

**UNIVERSIDADE FEDERAL DO RIO GRANDE DO SUL
INSTITUTO DE GEOCIÊNCIAS
PROGRAMA DE PÓS-GRADUAÇÃO EM GEOCIÊNCIAS**

**O MAGMATISMO DE ARCO CONTINENTAL PRÉ-COLISIONAL (790 Ma) E
A RECONSTITUIÇÃO ESPAÇO-TEMPORAL DO REGIME
TRANSPRESSIVO (650 Ma) NO COMPLEXO VÁRZEA DO CAPIVARITA,
SUL DA PROVÍNCIA MANTIQUEIRA**

MARIANA MATURANO DIAS MARTIL

ORIENTADORA – Prof.^a Dr.^a Maria de Fátima Bitencourt

CO-ORIENTADOR – Prof. Dr. Lauro Valentim Stoll Nardi

Porto Alegre – 2016

**UNIVERSIDADE FEDERAL DO RIO GRANDE DO SUL
INSTITUTO DE GEOCIÊNCIAS
PROGRAMA DE PÓS-GRADUAÇÃO EM GEOCIÊNCIAS**

**O MAGMATISMO DE ARCO CONTINENTAL PRÉ-COLISIONAL (790 Ma) E
A RECONSTITUIÇÃO ESPAÇO-TEMPORAL DO REGIME
TRANSPRESSIVO (650 Ma) NO COMPLEXO VÁRZEA DO CAPIVARITA,
SUL DA PROVÍNCIA MANTIQUEIRA**

MARIANA MATURANO DIAS MARTIL

ORIENTADORA – Prof.^a Dr.^a Maria de Fátima Bitencourt

CO-ORIENTADOR – Prof. Dr. Lauro Valentim Stoll Nardi

BANCA EXAMINADORA

**Prof^a. Dr^a. Maria do Carmo Gastal – Instituto de Geociências, Universidade Federal
do Rio Grande do Sul**

**Prof. Dr. Adejardo Francisco da Silva Filho – Centro de Tecnologia e Geociências ,
Universidade Federal de Pernambuco**

**Prof. Dr. Vinícius Tieppo Meira – Instituto de Geociências da Universidade Estadual
de Campinas**

**Tese de Doutorado apresentada como
requisito parcial para a obtenção do Título
de Doutor em Ciências.**

Porto Alegre – 2016

UNIVERSIDADE FEDERAL DO RIO GRANDE DO SUL

Reitor: Carlos Alexandre Netto

Vice-Reitor: Rui Vicente Oppermann

INSTITUTO DE GEOCIÊNCIAS

Diretor: André Sampaio Mexias

Vice-Diretor: Nelson Luiz Sambaqui Gruber

Martil, Mariana Maturano Dias

O magmatismo de Arco Continental pré-colisional (790 Ma) e a reconstituição espaço-temporal do regime transpressivo (650 Ma) no Complexo Várzea do Capivarita, Sul da Província Mantiqueira . / Mariana Maturano Dias Martil. - Porto Alegre: IGEO/UFRGS, 2016. [167 f.] il.

Tese (Doutorado).- Universidade Federal do Rio Grande do Sul. Programa de Pós-Graduação em Geocências. Instituto de Geociências. Porto Alegre, RS - BR, 2016.

Orientador(es): Maria de Fátima Bitencourt
Coorientador(es): Lauro Valentim Stoll Nardi

1. Tectônica transpressiva 2. Ortognaisses granulíticos 3.
Magmatismo de Arco Continental 4. Sul da Província da Mantiqueira I.
Título. CDU 55

Catalogação na Publicação

Biblioteca Instituto de Geociências - UFRGS

Sibila Francine T. Binotto

CRB 10/1743

And in the aeon of hope - A new sun will rise for you

And in the still of the night - The moonchild will watch you too

Tiamat – Light in Extension

Esta tese é dedicada a Daia, minha irmã,
pelo apoio incondicional
É dedicada também a todas as mulheres cientistas
E as geólogas que consagram seu trabalho a ciência

Agradecimentos

Agradeço a todos que apoiaram e contribuíram para a conclusão do meu doutorado. O incentivo de vocês foi fundamental.

"The love he receives is the love that is saved"

Agradeço também aos que não acreditaram. Vocês também me motivaram.

"Nada nascerá onde não houver o cultivo de um ser melhor"

Aos orientadores, Fátima e Lauro.

A minha vó Eunice pelo carinho.

As amigas de todas as horas: Rossana Goulart, Fernanda Zanettini, Carla Barreto. Por todo o apoio nos momentos difíceis e pela alegria compartilhada.

A Stephanie Carvalho. Amiga querida! Tua ajuda na formatação final do texto e as palavras de incentivo me tranquilizaram nos momentos finais que antecederam a entrega da tese.

RESUMO

Este estudo foca no Complexo Várzea do Capivarita (CVC), localizado no sul da Província da Mantiqueira (PM), Brasil. A fim de investigar a evolução geológica do CVC, uma abordagem multi-disciplinar foi utilizada, incluindo geologia de campo, geologia estrutural, petrografia, geoquímica de elementos maiores e traços, isótopos de Sr-Nd e geocronologia U-Pb em zircão (LA-MC-ICP-MS e SHRIMP). O complexo compreende uma variedade de orto- e paragnaisse de composição e idade diversa. Volumes subordinados de sienitos sintectônicos também perfazem o CVC. A deformação é particionada em zonas de cisalhamento do tipo thrust (D_1) e transcorrentes (D_2), o que sugere tectônica transpressiva. O arcabouço estrutural descrito é possivelmente relacionado a um evento colisional oblíquo. Os estudos petrológicos e geocronológicos enfatizaram os ortognaisses do CVC a fim de avaliar as fontes magmáticas e paleo-ambientes envolvidos. Idades de cristalização obtidas nos domínios de zircão com zonação tipicamente ígnea variaram entre 780 e 790 Ma. Por sua vez, idades entre 640 - 650 Ma foram obtidas em sobrecrecimentos de zircão, sendo interpretadas como o registro da idade do metamorfismo de alto grau e fusão parcial associada. Os dados geocronológicos apresentados também indicaram que ambos os regimes cinemáticos foram contemporâneos, oferecendo, dessa forma, evidencia adicional para a hipótese de colisão oblíqua. Os ortognaisses do Complexo têm composição tonalítica a granítica e são rochas calcioalcalinas meta- a peraluminosas, com razões elevadas de $^{87}\text{Sr}/^{86}\text{Sr}$ (i) variando de 0.71628 a 0.72509 e valores $\epsilon\text{Nd}_{(790)}$ entre -7.19 a -10.06. Sua composição e padrões de elementos traços sugerem que representem um magmatismo de arco maduro continental. O magmatismo registrado no CVC é compatível com outras sequências de arco de ca. 800 Ma, incluindo parte das metavulcânicas ácidas do Complexo Metamórfico Porongos (CMP) e os ortognaisses do Cerro Bori, Uruguai. Todas essas associações têm assinatura típica de orógenos acrecionários, contendo idade TDM Meso a Paleoproterozóica, além de forte evidência da participação de processos de assimilação crustal/ contaminação. Desta forma, o conjunto de dados apresentados permite interpretar essas associações como parte do mesmo magmatismo, ou pelo menos como fragmentos de arcos magmáticos.

Programa de Pós-Graduação em Geociências

similares. As assinaturas Sr-Nd e geoquímica sugere que ao menos parte das metavulcânicas do CMP represente os protólitos dos ortognaisses de alto grau inclusos no CVC. Adicionalmente, as evidencias isotópicas também apontam similaridade entre as rochas sedimentares de ambas as unidades, sugerindo que o CVC e o PMC são, ao menos em parte, expressões do mesmo contexto, onde a atividade magmática e sedimentar ocorreu em um mesmo ambiente de arco continental. A corroboração desta premissa é o objetivo principal de estudos de proveniência em andamento, cujos resultados prévios apontam para o caráter vulcano-sedimentar dos metapelitos do CVC e sua relação co-genética com os ortognaisses do CVC. Os dados isotópico Sr-Nd sugerem que os protólitos dos ortognaisses foram gerados por processos de assimilação crustal associados à cristalização fracionada. O modelamento binário (*binary mixing model*) realizado indica que o magmatismo estudado teria se originado de fontes mantélicas do tipo EM II. Uma seqüência paleoproterozóica de rochas TTG pertencente ao Complexo Arroio dos Ratos (CAR) é possivelmente o principal contaminante crustal assimilado. Em conjunto com as idades de herança descritas no CVC em ca. 2.0 Ga é sugerido que a fusão crustal que gerou o magmatismo do CVC em ca. 790-780 Ma foi predominantemente similar ao CAR.

Palavras-chave: Tectônica transpressiva, Ortognaisses granulíticos, Magmatismo de Arco Continental, Sul da Província da Mantiqueira

ABSTRACT

This study focuses in the Várzea do Capivarita Complex (VCC), exposed in the southern part of the Neoproterozoic Mantiqueira Province (PM), Brazil. To investigate the evolutionary processes that lead the VCC construction, a multi-disciplinary approach is taken, which includes field and structural geology, petrography, major and trace-element geochemistry, Sr-Nd isotope and U-Pb zircon geochronology by LA-MC-ICP-MS and SHRIMP. The complex comprises a compositional and age variety of ortho- and paragneisses tectonically interleaved during a high grade event. Subordinate volumes of syntectonic syenites are also part of CVC. The VCC deformation is partitioned into thrusting (D_1) and transcurrent (D_2) shear zones, suggestive of transpressive tectonics. This structural framework is possibly related to an oblique collision event. Petrological and geochronological studies emphasize the VCC orthogneisses in order to evaluate magmatic sources and related paleo-environments. Igneous crystallization ages obtained in the typical magmatic domains presenting oscillatory zoning in zircons vary between 780 and 790 Ma. Zircon overgrowths have ages mostly in the 650 – 640 Ma range and are interpreted to record the timing of high-grade metamorphism and associated partial melting. Geochronological data presented also indicates that both kinematic regimes are contemporaneous, offering, therefore, further evidence for the oblique collisional event hypothesis. The VCC ortogneisses comprise tonalitic to granitic compositions and are metaluminous to peraluminous, calc-alkaline rocks, with high $^{87}\text{Sr}/^{86}\text{Sr}$ ratios from 0.71628 to 0.72509 and $\epsilon\text{Nd}_{(790)}$ values from -7.19 to -10.06. Their geochemical composition and trace-element patterns are compatible with a continental mature arc. VCC magmatism is correlated with other ca. 800 Ma arc sequences from southern PM, including part of the Porongos Metamorphic Complex (PMC) metavolcanic rocks and the orthogneisses from Cerro Bori, Uruguay. All these associations show signatures typical of accretionary orogens, TDM and Meso to Paleoproterozoic inheritance ages, and present strong evidences of crustal assimilation/contamination. Thus, these sequences may be interpreted as part of the same magmatism, or at least as fragments of similar magmatic arcs. Geochemical and Sr-Nd signatures suggest that at least part of the PMC metavolcanic rocks may

Programa de Pós-Graduação em Geociências

represent the protoliths of the VCC high grade orthogneisses. This, together with the isotope evidence of similarity between the sedimentary fractions of both unities, suggest that the VCC and PMC are, at least in part, expressions of the same context, wherein the magmatic and sedimentary activity occurred in a single continental arc environment. The corroboration of this premise is the main goal of provenience studies in prep, which previous results points to the volcano-sedimentary character of part of the VCC metapelites and its co-genetic relation with the VCC orthogneisses. Sr-Nd isotope data suggest that the orthogneiss protoliths were generated by crustal assimilation processes associated with fractional crystallization. Binary mixing models indicate that the VCC magmatism originates from evolved EM II mantle sources. A Paleoproterozoic TTG association (ca. 2.0 Ga) from the Arroio dos Ratos Complex (ARC) seems to be the main crustal contaminant assimilated. Together with the small inheritance contribution at ca. 2.0, this suggests that the melted crust at ca. 790-800 Ma was predominantly like ARC.

Key-words: Transpressive tectonic, Granulitic orthogneisses, Continental Arc Magmatism, Southern of Mantiqueira Province

Programa de Pós-Graduação em Geociências

SUMÁRIO

RESUMO	1
ABSTRACT	3
ESTRUTURA E ORGANIZAÇÃO DA TESE	6
Capítulo I – INTRODUÇÃO.....	7
1. Caracterização do problema e motivação da pesquisa.....	7
2. Objetivos.....	8
3. A reconstrução de ambientes pré- e sin-colisionais em rochas de alto grau.....	9
3.1. Arquitetura de orógenos colisionais: arcabouço estrutural	10
3.2. Ortognaisses de alto grau: Relação entre preservação e obliteração da geoquímica original dos protólitos ígneos	11
3.3. Geoquímica isotópica e geocronologia em ortognaisses de alto grau	14
4. Contexto geológico da região estudada.....	16
4.1. O segmento meridional da Província da Mantiqueira	16
4.2. Evolução do conhecimento sobre o Complexo Várzea do Capivarita.....	17
5. Metodologia e métodos	20
5.1. Pesquisa bibliográfica	20
5.2. Trabalho de campo.....	21
5.3. Análise petrográfica e microestrutural.....	21
5.4. Geoquímica de elementos maiores e traços.....	21
5.5. Isótopos de Sr e Nd	22
5.6. Geocronologia U-Pb	23
Referências	24
Capítulo II – APRESENTAÇÃO DOS ARTIGOS CIENTÍFICOS	29
1. Artigo 1 - Structural Evolution of the Várzea do Capivarita Complex: a record of Cryogenian (ca. 650Ma) transpressive tectonics in southernmost Brazil	29
2. Artigo 2 - Cryogenian granulitic orthogneisses of the Várzea do Capivarita Complex thrust pile and implications of magmatic arc activity and continental collision in the southern Mantiqueira Province, Brazil	70
3. Artigo 3 - Pre-collisional Neoproterozoic (ca.790 Ma) arc magmatism in southernmost Brazil: tectono-stratigraphy of the Várzea do Capivarita Complex	113
Capítulo III – CONSIDERAÇÕES FINAIS.....	157
Referências	161

ESTRUTURA E ORGANIZAÇÃO DA TESE

Esta tese está disposta em 3 capítulos principais, incluindo introdução, artigos submetidos e considerações finais.

No Capítulo I estão enumerados os itens introdutórios da tese e que constituíram o arcabouço deste estudo. O item 1 inclui a caracterização do problema e o item 2 contém os objetivos pretendidos. No item 3 são apresentados alguns conceitos básicos sobre o conhecimento dos terrenos de alto grau e os problemas envolvidos em sua investigação. Informações a respeito da geologia da área e evolução do conhecimento do Complexo Várzea do Capivarita são encontrados no item 4. No item 5 estão listados os métodos envolvidos na pesquisa.

O Capítulo II é composto pelos artigos científicos submetidos que perfazem o corpo principal desta tese.

No Capítulo III são reunidas as considerações finais da tese com a síntese das principais conclusões obtidas nos artigos científicos submetidos.

- Capítulo I -

INTRODUÇÃO

1. Caracterização do problema e motivação da pesquisa

O Complexo Várzea do Capivarita (CVC) está localizado no segmento Meridional da Província Mantiqueira (PM), Brasil. O CVC é composto por orto- e paragnaisse de alto grau cujas relações estratigráficas e estruturais são pouco compreendidas.

Os trabalhos desenvolvidos durante a elaboração de mestrado da presente autora (Martil 2010, Martil et al., 2011) forneceram informações que permitiram um primeiro entendimento sobre as relações geológicas e estruturais do CVC. Compreenderam também a discussão dos dados de geoquímica de elementos maiores e traço obtidos para os gnaisses tonalíticos inclusos no CVC, cujo magmatismo foi atribuído a arco continental. No entanto, inúmeras questões permaneceram em aberto.

Os dados referentes à configuração estrutural do Complexo sugeriam a existência de dois regimes distintos. No CVC, a estrutura regional principal seria formada pela intercalação tectônica contemporânea ao metamorfismo de fácie granulito e formada possivelmente por movimentos de cavalgamento/empurrao. O Complexo seria também afetado por uma zona de cisalhamento de direção NNW e caráter transcorrente horário. Contudo, os dados levantados foram de natureza preliminar e, a fim de estabelecer os estilos tectônicos relacionados à construção do CVC, seria requerido o aprimoramento dos dados estruturais. A aquisição desses dados possibilitaria também investigar a possível correlação do complexo com os eventos colisionais envolvidos na construção do segmento meridional da Província Mantiqueira, até então pouco entendidos.

Durante trabalhos de mapeamento foram encontrados gnaisses de composição granítica que seriam parte da pilha de *thrust* descrita para o CVC. A comparação com as litologias tonalíticas poderia fornecer informações adicionais a respeito do magmatismo de margem continental registrado no CVC, ou ainda reforçar a hipótese de empilhamento tectônico, caso os ortognaisses possuíssem

Programa de Pós-Graduação em Geociências

assinaturas químicas ou mesmo idades distintas. Adicionalmente, o estudo de fontes magmáticas envolvidas na geração do magmatismo de arco já estabelecido propiciaria informações a respeito da gênese e evolução crustal desse segmento da PM.

Os dados geocronológicos disponíveis para o CVC são escassos e algo imprecisos. Até o presente momento, a idade ígnea da fração ortometamórfica permanece inédita na bibliografia. Além disso, as idades metamórficas citadas na literatura são controversas (Gross et al., 2006, Philipp et al., 2016) e uma investigação acurada se faz necessária a fim de balizar a possível colisão registrada no CVC.

2. Objetivos

O trabalho proposto teve como motivação principal investigar o Complexo Várzea do Capivarita através de uma abordagem integrada e multi-disciplinar de forma a obter uma visão integrada dos aspectos envolvidos na gênese do Complexo. Os resultados obtidos permitiram também contribuir para o avanço do conhecimento a respeito dos episódios tectônicos que levaram à construção do segmento meridional da Província Mantiqueira, assunto até então alvo de debate na literatura. Os objetivos específicos deste trabalho foram investigados numa série de etapas complementares:

- 1) *Detalhamento das relações geológicas e estratigráficas, bem como o aprimoramento do arcabouço estrutural do CVC;*
- 2) *Determinação da cronologia dos eventos magmáticos, metamórficos e estruturais envolvidos na construção do complexo;*
- 3) *Analizar do ponto de vista geoquímica e isotópico o magmatismo registrado no CVC, com o objetivo de determinar as fontes magmáticas e paleo-ambientes envolvidos;*

- 4) *Integração dos dados obtidos e comparação com a literatura disponível.*

3. A reconstrução de ambientes pré- e sin-colisionais em rochas de alto grau

Os terrenos metamórficos de alto grau constituem uma porção significativa da crosta continental exposta em cinturões orogênicos fanerozóicos e em cráticos pré-cambrianos. As rochas ortometamórficas representam um volume expressivo desses terrenos e o seu estudo permite tecer considerações sobre os estágios primitivos de gênese crustal.

O metamorfismo granulítico ocorre em uma gama de ambientes tectônicos e diversas são as hipóteses sob sua gênese e evolução. Contudo, inúmeras ocorrências de rochas de alto grau estão associadas a processos tectônicos relacionados ao encurtamento e espessamento da crosta e da litosfera gerados em limites colisionais e convergentes. As falhas de empurrão, bem como as dobras de grande escala, são as estruturas dominantes da arquitetura desses sistemas tectônicos onde constituem cinturões de cavalgamento e dobramento (*fold and thrust belts*).

Em terrenos de alto grau é em geral observada uma configuração polimetamórfica e polideformacional e muitos aspectos da história geológica precoce podem ser obscurecidos. Para desvendar a história tectônica de um terreno granulítico é necessária a aplicação de técnicas variadas, incluindo estudos detalhados de estrutural e petrografia para reconstrução da história metamórfica e deformacional e estudo de isótopos radiogênicos para fornecer a temporalidade absoluta desses processos. No caso de rochas ortognáissicas, a abordagem geoquímica é essencial para o entendimento dos ambientes formadores e fontes de magmatismo. Para tanto, é necessário averiguar quais características do protólito ígneo podem ser preservadas.

A seguir são abordadas algumas questões sobre que tipo de informações podem ser resgatadas em rochas de alto grau. Uma breve explanação sobre a geometria estrutural de áreas colisionais é apresentada. É também discutido que informações podem ser preservadas sobre as fontes e história magmática, além de quais critérios devem ser atendidos para abordagem geoquímica de rochas

Programa de Pós-Graduação em Geociências

ortoderivadas. Por fim, é realizada uma breve explanação sobre os dados que podem ser obtidas por meio de estudos geocronológicos e isotópicos em ortognaisses de alto grau.

3.1. Arquitetura de orógenos colisionais: arcabouço estrutural

Muitas variáveis governam as estruturas e condições metamórficas produzidas durante a formação de um orógeno, tais como as idades e características físicas das massas rochosas envolvidas, o tipo de movimento relativo das placas, etc.

As estruturas presentes em um orógeno colisional podem estar relacionadas ao tipo de movimento relativo entre os blocos produzido durante a colisão (Plujiin & Marshak, 2004). Nas **colisões frontais** predominam estruturas relacionadas a falhas de cavalgamento cujo movimento é perpendicular ao limite dos blocos envolvidos na colisão. Já **nas colisões oblíquas** o movimento relativo entre as placas não é perpendicular ao limite da convergência. Nesse caso, a distribuição das forças envolvidas na colisão são divididas em um componente de movimento do tipo *dip-slip* (cavalgamento) perpendicular a borda do orógeno e outro componente de cisalhamento paralelo a essa mesma margem (Fig.1a & 1b). As falhas transcorrentes ocorrem em uma variedade de locais ao longo da margem, incluindo a cunha acrecionária, o arco vulcânico e a região de *backarc*. O movimento direcional (*strike-slip*) comumente observado nessas falhas é geralmente acompanhado por um componente de encurtamento ou extensão. Especificamente, quando a **transpressão** ocorre, há uma combinação de movimento *strike-slip* e encurtamento, produzindo soerguimento das rochas ao longo da falha. Já a **transtracção** ocorre quando há a combinação de movimento *strike-slip* e extensão, e pode produzir subsidência nas porções adjacentes ao plano de falha. As falhas geralmente relacionadas à colisão são, pelo menos em um primeiro momento, de natureza transpressiva. As falhas transtratativas são mais comuns, mas não exclusivas, em áreas mais distais do orógeno.

Em alguns casos, o movimento das zonas de cisalhamento durante a colisão oblíqua pode ser responsável pela acresção de fatias ou fragmentos de terrenos

exóticos inteiros a uma dada orogenia (Fig.1c). Em geral, esses dois estilos colisionais – frontal e oblíquo – podem estar associados a diferentes ciclos de uma mesma orogenia.

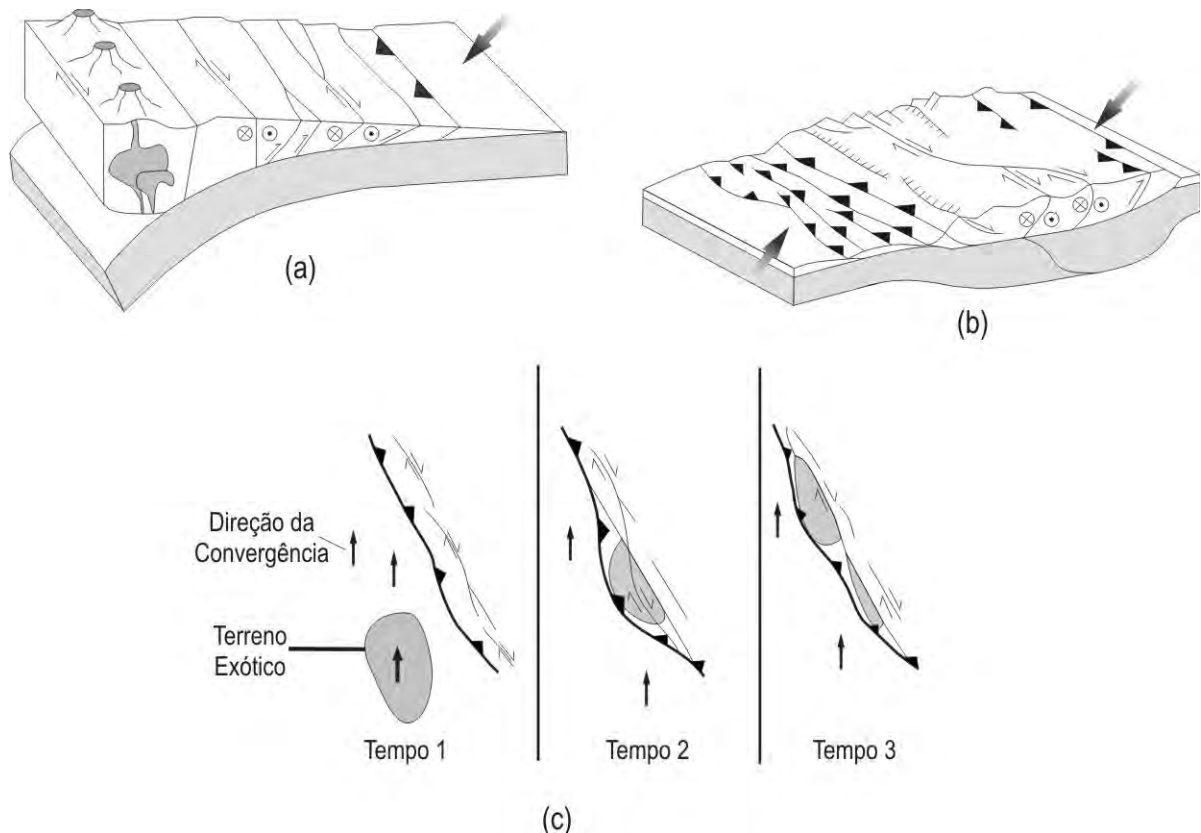


Figura 01 – (a) Falhas transcorrentes em uma margem convergente oblíqua. Notar que essas falhas ocorrem em vários locais ao longo do orógeno. A seta larga indica o movimento relativo da placa subjascente. (b) Falhas transcorrentes em um cinturão colisional já formado. (c) Cróqui esquemático demonstrando a acresção progressiva de um terreno exótico. No estágio final esse mesmo terreno é fatiado ao longo do orógeno pela atuação das falhas transcorrentes. Modificado de Pluigin & Marshak (2004).

3.2. Ortognaisses de alto grau: Relação entre preservação e obliteração da geoquímica original dos protólitos ígneos

Estudos geoquímicos e petrológicos de ortognaisses de alto grau constituem uma importante ferramenta para o entendimento dos processos relacionados à origem e a formação da crosta continental arqueana e também fanerozóica. Para obter tais informações, é necessário avaliar até que ponto os diversos eventos comumente envolvidos na história desses terrenos atuaram na modificação da química original dos protólitos ígneos dos gnaisses de alto grau. Ao mesmo tempo, é

Programa de Pós-Graduação em Geociências

preciso investigar que características geoquímicas podem ter sido relativamente bem preservadas.

Durante o metamorfismo, as rochas são submetidas a variações compostacionais mais ou menos intensas. As variações químicas que os protólitos podem sofrer dependem de inúmeros fatores, incluindo as condições de P-T do metamorfismo, a composição do protólito, a presença de fases fluídas e o transporte desses através das estruturas geradas durante inúmeros episódios de deformação.

No caso de rochas metamorfizadas sob alto grau, as reações de desidratação e anatexia constituem os principais processos mobilizadores, e os elementos químicos comumente fracionados durante este tipo de metamorfismo são aqueles que tendem a se concentrar na fase fluida ou no líquido resultante da fusão parcial. Desta modo, se é pretendido averiguar as características geoquímicas do protólito de rochas de alto grau, é importante se concentrar nas relações entre aqueles elementos relativamente imóveis durante o metamorfismo, além de se avaliar o grau de atuação dos fatores que tendem a alterar a composição química original em cada contexto geológico.

O fracionamento dos elementos litófilos de raio iônico grande, ou LILE (*Large Ion Lithophile Elements* - Cs, Sr, K, Rb, Ba) e de alguns elementos com comportamento químico similar (*i.e.*: raio iônico e carga similar) durante o metamorfismo é amplamente reconhecido na bibliografia. Os metais de transição, tais como Mn, Zn e Cu também tendem a ser mobilizados, particularmente sob altas temperaturas (Rollinson, 2005).

Caso os padrões químicos do ortognaisse estudado demonstrem algum fracionamento em seus padrões LILE e de seus elementos maiores, uma alternativa possível seria a utilização de diagramas que considerem elementos menos móveis durante o metamorfismo. Os elementos de raio iônico pequeno ou HFSE (High Field Strenght Elements) são tidos como pouco móveis e incluem os lantanídeos (elementos com número atômico entre 57 e 71) sendo estes também denominados de terras-raras (ETR - Sc, Y, Th, Zr, Hf, Ti, Nb, Ta e P). Os metais como Co, Ni, V e Cr também são relativamente imóveis (Rollinson, 2005). O teor de elementos traços que permanecerá no protólito durante o metamorfismo dependerá da quantidade inicial desses elementos no protólito e da mineralogia original do mesmo: o coeficiente de partição (K_d – equação 1) desses elementos em relação aos minerais

Programa de Pós-Graduação em Geociências

existentes é que vai controlar o teor de elementos traço que irá permanecer no restito (elementos compatíveis – $K_d > 1$) e os elementos que terão maior afinidade com o líquido originado pela fusão (incompatíveis – $K_d < 1$).

$$\text{Equação 1: } K_d_{\text{elemento}} = \frac{\text{Concentração}_{\text{elemento}} \text{ no mineral}}{\text{Concentração}_{\text{elemento}} \text{ na fusão}}$$

Os diagramas geoquímicos mais indicados são aqueles que lidam entre proporções desses elementos de baixa mobilidade, pois ainda que esses elementos tenham sido depletados, foram possivelmente empobrecidos na mesma proporção (*i.e.* tem características químicas similares). Exemplos de diagramas que lidam com esses elementos são demonstrados abaixo (Fig. 2):

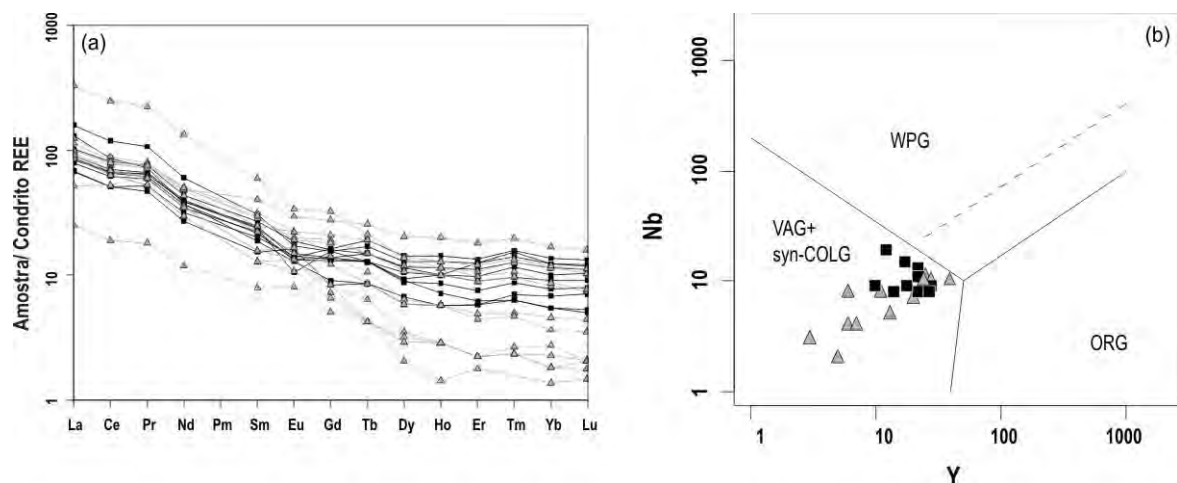


Figura 02 – Exemplos de diagramas geoquímicos clássicos que utilizam elementos imóveis. (a) Padrões ETR normalizados pelos valores condriticos (Nakamura, 1974). (b) Diagrama discriminatório Nb x Y de Pearce *et al.* (1984). Os padrões observados são de amostras de sequências ortognáissicas do Escudo Sul-rio-grandense. Modificado de Martil *et al.* (2011).

Uma vez sendo reconhecidos padrões geoquímicos preservados no ortognaisse de alto grau, uma ferramenta essencial para avaliar a química original do protólito seria a comparação da associação estudada com as séries magmáticas conhecidas. A classificação de rochas ígneas segundo sua composição química constitui importante ferramenta na construção de hipóteses no campo da petrogênese, estratigrafia, metalogenia e geotectônica (Nardi, 2011), sendo esta a

etapa precedente e base fundamental para qualquer estudo que envolva litologias ígneas.

As associações de rochas magmáticas derivadas de magmas parentais composicionalmente semelhantes podem ser agrupadas segundo suas características comuns, mesmo que durante os processos de diferenciação ocorra assimilação ou mistura com materiais externos. Os principais grupos assim identificados são denominados de séries ígneas (Fig. 3).

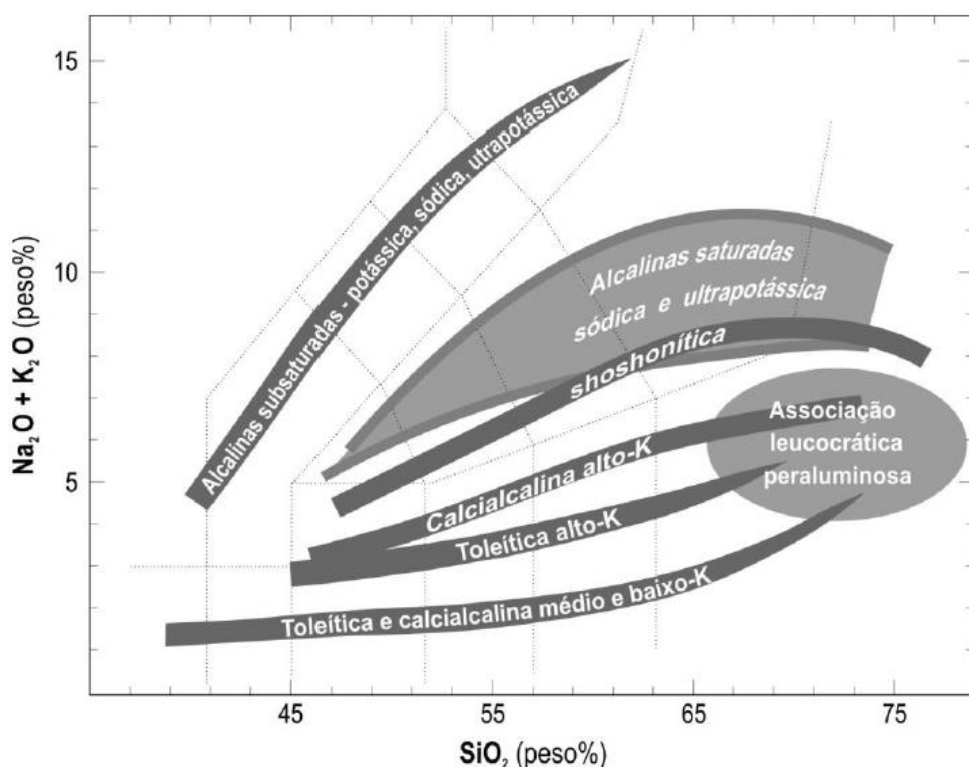


Figura 03 – Principais séries magmáticas e produtos de fusão crustal lançados no TAS. Modificado de Nardi (2011).

3.3. Geoquímica isotópica e geocronologia em ortognaisses de alto grau

A utilização de sistemas como Rb-Sr, Sm-Nd, Lu-Hf e U-Th-Pb (*p. ex.*), através da obtenção de dados de rocha-total e mineral, podem fornecer delimitações importantes sobre a evolução e idade de rochas de alto grau. Contudo, deve-se notar que todos esses sistemas são afetados em alguma extensão pela atuação do metamorfismo e da atividade de fluídos. Na investigação de ortognaisses, estudos isotópicos podem fornecer informações petrogenéticas e dados sobre as fontes magmáticas, a idade do protólito, bem como as idades dos diferentes eventos

Programa de Pós-Graduação em Geociências

deformacionais e metamórficos. No caso da existência de uma pilha de cavalgamento (*thrust pile*) é possível estabelecer as idades das diferentes fatias que constituem uma dada orogenia.

O uso de isótopos radiogênicos na investigação de terrenos de alto grau tem certas limitações que resultam do fato do metamorfismo de alto grau poder modificar as razões isotópicas originais bem como a razão entre elementos pai e filho, o que causaria a perda de dados sobre a história pré-metamórfica. Esse processo é denominado de homeogeneização isotópica ou *reset* do sistema (e.g. Faure, 1989). Por essa razão, quando são estudados ortognaisses de alto-grau, são geralmente utilizados de sistemas que lidem com elementos mais imóveis. É o caso, por exemplo, dos métodos Sm-Nd. O **método Sm-Nd** utiliza elementos que não se difundem facilmente e são muito pouco móveis no estado sólido. São também resistentes a processos de intemperismo e de lixiviação. O único processo realmente capaz de alterar as razões Sm-Nd é a extração mantélica, mas uma vez que a crosta é gerada, os processos tectono-metamórficos que ela possa vir a sofrer, em geral, não interferem nessa razão.

Minerais refratários, tais com zircão e monazita, são reconhecidos por preservarem características prévias de sua história magmática e metamórfica, sendo comumente utilizados na datação de rochas de alto grau. Uma abordagem amplamente utilizada na bibliografia para obter idades e metamórfica de ortognaisses de alto grau é o método **U-Pb em zircão**. O zircão constitui um sistema fechado que pode conter teores elevados de U e que de modo geral não contém Pb inicial (Pb não radiogênico) pois sua estrutura não possui sítios adequados para elementos de grande raio iônico. Logo o Pb presente na estrutura cristalina do zircão é tido como produto do decaimento do radioativo do U. No entanto, justamente devido a incompatibilidade do Pb com a estrutura cristalina do zircão pode haver perdas de Pb relacionadas a eventos que causem a abertura do sistema de forma a aumentar a relação U/Pb. Estudos modernos tentam superar o problema relacionado à perda de chumbo por meio de análises pontuais em grão isolados. Uma das técnicas mais sofisticadas é a realização de microanálises por microssonda iônica (Ex.: SHRIMP – *Sensitive High Resolution Ion Micropobe*) ou microssonda laser (Ex.: Laser Ablation-ICP-MS). Essas técnicas permitem análises pontuais muito precisas na superfície polida de um zircão. Por meio desse tipo de análise pode-se, por

exemplo, obter a idade de um núcleo ígneo e a idade metamórfica de um sobrecrecimento presente em um único grão de zircão.

4. Contexto geológico da região estudada

4.1. O segmento meridional da Província da Mantiqueira

A área estudada é parte do segmento Meridional da Província Mantiqueira (PM – Fig.1), que é em grande parte composto por granitóides neoproterozoicos intrusivos em embasamento metamórfico de idade predominante paleoproterozoica (Hartmann et al., 1999; Soliani Jr et al., 2000). A Província Mantiqueira desenvolveu-se durante o Ciclo Orogênico Brasiliano/Panafricano cuja evolução é principalmente caracterizada por episódios diacrônicos de subducção e de colisão do tipo arco-continente e continente-continente (e.g. Heilbron et al., 2004). No segmento meridional da PM (Fig.1). O ciclo Brasiliano/ Panafricano é caracterizado por um magmatismo de arco entre 900 e 700 Ma (e.g. Leite et al., 1998, Lenz et al., 2011, Siviero et al., 2009, Hartmann et al. 2000, 2011) e por amplo magmatismo pós-colisional, com idades entre 650 e 580 Ma (Bitencourt e Nardi, 2000). Idades de metamorfismo de alto grau relacionadas à colisão têm sido descritas em investigações recentes e variam entre ca. 670 Ma, no Escudo Uruguaio (Lenz et al., 2011) até ca. 620 Ma no Sul do Brasil (Philipp et al., 2016).

A distribuição dos grandes domínios litológicos deste segmento da PM indica a ocorrência de rochas paleoproterozóicas no extremo nordeste de Santa Catarina (SC), no sudoeste do Rio Grande do Sul (RS), e uma área mais significativa no Escudo Uruguaio (Fig. 1). As associações Neoproterozóicas do sul da PM ocorrem ao longo do Cinturão Dom Feliciano (CDF) e compreendem principalmente: rochas relacionadas a arco a oeste; uma faixa estreita de rochas metamórficas supracrustais de fácies anfibolito inferior a médio na região central; e na porção leste um cinturão granítico de direção NE que se estende de Santa Catarina ao Uruguai. Segundo Bitencourt e Nardi (2000), a atividade ígnea deste cinturão granítico teria sido controlada pela descontinuidade de escala litosférica denominada Cinturão de Cisalhamento Sul-brasileiro (CCSb). O complexo Metamórfico Várzea do Capivarita

ocorre como pendentes de teto de grande escala nos granitóides associados ao desenvolvimento do CCSb.

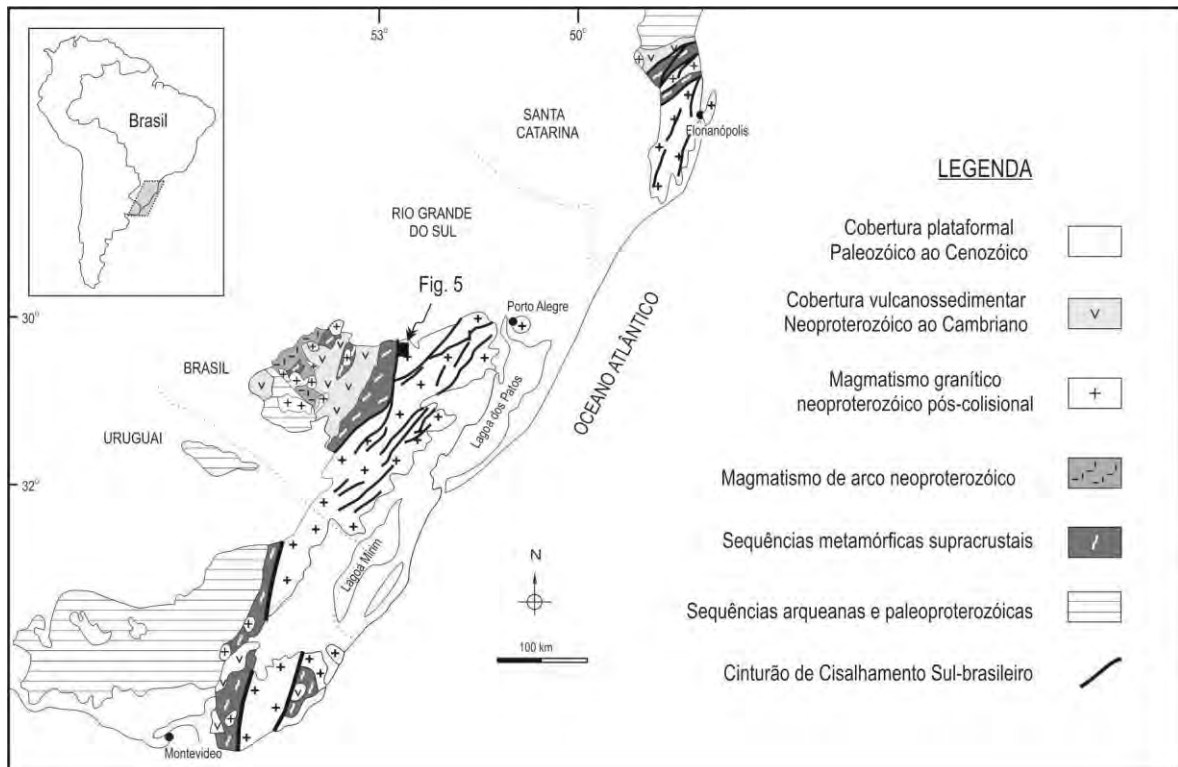


Figura 04 – Principais domínios geotectônicos do segmento meridional da Província Mantiqueira (modificado de Nardi e Bitencourt, 2007).

4.2. Evolução do conhecimento sobre o Complexo Várzea do Capivarita

A área estudada foi primeiramente definida e denominada como Complexo Metamórfico Várzea do Capivarita (CMVC – Frantz et al., 1984) e incluía as associações gnáissicas de alto grau que ocorrem na região de Encruzilhada do Sul, RS (Fig. 5). Este complexo era formado por paragnaisses aluminosos, calciosilicáticos e quartzo-feldspáticos, intercalados com ortognaisses de composição granodiorítica a tonalítica, além de meta-anortositos (Anortosito Capivarita).

Fernandes et al. (1988) propuseram o desmembramento desta unidade, retirando dela o Metanortosito Capivarita e denominando os paragnaisses de Suíte Metamórfica Várzea do Capivarita (SMVC). Os ortognaisses foram definidos como Complexo Gnáissico Arroio dos Ratos (CGAR), o qual compreenderia uma sucessão

Programa de Pós-Graduação em Geociências

de rochas plutônicas que ocorria como xenólitos e pendentes de teto de dimensões variáveis na SMVC e que também eram metamorfizadas em alto grau. A partir de então, diversos trabalhos (e.g. Porcher, 2000, Gross et al., 2006, Koester et al., 2008) referem estas duas unidades a uma história deformacional comum, registrada em uma trama originalmente subhorizontal, com lineação de estiramento indicativa de transporte tectônico de E para W (Fernandes et al. 1992).

Contudo, a área aflorante destas litologias foram redefinidas por uma série de mapeamentos (Niessing, 2007; Martil, 2007, UFRGS, 2008, UFRGS 2009), levando à reestruturação das concepções estratigráficas para esta área no que se refere às rochas metamórficas de alto grau. Grande parte das litologias encontradas na área atribuída por Porcher (2000) ao Complexo Gnáissico Arroio dos Ratos (ocorrência norte na Fig. 5) corresponde, na descrição de Niessing et al. (2008), a um sillimanita-biotita leucogranito foliado, denominado Granito Butiá. O Granito Butiá é interpretado como um exemplo de magmatismo sintectônico relacionado a zonas de transcorrência do Cinturão de Cisalhamento Sul-brasileiro (Niessing 2007, Niessing et al., 2008).

Na ocorrência atribuída à Suíte Metamórfica Várzea do Capivarita, a leste do Maciço Sienítico Piquiri (Fig. 5), Martil (2007, 2010) e Martil et al. (2011) descreve a intercalação de orto e paragnaisses em diversas escalas, o que torna impossível a separação em duas unidades distintas, como feito anteriormente por diversos autores (Fernandes et al., 1988, 1992; Porcher, 2000, entre outros). Relações similares são também encontradas na área maior de ocorrência destas litologias para leste e sul, conforme dados de sucessivos mapeamento de detalhe. A ocorrência pontual nessa região de ortagnaisses granodioríticos de fácies granulito é também descrita por Lima et al. (1997).

Nestas porções foram também identificados granitóides sintectônicos de composição dominante sienítica (Sienito Arroio das Palmas), intrusivos nas litologias gnáissicas. Para o conjunto de rochas gnáissicas para e sienitos sintectônicos foi então adotada a denominação de Complexo Várzea do Capivarita.

A continuidade deste trabalho de detalhamento e reestruturação das concepções estratigráficas e geológicas para o CVC é apresentado nos artigos inclusos nessa tese.

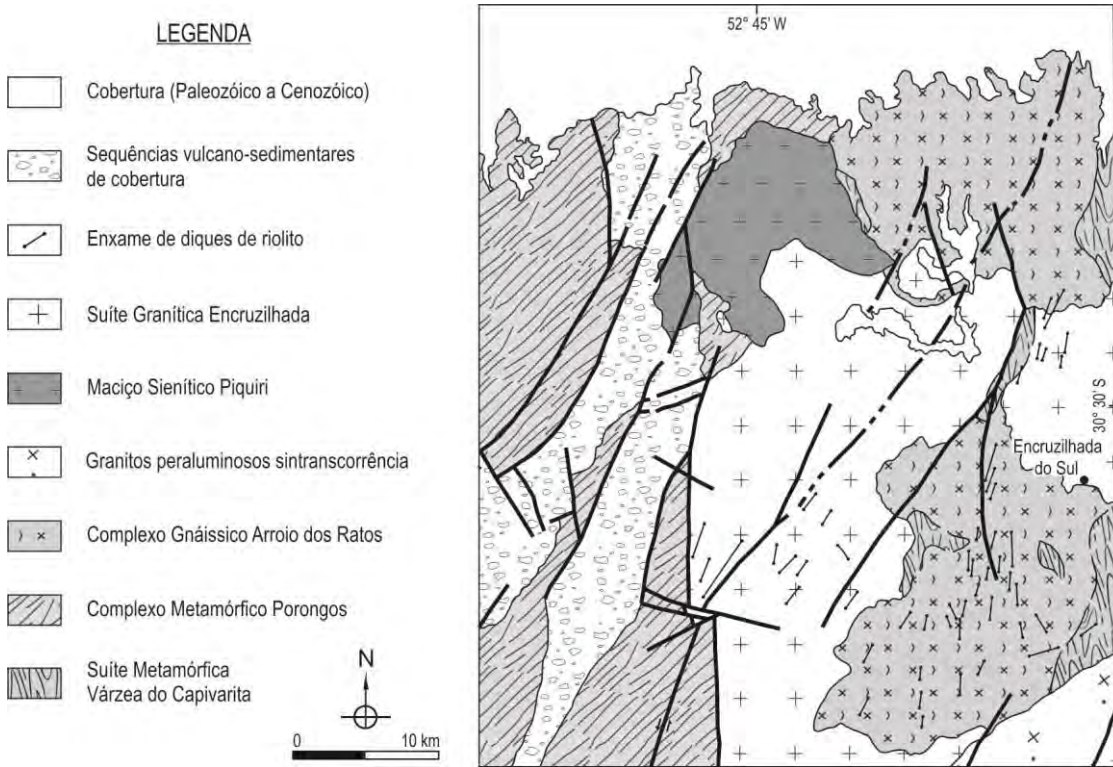


Figura 05 – Mapa geológico simplificado da porção leste da Folha Cachoeira do Sul, segundo os dados apresentados por Porcher et al. (2000); a área indicada corresponde à porção leste da Folha Passo das Canas, onde se localiza a área de estudo.

Os paragnaisse inclusos no CVC foram interpretados como uma sequência de sedimentos de plataforma, do tipo margem continental passiva (Fragoso Cesar, 1991), metamorfizada em condições de fácies anfibolito superior a granulito. Evidências de campo sugestivas de fusão parcial são encontradas em todos os tipos litológicos do Complexo, conforme já referido por Silva et al. (2002), embora sejam mais comum nos gnaisses pelíticos, na formas de bolsões e veios irregulares de leucogranitos. Gross et al. (2006) relacionam estas rochas a um evento tectono-termal com condições P-T entre 750-800°C e pressão entre 3-4 Kbar. Estes autores mencionam idades metamórficas obtidas em metapelitos entre 604 e 652 Ma (Sm-Nd granada vs. rocha total), com idade de pico entre ca. 604-626 Ma e erros altos associados. Recentemente, Phillip et al. (2016) baseando-se nas paragêneses Granada-cordierita-silimanita e biotita, estabeleceu condições de metamorfismo com temperatura de 720-820° C e pressão entre 8 e 9 kbar, caracterizando este metamorfismo como de alta temperatura e pressão intermediária. Dados geocronológicos (U-Pb SHRIMP em zircão) obtidos por estes autores indicaram

idade metamórfica de 619 ± 4.3 Ma. A idade magmática de um veio granítico determinada em 620 ± 6.3 Ma é interpretada como registro da fusão parcial para esta sequência (Phillip et al., 2016).

5. Métodos

Técnicas diversas foram utilizadas a fim de obter uma visão global dos aspectos estruturais, estratigráficos e tectônicos do Complexo Várzea do Capivarita, embora os estudos petrológicos tenham enfatizado principalmente os ortognaisses. O embasamento deste trabalho consistiu no mapeamento geológico estrutural da área de estudo, seguido pelo estudo petrográfico e microestrutural das rochas de alto grau do CVC. Foram selecionadas amostras dos diferentes tipos de ortognaisses para estudos geoquímicos e determinações isotópicas U-Pb, Rb-Sr e Sm-Nd. A pesquisa bibliográfica permeou toda a construção da tese.

5.1. Pesquisa bibliográfica

Para a pesquisa bibliográfica foram utilizados artigos científicos, livros e capítulos de livros texto nos temas relacionados à tese, notas de aula, bem como mapas e dados de mapeamento UFRGS e CPRM. Foi realizado o levantamento dos dados geológicos existentes para a área de estudo e adjacências a fim de obter um arcabouço prévio do estado do conhecimento das relações tectono-estratigráficas. Simultaneamente, procurou-se investigar os problemas envolvidos e a abordagem utilizada para investigação dos terrenos de alto grau. Esta revisão da literatura permitiu uma visualização ampla do contexto da área, bem como do tema investigado e das lacunas existentes. A investigação bibliográfica também possibilitou o desenvolvimento de estratégias de pesquisa em todas as etapas do doutorado.

5.2. Trabalho de campo

Em ordem de investigar o arcabouço estrutural e a história cinemática do CVC, foram realizados mapeamentos de detalhe na escala 1:10.000 em seções de interesse em uma área escolhida para detalhamento. Esta área foi escolhida de modo a contemplar os diferentes estágios de deformação registrada no CVC. Essa seleção foi feita a partir de dados de mapeamentos geológicos prévios na escala 1:25.000 (Martil, 2007, 2010, Martil et al., 2011, UFRGS, 2008).

Os dados levantados incluíram a descrição detalhada de cerca de 100 afloramentos. Os resultados deste trabalho de campo foram sintetizados em um mapa geológico revisado e numa série de seções estruturais. A análise geométrica consistiu na descrição e definição de grupos de estruturas. A análise cinemática envolveu a coleta das atitudes de lineações minerais e de estiramento e dos planos de foliação. Foram obtidas fotos e croquis das feições principais. Amostras orientadas foram coletadas para estudos petrográficos, microestruturais, e também amostras para caracterização geoquímica e obtenção de dados geocronológicos.

5.3. Análise petrográfica e microestrutural

Nesta etapa foi realizada a descrição petrográfica de detalhe das amostras de mão e de suas respectivas lâminas delgadas. Foram reconhecidas as feições microestruturais e texturais particulares, e subsequente obtenção de fotomicrografias das mesmas. São também correlacionadas as características de campo com as feições observadas na etapa de petrografia. A descrição petrográfica e microestrutural envolveu a seleção, a partir de dados de campo, de cerca de 80 amostras representativas. As lâminas delgadas foram confeccionadas no laboratório de preparação de amostras do IG-UFRGS.

5.4. Geoquímica de elementos Maiores e traços

As análises geoquímicas foram utilizadas para determinação dos conteúdos dos elementos maiores e traços em rocha a fim de investigar os protólitos ígneos

Programa de Pós-Graduação em Geociências

dos ortognaisses tonalíticos a graníticos, com o objetivo de estabelecer as séries magmáticas originárias e seus possíveis ambientes tectônicos. Para realização destes estudos, as amostras foram preparadas no Anexo do Laboratório de Geologia Isotópica do IG/UFRGS, envolvendo as seguintes etapas: (i) lavagem das amostras, (ii) moagem das amostras em prensa hidráulica, (iii) quarteamento das amostras e subsequente redução da granulação da fração escolhida em gral de porcelana, (iv) novo quarteamento de amostras com separação de 10g para moagem em moinho de bolas, (iv) redução da granulometria das amostras em gral de ágata até a obtenção da fração pó, (v) acondicionamento e envio das amostras para *AcmeLabs™*. Para as análises foram utilizadas as técnicas de ICP-OES (*Inductively Coupled Plasma Optical Emission Spectrometry*) para determinação dos elementos maiores e ICP-MS (*Inductively Coupled Plasma Mass Spectrometry*) para os elementos traços, após fusão com metaborato/tetraborato. Uma precisão melhor que 2% e 10% foi obtida para os elementos maiores e traços, respectivamente.

5.5. Isótopos de Sr e Nd

Estudos isotópicos foram realizados a fim de estudar as fontes e paleoambientes envolvidos na geração do magmatismo de arco registrado no CVC. Análises Rb-Sr e Sm-Nd foram obtidas no Laboratório de Geologia Isotópica of the Universidade Federal do Rio Grande do Sul (UFRGS) e no Laboratório de Geocronologia da Universidade de Brasília (UnB) utilizando um espectrometro de ionização termal (*TIMS - Thermal Ionization Mass Spectrometer*). Os equipamentos utilizados incluiram o multicoletor *VG Sector 54* (UFRGS) e o multicoletor *Finnigan MAT 262* (UnB). As determinações isotópicas seguiram as etapas propostas por Gioia and Pimentel (2000). Os procedimentos analíticos de ambos os laboratórios encontram-se descritos no item 4.2. do artigo 3, inserido no capítulo II.

5.6. Geocronologia U-Pb

Dados geocronológicos dos gnaisses graníticos e tonalíticos foram obtidos e comparados entre si. Essas análises propiciaram a determinação da idade do magmatismo de arco continental registrado no CVC. Os trabalhos realizados incluíram também o refinamento dos dados geocronológicos a respeito das idades de metamorfismo e fusão parcial. Adicionalmente, foram obtidas as idades absolutas dos sistemas de thrust e transcorrência inclusos no CVC a fim de investigar a hipótese de contemporaneidade entre ambos os regimes de cisalhamento.

As análises U-P em zircão por LA-MC-ICP-MS foram realizadas no Laboratório de Geologia Isotópica, Universidade Federal do Rio Grande do Sul (LGI – UFRGS) e no Laboratório de Geocronologia, Universidade de Brasília (UnB). As análises U-P em zircão por SHRIMP foram realizadas no Centro de Pesquisas Geocronológicas, Universidade de São Paulo (CPGeo-USP) e na *Research School of Earth Sciences, Australian National University* (RSES-ANU), Austrália. Os métodos analíticos e procedimentos destes laboratórios estão detalhados no Anexo A do artigo 2, inserido no capítulo II. Todas as idades foram calculadas usando o software Isoplot 3.0 (Ludwig, 2003).

Referências

- Bitencourt, M.F. e Nardi, L.V.S. 2000. Tectonic setting and sources of magmatism related to the Southern Brazilian Shear Belt. *Revista Brasileira de Geociências*, 30: 184-187.
- Faure, G., 1989. *Principles of Isotope Geology*. New York, John Wiley & Sons, 588p.
- Fernandes, L.A.D.; Tommasi, A.; Porcher, C.C.; Vieira Jr, N.; Marques-Toigo, M.Guerra-Sommer, M.; Piccoli, A.E. 1988. Mapa geológico de parte das folhas de Quitéria (SH 22-Y-B-I-4) e Várzea do Capivarita (SH 22-Y-B-I-3), RS. Porto Alegre, 1988. 1 mapa preto e branco. Escala 1:50.000.
- Fernandes, L.A.D, Tommasil, A., Porcher, C.C. 1992. Deformation patterns in the southern Brazilian branch of the Dom Feliciano Belt: a reappraisal. *Journal of South American Earth Sciences*, 5(1):77-96.
- Fragoso César, A.R.S. 1991. Tectônica de placas no Ciclo Brasiliano: As orogenias dos Cinturões Dom Feliciano e Ribeira no Rio Grande do Sul. São Paulo. 362 p. Tese de Doutorado em Geociências, Instituto de Geociências, Universidade de São Paulo.
- Frantz, J. C., Lima, E. F., Pinheiro-Machado, Naumann, M.P. 1984. Contribuição a geologia da região de Encruzilhada do Sul-RS. In: CONGRESSO BRASILEIRO DE GEOLOGIA, 33., Rio de Janeiro. Anais... Rio de Janeiro, SBG, v. 5. p. 2407-2416.
- Gioia, S.M.C., Pimentel, M., 2000. The Sm–Nd isotopic method in the Geochronology Laboratory of University of Brasilia. *Anais da Academia Brasileira de Ciências* 72, 219–245.
- Gross, A.O.M.S., Porcher, C.C., Fernandes, L.A.D., Koester, E. 2006. Neoproterozoic low-pressure/high-temperature collisional metamorphic evolution in

Programa de Pós-Graduação em Geociências

the Varzea do Capivarita metamorphic suite, RS Brazil: thermobarometric and Sm/Nd evidence. *Precambrian research*, 147:41-64.

Hartmann, L. A., Leite, J.A.D., McNaughton, N.J., Santos, J. O.S. 1999. Deepest exposed crust of Brazil - SHRIMP establishes three events. *Geology*, 27(10):947-950.

Heilbron, M., Pedrosa-Soares, A.C., Campos Neto, M., Silva, L.C., Trouw, R.A.J., Janasi, V.C. 2004. A Província Mantiqueira. In: Mantesso-Neto, V., Bartorelli, A., Carneiro, C.D.R., Brito Neves, B.B. (Eds.), *O desvendar de um continente: a moderna geologia da América do Sul e o legado da obra de Fernando Flávio Marques de Almeida*, pp. 203-234.

Koester, E., Chemale Jr., F., Porcher, C.C., Bertotti, A.L., Fernandes, L.A.D., 2008. U-Pb ages of granitoids from Eastern Sul-riograndense Shield. San Carlos de Bariloche, Argentina. In: VI South American Symposium on Isotope Geology, Annals.

Leite, J.A.D., Hartmann, L.A., McNaughton, N.J., Chemale Jr., F., 1998. SHRIMP U-Pbzircon geochronology of Neoproterozoic juvenile and crustal-reworked terranes in southernmost Brazil. *International Geological Review*. 40, 688–705.

Lenz, C., Fernandes, L.A.D., McNaughton, N.J., Porcher, C.C., Masquelin, H. 2011. U Pb SHRIMP ages for the Cerro Bori Orthogneisses, Dom Feliciano Belt in Uruguay: Evidences of a 800Ma magmatic and 650Ma metamorphic event. *Precambrian Research*, p. 149-163.

Lima, E.F. de, Porcher, C.A., Wildner, W. 1997. Identificação das Rochas Granulíticas da porção leste do Estado do Rio Grande do Sul, região da Várzea do Capivarita – Brasil. In: Congresso de Geoquímica dos países de Língua Portuguesa, 4., & Semana de Geoquímica, 10., 1997, Braga Portugal, Actas... Braga, p.73-76.

Programa de Pós-Graduação em Geociências

Ludwig, K.R., 2003. Isoplot 3.00: A Geochronological Toolkit for Microsoft Excel_(revised version). In: Special Publication 4. Berkeley Geochronological Center, Berkeley, CA, 70 pp.

Martil, M.M.D. 2007. Relações de Intrusão do Maciço Sienítico Piquiri, RS com Suas Encaixantes. Porto Alegre, 71p. Monografia de conclusão de curso, Curso de Geologia, Instituto de Geociências, Universidade Federal do Rio Grande do Sul.

Martil, M.M.D, 2010. Caracterização Estrutural e Petrológica do Magmatismo Pré-Colisional do Escudo Sul-Rio-Grandense: Os Ortognaisses do Complexo Metamórfico Várzea do Capivarita. Porto Alegre, 50p. Dissertação de Mestrado, Instituto de Geociências, Universidade Federal do Rio Grande do Sul.

Martil, M.M.D., Bitencourt, M.F. and Nardi, L.V.S. 2011. Caracterização estrutural e petrológica do magmatismo pré-colisional do Escudo Sul-rio-grandense: os ortognaisses do Complexo Metamórfico Várzea do Capivarita. Pesquisas em Geociências, 38(2): 181-201.

Nakamura N., 1974. Determination of REE, Ba, Fe, Mg, Na and K in carbonaceous and ordinary chondrites. *Geochimica et Cosmochimica Acta*, 38: 757-775.

Nardi, L.V.S. & Bitencourt, M.F. 2007. Magmatismo Granítico e Evolução Crustal no Sul do Brasil. In: J.C. Frantz; R. Ianuzzi (Org.). *Geologia do Rio Grande do Sul - 50 Anos do IG-UFRGS*. Porto Alegre, 2007.

Nardi, L.V.S. 2011. Granitóides e Séries Magmáticas: Classificação e interpretação. Notas de aula da disciplina GEP 48 - Quantificação de dados físicos e químicos em petrologia ígnea. Programa de Pós-Graduação em Geociências - UFRGS. 15p.

Niessing, M. 2007. Geology and stratigraphic definition of the Butiá Granite: a sillimanite-bearing syntectonic leucogranite from the Sul-rio-grandense Shield. Munique, 104p. Dissertação de Mestrado, Technische Universität München.

Programa de Pós-Graduação em Geociências

Niessing, M.; Bitencourt, M.F.; Kruhl, J.H.; Martil, M.M.D.; Gregory, T.R.; Centeno, A.P.; Fontana, E. & Knijnik, D.B. 2008. Magma emplacement and crystallization during regional stress: an example from the Sul-rio-grandense Shield (Southern Brazil). 86TH ANNUAL MEETING OF THE GERMAN MINERALOGICAL SOCIETY (DMG), 14-17 September 2008, Berlin/Germany, Book of Abstracts (CD-Rom), Symposium "Making and Breaking of Continents", Abstract n. S07P09.

Pearce, J.A., Harris, N.B.W. & Tindle, A.G., 1984. Trace element discrimination diagrams for the tectonic interpretation of granitic rocks. *Journal of Petrology*, 25:956-983.

Philipp, R.P., Bom, F.M., Pimentel, M.M., Junges, S. L., Zvirtes, G. 2016. SHRIMP U-Pb age and high temperature conditions of the collisional metamorphism in the Várzea do Capivarita Complex: Implications for the origin of Pelotas Batholith, Dom Feliciano Belt, Southern Brazil. *Journal of South American Earth Sciences*, 66: 196-207.

Pluigin, B.A.V.D. & Marshak, S. (2004). *Earth Structure: An Introduction to Structural Geology and Tectonics*. International Student Edition. New York/ London, W.W. Norton & Company, Inc., 444-474p.

Porcher, C.A. (Coord.) 2000. Programa Levantamentos Geológicos Básicos do Brasil, Folha Cachoeira SH.22-Y-A. Estado do Rio Grande do Sul. Escala 1:250.000. Brasília, CPRM, 131p.

Rollinson, H. R. & Tarney, J. 2005 Adakites – the key to understanding LILE depletion in granulites. *Lithos*, 79: 61– 81.

Silva, A.O.M.S., Porcher, C.C., Fernandes, L.A.D., Droop, G.T.R. 2002. Termobarometria da Suíte Metamórfica Várzea do Capivarita (RS): Embasamento do Cinturão Dom Feliciano. *Revista Brasileira de Geociências*, 32(4):419-432.

Programa de Pós-Graduação em Geociências

Siviero, R. S., Bruguier, O., Koester, E., Fernandes, L.A.D. 2009. Crustal evolution in the Lavras do Sul region, Southern Brazil and the amalgamation of West Gondwana. Goldschmidt Conference Abstracts. A1232.

Soliani Jr., E., Koester, E., Fernandes, L.A.D. 2000. A Geologia Isotópica do Escudo Sul-rio-grandense. Parte II: os dados isotópicos e interpretações petrogenéticas. In: Michael Holz & Luis Fernando De Ros. (Eds.). Geologia do Rio Grande do Sul. Porto Alegre: Editora da UFRGS/Centro de Investigação do Gondwana - Instituto de Geociências, p. 175-230.

UFRGS 2008. Mapeamento Geológico 1:25 000 de parte das folhas Passo das Canas SH22-Y-A-III-4 (MI2984/4) e Capané SH 22-Y-A-III-3 (MI2984/3), RS. Porto Alegre. 1 vol., 2 mapas. Curso de Geologia. Instituto de Geociências, Universidade Federal do Rio Grande do Sul.

UFRGS 2009. Mapeamento Geológico 1:25 000 de parte da Folha Passo das Canas SH22-Y-A-III-4 (MI2984/4), RS. Porto Alegre. 1 vol., 2 mapas. Curso de Geologia. Instituto de Geociências, Universidade Federal do Rio Grande do Sul.

- Capítulo II -

APRESENTAÇÃO DOS ARTIGOS CIENTÍFICOS

1. Artigo 1

Structural Evolution of the Várzea do Capivarita Complex: a record of Cryogenian (ca. 650Ma) transpressive tectonics in southernmost Brazil

Autores:

Mariana Maturano Dias Martil, Maria de Fátima Bitencourt, Lauro Valentim Stoll Nardi, Renata da Silva Schmitt, Roberto F. Weinberg

O foco deste trabalho foi estabelecer as principais feições geológicas, estratigráficas e estruturais do Complexo Várzea do Capivarita. A pesquisa realizada envolveu principalmente trabalho de campo, mas incluiu também estudos petrográficos e microestruturais, além do processamento dos dados geológicos e estruturais coletados. Os resultados obtidos serviram de base para a construção e desenvolvimento dos temas investigados nos demais artigos inclusos nesta tese.

O CVC forma duas ocorrências maiores a oeste da Zona de Cisalhamento Dorsal de Canguçu, onde são predominantes um conjunto de intrusões resultantes do magmatismo Neoproterozóico. Uma sequência de rochas gabro-anortosítica de ambiente intraplaca registra a mesma história estrutural do CVC, caracterizada pela formação de dobras de mega-escala que afetam o bandamento principal.

O CVC é principalmente composto por paragnaisse de composição pelítica além de rochas calciosilicáticas, lentes de mármore e quartizitos. Os ortognaisse tem composição tonalítica a granítica. Volumes subordinados de sienitos sintectonicos também fazem parte do complexo (Sienito Arroio das Palmas – SAP). O posicionamento do SAP teria sido concomitante ao episódio tectono-metamórfico que afeta os gnaisses do Complexo. Os diferentes gnaisses que compõem o CVC se alternam predominantemente em fatias tabulares ou lenticulares de dimensão métrica, mas podem atingir até dezenas de metro de espessura. Entretanto, a intercalação em camadas milimétricas é também observada. Essa sucessão

Programa de Pós-Graduação em Geociências

litológica se dá ao longo dos planos do bandamento gnáissico do CVC, onde estão alinhados minerais de alta temperatura, tais como hiperstênio e cordierita-espinélio. Tais evidências sugerem contemporaneidade entre o metamorfismo de fácies granulito e evento tectônico responsável pelo empilhamento destas rochas.

A fim de estabelecer a evolução estrutural e tectônica do CVC, uma área de estruturas bem preservadas foi escolhida para detalhamento. Relações estratigráficas e geológicas similares são encontradas em todo o Complexo e dessa forma, a história estrutural registrada na área de detalhe é tida como representativa para o Complexo como um todo.

Duas fases de deformação dúctil, formadas progressivamente e em condições de fácies granulito, foram reconhecidas para o Complexo: D₁ e D₂. O levantamento estrutural realizado indica que a deformação durante D₁ foi originada a partir de movimentos de empurrão/cavalgamento. O conjunto de evidências inclui: (i) a posição original subhorizontal de S₁; (ii) a lineação de estiramento com caiimento para leste e portanto alto ângulo de rake em relação a direção NNW do bandamento; (ii) os indicadores cinemáticos que demonstram a existência de cisalhamento durante D₁, com sentido de movimento de topo para oeste; (iii) a existência de dobras (F₁) assinalando um componente de encurtamento durante D₁; (iv) a natureza sem raiz destas mesmas dobras indicando transporte, bem como cisalhamento, ao longo dos planos de S₁; (v) a intercalação tectônica em diferentes escalas de tipos de composição e idade distintas, originando uma pilha de thrust.

As estruturas componentes da deformação D₂ apresentam desenvolvimento heterogêneo controlado principalmente pela intensidade da deformação e subordinamente pela variação litológica. O conjunto de estruturas da fase D₂ oblitera em grau variável as estruturas relacionadas a D₁. A estrutura principal desta fase é uma trama planar NNW de mergulho alto – S₂ que contem uma lineação de estiramento – L_{x2} que é originalmente subhorizontal. S₂ gradaciona desde uma clivagem plano-axial bem espaçada (entorno de 50 cm) em áreas de baixa deformação (*low strain zones*), passando para uma clivagem de transposição que, em zonas de alta taxa de deformação (*high strain zones*), forma uma foliação penetrativa de alto ângulo de mergulho. Evidência de cisalhamento ao longo dos planos de S₂ é fornecida pela rotação horária e gradual do bandamento S₁ em planos de mergulho moderado a alto, porfiroclastos rotados, *drag folds* do

Programa de Pós-Graduação em Geociências

bandamento prévio, bem como a geometria curva de L_{X1} próximo aos planos de S_2 . O cisalhamento progressivo ao longo de S_2 leva a geração de uma zona de cisalhamento NNW trancorrente à levemente oblíqua, a feição mais óbvia da deformação D_2 . A associação de uma fase dobramento (F_2) seguido de cisalhamento progressivo ao longo dos planos axiais destas mesmas dobras indica a coexistência de um componente de encurtamento e de um componente de cisalhamento simples para D_2 , o que pode sugerir um caráter transpressivo para esta deformação.

A evolução transicional entre a cinemática de cavalgamento- D_1 e a transcorrência- D_2 indica que ambas as fases são representativas de um único evento tectono-metamórfico que se partitiona em zonas de cisalhamento de baixo e alto ângulo, sugerindo um caráter oblíquo para este episódio. O arcabouço estrutural formado em condições de fácies granulito que compõe o CVC estabelece o Complexo como o registro de uma tectônica de espessamento crustal. O conjunto dados estruturais associados aos dados petro- e geocronológicos poderia sugerir que o Complexo originou-se em um ambiente colisional oblíquo.

Programa de Pós-Graduação em Geociências

[Início](#)
[Mail](#)
[Notícias](#)
[Esportes](#)
[Finanças](#)
[Celebridades](#)
[Vida e Estilo](#)
[Cinema](#)
[Respostas](#)
[Flickr](#)
[Mais](#) ▾

[Todas](#)
[Buscar](#)
[Buscar no Mail](#)
[Buscar na Web](#)
 [Início](#)
Mariana


Escrever
Arquivar
Mover
Apagar
Spam
Mais

Submission Confirmation

Journal of Structural Geology <ees.sg.0.3b3eb8.ad99c15e@eesmail.elsevier.com> Hoje em 17:08
Para: marianamdmartil@yahoo.com.br

Full Length Article

Dear Ms. Mariana Maturano Dias Martil,

Your submission entitled "Structural Evolution of the Várzea do Capivari Complex: a record of Cryogenian (ca. 650Ma) transpressive tectonics during oblique collision in southernmost Brazil" has been received by the Journal of Structural Geology.

You may check on the progress of your paper by logging on to the Elsevier Editorial System as an author. The URL is <http://ees.elsevier.com/sg/>.
Your username is: marianamdmartil@yahoo.com.br
If you need to retrieve password details, please go to: http://ees.elsevier.com/SG/automail_query.asp

Your manuscript will be given a reference number once an Editor has been assigned.

Thank you for submitting your work to this journal.

Kind regards,

Elsevier Editorial System
Journal of Structural Geology

[Responder](#)
[Responder a todos](#)
[Encaminhar](#)
[Mais](#)

Clique para Responder, Responder a todos ou Encaminhar:

Structural Evolution of the Várzea do Capivarita Complex: a record of Cryogenian (ca. 650Ma) transpressive tectonics during oblique collision in southernmost Brazil

Martil^{a*}, Mariana Maturano Dias, Bitencourt^b, Maria de Fátima, Schmitt^c, Renata da Silva, Weinberg^d, Roberto Ferrez

a - Programa de Pós-Graduação em Geociências, Instituto de Geociências, Universidade Federal do Rio Grande do Sul, Av. Bento Gonçalves, 9500, Porto Alegre 91500-000, RS, Brazil. marianamdmartil@yahoo.com.br

b - Centro de Estudos em Petrologia e Geoquímica, Instituto de Geociências, Universidade Federal do Rio Grande do Sul, Av. Bento Gonçalves, 9500, Porto Alegre 91500-000 RS, Brazil. fatimab@ufrgs.br

c- Instituto de Geociências, Universidade Federal do Rio de Janeiro, Av. Athos da Silveira Ramos 274, Cidade Universitária, Rio de Janeiro 21941-916, RJ, Brazil. renatagondwana@uol.com.br

d- School of Geosciences, Monash University, Clayton, Victoria 3800, VIC, Australia.
Roberto.Weinberg@monash.edu

*Corresponding author. Present Adress: Programa de Pós-Graduação em Geociências, Instituto de Geociências, Universidade Federal do Rio Grande do Sul, Av. Bento Gonçalves, 9500, Porto Alegre 91500-000, RS, Brazil. E-mail address: marianamdmartil@yahoo.com.br (M.M.D. Martil). Phone number: +55-51-8061-0714

Key-words: deformation partitioning, transpressive tectonics, Cryogenian oblique collision

Abstract

The Várzea do Capivarita Complex (VCC), southern part of the Neoproterozoic Mantiqueira Province, Brazil, comprises ortho- and paragneisses of variable age and composition, and subordinate volumes of syntectonic syenites. Two progressive deformation phases – D₁ and D₂, are identified in this complex, both formed under granulite facies metamorphic conditions (ca. 650 Ma). The gneisses were tectonically interleaved during D₁ along a subhorizontal banding and formed a thrust stack with top-to-the-west shear sense. D₂ is marked by folding and strain concentration along their axial planes which in turn become NNW-trending, subvertical, strike-slip to oblique dextral shear zones. Stretching lineations are progressively rotated from dip towards strike marking the swapping of tectonic axes X and Y that follow strain partitioning into contractional and transcurrent regimes, as expected during transpression. The age of VCC tectono-metamorphic activity is consistent with the one previously determined for a collisional event in this area and the kinematic picture determined here points towards an oblique character of the collision. Such conditions are also consistent with the ones determined for the initial stages of the Southern Brazilian Shear Belt, formed during late Brasiliano Cycle transpressive regime.

1. Introduction

Metamorphic high-grade terranes make up a significant volume of the continental crust exposed in cratons and orogenic belts worldwide. A large proportion of these terranes are related to processes of crustal shortening and thickening at convergent plate margins, and therefore, the investigation of the common structural associations in such terranes is important for elucidating orogenic and continental crust-forming processes.

The study area is part of the southern segment of the Mantiqueira Province (MP), largely composed of Neoproterozoic granitic rocks intrusive in a metamorphic basement of predominant Paleoproterozoic age (Hartmann et al., 1999, Gregory et al. 2015). It was built during the Brasiliano / Pan-African Orogenic Cycle, and its evolution involved diachronic episodes of plate subduction and arc-continent or continent-continent collision (Heilbron et al., 2004). According to several authors (e.g. Fernandes et al., 1992a) the tectonic framework of this province includes a complex system of thrust and fold belts associated with a late

lateral escape tectonics, governed by transcurrent fault systems. Although the events leading to the formation of this province have been the subject of numerous studies over the past decades, specific structural and tectonic studies are rare, and therefore the tectonic episodes in the southern segment are still poorly-constrained.

The Várzea do Capivarita Complex (VCC) presently studied is part of the Neoproterozoic collisional record in southern Brazil, and although several papers mention its connection to transpressive tectonics (e.g. Philipp et al., 2016a, b), no structural arguments are presented. The purpose of this paper is to contribute to the investigation of the Mantiqueira Province southern segment by building detailed description and interpretation of structures related to Neoproterozoic tectonism. Determination of the spatio-temporal relations is achieved by integrating the results with other data obtained for the VCC, including U-Pb zircon geochronological data (Martil et al., submitted a), and other isotope and field data (Martil, 2016, Martil et al., submitted b).

2. Geological Setting: Southern Mantiqueira Province overview

The distribution of major lithotectonic domains in the southern segment of the Mantiqueira Province (MP) shows Archean to Paleoproterozoic rocks in northeast Santa Catarina (SC), in southwestern Rio Grande do Sul (RS) and in a large area of the Uruguayan Shield (Fig. 1). These ancient blocks are partly surrounded by Neoproterozoic associations along the Dom Feliciano Belt which comprises mainly arc-related rocks, supracrustal metamorphic sequences, and the products of voluminous post-collisional magmatism (Fig. 1).

In western RS, Neoproterozoic rock sequences are attributed to one or more juvenile arcs (e.g. Babinski et al., 1996, Leite et al., 1998, Saalmann et al., 2005a, b, Hartmann et al., 2011, Philipp et al., 2016b). Ages of magmatic-arc activity in this area are summarized by Philipp et al. (2016b and references therein) at the intervals of 0.89 – 0.86 Ga and 0.77 – 0.68 Ga.

Neoproterozoic continental magmatic arc activity at ca. 800 Ma is described in the southeastern part of the Uruguayan Shield (Lenz et al., 2011, 2013, Oyhantçabal et al., 2009) as the high grade Cerro Bori Orthogneisses comprised of tectonically interleaved, calc-alkaline, tonalitic and granodioritic gneisses, which are dominant over tholeiitic and ultrapotassic mafic gneisses. In the central and eastern part of the Dom Feliciano Belt, Saalmann et al. (2006, 2011), Golmann et al. (2008) and Martil et al. (2016) report acidic

Programa de Pós-Graduação em Geociências

metavolcanic rocks formed in a Tonian continental arc environment (ca. 790 Ma). Among the basement inliers found on late Neoproterozoic granites of the MP esater portion, tonalitic gneisses are reported by Koester et al. (2016) as related to a ca. 800 Ma magmatic arc.

A narrow strip of supracrustal, amphibolite facies metamorphic rocks (Fig. 1) occurs in the central region of the DFB. It comprises metapelites, quartzites, metavolcano-sedimentary and metavolcanic rocks. Interpretations of this association tectonic setting to date are controversial, and range from passive margin (Jost and Bitencourt, 1980), passive margin and/or intracontinental setting (Hartmann et al., 2004, Saalmannet al., 2006, Gruber et al., 2011) to back-arc basin (Fernandes et al., 1992a,b, Marques et al., 1998, Babinski et al., 1997, Hartmann et al., 1999, Gollmann et al., 2008).

On the eastern portion of the Mantiqueira Province a granitic belt extends from southern Brazil to Uruguay (Fig. 1). According to Bitencourt and Nardi (1993, 2000), this granitic belt developed in a post-collisional setting between 650 and 580 Ma. The igneous activity was probably controlled by the trans-lithospheric structures composing the Southern Brazilian Shear Belt (SBSB - Fig. 1), closely associated to the Brasiliano/Pan-African tectonic events in a transpressive regime. Flat-lying structures are only locally preserved and are often obliterated by the main transcurrent shear zones. The host rocks of these granitic intrusions are often exposed as inliers, most of them representing km-scale roof-pendants, comprising Paleo-, Meso- or Neoproterozoic metamorphic sequences (Fig. 1 and 2). One of them – the Várzea do Capivarita Complex - is the focus of this study.

Programa de Pós-Graduação em Geociências

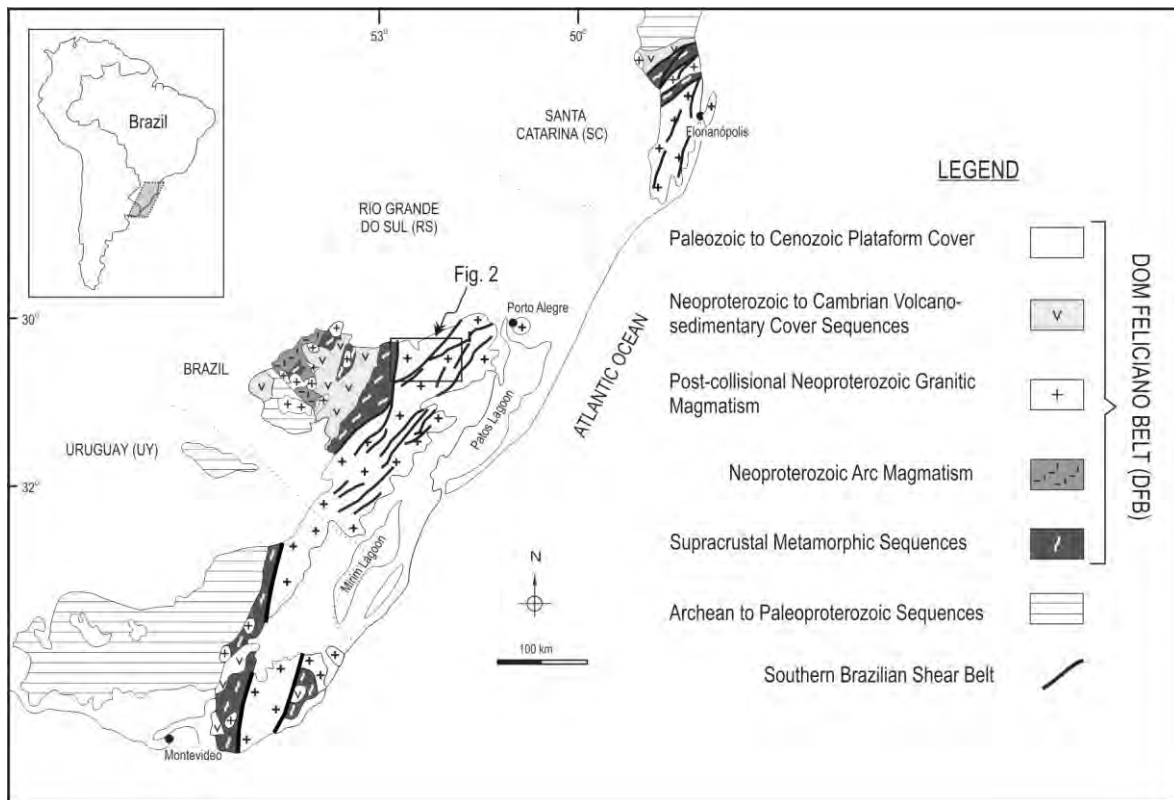


Figure 1 – Main tectonic domains for the Southern Mantiqueira Province, with indication of figure 2 (modified from Nardi and Bitencourt, 2007).

3. The Várzea do Capivarita Complex

The Várzea do Capivarita Complex (VCC) forms two major areas to the west of the Dorsal de Canguçu Transcurrent Shear Zone (DCTSZ – Fig. 2), where Neoproterozoic granitic magmas are dominant. In the northeastern area of VCC rocks, an intraplate gabbro-anorthosite sequence (Chemale Jr. et al., 2011) registers the same structural history as the VCC, featuring large-scale folds of the main banding (Fig. 2). These gabbro-anorthositic rocks yield magmatic U-Pb ages of ca. 1572 and 1530 Ma (zircon and titanite, respectively) and metamorphic U-Pb ages between 651 and 600 Ma (LA-MC-ICP-MS, Chemale Jr. et al., 2011).

The complex stratigraphic relation between the VCC rocks and the gabbro-anorthosites is partly obliterated by successive intrusions of Neoproterozoic plutons and regional folds (Fig. 2). These are nearly upright folds of NW-trending, shallow-plunging general axes. The geological correlation between the VCC rocks and the other supracrustal sequences to the

Programa de Pós-Graduação em Geociências

west (Fig. 2) are still poorly constrained. To the east, syntectonic granites are found along two main transcurrent shear zones that partly envelop an elongate, NE-trending Paleoproterozoic area known as Arroio dos Ratos Complex (Gregory et al. 2015). A large volume of late Neoproterozoic granitic rocks lies to the east, where the VCC rocks are found only as xenoliths of variable size.

The Várzea do Capivarita Complex comprises mainly pelitic gneisses with subordinate calc-silicate rocks and some marble lenses, as well as rare quartzite layers. Orthogneisses are found as concordant tabular or lens like bodies. Subordinate volumes of syntectonic syenites are also part of the complex, with magmatic ages of $642 \pm \text{Ma}$ (U-Pb zircon, LA-MC-ICP-MS – Bitencourt et al., 2011).

The VCC orthogneisses are metaluminous to peraluminous, calc-alkaline rocks whose composition and trace-element patterns are compatible with continental mature arc magmatism (Martil et al., 2011). Sr and Nd isotope data reported by Martil et al. (submitted b) suggest that the orthogneiss protoliths were generated by crustal assimilation processes associated with fractional crystallization. Zircon data from several samples of VCC orthogneisses indicate a magmatic age of ca. 790 Ma (U-Pb in zircon by LA-MC-ICP-MS and SHRIMP - Martil et al., submitted a). The VCC magmatism is correlated with other ca. 800 Ma arc sequences from southern MP, including part of the supracrustal metavolcanic rocks from southernmost Brazil, and high-grade orthogneiss sequences in Uruguay (Fig. 1), as discussed in Martil et al (submitted b). Despite the references to interleaving of the VCC paragneisses with the Arroio dos Ratos Complex orthogneisses (e.g. Philipp et al., 2016b), such relation is not observed, and several age determinations in the VCC orthogneisses resulted in ca. 800 Ma magmatic ages, as opposed to Paleoproterozoic ages of the Arroio dos Ratos Complex reported by Gregory et al. (2015).

The VCC paragneisses were previously interpreted to represent a platform sequence of passive continental margin type (Fragoso Cesar, 1991). Nevertheless, recent provenance studies (Martil, 2016) indicate the volcano-sedimentary character of part of the VCC metapelites and its co-genetic relation with the VCC orthogneisses. The same author also interprets acidic metavolcanic rocks from the supracrustal sequence (Fig. 2) to be the protoliths of the high grade VCC orthogneisses, and therefore relates these high- and medium-grade rocks to the same paleoenvironment. Metamorphic conditions of $720\text{-}820^\circ \text{C}$ and 8 to 9 kbar are referred by Philipp et al. (2016) based on the paragenesis garnet-cordierite-sillimanite-biotite. Although local partial melting evidence is found in all VCC gneisses, as

Programa de Pós-Graduação em Geociências

already mentioned by Silva et al. (2002), they are more frequent in the pelitic gneiss, as irregular, garnet-bearing, leucogranitic pockets (leucosomes). Provenance studies for metapelites of the Várzea do Capivarita Complex (Gruber, 2016) report detritic zircons of Paleoproterozoic (ca. 2.2-2.0 Ga) and Mesoproterozoic (1.4 Ga) ages. This author also refers a maximum depositional age of 714.3 ± 3.9 Ma and metamorphic rim ages of 618 ± 7.3 Ma (U-Pb in zircon by LA-MC-ICP-MS).

Zircon overgrowths of 640 - 650 Ma in the VCC orthogneisses (U-Pb in zircon by LA-MC-ICPMS and SHRIMP - Martil et al., submitted a) are interpreted to register the high-grade metamorphic event. This agrees with those obtained in VCC syntectonic syenites at 642 ± 10 Ma (U-Pb zircon - LA-MC-ICP-MS - Bitencourt et al., 2011). Similar ages are also reported by Chemale Jr. et al. (2011) for the upper amphibolite facies metamorphic event in the nearby metagabbro-anorthosite association (Fig. 2). Younger metamorphic ages obtained in the VCC metapelites and leucogranite veins of ca. 620 Ma reported in previous studies (zircon U-Pb SHRIMP - Philipp et al., 2016a), are interpreted as related to partial melting during thermal relaxation that commonly follows the main collisional stage in orogens (e.g. Jamieson et al., 2004).

In order to establish the structural and tectonic evolution of the VCC, an area of well-preserved structures was selected for detailed work (Fig. 3, indicated in Fig. 2). Similar stratigraphic and geological relations are found in all the VCC areas shown in figure 2, and therefore the structural history in the study area is taken as representative for the entire complex.

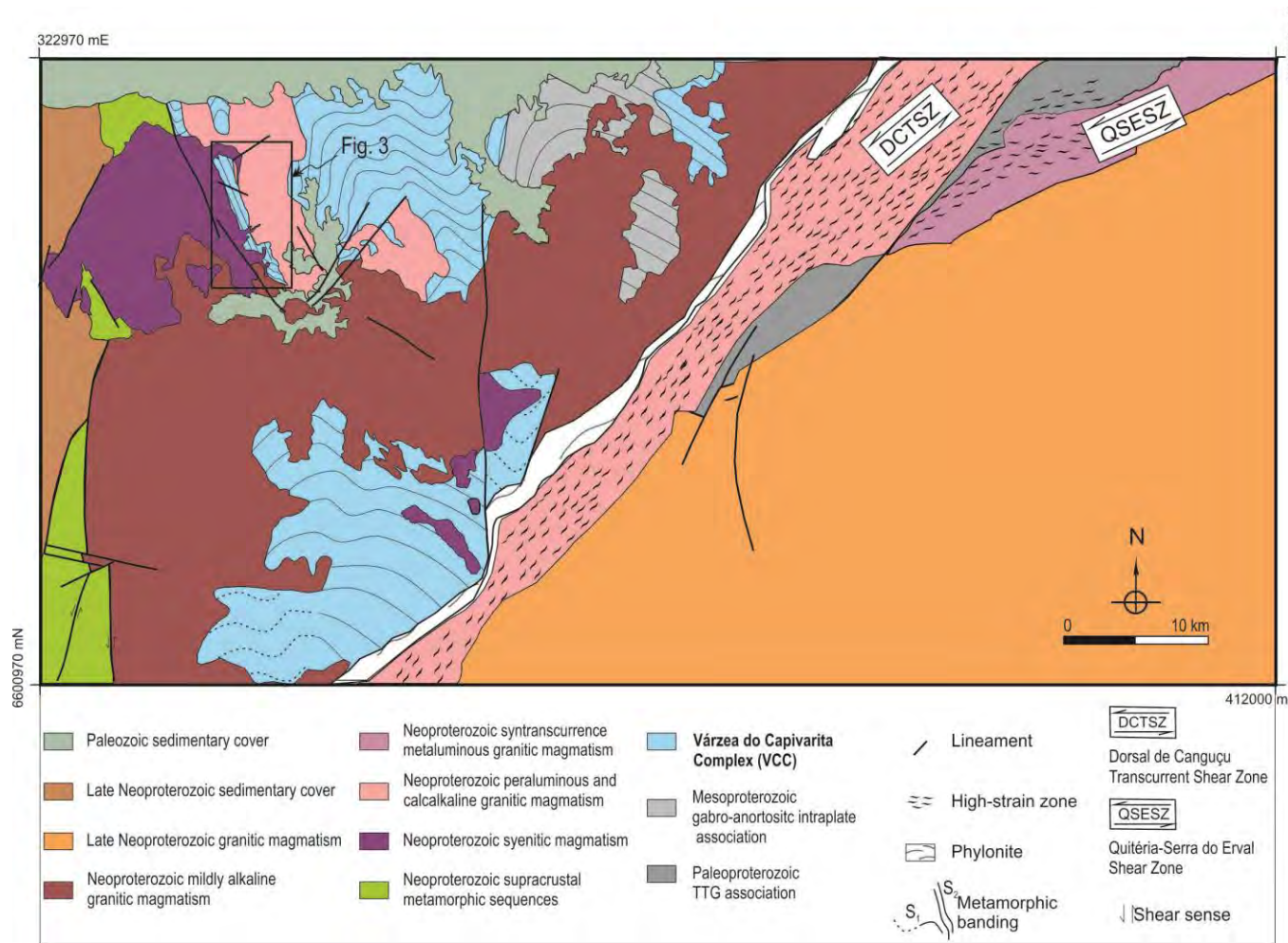


Figure 2 – Regional setting of the Várzea do Capivarita Complex featuring its areal extension and surrounding units. Location of the study area is indicated as Fig. 3.

4. Analytical Procedures

In order to investigate the structural and kinematic history of the Várzea do Capivarita Complex, detailed geological and structural mapping was carried out. Mesoscopic structural data were collected at nearly 100 outcrop stations. The results of this field-based work are synthesized in a revised geological map and in a series of cross-sections (Fig. 3). Geometric analysis consists of description and definition of groups of structures. Kinematic analysis was based on a dataset of measured stretching and mineral lineations and foliation planes. The determination of shear sense was based on the interpretation of asymmetric structures. Illustrations consist of outcrop photographs and photomicrographs, and refer mostly to the XZ sections of the finite strain ellipsoid.

The set of VCC structures was attributed to two ductile deformation phases – D₁ and D₂. The planar and linear structures were grouped according to the deformation phase they belong to and their labeling relies on geometry, kinematics and crosscutting relations, so that foliations S₁ and S₂, and stretching lineation L_{X1} and L_{X2} are assigned respectively to D₁ and D₂ phases. However, within the frame of D₂ phase, the local development of an additional antithetic cleavage is observed, and labeled as S_{2'}.

Four structural domains (SD) have been established in the area (Fig. 3). They are distributed and named from south to north from SD1 to SD4. The division was based on the distribution of mesoscale structural features and according to the relation between preservation/obliteration of D₁-related structures and progression to the D₂ phase.

5. Results

5.1. Várzea do Capivarita Complex internal stratigraphy

In the study area (Fig. 3) all VCC rock types are exposed, with the exception of marbles. Pelitic gneisses are dominant over calcsilicate rocks, syenites, orthogneisses and quartzites, all of them interleaved along the main gneissic banding S₁. The rock types alternate mostly as m-thick layers. However, mm-thick layers are also common, and they may reach as much as tens of meters in thickness.

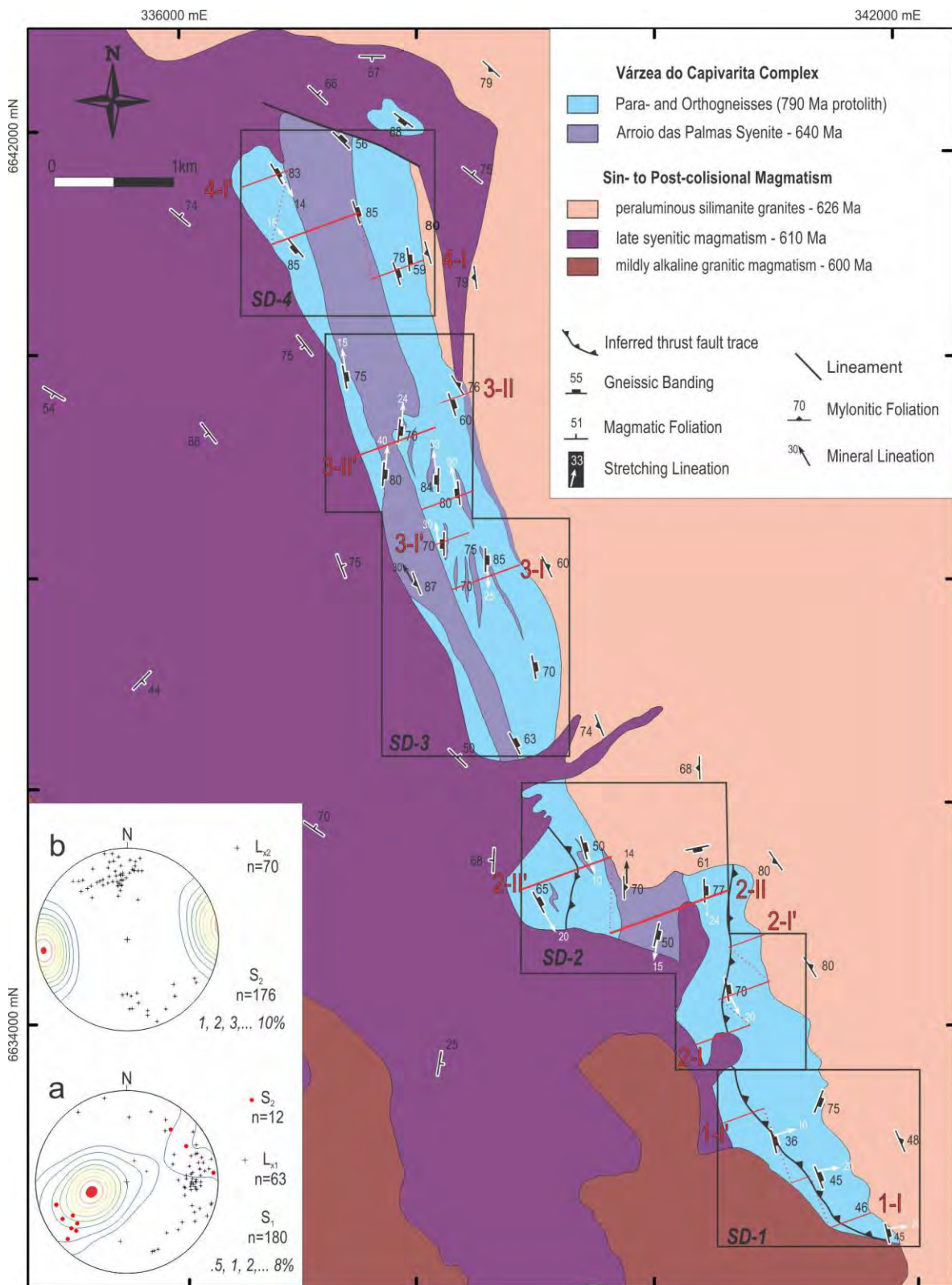


Figure 03 – Várzea do Capivarita Complex study area. Structural domains (SD) and composite cross-sections are indicated and correspond to Figs. 08, 10, 11 and 13. (a-b) Lower hemisphere, equal area stereonet projections. (a) Distribution of poles to banding S_1 and stretching lineation L_{x1} and S_2

Programa de Pós-Graduação em Geociências

foliation in the southern part of the study area. (b) Distribution of poles to S_2 foliation and L_{x2} lineation in the northern part of the study area.

The dominant VCC metapelites are fine to medium-grained gneisses with alternating dark and light layers. The dark layers are usually fine-grained, biotite-rich and contain also cordierite, green spinel (hercynite) (Fig. 4a), sillimanite and garnet. Leucocratic bands contain quartz, plagioclase and K-feldspar. Quartz-feldspar rich metapelite varieties tend to form more competent, continuous and thick bands (1 m – 60 m). In contrast, cordierite-biotite gneisses form thinner layers (< 1 cm to up 30 cm) and commonly form disrupted lenticular fragments in quartz-feldspar layers (Fig. 4a). Quartzites are rare and commonly form tabular bands (0.3 m – 1m thick).

Two main varieties of calcsilicate rocks are recognized: diopside gneisses and hypersthene-Mg-amphibole calcsilicate rocks. The diopside gneisses typically form discontinuous, grayish-green layers and lenses (0.3 m -1.0 m thick). They show an internal mm- to cm-thick metamorphic banding marked by alternating biotite-diopside rich bands with plagioclase and quartz-rich layers. Plagioclase-rich compositions are rare, and form competent, partly rotated bands enveloped by the weaker metapelites (Fig. 4c and 4d).

Magnesium-rich calcsilicate rocks are dark, massive and fine-grained. They are more common as small rounded lenses (5 cm- 10 cm) within metapelites but they also form continuous bands of variable dimensions (mm to tens of meters). They are mostly composed of Ca-plagioclase, biotite, Mg-amphibole and minor amounts of hypersthene crystals.

The orthogneisses form lenses or tabular slices (30 cm to tens of meters), which are interleaved with paragneisses. The VCC ortogneisses are fine- to medium-grained rocks and comprise tonalitic (Fig. 5a) to granitic compositions (Fig. 5b) of very regular geochemical composition (Martil et al., submitted b). The metamorphic banding is marked by alternating mafic and felsic, mm-thick, regular bands and contains a well-developed stretching lineation (L_x - Fig. 5c) marked by quartz-feldspathic lenticular aggregates. In the tonalitic gneisses biotite, hypersthene, and diopside are found in the mafic bands. In rocks of granitic compositions, biotite is the dominant mafic phase, and garnet occurs as fine-grained crystals. Successive generations of granitic veins (Fig. 5a, b) enhance deformational features.

The VCC syenites (Fig. 3) comprise mainly porphyritic rocks emplaced during the main tectono-metamorphic episode that affect the VCC gneisses (Bitencourt et al., 2011; De Toni et al., 2016).

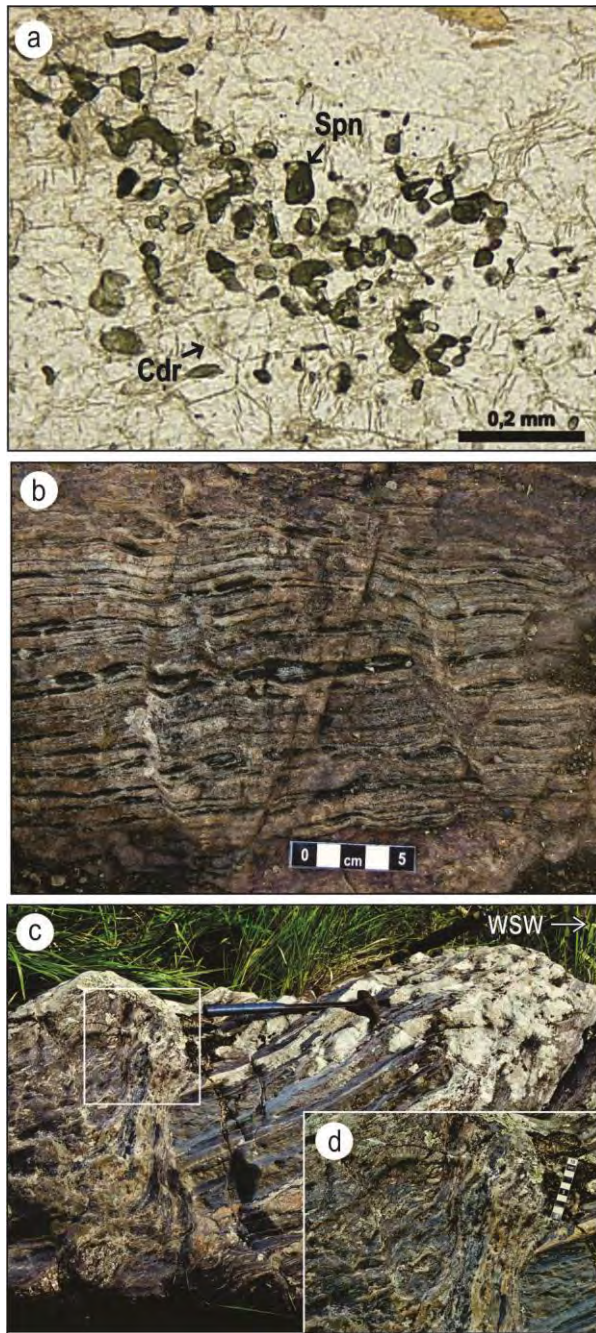


Figure 04 – Main features of the Várzea do Capivarita Complex paragneisses. (a) XZ-plane thin section of metapelitic high-grade paragenesis, with cordierite (Cdr) and spinel (Spn). (b) Alternating bands of different pelitic compositions with boudinaged cordierite-bearing, fine-grained bands. (c) Disrupted and partly rotated plagioclase-rich calc-silicate bands in pelitic gneiss. (d) Detail showing the flow and folding of metapelites around the broken, more competent calc-silicate rock.

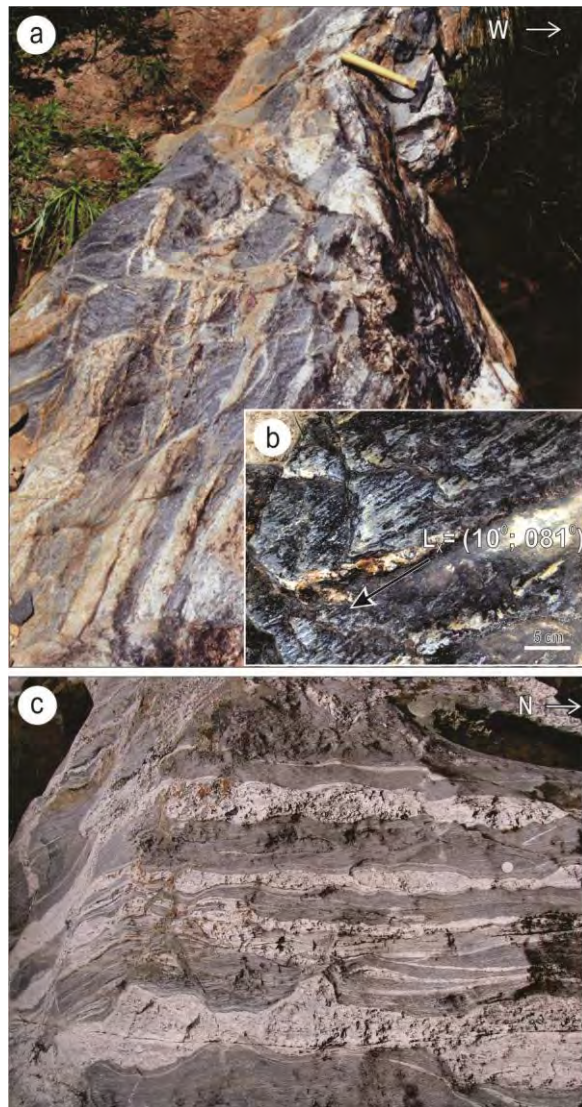


Figure 05 – Main features of the Várzea do Capivarita Complex orthogneisses. (a) Tonalitic gneiss with sub-horizontal metamorphic banding. (b) Pronounced stretching lineation (L_{x1}). (c) Granitic gneiss with concordant, deformed leucogranitic veins showing pinch-and-swell.

5.2. Structural Framework

5.2.1. General features of ductile deformation phase D₁

The main planar structure in the VCC is a pervasive, NNW-trending gneissic banding – S₁ with variable dip angle towards NE and SW forming a complete girdle (Fig. 3a). It is a composite banding, where a variable-scale interleaving takes place between lithological varieties and unrelated compositional bands. The dominant fabric is granoblastic (Fig. 6a). S₁ bears a penetrative stretching lineation L_{X1} (Fig. 5c) defined by elongate quartz and feldspar aggregates found in all VCC rock types. A poorly-developed mineral lineation parallel to L_{X1} is best preserved in paragneisses, given either by sillimanite or diopside, but is also marked in othogneisses by hypersthene (Fig. 6b). The stretching lineation measurements are scattered along a great circle (Fig. 3a) roughly parallel to the average S₂ foliation (Fig. 3b).

Leucocratic veins, either parallel or at high angles to S₁, register the same stretching lineation found in the host gneisses. Parallel veins may form elongate, disrupted lenses within S₁. Cm-scale fold hooks and rootless folds (F₁) of leucogranitic material are locally preserved along S₁ planes, especially in paragneisses (Fig. 6c), and the leucosome nature of this material is suggested by their diffuse, irregular outlines and the local presence of garnet.

The succession of VCC gneisses along S₁ follows three different morphologies: (i) paragneisses form thick packages containing gradational compositional variation between pelitic gneisses and calcsilicate rocks, occasionally containing orthogneiss layers; (ii) ortho- and paragneisses form mm- to m-thick slices within one package where they show abrupt contacts bearing no evidence of depositional progression or gradation; (iii) a combination of the two other types, observed in thicker piles. The successions described in the last two cases are interpreted as due to tectonic interleaving during D₁. Since the mineral assemblages aligned in S₁-L_{X1} fabrics are typical high-temperature minerals, such as hypersthene and cordierite-spinel, D₁ deformation is interpreted as related to high-grade metamorphic conditions.

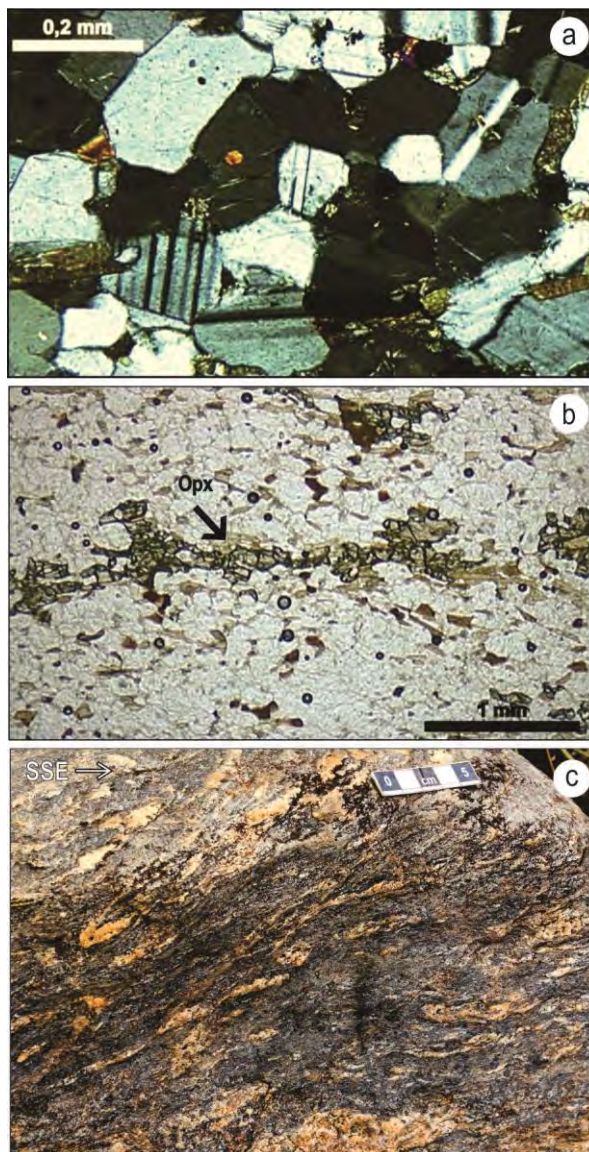


Figure 06 – General features of ductile deformation phase D_1 . (a) Well-developed polygonal texture in tonalitic orthogneiss. (b) XZ-plane thin section from tonalitic gneiss showing orthopyroxene (Opx) grains aligned parallel to L_x . (c) Vertical cut showing fold hooks and rootless folds (F_1) over quartz-feldspathic veins (leucosomes) in pelitic gneiss.

5.2.2. General features of ductile deformation phase D_2

The most conspicuous D_2 structures are F_2 folds and S_2 axial-planar cleavage. F_2 folds are meso to mega-scale features that control the outcrop pattern in the study area, with NNW-trending, steeply-dipping to nearly upright axial planes (Figs. 7a, 7c). The associated planar feature, S_2 , is a heterogeneously-developed, NNW-striking and steeply-dipping fabric which

Programa de Pós-Graduação em Geociências

bears a gently-plunging stretching lineation with subordinate higher plunge values (Fig. 3b). The D₂ structures partly obliterate the former ones, as discussed in detail for each structural domain. In low strain zones, S₂ is an axial-planar cleavage spaced up to 50 cm (Fig. 7a) defined by biotite alignment and commonly filled by leucogranitic veins. It grades into a transposition cleavage spaced up to 10 -15 cm (Fig. 7b), and in high strain zones it forms a steeply-dipping, penetrative foliation. The heterogeneous development of S₂ is controlled mostly by strain intensity, but also by lithological variation, in that biotite-rich gneisses and hypersthene-Mg-amphibole calcsilicate rocks show more pervasive S₂ planes than other VCC gneisses. Nevertheless, once high-strain zones of D₂ are established such differences are no longer noticeable. Accordingly, L_{x2} varies from poorly to very well developed stretching lineation, and in high-strain zones it is no longer distinguished from L_{x1}. It is parallel to the hinge lines of F₂ folds; plunging 05°- 40° to NNW or SSE (Fig. 3b and 7c).

High-grade metamorphic conditions of D₂-related foliation and lineation are marked by the same mineral assemblages reported for D₁ phase, including Opx (Fig. 7d). Progressive shearing along S₂ planes gradually displaces original S₁ planes and concentrates in steeply-dipping, NNW-trending shear zones (Fig. 3).

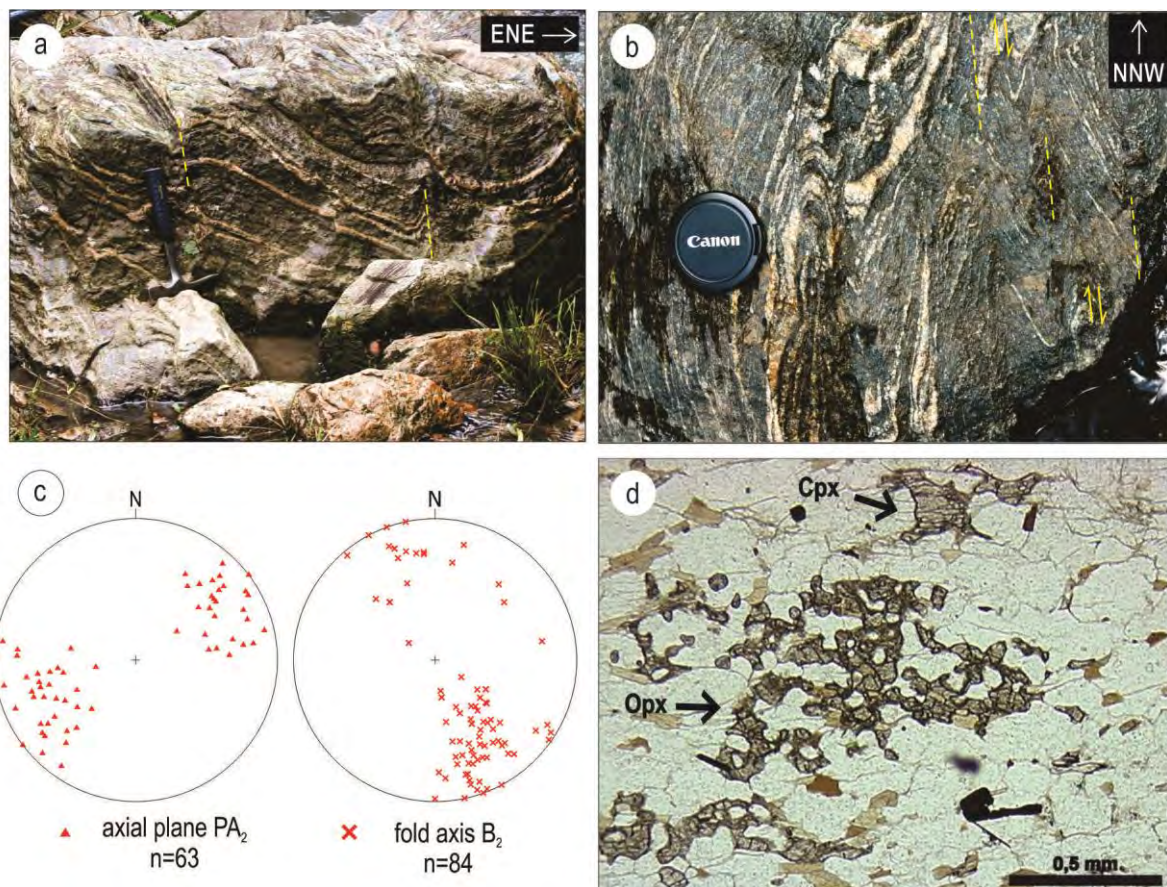


Figure 07 – Structural features of ductile deformation D_2 (a) Asymmetric folds (F_2) in quartz-feldspar metapelites, close to the profile plane, with poorly-developed axial-planar cleavage marked by the yellow dashed lines. (b) Dextral shearing of orthogneisses along well-developed, axial-planar transposition cleavage (S_2) (horizontal-plane view). (c) Lower hemisphere, equal-area stereonet projection showing the distribution of poles to axial planes (PA_2) and fold axis (B_2) of F_2 folds. (d) Tonalitic gneiss showing that the high-grade metamorphic conditions of D_2 -related foliation and lineation are marked by the same polygonal texture and mineral assemblages related to D_1 phase. Arrows indicate orthopyroxene (Opx) and clinopyroxene (Cpx).

5.3 Structural Domains and Cross Sections

Due to the discontinuous nature of the outcrops, cross sections were built from displaced, parallel segments, as shown in figure 3. The investigated sections comprise VCC granulitic gneisses and syntectonic syenites, as well as late granite and syenite, large-scale tabular bodies. Wherever possible, different generations of structures are given specific reference, such as S_1 , S_2 . However, within high-strain zones it is no longer possible to distinguish them, and they are therefore referred by common terms such as “banding” and “ L_x ”.

5.3.1. Structural Domain 1 (SD-1)

The structures related to D₁ are best preserved in the south, in Structural Domain 1 (Figs. 3 and 8a). The strata in this cross-section dip gently to moderately toward east-northeast. Contacts are sharp and the general configuration is that of a W-verging, F₂ mega-antiformal fold developed over the main S₁ banding. The distribution of poles to S₁ in this subarea (Fig. 8b) is compatible with such geometry. The dominance of eastward plunging L_{X1} is in agreement with that observed in map scale (Fig. 3). However, the distribution of L_{X1} along a great circle (Fig. 8a) roughly parallel to the orientation of S₂ suggests that these are mainly shear planes. Extracting the fold effects, the original sub-horizontal position of S₁ is apparent, as well as the high angle of rake of its lineation L_{X1}.

D₂ structures are found in discrete zones along SD-1. L_{X2} is poorly-developed in this subdomain, with shallow plunge toward SSE. Therefore, this subdomain features the best preserved relations between D₁ and D₂ as well as the nearly original geometry of D₁ elements. The sub-horizontal position of S₁ is depicted between S₂ planes, and in such places kinematic indicators, such as feldspar porphyroclasts and asymmetric intrafolial folds indicate top-to-the-W shear sense (Fig. 9a) for D₁.

Outcrop scale F₂ folds are asymmetric, with a steep western flank and a gently-dipping eastern one (Fig. 7a), and sub-horizontal hinge lines. The geometry of F₂ folds may also vary according to rock type, the most competent varieties exhibiting large wavelength (Fig. 7a) and weaker ones having larger amplitude and shorter wavelength (Fig. 9b).

S₂ high-strain zones of 10 cm to 1 m thickness are widely-spaced along this subdomain (Fig. 8a). Evidence of shearing along S₂ is provided by dextral rotation of S₁ onto moderately-dipping planes, as well as by the curved geometry of L_{X1} near S₂ planes. Shearing along the S₂ steeply-dipping planes tends to partly obliterate the short, steeper limbs of F₂ folds, nearly placing two antiforms side by side, as depicted from the inset of figure 8a.

Boudins are common mesoscopic features of SD-1, and comprise: (i) cm-thick, rounded lenses of fine-grained black material (either pelite or calc-silicate) interlayered in the main S₁ banding (Fig. 4a); (ii) elongate and disrupted former layers of greyish green, diopside-rich calc-silicate rocks alternated with pelitic gneiss, both types related to D₁, and (iii) m-scale angular fragments of plagioclase-rich calc-silicate bands rotated by shearing along S₂ (Fig. 4c).

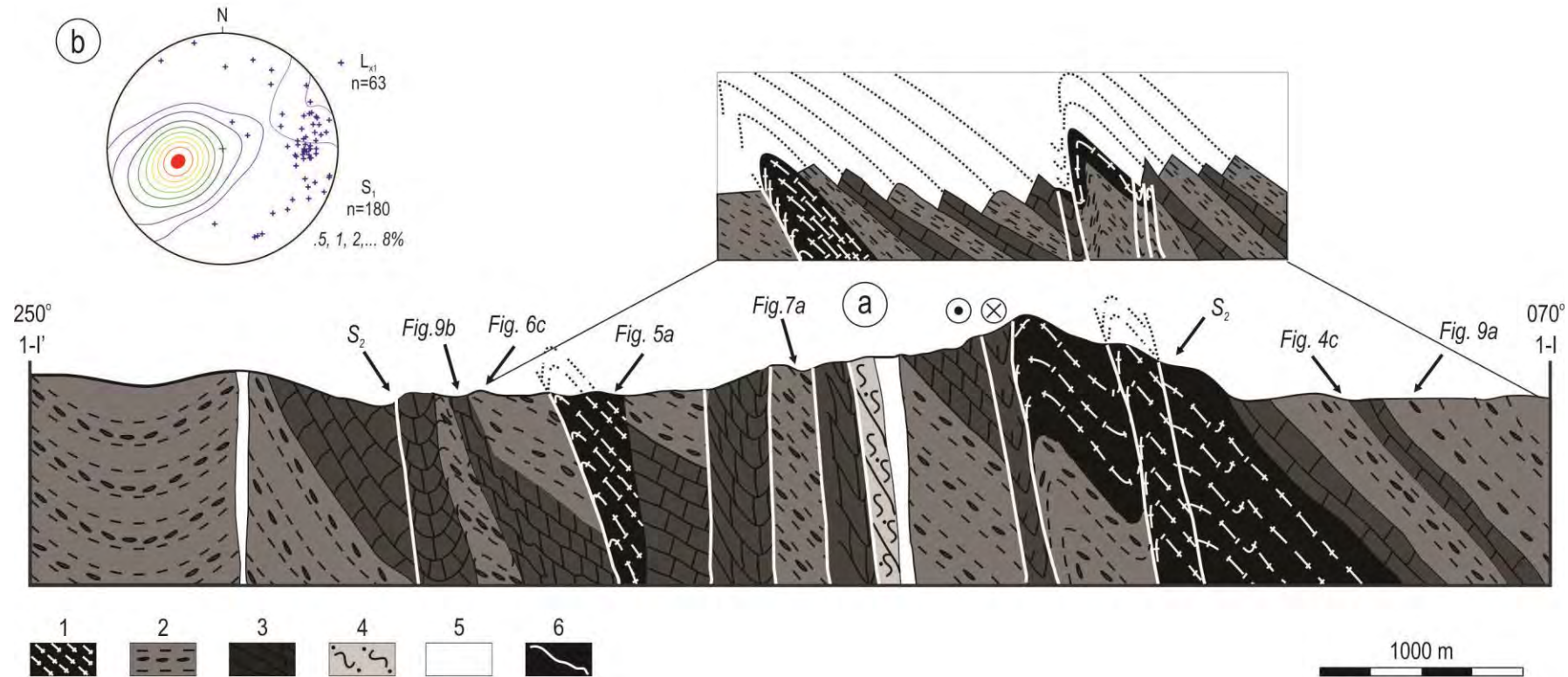


Figure 08 – Schematic cross-section from WSW to ENE. (a) Structural domain 1 – SD-1 with F_2 mega-antiformal fold indicated. (b) (a) Lower hemisphere, equal-area stereonet projection showing the distribution of poles to banding – S_1 indicating NNW-striking planes of low to moderate dip. The stretching lineation (L_{x1}) is scattered along a great circle, which indicates its rotation along planes that are possibly related to S_2 . 1 – Orthogneisses; 2 – Metapelites with boudinaged fragments; 3 – Calc-silicate rocks; 4- Arroio das Palmas Syenite with mylonitic foliation; 5 –Granitic veins; 6 – S_2 foliation. Location of structural features shown in figures 04, 05, 06 and 09 are indicated.

5.3.2. Structural Domain 2 (SD-2)

Pelitic gneisses are dominant in Structural Domain 2. The main banding S_1 is folded and partly transposed onto S_2 along more closely spaced high-strain zones (Fig. 10a). D_2 high-strain zones may be as wide as 6km (Fig. 10b) and S_1 is observed to become increasingly steeper near them. Lx_2 is also better developed in these high-strain zones than observed in SD-1. However, upright folds of S_1 are still a very important feature of SD-2, indicating a considerable amount of E-W shortening. Dextral shearing along S_2 is also significant, and shear zones are established on the axial planes of F_2 folds, and syntectonic syenites are positioned parallel or at low angles to these structures (Fig. 10a, b).

The distribution of poles to S_1 in each cross-section of SD-2 (Fig. 10c and d) illustrates the progression, from south to north, of medium to steep dips of the older planar structure. As a consequence, the contoured S_1 diagram for all measurements from this subdomain (Fig. 10e) produces a void relative to the girdle in figure 8b, compatible with the dominance of steeply-dipping S_1 planes in SD-2. The position of L_{X1} is also more clearly concentrated in subhorizontal clusters, as shown in figures 10c to d.

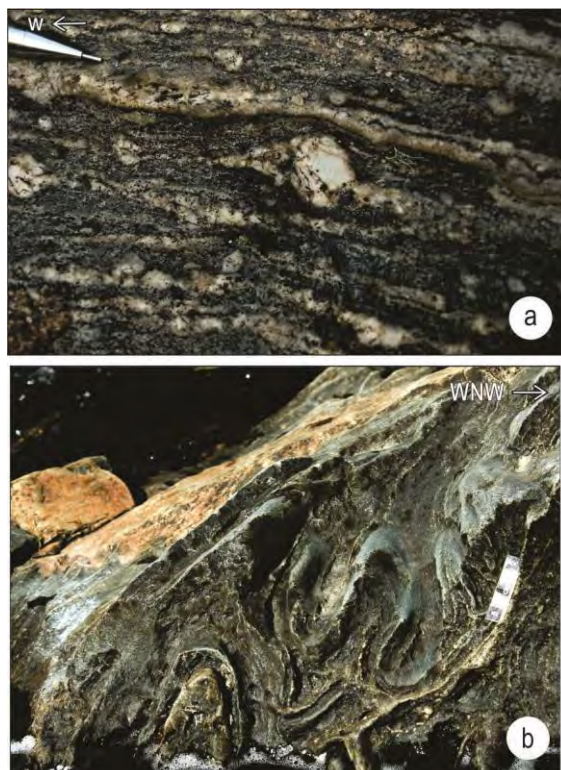


Figure 09 – (c) Asymmetric eldspar porphyroclasts indicating top-to-the-west shear sense - vertical exposure parallel to stretching lineation. (b) Large amplitude F_2 folds in calc-silicate bands – scale is 5 cm long.

Instituto de Geociências
Programa de Pós-Graduação em Geociências

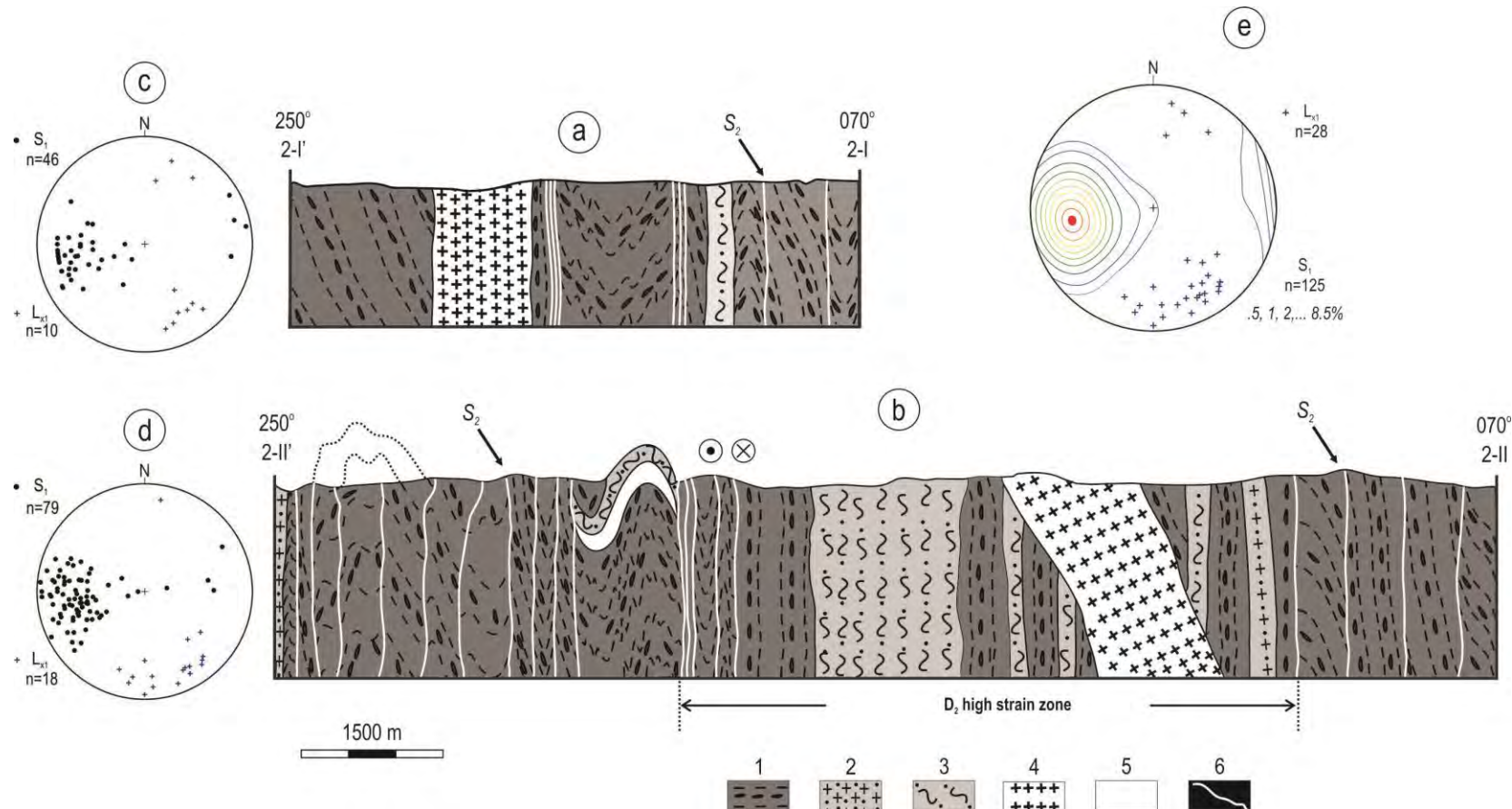


Figure 10 – Schematic cross-sections for structural domain 2 (SD-2). (a) Cross-section 2-I – 2-I'. (b) Cross-section 2-II – 2-II'. (c-e) Lower hemisphere, equal-area stereonet projection of S_1 -gneissic banding and L_{x1} stretching lineation (c) for cross-section 2-I – 2-I', (d) for cross-section 2-II – 2-II', (e) Integrated contoured S_1 diagram for SD-2 showing the dominance of subvertical S_1 planes. L_{x1} concentrates in sub-horizontal clusters trending approximately N-S. 1 –Metapelites with boudinaged fragments; 2 – Arroio das Palmas Syenite with magmatic foliation; 3 – Arroio das Palmas Syenite with mylonitic foliation; 4 – Late syenite – 610 Ma; 5 – Granitic veins; 6 – S_2 foliation.

5.3.3. Structural Domain 3 (SD-3)

Structural Domain 3 (Fig. 11) features the best record of phase D₂ and represents the maximum development of S₂ in the study area. In the southern portion of SD-3, folding and transposition of S₁ is advanced (Section 3I-3I', Fig. 11a), but it is still locally recognizable as original sub-horizontal planes which rotate onto increasingly steeper positions next to D₂ high-strain zones. Towards the north (section 3II-3II' - Fig. 11b) it is no longer possible to distinguish S₁ except for very local, small-scale lenticular microlithons (Fig. 12a, b), and S₂ forms a steeply-dipping penetrative banding. Different rock types alternate as thin bands along S₂, as shown in figure 12c. In both SD-3 cross sections, a very well developed stretching lineation L_{X2} is registered, and remnants of L_{X1} are only locally found.

Progressive dextral shearing along S₂ leads to the formation of a NNW-trending, regional strike-slip shear zone, as shown by steeply-dipping mylonitic foliations bearing a shallow-plunging stretching lineation (Fig. 11c, d, e). Similar features are described in the syntectonic syenites by De Toni et al. (2016).

F₂ fold axes show a systematic variation throughout SD-3, whilst their axial planes keep a fairly constant orientation. The data presented in figure 11f were taken from a small area representing a roof pendant of VCC rocks on the peraluminous granites (Fig. 3). This diagram shows a regular spread of B₂ orientations along a great circle which is approximately the orientation of S₂. Such variation is compatible with shearing along S₂ which may eventually disrupt early-formed F₂-folds. Dextral shear sense of S₂ shear zones is indicated by drag folds on S₁ and rotated porphyroclasts (Fig. 12d).

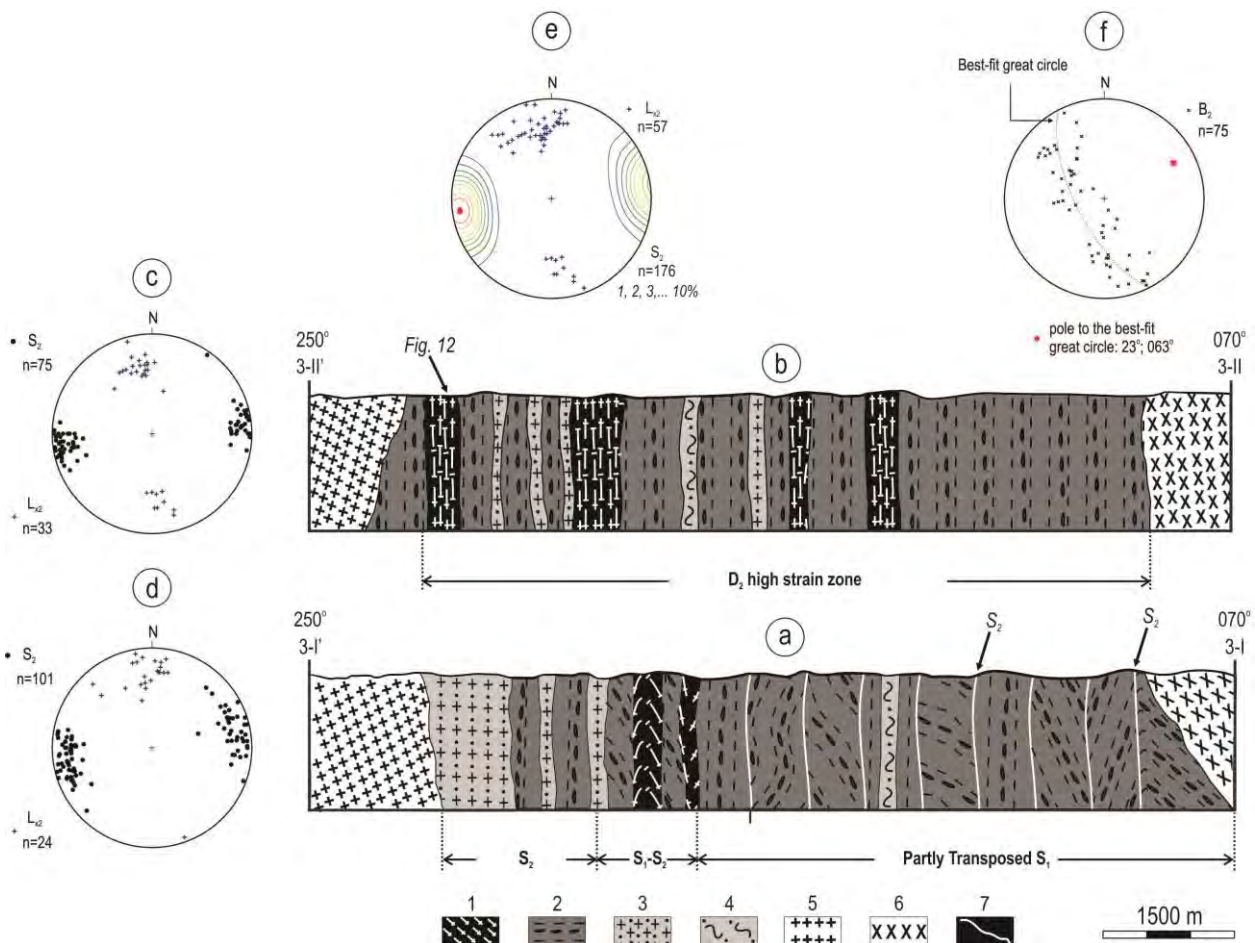


Figure 11 – Schematic cross-sections for structural domain 3 (SD-3). (a) Cross-section 3-I – 3-I'. (b) Cross-section 3-II – 3-II'. (c-f) Lower hemisphere, equal-area stereonet projection of S₂ gneissic banding and L_{x2} stretching lineation: (c) for cross-section 3-I – 3-I' (d) for cross-section 3-II – 3-II'. (e) Integrated contoured S₂ for SD-3 showing the dominance of subvertical NNW- trending planes and a preferred shallow, NNW-SSEplunging stretching lineation. (f) F₂ folds axes showing a regular spread of B₂ orientations along a great circle which is approximately the orientation of S₂. 1 – Orthogneisses; 2 – Metapelites including boudinaged fragments; 3 – Arroio das Palmas Syenite - magmatic foliation; 4 - Arroio das Palmas Syenite - mylonitic foliation; 5 – late syenites - 610 Ma; 6 – peraluminous sillimanite granites - 626 Ma; 7 – S₂ foliation. Location of structural features shown in figure 12 are indicated.

5.3.4. Structural Domain 4 (SD-4)

D₂-related structures are dominant also in Structural Domain 4 (Fig. 13a), where former structures are partly transposed by shearing along S₂. However, cm- to m-thick pods are common in this domain where D₁-or early D₂-structures are well-preserved (Fig. 14a). Within these pods F₂ folds are well-preserved and affect former concordant granite intrusions along the main banding (S₁) of calc-silicate gneisses. Geochronological studies were performed by Martil et al. (submitted a) on a granite sample taken from one of these intrusions (Fig. 14b) and the observed structural relations are used to constrain the results.

The distribution of poles to S₂ (Fig. 13b) is compatible with the rotation of structures to the west of the main shear zone from SD-3. Stretching lineation (L_{X2}) is less developed than in SD-3, but maintains approximately the same orientation.

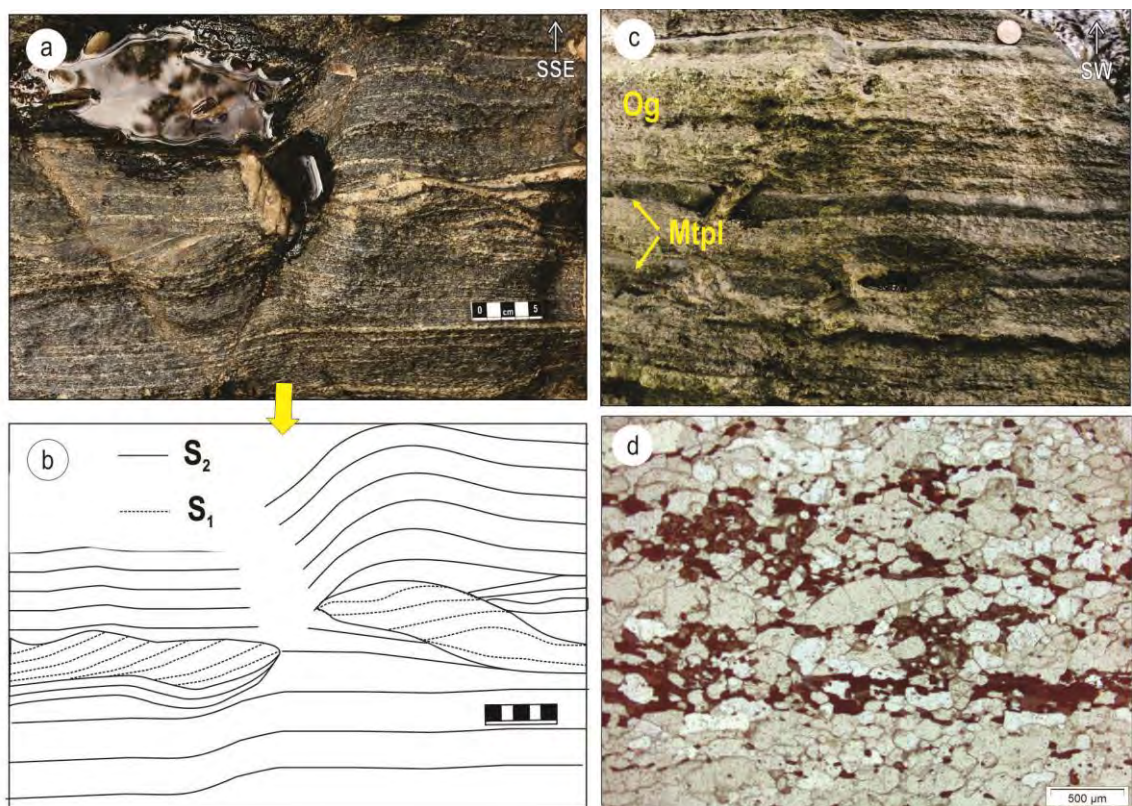


Figure 12 – High-strain features of SD-3. (a-b) S₁ lenticular microlithons. (c) Orthogneiss (Og) and metapelitic (Mtpl) layers thinned due to shortening. (d) Dextral shear sense of S₂ indicated by a rotated porphyroblast.

5.4. Antithetic structures

As part of the frame of D₂ phase the local development of an antithetic cleavage, labeled as S_{2'} is observed. It forms widely-spaced surfaces (Fig. 14c) in SD-1 and SD-2, and acquires a more narrow spacing in SD-4 (Fig. 14d), but is virtually absent from SD-3. The presence of antithetic cleavages suggests that a pure shear component for D₂ is significant in SD-1, SD-2 and SD-4. Its absence from SD-3 may result from the very intense shearing along S₂ taking place in this domain.

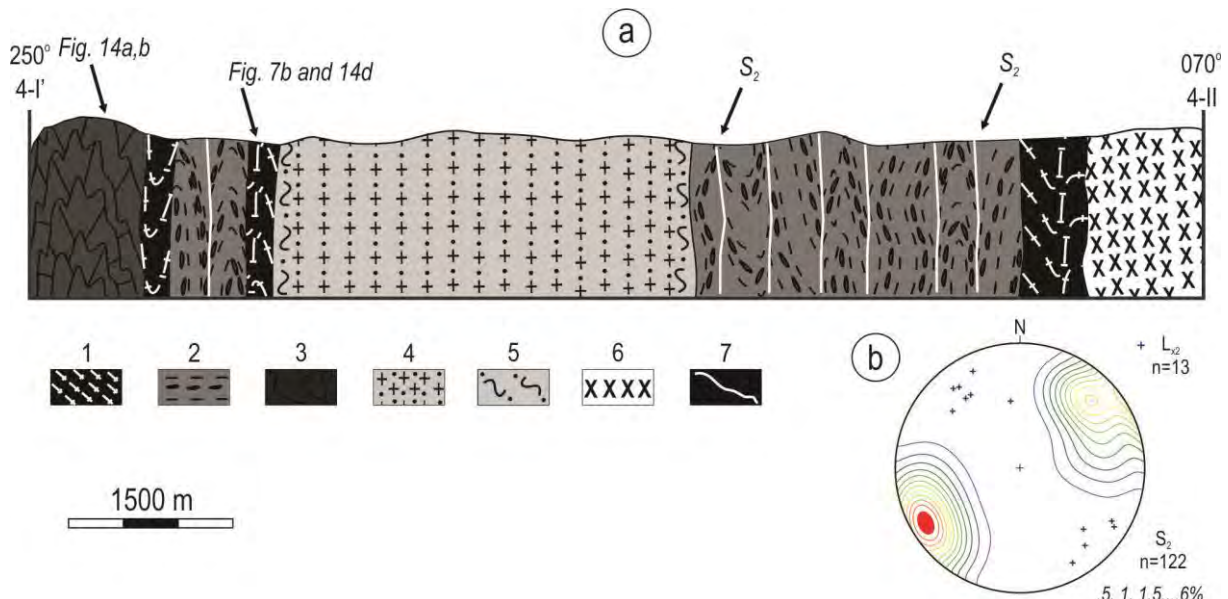


Figure 13 – Schematic cross-sections for structural domain 4 (SD-4). (a) Cross-section 4-I – 4-I'. (b) Lower hemisphere, equal-area contoured diagram for the distribution of poles to S₂ banding and L_{x2} stretching lineation. 1 – Orthogneisses; 2 – Metapelites including boudinaged fragments; 3 – Calc-silicate rocks; 4 – Arroio das Palmas Syenite- igneous foliation; 5 - Arroio das Palmas Syenite - mylonitic foliation; 6 – peraluminous sillimanite granites - 626 Ma; 7 – S₂ foliation. Locations of structural features shown in figure 14 a,b and d are indicated.

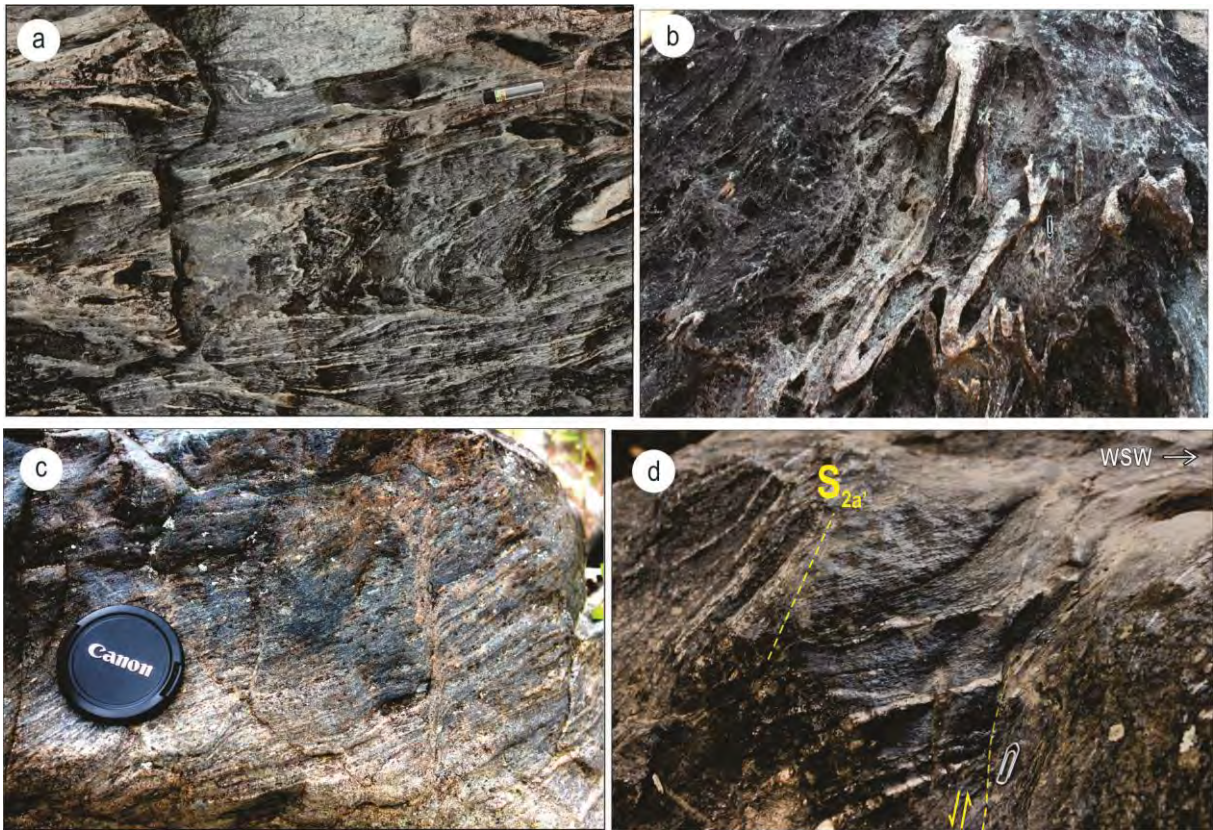


Figure 14 – (a) Metre-thick pod with S_1 remains and early D_2 -structures. (b) Granitic vein affected by F_2 folds and sampled for geochronological studies. (c -d) S_2' antithetic cleavage, widely spaced in (c) and tightly spaced in (d).

6. Discussion

Deformation phase D_1 was responsible for the generation of a sub-horizontal, NNW-trending gneissic banding (S_1) and eastward-plunging stretching lineation (L_{X1}) under high grade metamorphic conditions. Kinematic indicators, together with the position of stretching lineation in the banding surface are compatible with top-to-the-west thrusting during D_1 . Tectonic interleaving of contrasting rock types at variable scales is thought to have taken place during this phase, and is responsible for the wide variation of unrelated compositions observed in all structural domains. The multiple provenance ages reported by Gruber (2016) from VCC pelitic gneisses contrast with the highly similar zircon populations found by Martil (2016) in the VCC orthogneisses and pelitic gneisses (ca. 800 Ma). Such contrasting provenance data is taken as additional evidence for tectonic interleaving. Further evidence to support this interpretation is taken from geochronological data reported by Martil et al.

Programa de Pós-Graduação em Geociências

(submitted a). Crystallization ages of *ca.* 770 -780 Ma are reported for granitic veins which crosscut calc-silicate gneisses and are deformed by F_2 . Such are the same values reported for the VCC tonalitic orthogneisses, and therefore these calc-silicate gneisses must be older.

Despite the expressive regional distribution of S_1 , as shown in figure 2, the data obtained in the study area (Fig. 3) indicate a concentration of strain along the axial planes of F_2 folds which lead to the generation of large-scale shearing along subvertical planes. The progression of flat-lying structures toward a subvertical shear zone may be followed from southeast to northwest, from SD-1 to SD-3. Thus, structural domains 1 and 2 record increasing deformation intensity due to D_2 phase, leading to maximum strain concentration along the NNW-trending transcurrent shear zone of SD-3 (Fig. 11). Structural relations in SD-4 are similar to the ones found in SD-2, which confirms that structural features of SD-3 result from peak deformation and maximum strain concentration during D_2 . The consistency of kinematic picture and shear sense determined for S_2 in different structural domains suggests variable development of a single deformation episode (D_2) rather than multiple episodes. Additionally, it demonstrates the increasing importance of shearing relative to shortening towards SD-3. The distribution of B_2 orientations along S_2 planes (Fig. 11f) may indicate the transport of the early- F_2 folds during the progressive transcurrent shearing of D_2 phase.

The distribution of L_{X1} measurements along a great circle (Figs. 3a, 8b) indicates its rotation within such surface which is in this case compatible with the average orientation of S_2 . Such feature again points to a considerable amount of shearing taking place along S_2 . The stretching lineation L_{X2} is ill-defined in SD-1 and becomes increasingly well developed towards SD-3 (Fig. 10 and 11). L_{X2} plunge values range from 15 to 35° even in the highest strain zones of D_2 , which is compatible with a significant oblique component to the strike-slip deformation. Considering the dominantly down-dip position of L_{X1} which is characteristic of D_1 , the nearly directional position of L_{X2} indicates the swapping of tectonic axes X and Y as deformation progresses, which is expected in transpressive regimes (Sanderson and Marchini, 1984, Tikoff and Tessier, 1994)..

The relative coexistence/ transitional evolution between thrust kinematics - D_1 and strike-slip to oblique shearing - D_2 is shown by structural, petrological and field evidence: (i) as indicated by the mineral assemblages, S_1 and S_2 were generated under the same granulite facies metamorphic conditions, and since no evidence is found of two high grade events in the region, it is expected that both phases are part of the same tectono-metamorphic episode; (ii) the D_1 structures are gradually rotated, deflected and transposed into the D_2 high-strain zones,

as demonstrated in the cross-sections for different subdomains; (iii) the top-to-the-west shear sense of contractional D₁ phase is compatible with the dextral transcurrent movement of D₂.

Recent geochronological results are in agreement with the hypothesis of relative simultaneity between D₁ and D₂, since the same metamorphic age values (ca. 650 Ma) were obtained in VCC samples taken from different structural domains (Martil et al., submitted a). Additional evidence of such timing comes from the syntectonic syenite ages reported by Bitencourt et al. (2011).

7. Conclusions

The structural investigation of the Várzea do Capivarita Complex reveals that deformation phases D₁ and D₂ result from one single tectono-metamorphic event which was partitioned into thrusting and oblique transcurrent under granulite facies conditions. During D₁ the VCC gneisses were tectonically interleaved along a subhorizontal banding, generating a thrust stack with top-to-the-west shear sense. D₂ is marked by strike-slip to slightly oblique, NNW-trending vertical, dextral shear zones.

Such structural history developed under high temperature conditions establish the Várzea do Capivarita Complex as a record of a thick-skinned thrust tectonics at deep to mid-crustal levels. The age of metamorphism (ca. 650 Ma) is consistent with the initial stages of the Southern Brazilian Shear Belt, whose genesis is attributed to a transpressive regime during late Brasiliano Cycle, best recorded to the north of the study area. Similar metamorphic ages (ca. 670-650 Ma) obtained in Tonian (ca. 800 Ma) arc-related sequences from the Uruguayan Shield indicate that it is part of a larger framework. Taken altogether, the different lines of evidence point to the VCC as a possible record of an oblique collision event.

Acknowledgements

This work is part of the Ph.D. thesis of Mariana M. D. Martil. We acknowledge financial support of the 141209/2010-0 (PhD Grant) and the scholarship from Ciência sem Fronteiras Program of National Research Council (CSF-CNPq # 400252/2012-0). This research was also supported by the State Research Foundation (FAPERGS, 10/0045- 6) and by CNPq Universal Program (471266/2010-8) granted to M.F. Bitencourt.

References

- Babinski, M., Chemale Jr., F., Hartmann, L.A., Van Schmus, W.R., Silva, L.C., 1996. Juvenile accretion at 750–700 Ma in southern Brazil. *Geology* 24, 439–442.
- Babinski, M., Chemale Jr., F., Van Schmus, W.R., Hartmann, L.A., Silva, L.C., 1997. U-Pb and Sm-Nd Geochronology of the Neoproterozoic Granitic-Gneissic Dom Feliciano Belt, southern Brazil. *Journal of South American Earth Science* 10, 263–274.
- Bitencourt, M.F., Nardi, L.V.S., 1993. Late to Post-collisional Brasiliano Magmatism in Southernmost Brazil. *Annals of the Brazilian Academy of Science* 65, 3-16.
- Bitencourt, M.F., Nardi, L.V.S., 2000. Tectonic setting and sources of magmatism related to the Southern Brazilian Shear Belt. *Revista Brasileira de Geociências* 30, 184-187.
- Bitencourt, M.F., De Toni, G.B., Florisbal, L.M., Martil, M.M.D., Niessing, M., Gregory, T.R., Nardi, L.V.S., Heaman, L.M., Dufrane, S.A., 2011. Structural geology and U-Pb age of unusual Neoproterozoic syn-collisional syenite-tonalite association from southernmost Brazil. In: Seventh Hutton Symposium on Granites and Related Rocks, 2011, Avila. Abstracts Book, p. 21.
- Chemale Jr., F., Philipp, R.P., Dussin, I.A., Formoso, M.L.L., Kawashita, K., Bertotti, A.L., 2011. Lu-Hf and U-Pb age determinations of Capivarita Anorthosite in the Dom Feliciano Belt, Brazil. *Precambrian Research* 186, 117-126.
- De Toni, G.B., Bitencourt, M.F., Nardi, L.V.S., 2016. Strain partitioning into dry and wet zones and the formation of Ca-rich myrmekite in syntectonic syenites: a case for melt-assisted dissolution-replacement creep under granulite facies conditions. *Journal of Structural Geology*. Accepted for publication.
- Fernandes, L.A.D., Tommasi, A., Porcher, C.C., 1992a. Deformation patterns in the southern Brazilian branch of the Dom Feliciano Belt: a reappraisal. *Journal of South America Earth Science* 5, 77-96.

Fernandes, L.A.D., Tommasi, A., Porcher, C.C., Koester, E., Kraemer, G., Scherer, C.M., Menegat, R., 1992b. Granitoides precoces do Cinturão Dom Feliciano: caracterização geoquímica e discussão estratigráfica. *Pesquisas* 19, 197-218.

Fragoso César, A.R.S., 1991. Tectônica de placas no Ciclo Brasiliense: As orogenias dos Cinturões Dom Feliciano e Ribeira no Rio Grande do Sul. PhD Thesis, Universidade de São Paulo.

Gollmann, K., Marques, J.C., Frantz, J.C., Chemale Jr., F., 2008. Geoquímica e Isotópos de Nd de Rochas Metavulcânicas da Antiforme Capané, Complexo Metamórfico Porongos, RS. *Pesquisas em Geociências* 35, 83-95.

Gregory, T.R., Bitencourt, M.F., Nardi, L.V.S., Florisbal, L.M., Chemale Jr., F., 2015. Geochronological data from TTG-type rock associations of the Arroio dos Ratos Complex and implications for crustal evolution of southernmost Brazil in Paleoproterozoic times. *Journal of South American Earth Sciences* 57, 49–60.

Gruber, L., Porcher, C.C., Lenz, C., Fernandes, L.A.D., 2011. Proveniência de metassedimentos das sequências Arroio Areião, Cerro Cambará e Quartz Milonitos no Complexo Metamórfico Porongos, Santana da Boa Vista, RS. *Pesquisa em Geociências* 38, 205-223.

Gruber, L., 2016. Geologia isotópica e geocronologia do Complexo Metamórfico Porongos e Suíte Metamórfica Várzea do Capivarita, Cinturão Dom Feliciano, Sul do Brasil: Implicações para a evolução do Gondwana em sua margem ocidental. PhD thesis, Universidade Federal do Rio Grande do Sul, Porto Alegre, p. 117.

Hartmman, L.A., Leite, J.A.D., McNaughton, N.J., Santos, J.O.S., 1999. Deepest exposed crust of Brazil - SHRIMP establishes three events. *Geology* 27, 947-950.

Programa de Pós-Graduação em Geociências

Hartmann, L.A., Philipp, R.P., Liu, D., Wan, Y., Wang, Y., Santos, J.O.S., Vasconcellos, M.A.Z., 2004. Paleoproterozoic magmatic provenance of Detrital Zircons, Porongos complex quartzites, southern Brazilian shield. International Geological Review 46, 127–157.

Hartmann, L.A., Philipp, R.P., Santos, J.O.S., McNaughton, N.J., 2011. Time frame of the 753–680 Ma juvenile accretion during the São Gabriel orogeny, Southern Brazilian shield. Gondwana Research 19, 84–99.

Heilbron M., Pedrosa-Soares, A.C., Campos Neto, M., Silva, L.C., Trouw, R.A.J., Janasi, V.C., 2004. A Província Mantiqueira. In: V. Mantesso-Neto, A. Bartorelli, C.D.R. Carneiro, B.B. Brito Neves (Eds.), *O Desvendar de um Continente: A Moderna Geologia da América do Sul e o Legado da Obra de Fernando Flávio Marques de Almeida*, São Paulo, 203-234.

Jamieson, R. A., Beaumont, C., Medvedev, S., Nguyen, M.H., 2004. Crustal channel flows: 2. Numerical models with implications for metamorphism in the Himalayan –Tibetan orogen. Journal of Geophysical Research, 109, B06406, doi:10.1029/2003JB002811.

Jost, H., Bitencourt, M.F., 1980. Estratigrafia e tectônica de uma fração da faixa de Dobramentos de Tijucas no Rio Grande do Sul. Acta Geologica Leopoldensia 4, 27-60.

Koester, E., Porcher, C.C., Pimentel, M.M., Fernandes, L.A.D., Vignol-Lelarge, M.L., Oliveira, L.D., Ramos, R.C., 2016. Further evidence of 777 Ma subduction-related continental arc magmatism in Eastern Dom Feliciano Belt, southern Brazil: The Chácara das Pedras Orthogneiss. Journal of South American Earth Sciences 68, 155-166.

Leite, J.A.D., Hartmann, L.A., McNaughton, N.J., Chemale Jr., F., 1998. SHRIMP U-Pb zircon geochronology of Neoproterozoic juvenile and crustal-reworked terranes in southernmost Brazil. International Geological Review 40, 688–705.

Lenz, C., Fernandes, L.A.D., McNaughton, N.J., Porcher, C.C., Masquelin, H., 2011. U-Pb SHRIMP ages for the Cerro Bori Orthogneisses, Dom Feliciano Belt in Uruguay: Evidences of a 800Ma magmatic and 650 Ma metamorphic event. Precambrian Research 185, 149-163.

Programa de Pós-Graduação em Geociências

Lenz, C., Porcher, C.C., Fernandes, L.A.D., Masquelin, H., Koester, E., Conceição, R.V., 2013. Geochemistry of the Neoproterozoic (800 - 767 Ma) Cerro Bori orthogneisses, Dom Feliciano Belt in Uruguay: tectonic evolution of an ancient continental arc. *Mineralogy and Petrology* 107, 785–806.

Marques, J.C., Jost, H., Roisenberg, A., Frantz, J.C., 1998. Eventos ígneos da Suíte Metamórfica Porongos na área da Antiforme Capané, Cachoeira do Sul. RS. *Revista Brasileira de Geociências* 28, 419-430.

Martil, M.M.D., Bitencourt, M.F., Nardi, L.V.S., 2011. Caracterização Estrutural e Petrológica do Magmatismo Pré-colisional do Escudo Sul-rio-grandense: os ortognaisses do Complexo Metamórfico Várzea do Capivarita. *Pesquisas em Geociências* 38, 181-201.

Martil, M.M.D., 2016. O magmatismo de arco continental pré-colisional (790 Ma) e a reconstituição espaço-temporal do regime transpressivo (650 Ma) no Complexo Várzea do Capivarita, sul da Província Mantiqueira. PhD Thesis, Universidade Federal do Rio Grande do Sul Porto Alegre, p. 120.

Martil, M.M.D., Bitencourt, M.F., Nardi, Armstrong, R., L.V.S., Pimentel, M.M., Schmitt, R.S., Florisbal, L.M., Chemale Jr., F., Cryogenian granulitic orthogneisses of the Várzea do Capivarita Complex thrust pile and implications for the timing of magmatic arc activity and continental collision in the southern Mantiqueira Province, Brazil. *Precambrian Research* (submitted, a).

Martil, M.M.D., Bitencourt, M.F., Nardi, L.V.S., Koester, E., Pimentel, M.M., Pre-collisional, Neoproterozoic (ca. 790 Ma) arc magmatism in southernmost Brazil: tectono-stratigraphy of the Várzea do Capivarita Complex. *Lithos* (submitted, b).

Nardi, L.V.S., Bitencourt, M.F., 2007. Magmatismo Granítico e Evolução Crustal no Sul do Brasil. In: J.C. Frantz & R. Ianuzzi (Eds.). *Geologia do Rio Grande do Sul - 50 Anos do IG-UFRGS*. Porto Alegre, Ed. Comunicação e Identidade. CIGO e IG-UFRGS, p. 125-141.

Programa de Pós-Graduação em Geociências

Oyhantçabal, P., Siegesmund, S., Wemmer, K., Presnyakov, S., Layer, P., 2009. Geochronological constraints on the evolution of the southern Dom Feliciano Belt. *Journal of the Geological Society (Uruguay)*. *Journal of the Geological Society* 166, 1075-1084.

Philipp, R.P., Bom, F.M., Pimentel, M.M., Junges, S.L., Zvirtes, G., 2016a. SHRIMP U-Pb age and high temperature conditions of the collisional metamorphism in the Várzea do Capivarita Complex: Implications for the origin of Pelotas Batholith, Dom Feliciano Belt, Southern Brazil. *Journal of South American Earth Sciences* 66, 196-207.

Philipp, R.P., Pimentel, M.M., Chemale Jr., F., 2016b. Tectonic evolution of the Dom Feliciano Belt in Southern Brazil: Geological relationships and U-Pb geochronology. *Brazilian Journal of Geology* 46(Suppl 1), 83-104.

Saalmann, K., Remus, M.V.D., Hartmann, L.A., 2005a. Geochemistry and crustal evolution of volcano-sedimentary successions and orthogneisses in the São Gabriel Block, southernmost Brazil—relics of Neoproterozoic magmatic arcs. *Gondwana Research* 8:143–161.

Saalmann, K., Hartmann L.A., Remus, M.V.D., Koester, E., Conceição, R.V., 2005b. Sm-Nd isotope geochemistry of metamorphic volcanosedimentary successions in the São Gabriel Block, southernmost Brazil: evidence for the existence of juvenile Neoproterozoic oceanic crust to the east of the Rio de la Plata craton. *Precambrian Research* 136:159–175.

Saalmann, K., Remus, M.V.D., Hartmann, L.A., 2006. Structural evolution and tectonic setting of the Porongos belt, southern Brazil. *Geological Magazine* 143:59–88.

Saalmann, K., Gerdes, A., Lahaye, Y., Hartmann, L.A., Remus, M.V.D., Läufer, A., 2011. Multiple accretion at the eastern margin of the Rio de la Plata craton: the prolonged Brasiliano orogeny in southernmost Brazil. *International Journal of Earth Sciences* 66, 355-378.

Sanderson, D.J., Marchini, W.R.D., 1984. Transpression. *Journal of Structural Geology* 6, 449– 458.

Silva, A.O.M.S., Porcher, C.C., Fernandes, L.A.D., Droop, G.T.R., 2002. Termobarometria da Suíte Metamórfica Várzea do Capivarita (RS): Embasamento do Cinturão Dom Feliciano. *Revista Brasileira de Geociências* 32, 419-432.

Tikoff, B., Tessier, C., 1994. Strain modeling of displacement field partitioning in transpressional orogens. *Journal of Structural Geology* 11, 1575-1588.

Figure Captions

Figure 1 – Main tectonic domains for the Southern Mantiqueira Province, with indication of figure 2 (modified from Nardi and Bitencourt, 2007).

Figure 2 – Regional setting of the Várzea do Capivarita Complex featuring its areal extension and surrounding units. Location of the study area is indicated as Fig. 3.

Figure 03 – Várzea do Capivarita Complex study area. Structural domains (SD) and composite cross-sections are indicated and correspond to Figs. 08, 10, 11 and 13. (a-b) Lower hemisphere, equal area stereonet projections. (a) Distribution of poles to banding S_1 and stretching lineation L_{x1} and S_2 foliation in the southern part of the study area. (b) Distribution of poles to S_2 foliation and L_{x2} lineation in the northern part of the study area.

Figure 04 – Main features of the Várzea do Capivarita Complex paragneisses. (a) XZ-plane thin section of metapelitic high-grade paragenesis, with cordierite (Cdr) and spinel (Spn). (b) Alternating bands of different pelitic compositions with boudinaged cordierite-bearing, fine-grained bands. (c) Disrupted and partly rotated plagioclase-rich calc-silicate bands in pelitic gneiss. (d) Detail showing the flow and folding of metapelites around the broken, more competent calc-silicate rock.

Programa de Pós-Graduação em Geociências

Figure 05 – Main features of the Várzea do Capivarita Complex orthogneisses. (a) Tonalitic gneiss with sub-horizontal metamorphic banding. (b) Pronounced stretching lineation (L_{x1}). (c) Granitic gneiss with concordant, deformed leucogranitic veins showing pinch-and-swell.

Figure 06 – General features of ductile deformation phase D_1 . (a) Well-developed polygonal texture in tonalitic orthogneiss. (b) XZ-plane thin section from tonalitic gneiss showing orthopyroxene (Opx) grains aligned parallel to L_x . (c) Vertical cut showing fold hooks and rootless folds (F_1) over quartz-feldspathic veins (leucosomes) in pelitic gneiss.

Figure 07 – Structural features of ductile deformation D_2 (a) Asymmetric folds (F_2) in quartz-feldspar metapelites, close to the profile plane, with poorly-developed axial-planar cleavage marked by the yellow dashed lines. (b) Dextral shearing of orthogneisses along well-developed, axial-planar transposition cleavage (S_2) (horizontal-plane view). (c) Lower hemisphere, equal-area stereonet projection showing the distribution of poles to axial planes (PA_2) and fold axis (B_2) of F_2 folds. (d) Tonalitic gneiss showing that the high-grade metamorphic conditions of D_2 -related foliation and lineation are marked by the same polygonal texture and mineral assemblages related to D_1 phase. Arrows indicate orthopyroxene (Opx) and clinopyroxene (Cpx).

Figure 08 – Schematic cross-section from WSW to ENE. (a) Structural domain 1 – SD-1 with F_2 mega-antiformal fold indicated. (b) (a) Lower hemisphere, equal-area stereonet projection showing the distribution of poles to banding – S_1 indicating NNW-striking planes of low to moderate dip. The stretching lineation (L_{x1}) is scattered along a great circle, which indicates its rotation along planes that are possibly related to S_2 . 1 – Orthogneisses; 2 – Metapelites with boudinaged fragments; 3 – Calc-silicate rocks; 4- Arroio das Palmas Syenite with mylonitic foliation; 5 –Granitic veins; 6 – S_2 foliation. Location of structural features shown in figures 04, 05, 06 and 09 are indicated.

Figure 09 – (c) Asymmetric eldspar porphyroclasts indicating top-to-the-west shear sense - vertical exposure parallel to stretching lineation. (b) Large amplitude F_2 folds in calc-silicate bands – scale is 5 cm long.

Programa de Pós-Graduação em Geociências

Figure 10 – Schematic cross-sections for structural domain 2 (SD-2). (a) Cross-section 2-I – 2-I'. (b) Cross-section 2-II – 2-II'. (c-e) Lower hemisphere, equal-area stereonet projection of S_1 -gneissic banding and L_{x1} stretching lineation (c) for cross-section 2-I – 2-I', (d) for cross-section 2-II – 2-II', (e) Integrated contoured S_1 diagram for SD-2 showing the dominance of subvertical S_1 planes. L_{x1} concentrates in sub-horizontal clusters trending approximately N-S. 1 – Metapelites with boudinaged fragments; 2 – Arroio das Palmas Syenite with magmatic foliation; 3 – Arroio das Palmas Syenite with mylonitic foliation; 4 – Late syenite – 610 Ma; 5 – Granitic veins; 6 – S_2 foliation.

Figure 11 – Schematic cross-sections for structural domain 3 (SD-3). (a) Cross-section 3-I – 3-I'. (b) Cross-section 3-II – 3-II'. (c-f) Lower hemisphere, equal-area stereonet projection of S_2 gneissic banding and L_{x2} stretching lineation: (c) for cross-section 3-I – 3-I' (d) for cross-section 3-II – 3-II'. (e) Integrated contoured S_2 for SD-3 showing the dominance of subvertical NNW- trending planes and a preferred shallow, NNW-SSEplunging stretching lineation. (f) F_2 folds axes showing a regular spread of B_2 orientations along a great circle which is approximately the orientation of S_2 . 1 – Orthogneisses; 2 – Metapelites including boudinaged fragments; 3 – Arroio das Palmas Syenite - magmatic foliation; 4 - Arroio das Palmas Syenite - mylonitic foliation; 5 – late syenites - 610 Ma; 6 – peraluminous sillimanite granites - 626 Ma; 7 – S_2 foliation. Location of structural features shown in figure 12 are indicated.

Figure 12 – High-strain features of SD-3. (a-b) S_1 lenticular microlithons. (c) Orthogneiss (Og) and metapelitic (Mtpl) layers thinned due to shortening. (d) Dextral shear sense of S_2 indicated by a rotated porphyroblast.

Figure 13 – Schematic cross-sections for structural domain 4 (SD-4). (a) Cross-section 4-I – 4-I'. (b) Lower hemisphere, equal-area contoured diagram for the distribution of poles to S_2 banding and L_{x2} stretching lineation. 1 – Orthogneisses; 2 – Metapelites including boudinaged fragments; 3 – Calc-silicate rocks; 4 – Arroio das Palmas Syenite- igneous foliation; 5 - Arroio das Palmas Syenite - mylonitic foliation; 6 – peraluminous sillimanite granites - 626 Ma; 7 – S_2 foliation. Locations of structural features shown in figure 14 a,b and d are indicated.

Programa de Pós-Graduação em Geociências

Figure 14 – (a) Metre-thick pod with S_1 remains and early D_2 -structures. (b) Granitic vein affected by F_2 folds and sampled for geochronological studies. (c -d) S_2 , antithetic cleavage, widely spaced in (c) and tightly spaced in (d).

2. Artigo 2

Cryogenian granulitic orthogneisses of the Várzea do Capivarita Complex thrust pile and implications of magmatic arc activity and continental collision in the southern Mantiqueira Province, Brazil

Autores: Mariana Maturano Dias Martil, Maria de Fátima Bitencourt, Richard Armstrong, Lauro Valentim Stoll Nardi, Márcio Martins Pimentel, Renata da Silva Schmitt, Luana Moreira Florisbal, Farid Chemale Junior

Submetido a Revista Precambrian Research

A fim de estabelecer as idades magmáticas e metamórficas envolvidas na construção do Complexo Várzea do Capivarita foram selecionadas 5 amostras para análise U-Pb em zircão utilizando os métodos LA-MC-ICP-MS e SHRIMP. Estas amostras também foram selecionadas de forma a representar ambas as fases de deformação D₁ e D₂ e são representantes dos diferentes tipos de ortognaisses além de um veio granítico associado.

Boas partes dos zircões destas litologias apresentavam zonação, forma prismática e teores elevados de Th/U, o que é considerado típico de zircões ígneos. Os dados referentes às idades de magmatismo demonstraram coerência entre si e indicaram idade de cristalização em ca. 780-790 Ma para os protólitos dos ortognaisses. Adicionalmente, a semelhança morfológica entre os cristais de zircão dos diferentes tipos protólitos composicionais é consistente com a hipótese de uma fonte magnética comum para os ortognaisses tectonicamente intercalados.

Em sobrecrecimentos de zircão foram obtidas idades entre 640 - 650 Ma. Estes sobrecrecimentos apresentaram baixas razões Th/U (tipicamente 0.02–0.1) sugerindo gênese metamórfica. Dessa forma as idades obtidas foram interpretadas como o registro do evento de alto grau que afeta os gnaisses do CVC. Essas idades são também consistentes com as referidas por Chemale Jr. et al. (2011) para o metamorfismo de fácies anfibolito que afeta a associação metagabro-anortosítica (Anortosito Capivarita) encontrada na região, bem como com a idade ígnea dos

Programa de Pós-Graduação em Geociências

sienitos sintectônicos inclusos no CVC (Sienitos Arroio das Palmas) obtida por Bitencourt et al. (2011). Adicionalmente, os dados geocronológicos deste trabalho indicaram contemporaneidade para ambos as fases deformacionais D₁ e D₂, oferecendo uma evidencia adicional para o caráter oblíquo do evento colisional.

Uma grande variedade de idades de herança, desde ca. 3.1 até 1.0 Ga foi obtida em núcleos de zircão herdado encontrados nas litologias do CVC, o que sugere a participação de fontes crustais antigas durante a geração dos magmatismo registrado no CVC. Ademais, a predominância de herança Paleoproterozóica é compatível com as associações TTG encontradas regionalmente.

Idades magmáticas e de herança obtidas neste trabalho também apontam similaridade com outras sequências magmáticas neoproterozóicas do Cinturão Dom Feliciano.

As idades de cristalização (ca. 770 Ma) e de herança obtidas no veio granítico são coerentes com aquelas apresentadas para os ortognaisses do CVC, sugerindo que estas litologias são possivelmente correlatas. Visto que este veio é intrusivo em uma rocha calciosilicática é possível que pelo menos parte dos paragnaisses do Complexo sejam mais antigos que este evento magmático. Dessa forma, os dados geocronológicos obtidos neste trabalho em associação com o arcabouço estrutural descrito no artigo anterior indicam que rochas de diferentes composições e idades foram tectonicamente intercaladas em uma pilha de thrust, possivelmente durante um evento colisional oblíquo.

Programa de Pós-Graduação em Geociências

08/08/2016 (21 não lidos) - marianamdmartil - Yahoo Mail

Início Mail Notícias Esportes Finanças Celebridades Vida e Estilo Cinema Respostas Flickr Mais

Todas Buscar Buscar no Mail Buscar na Web Início Mariana

Escrever Resultados da busca Arquivar Mover Apagar Spam Mais

Submission PRECAM_2016_46 received by Precambrian Research

Precambrian Research <EvideSupport@elsevier.com> Para marianamdmartil@yahoo.com.br Mai 21 em 7:41 PM

This message was sent automatically. Please do not reply.
Ref: PRECAM_2016_46
Title: Cryogenian granulitic orthogneisses of the Várzea do Capivari Complex thrust pile and implications for the timing of magmatic arc activity and continental collision in the southern Mantiqueira Province, Brazil
Journal: Precambrian Research
Dear Ms. Martil,
Thank you for submitting your manuscript for consideration for publication in Precambrian Research. Your submission was received in good order.
To track the status of your manuscript, please log into EVIDE at:
http://www.evise.com/evise/faces/pages/navigation/NavController.jsp?JRNL_ACR=PRECAM and locate your submission under the header 'My Submissions with Journal' on your 'My Author Tasks' view.
Thank you for submitting your work to this journal.
Kind regards,
Precambrian Research
Have questions or need assistance?
For further assistance, please visit our [Customer Support](#) site. Here you can search for solutions on a range of topics, find answers to frequently asked questions, and learn more about EVIDE via interactive tutorials. You can also talk 24/5 to our customer support team by phone and 24/7 by live chat and email.
Copyright © 2016 Elsevier B.V. | [Privacy Policy](#)
Elsevier B.V., Radarweg 29, 1043 NX Amsterdam, The Netherlands, Reg. No. 33156677.

Responder Responder a todos Encaminhar Mais

Clique para Responder, Responder a todos ou Encaminhar

Enviar +

Cryogenian granulitic orthogneisses of the Várzea do Capivarita Complex thrust pile and implications for the timing of magmatic arc activity and continental collision in the southern Mantiqueira Province, Brazil

Mariana Maturano Dias Martil^{a1}, Maria de Fátima Bitencourt^{b2}, Richard Armstrong^c, Lauro Valentim Stoll Nardi^{b3}, Márcio Martins Pimentel^d, Renata da Silva Schmitt^e, Luana Moreira Florisbal^f, Farid Chemale Junior^g

a - Programa de Pós-Graduação em Geociências, Instituto de Geociências, Universidade Federal do Rio Grande do Sul, Av. Bento Gonçalves, 9500, Porto Alegre 91500-000, RS, Brazil. marianamdmartil@yahoo.com.br

b - Centro de Estudos em Petrologia e Geoquímica, Instituto de Geociências, Universidade Federal do Rio Grande do Sul, Av. Bento Gonçalves, 9500, Porto Alegre 91500-000 RS, Brazil. ^{b2}fatimab@ufrgs.br/ ^{b3}lauro.nardi@ufrgs.br

c- College of Physical and Mathematical Sciences, Australian National University, Canberra, ACT 0200, Australia. richard.armstrong@anu.edu.au

d- Laboratório de Geocronologia, Instituto de Geociências, Universidade de Brasília, Caixa Postal 04465, Brasília-DF 70910-000, Brazil. marcio@unb.br

e-Instituto de Geociências, Universidade Federal do Rio de Janeiro, Av. Athos da Silveira Ramos 274, Cidade Universitária, Rio de Janeiro 21941-916, RJ, Brazil. renatagondwana@uol.com.br

f- Centro de Filosofia e Ciências Humanas, Departamento de Geociências, Universidade Federal de Santa Catarina, Campus Universitário Reitor João David Ferreira Lima, Trindade, Florianópolis 88.040-900 SC, Brazil. luana.florisbal@ufsc.br

g - Universidade do Vale do Rio dos Sinos, Centro de Ciências Exatas e Tecnológicas, Área de Conhecimento e Aplicação de Geociências. Avenida Unisinos, São João Batista 93022000 - São Leopoldo, RS - Brazil. faridchemale@gmail.com

¹Corresponding author. Present Adress: Programa de Pós-Graduação em Geociências, Instituto de Geociências, Universidade Federal do Rio Grande do Sul, Av. Bento Gonçalves, 9500, Porto Alegre 91500-000, RS, Brazil. E-mail address: marianamdmartil@yahoo.com.br (M.M.D. Martil).

Abstract

This paper presents the first LA-MC-ICP-MS and SHRIMP U-Pb data for continental arc orthogneisses of the Várzea do Capivarita Complex (VCC), exposed in the southern part of the Neoproterozoic Mantiqueira Province, Brazil. The complex comprises ortho- and paragneisses of variable age and composition that were tectonically interleaved during thrusting under granulite facies metamorphism. The VCC deformation is partitioned into thrusting (D_1) and steeply-dipping shear zones (D_2), suggestive of transpressive tectonics with an oblique component. Four tonalitic to granitic orthogneisses and one associated granitic vein, were selected in order to establish the chronology of magmatic and metamorphic events that have led to the VCC construction. These samples are also representative of both D_1 and D_2 kinematics. Igneous crystallization ages obtained in the typical oscillatory magmatic domains in zircons from orthogneisses and from the granitic vein vary between 770 and 790 Ma. Zircon overgrowths of the VCC rocks have ages mostly in the 650 – 640 Ma range, with generally low Th/U ratios (typically 0.02–0.1) suggesting that they are metamorphic, and are therefore interpreted to record the timing of high-grade metamorphism and associated partial melting. Geochronological data presented here also indicates that both kinematic regimes are contemporaneous, offering, therefore, further evidence for the oblique character of the collisional event. Zircon cores inheritance ages have a broad range varying between ca.3.1 and 1.0 Ga. This suggests crustal recycling or the participation of different crustal sources and is consistent with previous petrological data that indicate a mature-arc setting for the magmatism. Furthermore, the predominance of Paleoproterozoic inheritance is compatible with the TTG associations recognized regionally. U-Pb zircon ages reported here reveal a long evolutionary history for the Complex. The orthogneisses were part of a continental magmatic arc at ca. 780 Ma, and their correlation with other Neoproterozoic arc sequences in the southern portion of the Mantiqueira Province is suggested. The Cryogenian (ca. 780 Ma) continental arc rocks were tectonically interleaved with different composition and origin sequences during a Late Cryogenian (ca. 650 Ma) high-grade event. The Várzea do Capivarita Complex represents, therefore, an important component of the oblique-collisional record in the southern Mantiqueira Province.

Key-words: Granulitic orthogneisses, U-Pb geocronology, Cryogenian continental arc, Brasiliano /Pan-African collision, Várzea do Capivarita Complex, Mantiqueira Province.

1. Introduction

Metamorphic high-grade terrains make up a significant volume of the continental crust exposed in Phanerozoic orogenic belts and Precambrian cratons and mobile belts. Orthogneisses are dominant in such environments, and their study provides important clues to the genesis of the primitive crust. Although these rocks are found in a large variety of tectonic settings, a large proportion of them are related to processes of crustal shortening and thickening at convergent plate margins.

In southern Brazil, high grade associations are rare and poorly investigated. Thus, the more detailed approach used in the present study may help to clarify the processes and tectonic events that have led to the construction of this crustal segment.

The study area is part of the southern segment of the Mantiqueira Province (MP). The MP is largely composed of Neoproterozoic granitic rocks intrusive in a metamorphic basement of predominant Paleoproterozoic age (Hartmann et al., 1999, Soliani Jr. et al., 2000). It was built during the Brasiliano / Pan-African Orogenic Cycle, and its evolution involved diachronic episodes of plate subduction and arc-continent or continent-continent collision (Heilbron et al., 2004). In the southern MP (Fig. 1), this orogen is characterized by arc magmatism between 850 and 700 Ma (*e.g.* Leite et al., 1998, Lenz et al., 2011, Siviero et al., 2009), as well as by a long-lived and voluminous post-collisional magmatism active from 650 to 580 Ma (Bitencourt and Nardi, 2000).

Although the events leading to the formation of this province have been the subject of numerous studies over the past decades, the discrimination of accretionary episodes in the southern Mantiqueira Province is still a matter of dispute. In particular, the nature of the collisional event is poorly-constrained from the structural viewpoint. Ages of collision-related, high-grade metamorphic rocks are reported from ca. 670 Ma, in the Uruguayan Shield (Lenz et al., 2011) to ca. 620 Ma in southernmost Brazil (Philipp et al., 2016).

This paper focuses on LA-MC-ICP-MS and U-Pb SHRIMP zircon dating of high grade orthogneisses which comprise the southern MP. The main goal is to unravel the chronology of magmatic and metamorphic events and thus contribute to understand the geodynamic evolution of this crustal segment in South America.

2. Geological setting

In addition to the large Neoproterozoic granite batholiths, the southern part of the comprises Archean to Paleoproterozoic rocks in northeast Santa Catarina (SC), southwestern Rio Grande do Sul (RS) and in a large area of the Uruguayan Shield (Fig. 1).

In RS, the oldest rock association is a granulite facies complex comprising a bimodal tholeiitic suite, with subordinate metapyroxenites, metapelites and BIF's (Hartmann, 1998) crystallized and metamorphosed respectively at 2489 ± 6 and 2006 ± 3 Ma (zircon U-Pb SHRIMP - Hartmann et al., 2008). Two other Paleoproterozoic orthogneiss associations of typical continental magmatic-arc signature are recognized, both not very expressive in volume. They are comparable to TTG associations. The Encantadas Complex (EC –Philipp et al., 2008) is exposed as a window within supracrustal metamorphic rocks (Fig. 1), whilst the Arroio dos Ratos Complex (ARC – as defined by Gregory et al., 2011) forms septa and roof pendants on granitoids associated with the Southern Brazilian Shear Belt (Fig. 1 and 2). SHRIMP U-Pb zircon data from the EC indicate crystallization age of $2,234 \pm 28$ Ma and metamorphism between 2000 – 2100Ma (Saalmann et al., 2011). In the ARC three metaigneous associations with ages between 2150 ± 28 and 2077 ± 13 Ma (zircon U-Pb LA-MC-ICP-MS data) are recognized by Gregory et al. (2015).

An extensional, Mesoproterozoic, intraplate gabbro-anorthosite association is also described in the southern MP (Fig. 2). U–Pb ages of magmatic and metamorphic zircons are 1573 ± 21 Ma and 606 ± 6 Ma, respectively, whereas titanite yielded a crystallization age of 1530 ± 33 Ma and metamorphic ages of 651 ± 9 Ma and 601 ± 5 Ma (LA-MC-ICP-MS, Chemale Jr. et al., 2011).

Neoproterozoic associations in southern MP occur along the Dom Feliciano Belt (DFB) comprising mainly arc-related rocks, a supracrustal metamorphic sequence, and the products of voluminous post collisional magmatism (Fig.1).

In western RS, Neoproterozoic rock sequences represent a juvenile arc (e.g. Babinski et al., 1996, Machado et al., 1990, Saalmann et al., 2005a,b), which later evolved to magmatism in a post-collisional environment (Garavaglia et al., 2006, Nardi and Bitencourt, 2007). Ages of magmatic-arc activity in this area vary between 750 and 700 Ma (e.g. Babinski et al., 1996, Machado et al., 1990). However, sparse data from this region suggest the existence of a continental crust at ca. 908 Ma and an older continental magmatic arc unit at ca. 848-828 Ma (Siviero et al., 2009).

Programa de Pós-Graduação em Geociências

Neoproterozoic continental arc magmatism at ca. 800 Ma is described in the southeastern part of the Uruguayan Shield (Lenz et al. 2011, 2013) in the high grade Cerro Bori Orthogneisses which comprise tectonically interleaved, calc-alkaline tonalitic and granodioritic gneisses which are dominant over tholeiitic and ultrapotassic mafic gneisses. In the central part of the DFB Saalmann et al. (2006, 2011), Golmann et al. (2008) and Martil et al. (submit.) report acidic metavolcanic rocks formed in a continental arc environment. Neoproterozoicarc-related rocks are interpreted as roof pendants on the DFB granitoids to the east (Koester et al., 2012, Silva et al., 1999).

A narrow strip of supracrustal, amphibolite facies metamorphic rocks (Fig. 1) is exposed in the central region of the DFB, comprising metapelites, quartzites, metavolcano-sedimentary and metavolcanic rocks. Its tectonic setting of formation is still controversial, and models range from passive margin deposits (Jost and Bitencourt, 1980), passive margin and/or intracontinental setting (Gruber et al., 2011, Hartmann et al., 2004, Saalmann et al., 2006) to back-arc setting (Babinski et al., 1997, Fernandes et al., 1992a,b, Hartmann et al., 1999, Gollmann et al., 2008, Marques et al., 1998). Provenance studies of metasedimentary rocks in this region indicate a variety of source areas, with significant contribution of Paleoproterozoic ages (Gruber et al., 2011, Hartmann et al., 2004, Pertille et al., 2015, Saalmann et al. 2011). According to Pertille et al. (2015) deposition took place in a foreland tectonic setting at 650-570 Ma. U-Pb zircon data (SHRIMP) from acidic to intermediate metavolcanic rocks in these areas produced ages of ca. 780-790 (Saalmann et al., 2011).

At the eastern portion of the MP a granitic belt extends from southern Brazil to Uruguay (Fig.1). According to Bitencourt and Nardi (1993, 2000), this granitic belt developed in a post-collisional setting between 650 and 580 Ma. The igneous activity was probably controlled by the translithospheric structures composing the Southern Brazilian Shear Belt (SBSB - Fig. 1), closely associated with transpressive tectonics of the Brasiliano/Pan-African tectonic events.

Programa de Pós-Graduação em Geociências

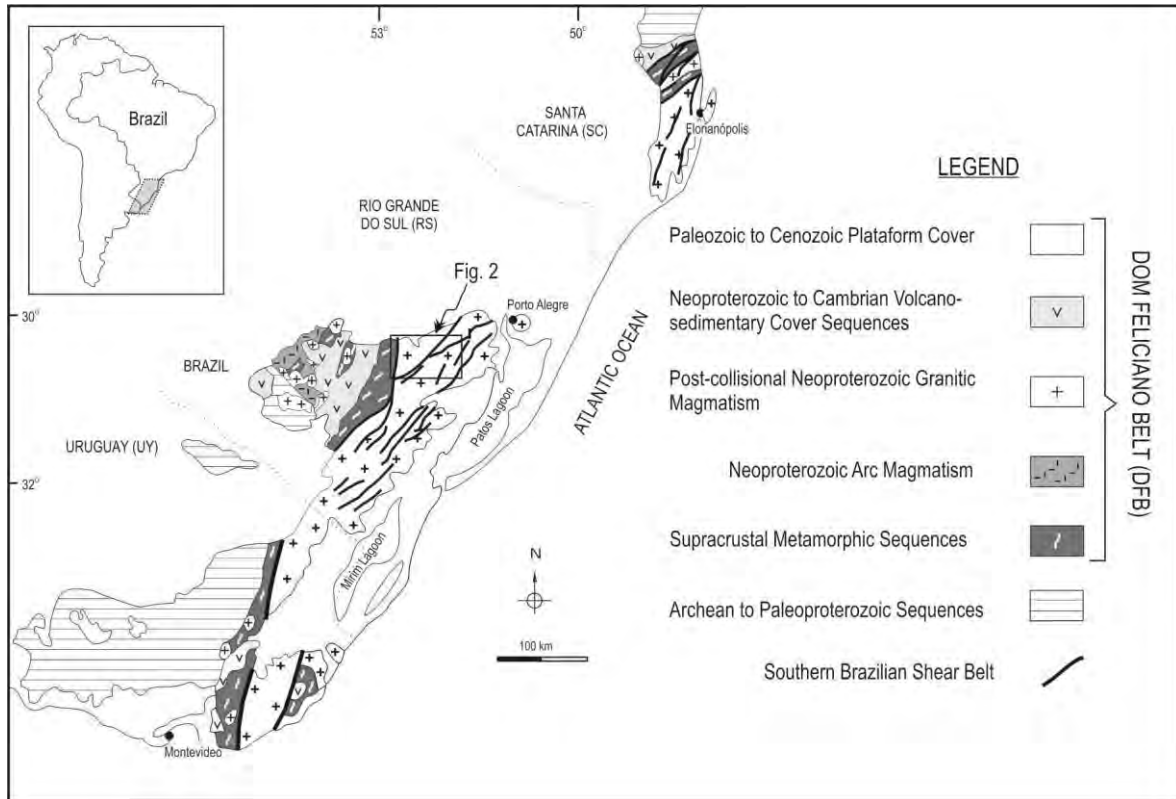


Figure 1 – Main tectonic domains for the southern Mantiqueira Province with location of figure 2 indicated (modified from Nardi and Bitencourt, 2007).

3. Geology of the Várzea do Capivarita Complex

The Várzea do Capivarita Complex (Fig. 2) comprises pelitic and calc-silicate paragneisses which predominate over orthogneisses. Subordinate volumes of syntectonic syenites are also part of the complex. The lithological types are tectonically interleaved as tabular or lenticular, decimeter- to meter-thick slices (Martil et al., 2011, Martil et al. b, submit.).

The VCC metapelites are finely laminated, with mafic and felsic layers. They also contain calc-silicate bands that commonly form disrupted, elongate boudins. The metapelitic high grade paragenesis is garnet + sillimanite + cordierite + spinel, whilst calc-silicate gneisses have more variable composition suchas alternating pyroxene-rich bands and fine-grained bands of biotite and Mg-rich amphibole. Although local partial melting evidences are identified in all VCC lithological types, as pointed out by Silva et al. (2002), they are more frequent in the pelitic gneiss, represented by irregular, garnet-bearing leucogranitic pockets.

Instituto de Geociências
Programa de Pós-Graduação em Geociências

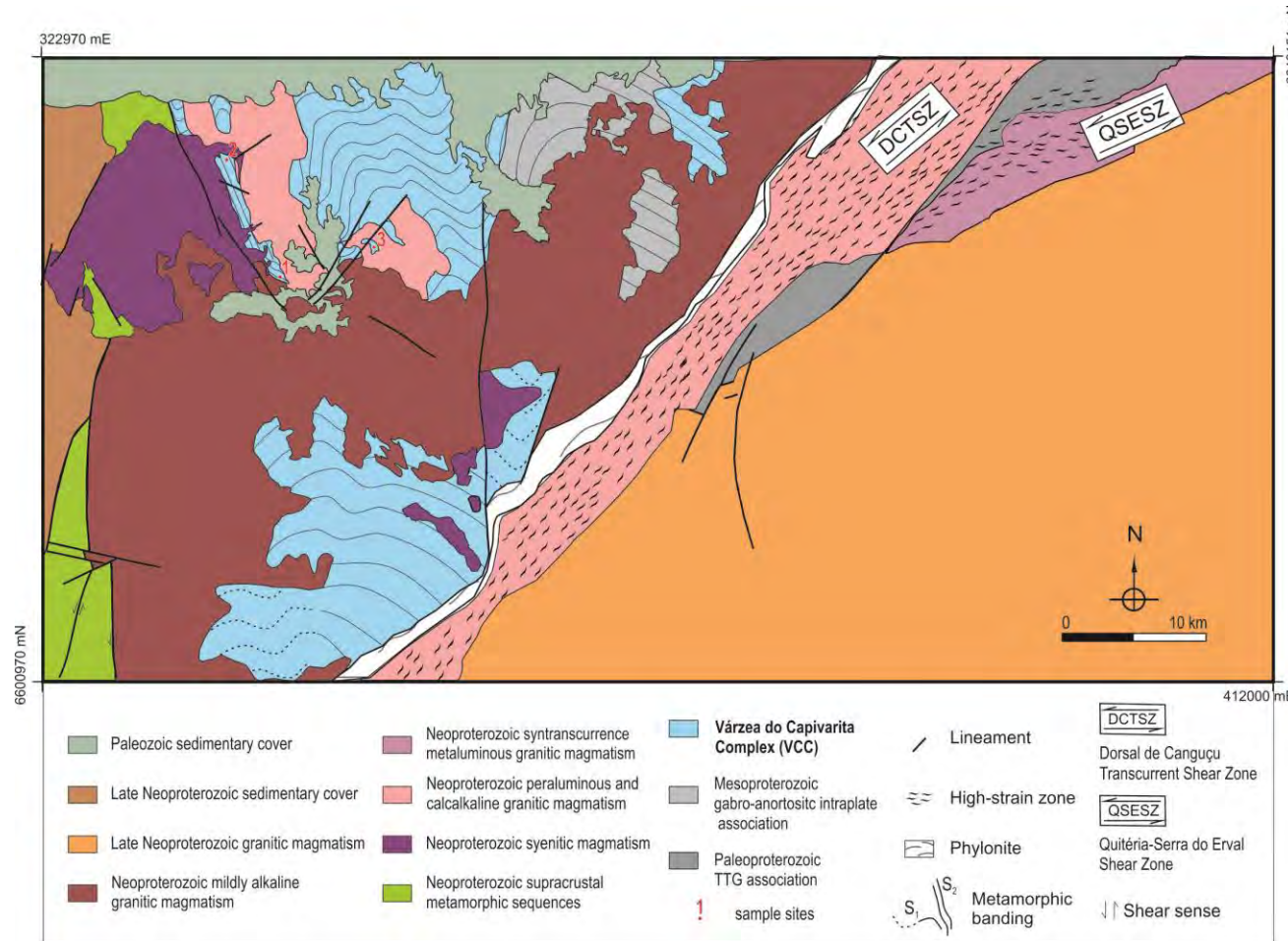


Figure 2 – Regional setting of the Várzea do Capivarita Complex featuring its areal extension and surrounding units. Sample sites: 1 – Samples TM 36B, TM 36 L and TM 01 E; 2 – TM 96 A; 3 – TM 45 G.

The orthogneisses are fine- to medium-grained rocks (Fig. 3a and 3b) of tonalitic to granitic compositions. The metamorphic banding is marked by alternating mafic and felsic, mm-thick, regular bands containing a well-developed stretching lineation (L_X - Fig. 3c) marked by quartz-feldspathic lenticular aggregates. Grain-size banding is also common. Successive generations of granitic veins enhance deformational features.

The dominant texture is polygonal granoblastic (Fig. 3d), with well-developed chessboard-pattern subgrains in quartz. In the tonalitic gneisses (Fig. 3a) felsic bands contain plagioclase, K-feldspar and quartz, whereas biotite, hypersthene (Fig. 3e), and diopside form the mafic assembly. The foliation is sigmoidal and contours plagioclase lenses and large quartz grains. The paragenesis Pl + Bt + Kfs + Qtz + Opx + Cpx indicates metamorphism under granulite facies conditions. In rocks of granitic composition, biotite is the dominant mafic phase, and garnet occurs as fine crystals.

The VCC orthogneisses are calc-alkaline, metaluminous to peraluminous rocks with major and trace-element patterns which are compatible with continental mature arc setting (Martil et al., 2011, Martil et al. c, submit.).

The regional structural framework is marked by two foliations, S_1 and S_2 , formed progressively, both under granulite facies conditions. S_1 is an originally sub-horizontal, NNW-trending gneissic banding (Fig. 3a, 4a and 4b) formed during a thrusting deformational phase – D_1 which resulted in the interleaving of the different VCC rock types and development of strong stretching lineation L_{X1} . In areas where the original sub-horizontal position of S_1 is preserved, kinematic indicators such as feldspar porphyroclasts and asymmetric intrafolial folds indicate top-to-the-W shear sense. The distribution of L_{X1} measurements along a single girdle (Fig. 4a) is consistent with subsequent folding during D_2 deformational phase. The F_2 folds are nearly upright, asymmetric folds with gently-plunging axis towards NNW (Fig. 4b). Their axial-planar cleavage grades into a dextral transposition cleavage (Fig. 4c), and eventually forms a steeply-dipping, S_2 , penetrative foliation (Fig. 4d). Progressive dextral shearing along S_2 leads to the formation of NNW-trending, regional strike-slip shear zones, the most obvious D_2 structural feature (Fig. 2).

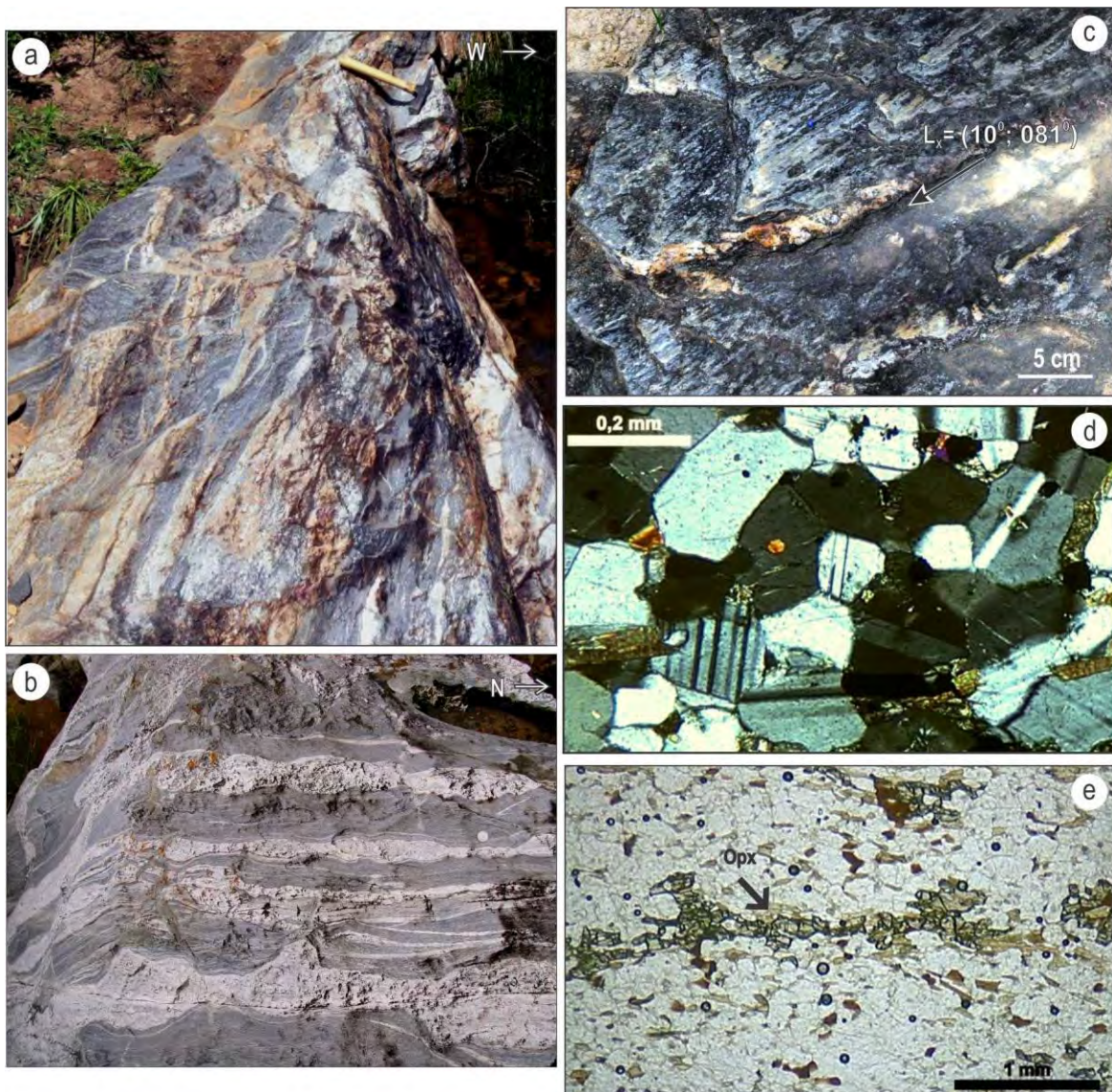


Figure 3 – Main features of the Várzea do Capivarita Complex orthogneisses. (a) Tonalitic gneiss with sub-horizontal metamorphic banding. (b) Granitic gneiss with concordant, deformed leucogranitic veins. (c) Pronounced stretching lineation in orthogneiss. (d) Well-developed polygonal texture in orthogneiss. (e) X-Z plane thin section from tonalitic gneiss showing orthopyroxene (Opx) grains aligned parallel to L_x .

Gross et al. (2006) determined metamorphic conditions between 750-800°C and 3-4 kbars for the VCC metapelites. Ultrahigh temperature (850-1000 °C) and medium pressure (6 to 11 kbars) conditions are reported for the VCC metapelites by Bom et al. (2014). Philipp et al. (2015) based on the paragenesis garnet-cordierite-sillimanite-biotite, established metamorphic conditions of 720-820° C and 8 to 9 kbar, characterizing it as of intermediate pressure and high temperature series.



Figure 4 – Várzea do Capivarita Complex structural features. (a) Lower hemisphere, equal-area contour plot diagram for the distribution of poles to banding – S_1 indicating preferred orientation along NNW-striking planes of low to moderate dip. The stretching lineation (L_{x1}) is scattered along a single girdle due to regional folding (F_2). (b) Asymmetric folds (F_2) in paragneisses, close to the profile plane, with poorly-developed axial-planar cleavage. (c) Dextral shearing of orthogneisses along well-developed, axial-planar transposition cleavage (S_2). (d) Lower hemisphere, equal-area contour plot

Programa de Pós-Graduação em Geociências

diagram showing distribution of poles to S_2 foliation and L_{x2} lineation which are the main features of D_2 strike-slip deformation. Contours and number of measurements are indicated in stereoplots.

4. Geochronology

4.1 Previous geochronological data from the Dom Feliciano Belt high-grade sequences

Geochronological data for the Várzea do Capivarita Complex (Table 1) are scarce and somewhat imprecise. No igneous age data have been reported to date. Metamorphic age values obtained from Sm-Nd garnet-whole rock isochrones in metapelites are reported by Gross et al. (2006) and range from 604 to 652 Ma, with high associated errors. Peak age value is at ca. 604-626 Ma. U-Pb SHRIMP data reported by Philipp et al. (2016) indicate metamorphic age of 619 ± 4.3 Ma. A 620 ± 6.3 Ma zircon age for a leucogranite vein is interpreted to indicate partial melting of the sequence (Tab. 1). U-Pb SHRIMP zircon age data reported by Lenz et al. (2011) in Uruguay (Tab. 1) indicate magmatic ages between ca. 800 and 767 Ma, metamorphic ages of 673 - 666 Ma and partial melting at 654 ± 3 Ma.

Localization	Rock type - Unit	Method	Age	Interpretation	Reference
Southern Brazil- RS	grt-sill-sp-crd-bt gneiss Várzea do Capivarita Complex	Sm-Nd garnet-whole rock U-Pb SHRIMP zircon	605.9 \pm 2.4 Ma 614 \pm 12 Ma 652 \pm 25 Ma	metamorphism (peak at 604-626 Ma)	Gross et al. (2006)
	grt-sill-bt gneiss Várzea do Capivarita Complex		619 \pm 4.3 Ma	metamorphism	Philipp et al. (2015)
	peraluminous leucogranite vein Várzea do Capivarita Complex		620 \pm 6.3 Ma	cristalization and anatexis	
Southeastern Uruguay	Tonalitic and mafic orthogneisses Cerro Bori Orthogneiss	U-Pb SHRIMP zircon	666 – 673 Ma	Maximum metamorphic ages	Lenz et al. (2011)
			654 \pm 3 Ma	Partial melting	
			802 – 767 Ma	crystallization ages	
			1.0 to 2.2 Ga	Inheritance ages	

Table 1 – Previous geochronological data for the Dom Feliciano Belt high-grade sequences in southern Brazil and Uruguay.

4.2 Analytical procedures

Five samples were selected for LA-MC-ICP-MS and SHRIMP U-Pb analyses. All samples were fragmented in hydraulic press, sieved and then milled in a disk mill at Laboratório de Geologia Isotópica (LGI-UFRGS). Heavy minerals were concentrated by panning and zircon concentrates were obtained using a magnetic separator, followed by manual separation. Zircon grains of different shapes and roundnesses were hand-picked under a binocular microscope, mounted in epoxy resin together with standards, and then polished until the central portion of the grains are exposed. The epoxy mounts were carbon- or gold-coated and then BSE, and cathodoluminescence (CL) images were taken in order to investigate internal structures of zircon grains and evaluate the best spot location, avoiding inclusions, mixed zones, and fractures. The U-Pb analyses were carried out at 4 different laboratories, whose analytical methods and procedures are detailed in appendix A. All the age calculations were performed with Isoplot 3.0 (Ludwig, 2003).

4.3 Samples and results

The analysed samples (Table 2) are located in figure 2. Four of them represent tonalitic and granitic orthogneisses collected from different structural domains in the VCC. Samples TM 01 E, TM 36 B e TM 36 L were collected at sites where D₁ sub-horizontal structures are well preserved, and only minor effects of D₂ are observed. Sample TM 01 E is a tonalitic orthogneisses and samples TM 36 B and TM 36 L are collected along a single, mafic-rich tabular body interleaved with the main tonalitic gneisses. Sample TM 45 G is a granitic orthogneiss collected from a D₂ high-strain zone, and sample TM 96 A was taken from a granitic vein intrusive into calc-silicate gneisses. This vein is affected by F₂ folds along a D₂ high-strain zone.

Sample	UTM N	UTM E	Rock type	Structural site
TM 01 E	6632 687	341 280	Tonalitic gneiss	Flat-lying foliation (D_1)
TM 36 B				
TM 36 L	6632 227	341 622	Mafic gneiss	Flat-lying foliation (D_1)
TM 45 G	6634 440	348 665	Granitic gneiss	Subvertical shear zone (D_2)
TM 96 A	6641 016	336 958	Granitic vein	Folded in D_2

UTM data – fuse: 22J; datum: Córrego Alegre

Table 2 – UTM coordinates of the sample collection sites.

4.3.1 Zircon texture

Despite the compositional differences, zircon crystals from the VCC orthogneisses have similar characteristics, as shown in CL images (e.g. Fig. 5). The zircon populations comprise elongate, prismatic, subrounded grains, rarely showing well-preserved bipyramidal faces. The zircon grains are 50 to 300µm long and have variable aspect ratios. The zoning patterns are mostly concentric and regular. Bright rims resulting from secondary recrystallization and/or overgrowth are present in most samples, but only two of them (TM 36 B and TM 36 L) were wide enough to be analysed. Some zircon grains display darker cores, sometimes with a well-defined zoning. We interpret the rounded cores as inherited and the zoned overgrowths or rims as magmatic zircon grown during melt crystallization. The zircon population from the granitic vein (sample TM 96 A) is similar to those described for the VCC orthogneisses. However, brighter and dark rims are more common and wider.

4.3.2 Mafic orthogneisses – Samples TM 36 B and TM 36 L

Nineteen LA-MC-ICP-MS analyses (Fig. 5) were performed on sample **TM 36 B** and the results are presented in table 3. In this set, 9 spots represent selected results, since spots with discordance higher than 5% were excluded. The zircon grains define a discordia line with an upper intercept age of 790 ± 34 Ma (MSWD = 0.26, n=5) (Fig. 6), which is also in accordance

Programa de Pós-Graduação em Geociências

with individuals ages obtained with discordance less than 5% (Table 3). The Th/U ratio values for this group of analyses (between 0.34-0.54) are typical of magmatic zircons. Four concordant analyses (#03, #05, 14 and #15) define an upper intercept age of 648 ± 18 Ma (MSWD = 0.021 – Fig. 6). These values are related to the dark luminescent rims, with low Th/U ratios, between 0.02-0.12, which, together with the textures, are typical of metamorphic zircon overgrowth. The upper intercept age of 790 ± 34 is interpreted to date the crystallization of the protolith, whereas the upper intercept of 648 ± 18 Ma is the time of the thermal input that formed the metamorphic zircon overgrowths. Two indications of inherited core ages are shown in table 3, one is 1083 Ma old (98% concordance, spot #02) and the other one is discordant (ca. 10%) and crosscut by a later magmatic domain (spot#17), with an age of ca. 1100 Ma (Table3).

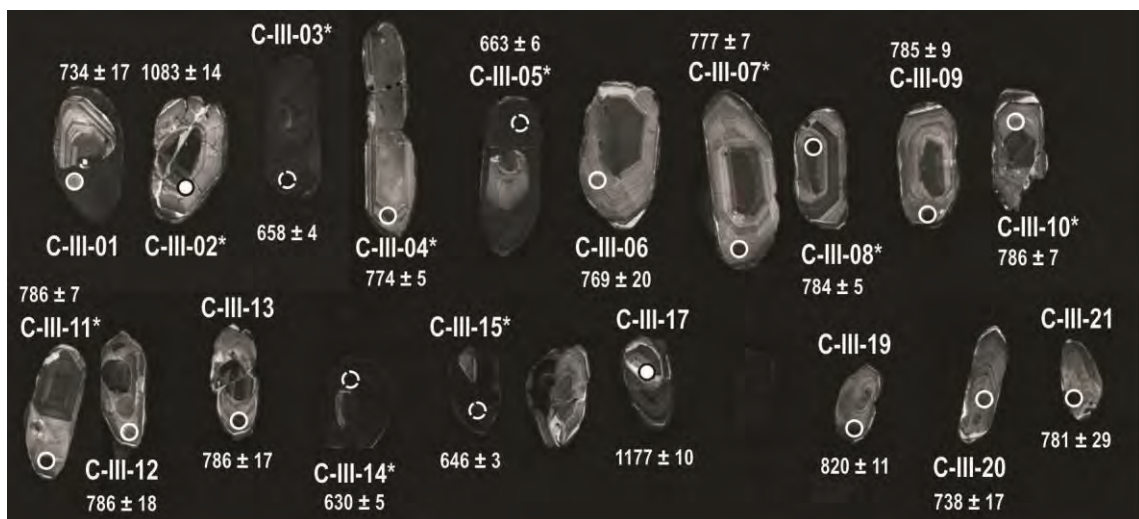


Figure 5 – Cathodoluminescence (CL) images of zircon grains from mafic orthogneiss(TM 36 B sample) dated by LA-MC-ICP-MS. Solid line –igneous age; dashed white line – metamorphic age; white-filled circle with solid black outline – inherited age. $^{206}\text{Pb}/^{238}\text{U}$ magmatic, metamorphic and inheritance ages with discordance less than 5% (*) and $^{207}\text{Pb}/^{206}\text{Pb}$ for high error analyses (*).

Instituto de Geociências

Programa de Pós-Graduação em Geociências

TM 36 B spot	isotopic ratios											Ages (Ma)						
	Pb (ppm)	U (ppm)	Th (ppm)	232Th/	207Pb/	1s	206Pb/	1s	207Pb/	1s	206Pb/	1s	207Pb/	1s	%			
	238U	235U	[%]	238U	[%]	Rho ^c	206Pbd	[%]	238U	abs	235U	abs	206Pb	abs	conc			
Magmatic Age - % discordance less than 5%																		
C-III-04	87	175	26	0.50	1.143	1.78	0.1275	0.58	0.33	0.065	1.69	774	5	774	14	776	13	100
C-III-07	43	112	17	0.39	1.146	2.19	0.1282	0.95	0.43	0.065	1.98	777	7	775	17	768	15	101
C-III-08	139	258	38	0.54	1.161	1.24	0.1292	0.60	0.49	0.065	1.09	784	5	782	10	779	8	101
C-III-10	55	113	17	0.49	1.159	1.89	0.1298	0.89	0.47	0.065	1.67	786	7	781	15	766	13	103
C-III-11	38	111	16	0.34	1.170	2.33	0.1297	0.87	0.37	0.065	2.16	786	7	787	18	787	17	100
Magmatic Age - % discordance > 5%																		
C-III-01	42	153	32	0.27	0.919	2.56	0.1046	1.05	0.41	0.064	2.33	641	7	662	17	734	17	87
C-III-06	26	72	10	0.36	1.058	2.75	0.1184	0.81	0.30	0.065	2.63	721	6	733	20	769	20	94
C-III-09	41	145	19	0.29	1.079	1.54	0.1198	0.98	0.64	0.065	1.18	729	7	743	11	785	9	93
C-III-12	29	80	13	0.37	1.089	2.5	0.1209	0.89	0.36	0.065	2.33	736	7	748	19	786	18	94
C-III-13	39	113	17	0.35	1.075	2.41	0.1193	1.02	0.42	0.065	2.19	726	7	741	18	786	17	92
C-III-19	93	235	29	0.40	1.162	1.42	0.1269	0.54	0.38	0.066	1.31	770	4	783	11	820	11	94
C-III-20	33	92	11	0.36	0.958	2.49	0.1087	0.77	0.31	0.064	2.37	665	5	682	17	738	17	90
C-III-21	34	111	15	0.31	1.081	4.7	0.1203	2.91	0.62	0.065	3.69	732	21	744	35	781	29	94
Inheritance core ages																		
C-III-02	34	130	21	0.26	1.923	2.28	0.1829	1.32	0.58	0.076	1.86	1083	14	1089	25	1103	20	98
C-III-17	21	77	16	0.27	2.414	2.33	0.2004	0.81	0.35	0.087	2.18	1177	10	1247	29	1369	30	86
Metamorphic rim ages																		
C-III-03	41	827	91	0.05	0.904	1.56	0.1075	0.66	0.42	0.061	1.42	658	4	654	10	640	9	103
C-III-05	57	537	57	0.11	0.909	2.07	0.1084	0.90	0.43	0.061	1.86	663	6	657	14	633	12	105
C-III-14	93	751	88	0.12	0.871	1.49	0.1026	0.74	0.50	0.062	1.29	630	5	636	9	658	9	96
C-III-15	37	1954	268	0.02	0.893	1.35	0.1055	0.42	0.31	0.061	1.28	646	3	648	9	653	8	99

Table3 – LA-MC-ICP-MS U-Pb data for sample TM 36 B.

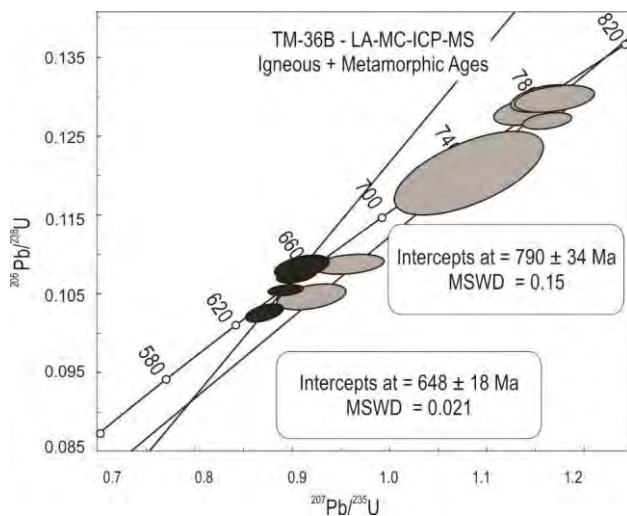


Figure 6 – LA-MC-ICP-MS concordia diagram for mafic orthogneiss (TM 36 B sample) showing igneous and metamorphic intercepts.

In order to refine the data obtained by LA-MC-ICPMS, twelve additional SHRIMP analyses were performed on sample TM 36 B (Table 4, Fig. 7a). The data (figure 7b) indicate the igneous age of $782 \pm 9.7 \text{ Ma}$ (MSWD = 0.15). One spot (# 3.1 – Table 4) has an identical metamorphic age as those from LA-MC-ICPMS data, which could be recalculated to $650 \pm 22 \text{ Ma}$ with MSWD of 1.11 and probability of 0.29.

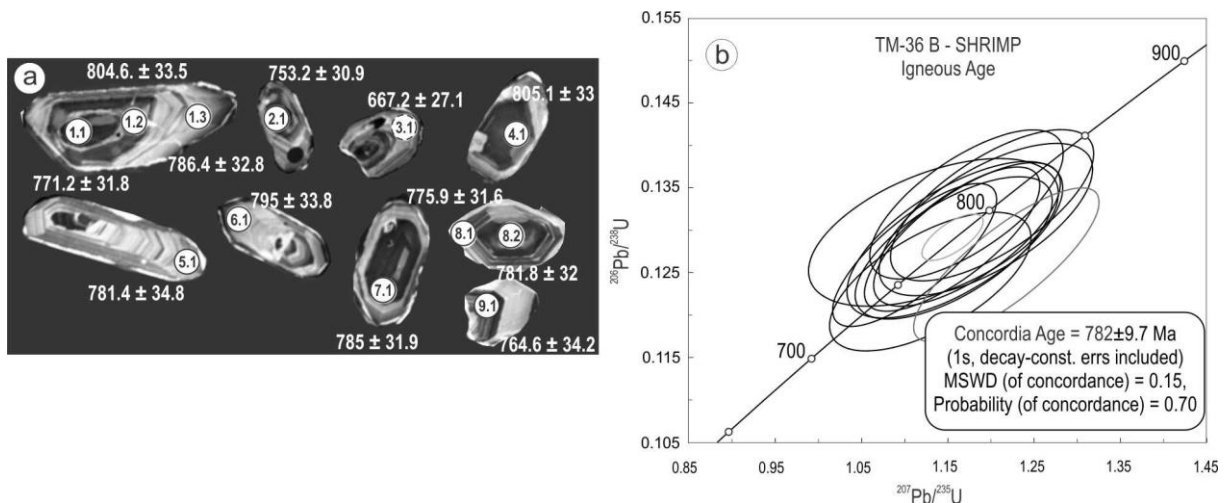


Figure 7 – SHRIMP analyses on mafic orthogneiss – TM 36 B sample. (a) – Cathodoluminescence (CL) images of zircon crystals. Solid line – igneous age; dashed line – metamorphic age. $^{206}\text{Pb}/^{238}\text{U}$ data for magmatic and metamorphic ages. (b) Concordia plot for igneous ages.

Programa de Pós-Graduação em Geociências

TM 36 B spot	%	ppm	ppm	^{232}Th	(1) ^{238}U	%	207r	%	207r	%	206r	%	err	(1) $^{206}\text{Pb}/$	1σ	(1) $^{207}\text{Pb}/$	1σ
	$^{206}\text{Pb}_c$	U	Th	/ ^{238}U	/ ^{206}r	err	206r	err	/235	err	/238	err	corr	^{238}U Age	err	^{206}Pb Age	err
TM_36-1.1	0.51	225	125	0.57	7.87	4.4	.0634	3.5	1.11	5.6	.1271	4.4	.776	771.2	31.8	723	75
TM_36-1.2	0.70	137	64	0.48	7.52	4.4	.0655	4.7	1.20	6.5	.1329	4.4	.684	804.6	33.5	792	99
TM_36-1.3	1.19	149	55	0.38	7.70	4.4	.0634	7.1	1.13	8.4	.1297	4.4	.525	786.4	32.8	720	152
TM_36-2.1	1.11	301	199	0.68	8.06	4.3	.0661	5.2	1.13	6.8	.1239	4.4	.638	753.2	30.9	810	110
TM_36-3.1r	0.25	1263	314	0.26	9.17	4.3	.0604	1.8	0.91	4.6	.1090	4.3	.924	667.2	27.1	617	38
TM_36-4.1	0.69	241	132	0.56	7.51	4.4	.0639	4.5	1.17	6.3	.1330	4.4	.691	805.1	33.0	738	97
TM_36-5.1	0.86	135	54	0.42	7.75	4.7	.0652	5.3	1.16	7.1	.1289	4.7	.663	781.4	34.8	780	112
TM_36-6.1	0.54	181	71	0.40	7.62	4.5	.0660	5.1	1.19	6.8	.1313	4.5	.660	795.0	33.8	806	107
TM_36-7.1	0.43	331	185	0.58	7.72	4.3	.0657	4.3	1.17	6.1	.1295	4.3	.708	785.0	31.9	795	90
TM_36-8.1	1.05	286	162	0.58	7.81	4.3	.0656	4.8	1.16	6.5	.1279	4.3	.664	775.9	31.6	794	102
TM_36-8.2	0.51	225	144	0.66	7.75	4.3	.0650	3.8	1.16	5.8	.1289	4.3	.749	781.8	32.0	773	81
TM_36-9.1	0.46	243	101	0.43	7.94	4.7	.0701	3.4	1.22	5.8	.1259	4.7	.815	764.6	34.2	932	69

Table 4 – Summary of SHRIMP U-Pb zircon data for sample TM 36 B.

Twenty three SHRIMP analyses were carried out on fourteen different zircon grains (Table 5, Fig. 8) from sample **TM 36 L** and the results are shown in figure 9. Four analyses are significantly discordant ($> 5\%$), and were excluded from the age calculation. Thirteen analyses, with Th/U ratios between 0.27 and 0.78 define a concordia age of 788 ± 5.3 Ma, the best estimate for crystallization of the orthogneiss protholith. Six analyses on the rims (Th/U = 0.02-0.1) were used to calculate the age of metamorphism of 648.4 ± 5.4 Ma.

Instituto de Geociências

Programa de Pós-Graduação em Geociências

TM 36 L spot	%	ppm	ppm	^{232}Th	\pm	(1) ppm	(1) $^{206}\text{Pb}/$	(1) $^{207}\text{Pb}/$	%	(1) $^{207}\text{Pb}^*$	\pm	(1) $^{207}\text{Pb}^*/$	\pm	$^{206}\text{Pb}^*/$	\pm	err		
	$^{206}\text{Pb}_c$	U	Th	/ ^{238}U	%	$^{206}\text{Pb}^*$	^{238}U Age	^{206}Pb Age	disc	/ $^{206}\text{Pb}^*$	[%]	^{235}U	[%]	^{238}U	[%]	corr		
1.1	0.05	166	66	0.41	0.33	0.05	793	± 12	794	± 40	+0	0.06560	1.92	1.185	2.5	0.1310	1.6	0.65
1.2	0.11	151	40	0.27	0.85	0.11	803	± 18	800	± 24	-0	0.06581	1.17	1.204	2.7	0.1326	2.4	0.90
2.1	0.00	440	242	0.57	0.53	0.00	795	± 10	788	± 12	-1	0.06542	0.57	1.184	1.5	0.1313	1.4	0.92
3.1	0.02	321	157	0.50	0.56	0.02	792	± 13	808	± 14	+2	0.06605	0.69	1.191	1.9	0.1308	1.7	0.93
3.2	0.09	565	52	0.10	0.84	0.09	649	± 11	655	± 14	+1	0.06146	0.66	0.897	1.9	0.1058	1.8	0.94
4.1	0.02	348	121	0.36	0.26	0.02	766	± 11	777	± 15	+2	0.06508	0.69	1.132	1.7	0.1261	1.6	0.91
4.2	0.01	380	285	0.78	0.23	0.01	774	± 12	758	± 13	-2	0.06450	0.63	1.134	1.8	0.1276	1.7	0.93
5.1	0.16	933	96	0.11	0.67	0.16	809	± 12	758	± 15	-7	0.06451	0.72	1.189	1.7	0.1337	1.5	0.90
6.1	0.38	190	71	0.38	0.32	0.38	781	± 13	765	± 31	-2	0.06470	1.46	1.149	2.3	0.1288	1.8	0.78
6.2	0.03	472	242	0.53	0.50	0.03	780	± 10	802	± 12	+3	0.06587	0.59	1.167	1.5	0.1285	1.4	0.92
7.1	0.03	280	86	0.32	0.29	0.03	801	± 12	811	± 27	+1	0.06615	1.27	1.207	2.0	0.1323	1.6	0.77
8.1	0.02	1042	66	0.07	0.29	0.02	652	± 9	644	± 9	-1	0.06115	0.41	0.897	1.5	0.1064	1.5	0.96
8.2	0.10	430	60	0.14	0.31	0.10	660	± 12	627	± 17	-6	0.06064	0.77	0.901	2.0	0.1078	1.9	0.92
9.1	0.23	47	4	0.08	1.32	0.23	653	± 9	635	± 66	-3	0.06088	3.06	0.895	3.4	0.1066	1.4	0.41
9.2	--	383	241	0.65	0.35	--	786	± 11	784	± 13	-0	0.06529	0.63	1.167	1.6	0.1296	1.4	0.91
10.1	0.02	175	69	0.41	0.32	0.02	776	± 12	766	± 32	-1	0.06473	1.52	1.141	2.3	0.1278	1.7	0.74
10.2	0.31	417	86	0.21	0.75	0.31	1068	± 15	1304	± 20	+20	0.08449	1.02	2.099	1.8	0.1802	1.5	0.83
11.1	--	516	320	0.64	1.28	--	804	± 13	797	± 18	-1	0.06571	0.87	1.204	1.9	0.1329	1.7	0.89
12.1	0.05	1982	41	0.02	0.67	0.05	654	± 6	649	± 6	-1	0.06128	0.30	0.902	1.1	0.1067	1.0	0.96
13.1	0.00	317	166	0.54	0.24	0.00	642	± 13	642	± 16	+0	0.06107	0.74	0.881	2.3	0.1046	2.2	0.95
13.2	0.20	551	185	0.35	1.20	0.20	709	± 17	806	± 47	+13	0.06600	2.25	1.057	3.4	0.1162	2.6	0.75
14.1	--	235	95	0.42	1.31	--	799	± 8	772	± 16	-4	0.06491	0.78	1.180	1.4	0.1319	1.1	0.82
14.2	0.24	330	6	0.02	0.88	0.24	640	± 7	641	± 26	+0	0.06106	1.23	0.879	1.6	0.1044	1.1	0.66

Table 5 – Summary of SHRIMP U-Pb zircon data for sample TM 36 L.

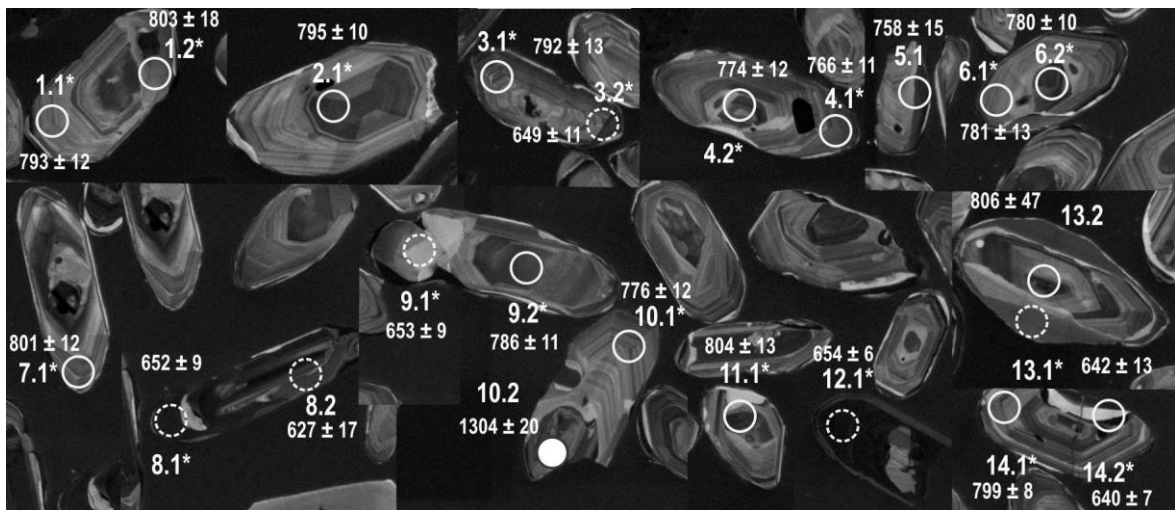


Figure 8 – Cathodoluminescence (CL) images of zircon grains from mafic orthogneiss (TM 36 L sample) dated by SHRIMP. Solid line – igneous age; dashed white line – metamorphic age; white-filled circle with solid black outline – inherited age. $^{206}\text{Pb}/^{238}\text{U}$ magmatic, metamorphic and inheritance ages with discordance less than 5% (*) and $^{207}\text{Pb}/^{206}\text{Pb}$ for high errors analysis (*).

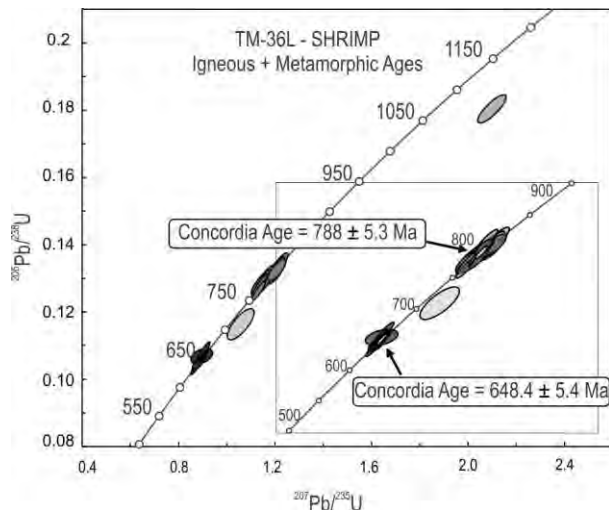


Figure 9 – SHRIMP concordia plot for mafic orthogneiss (TM 36 L); inset shows crystallization and metamorphic ages.

4.3.3 Tonalitic orthogneiss – Sample TM 01 E

Thirty six LA-MC-ICP-MS spots were analysed and from this set twenty two spots (Fig. 10) yielded concordant to nearly concordant values, with Th/U ranging from 0.25 to 0.69 (Table 6), which were recalculated and plotted on the concordia diagram of figure 11. These analyses align along a discordia with upper intercept age of 791 ± 30 Ma (MSWD = 0.36), which

Programa de Pós-Graduação em Geociências

agrees with the crystallization age obtained for the previous samples. Seven spots, with associated discordances less than 10%, yielded older $^{206}\text{Pb}/^{238}\text{U}$ ages, that represent inheritance, around 1.6, 1.8 and 3.1 Ga (Table 6). Inheritance data for these rock fix one upper intercept with age of 1848 ± 54 (MSWD = 0.15).

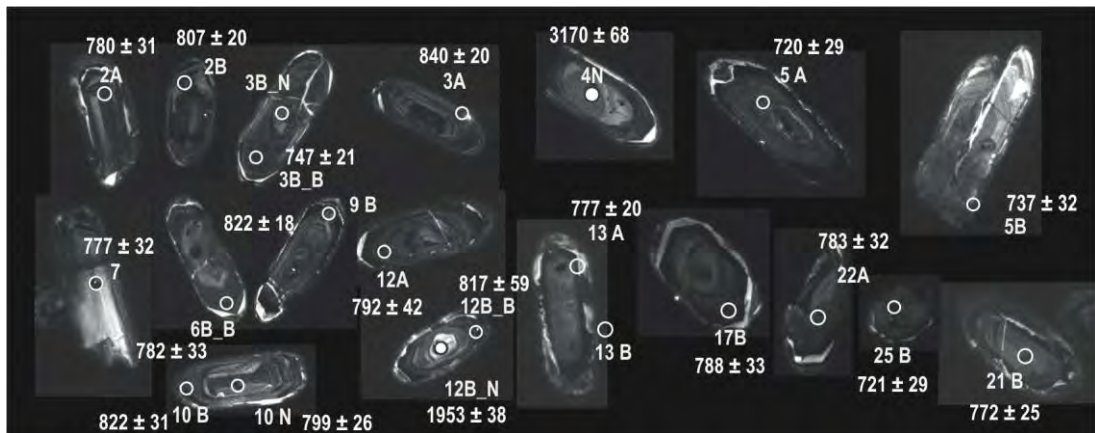


Figure 10 – Cathodoluminescence (CL) images of zircon grains from tonalitic gneiss(TM 01 E) dated by LA-MC-ICP-MS. Solid line – igneous age; white-filled circle with solid black outline – inherited age. $^{206}\text{Pb}/^{238}\text{U}$ ages for magmatic and inheritance ages with discordance less than 5% (*).

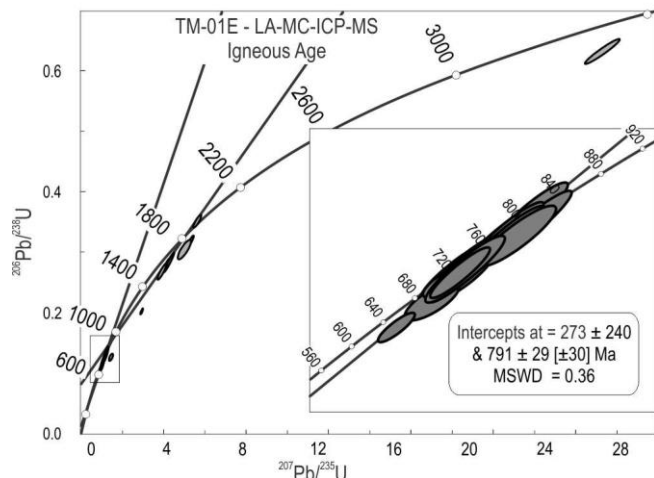


Figure 11 – LA-MC-ICP-MS Concordia plots for tonalitic gneiss(TM 01 E); inset shows crystallization age.

Instituto de Geociências

Programa de Pós-Graduação em Geociências

TM 01 E spot	isotopic ratios										Ages (Ma)							
	Pb (ppm)	U (ppm)	Th (ppm)	^{232}Th ^{238}U	$^{207}\text{Pb}/^{235}\text{U}$	1s [%]	$^{206}\text{Pb}/^{238}\text{U}$	1s [%]	Rho ^c	$^{207}\text{Pb}/^{206}\text{Pb}$	1s [%]	$^{206}\text{Pb}/^{238}\text{U}$	1s abs	$^{207}\text{Pb}/^{235}\text{U}$	1s abs	$^{207}\text{Pb}/^{206}\text{Pb}$	1s abs	% conc
	Magmatic Age - % discordance less than 5%																	
004-Z2A	36	155	273	0.57	1.166	4.41	0.1286	4.03	0.91	0.066	1.78	780	31	785	35	798	14	98
008-Z3B_B	47	156	388	0.40	1.091	3.23	0.1229	2.82	0.87	0.064	1.57	747	21	749	24	754	12	99
013-Z5A	22	58	140	0.42	1.034	4.44	0.1181	4.09	0.92	0.063	1.73	720	29	721	32	725	13	99
014-Z5B	15	44	93	0.47	1.073	4.73	0.1211	4.29	0.91	0.064	1.98	737	32	740	35	752	15	98
016-Z6B_B	41	101	240	0.42	1.164	4.4	0.129	4.17	0.95	0.065	1.41	782	33	784	35	789	11	99
017-Z7	24	54	140	0.39	1.144	4.47	0.128	4.18	0.93	0.065	1.59	777	32	774	35	768	12	101
020-Z10N	45	169	246	0.69	1.185	3.6	0.132	3.24	0.90	0.065	1.56	799	26	794	29	778	12	103
023-Z10B	40	84	207	0.41	1.226	4.13	0.136	3.76	0.91	0.065	1.70	822	31	812	34	786	13	105
024-Z12A	53	112	301	0.37	1.208	5.64	0.1308	5.33	0.95	0.067	1.84	792	42	804	45	838	15	95
027-Z13A	34	74	194	0.38	1.167	3.21	0.1282	2.58	0.80	0.066	1.92	777	20	785	25	807	15	96
036-Z17B	75	183	444	0.41	1.167	4.51	0.13	4.16	0.92	0.065	1.75	788	33	785	35	777	14	101
038-Z19B	16	34	109	0.32	1.017	3.08	0.1155	2.41	0.78	0.064	1.91	705	17	713	22	737	14	96
043-Z21B	20	68	125	0.55	1.148	3.58	0.1272	3.21	0.90	0.065	1.58	772	25	777	28	790	13	98
044-Z22A	67	99	403	0.25	1.171	4.45	0.1291	4.08	0.92	0.066	1.76	783	32	787	35	799	14	98
049-Z25B	26	71	177	0.40	1.055	4.31	0.1183	3.98	0.92	0.065	1.65	721	29	731	31	764	13	95
005-Z2B	51	219	357	0.62	1.222	3.18	0.1334	2.53	0.80	0.066	1.92	807	20	811	26	820	16	98
006-Z3A	55	212	415	0.52	1.262	2.98	0.1391	2.43	0.82	0.066	1.73	840	20	829	25	800	14	105
026-Z12B_B	64	127	347	0.37	1.240	7.4	0.1351	7.25	0.98	0.067	1.46	817	59	819	61	824	12	99
034-Z16	80	278	448	0.62	1.346	5.29	0.1462	3.70	0.70	0.067	3.77	879	33	866	46	832	31	106
019-Z9B	82	184	456	0.41	1.235	2.63	0.136	2.16	0.82	0.066	1.50	822	18	816	21	801	12	103

Table 6 – LA-MC-ICP-MS U-Pb data for sample TM 01 E.

Cont. tab. 6

TM 01 E spot	isotopic ratios												Ages (Ma)						
	Pb (ppm)	U (ppm)	Th (ppm)	^{232}Th ^{238}U	$^{207}\text{Pb}/$ ^{235}U	1s [%]	$^{206}\text{Pb}/$ ^{238}U	1s [%]	Rho ^c	$^{207}\text{Pb}/$ $^{206}\text{Pb}_{\text{d}}$	1s [%]	$^{206}\text{Pb}/$ ^{238}U	1s abs	$^{207}\text{Pb}/$ ^{235}U	1s abs	$^{207}\text{Pb}/$ ^{206}Pb	1s abs	% conc	
Magmatic Age - % discordance > 5%																			
015-Z6B_N	22	48	138	0.35	1.060	4.5	0.1173	3.90	0.87	0.066	2.25	715	28	734	33	791	18	90	
033-Z15	31	98	222	0.44	0.991	4.16	0.1101	3.18	0.76	0.065	2.69	673	21	699	29	783	21	86	
037-Z18	77	276	533	0.52	1.056	4.44	0.1173	4.15	0.93	0.065	1.59	715	30	732	33	783	12	91	
040-Z20B	96	124	645	0.19	0.909	3.07	0.1028	2.67	0.87	0.064	1.51	631	17	656	20	745	11	85	
046-Z23	21	91	128	0.72	1.187	4.94	0.1286	4.40	0.89	0.067	2.26	780	34	794	39	835	19	93	
047-Z24	13	33	82	0.41	1.067	5.65	0.1193	5.20	0.92	0.065	2.20	726	38	737	42	770	17	94	
028-Z13B	115	242	609	0.40	1.257	6.81	0.1331	6.12	0.90	0.068	2.99	806	49	826	56	882	26	91	
010-Z4B	61	161	473	0.34	1.434	4.64	0.1291	3.06	0.66	0.081	3.49	783	24	903	42	1210	42	65	
Inheritance core ages																			
025-Z12B_N	31	69	64	1.08	5.621	2.25	0.3538	1.95	0.87	0.115	1.12	1953	38	1919	43	1883	21	104	
009-Z4N	86	90	141	0.64	25.309	2.23	0.6351	2.14	0.96	0.289	0.62	3170	68	3320	74	3412	21	93	
029-Z14	48	98	129	0.76	4.184	1.95	0.2849	1.70	0.87	0.106	0.94	1616	27	1671	32	1740	16	93	
035-Z17N	59	107	159	0.68	4.256	3.94	0.286	3.79	0.96	0.108	1.07	1622	61	1685	66	1765	19	92	
045-Z22B	28	53	79	0.68	3.907	3.46	0.2704	3.11	0.90	0.105	1.52	1543	48	1615	56	1711	26	90	
007-Z3B_N	83	149	259	0.58	5.254	2.52	0.3193	2.29	0.91	0.119	1.05	1786	41	1861	47	1946	20	92	
048-Z25	86	113	244	0.47	4.991	4.19	0.3071	3.46	0.82	0.118	2.37	1726	60	1818	76	1925	46	90	
018-Z9N	99	111	382	0.29	2.919	1.89	0.2051	1.53	0.81	0.103	1.11	1203	18	1387	26	1683	19	71	

Table 6 – LA-MC-ICP-MS U-Pb data for sample TM 01 E.

4.3.4 Granitic orthogneiss – Sample TM 45 G

Twenty-two SHRIMP analyses were performed on this granitic orthogneiss and 11 spots (Fig. 12) were selected for age calculation, with associated discordance lower than 5% and Th/U ratios ranging from 0.16 to 0.54. The results are listed in table 7 and plotted in figure 13. The pattern is complex, with a great deal of Paleoproterozoic and possibly Archaean inheritance. The population of 11 analyses that cluster close to the concordia yielded the mean $^{207}\text{Pb}/^{206}\text{Pb}$ age of 789.7 ± 7 Ma (MSWD = 0.69; probability = 0.73). Despite the highly discordant data for most inherited grains (Table 7), at least 2 spots (# 9.1 and # 13.1) indicated concordant ages at ca. 1.8 and 2.0 Ga.

Instituto de Geociências

Programa de Pós-Graduação em Geociências

TM 45 G spot	%	ppm	ppm	^{232}Th	\pm	(1) ppm	(1) $^{206}\text{Pb}/^{238}\text{U}$	(1) $^{207}\text{Pb}/^{206}\text{Pb}$ Age		%	(1) $^{207}\text{Pb}^*$	\pm	(1) $^{207}\text{Pb}^*/^{235}\text{U}$	\pm	$^{206}\text{Pb}^*/^{238}\text{U}$	\pm	err	
	$^{206}\text{Pb}_c$	U	Th	/ ^{238}U	%	$^{206}\text{Pb}^*$		disc	/ $^{206}\text{Pb}^*$	[%]	^{235}U	[%]	^{238}U	[%]	corr			
1.1	0.09	316	124	0.41	0.25	34	754	± 10	772	± 18	+3	0.06493	0.84	1.110	1.6	0.1240	1.4	0.86
1.2	0.07	503	219	0.45	4.42	54	759	± 19	776	± 13	+2	0.06506	0.62	1.121	2.8	0.1250	2.7	0.97
2.1	--	736	197	0.28	0.45	84	802	± 13	800	± 10	-0	0.06579	0.46	1.202	1.8	0.1325	1.7	0.97
3.1	0.33	368	151	0.42	1.19	41	795	± 9	1410	± 27	+46	0.08927	1.39	1.615	1.9	0.1312	1.2	0.66
4.1	0.01	2575	389	0.16	1.62	284	778	± 9	792	± 12	+2	0.06556	0.57	1.160	1.3	0.1283	1.2	0.90
4.2	0.00	1109	786	0.73	2.96	341	1974	± 43	2648	± 21	+29	0.17943	1.28	8.865	2.8	0.3583	2.5	0.89
5.1	0.00	1180	114	0.10	2.94	356	1939	± 36	2842	± 9	+37	0.20197	0.53	9.772	2.2	0.3509	2.1	0.97
5.2	0.15	4307	692	0.17	0.70	453	744	± 15	783	± 26	+5	0.06528	1.24	1.101	2.4	0.1224	2.1	0.86
6.1	0.05	239	247	1.07	0.25	61	1684	± 34	1904	± 9	+13	0.11653	0.48	4.796	2.3	0.2985	2.3	0.98
6.2	--	333	120	0.37	0.29	36	771	± 14	807	± 20	+5	0.06601	0.93	1.156	2.2	0.1270	2.0	0.90
7.1	0.22	413	111	0.28	0.41	46	785	± 32	784	± 32	-0	0.06531	1.52	1.167	4.6	0.1296	4.4	0.94
8.1	0.58	124	106	0.88	0.72	29	1578	± 21	1945	± 18	+21	0.11922	1.01	4.559	1.8	0.2773	1.5	0.83
4.3	0.06	876	615	0.73	0.32	264	1940	± 28	2804	± 5	+36	0.19725	0.32	9.552	1.7	0.3512	1.7	0.98
2.2	0.01	447	173	0.40	0.23	51	798	± 11	787	± 13	-2	0.06540	0.61	1.189	1.5	0.1319	1.4	0.92
9.1	0.06	412	193	0.48	2.09	126	1965	± 36	1966	± 14	+0	0.12063	0.76	5.929	2.3	0.3565	2.1	0.94
7.2	0.04	476	215	0.47	0.43	52	776	± 10	778	± 13	+0	0.06511	0.60	1.148	1.5	0.1279	1.4	0.92
10.1	0.02	383	156	0.42	1.67	79	1384	± 21	1638	± 19	+17	0.10075	1.02	3.326	2.0	0.2394	1.7	0.85
10.2	14.46	382	108	0.29	2.53	11	210	± 18	1066	± 232	+82	0.07492	12	0.342	14.5	0.0331	8.8	0.60
11.1	0.24	454	151	0.34	0.72	63	962	± 18	1203	± 30	+22	0.08024	1.52	1.781	2.5	0.1610	2.0	0.80
12.1	0.02	468	160	0.35	0.41	51	769	± 8	800	± 13	+4	0.06579	0.60	1.150	1.2	0.1268	1.1	0.88
13.1	0.03	209	110	0.54	0.27	59	1822	± 25	1829	± 16	+0	0.11182	0.86	5.036	1.8	0.3266	1.6	0.88
14.1	0.01	216	63	0.30	0.53	49	1512	± 22	1985	± 53	+27	0.12197	2.96	4.446	3.4	0.2644	1.6	0.48

Table 7 – Summary of SHRIMP U-Pb zircon data for sample TM 45 G.

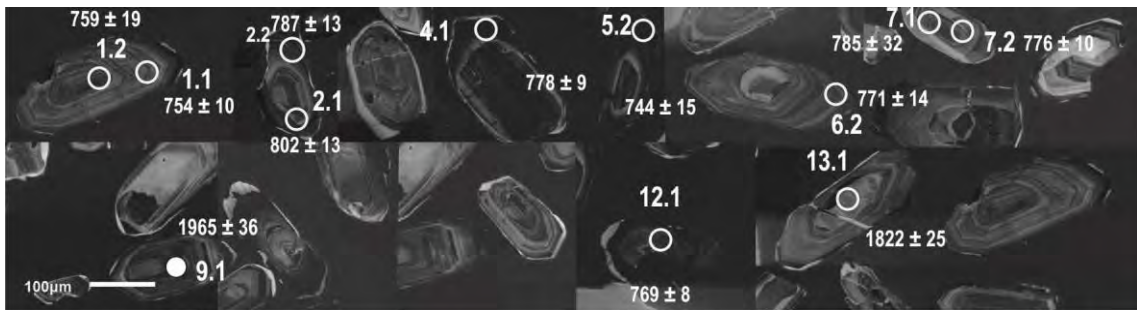


Figure 12 – Cathodoluminescence (CL) images of zircon grains from granitic gneiss(TM 45 G) dated by SHRIMP. Solid line –igneous age; white-filled circle with solid black outline – inherited age. $^{206}\text{Pb}/^{238}\text{U}$ ages for magmatic and inheritance ages with discordance less than 5% (*).

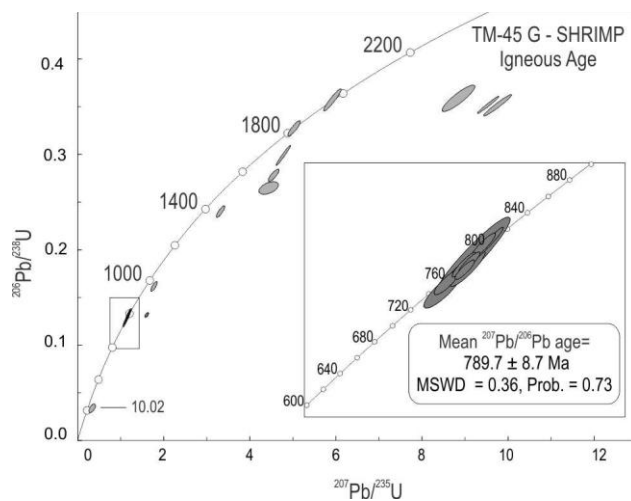


Figure 13 – SHRIMP concordia plot for granitic orthogneiss (TM 45 G); inset shows crystallization age.

4.3.5 Granite vein – Sample TM 96 A

Sixteen grains from a granitic vein (Fig. 14a) were analysed by SHRIMP comprising a total of 20 spots (Table 8). Seven spots were selected for age calculation (Fig. 14b), and the results are plotted in figure 14c and 14d. The pattern is complex, indicating inheritance and also Pb loss. Six analyses with Th/U ratios between 0.27 and 0.63 define a concordia age of 770 ± 9.9 Ma, which is considered here to be the best estimate for the crystallization of this granite vein. This sample shows one crystal rim with a younger concordant age ($^{206}\text{Pb}/^{238}\text{U}$ age at 666 ± 25 Ma). This is a very dark overgrowth, with high U content - 2762 ppm. The low Th/U (0.04) value is an indication of its metamorphic origin. Five spot analyses carried out on the brighter and darker rims show discordant younger ages, probably due to Pb-loss. One spot yields an older and slightly discordant (7%) $^{206}\text{Pb}/^{238}\text{U}$ age, which indicates an

Programa de Pós-Graduação em Geociências

inherited core age around 1.8 Ga (Table 8 and Fig. 14b). Magmatic, metamorphic and inherited ages of TM 96 A are similar to those obtained for the orthogneisses.

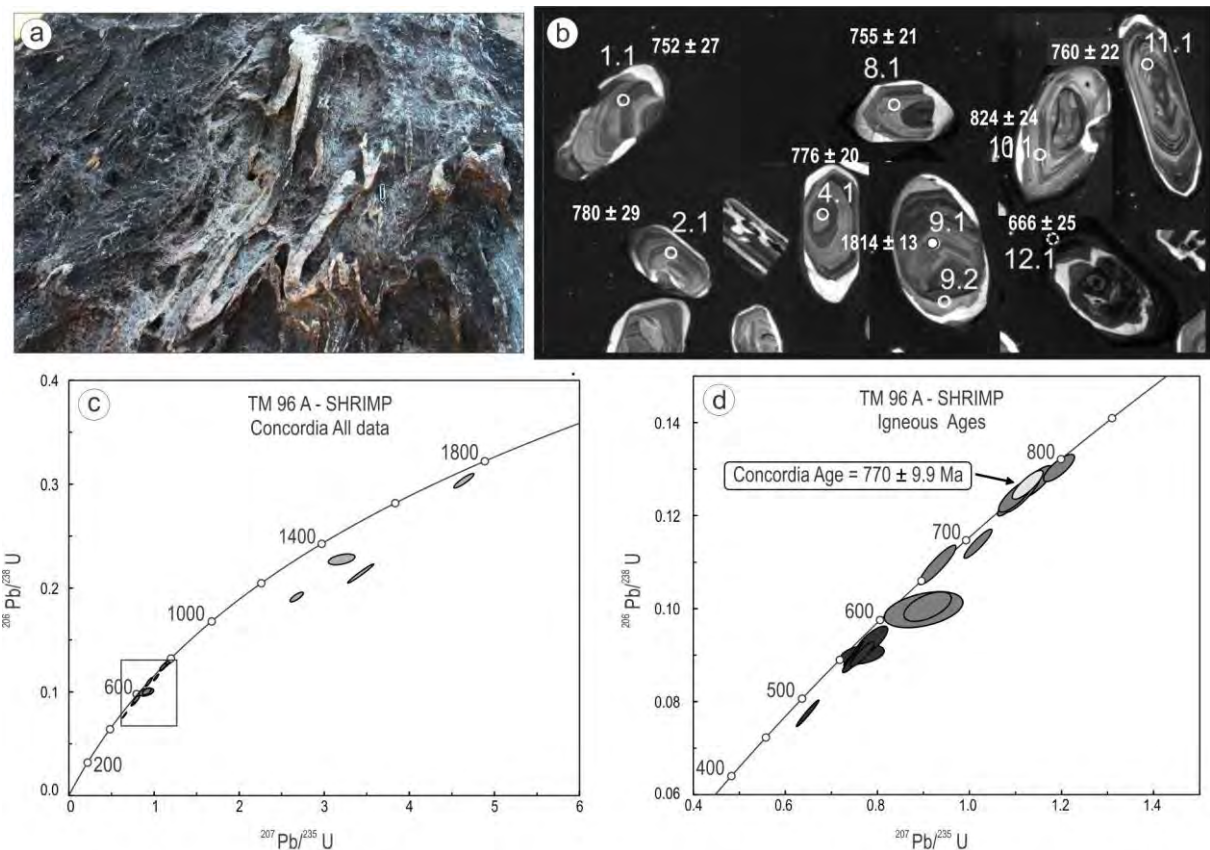


Figure 14 – (a) Sample TM 96 A, a granite vein affected by F_2 folds. (b) Cathodoluminescence (CL) images of zircon grains. Solid line – igneous age; dashed white line – metamorphic age and white-filled circle with solid black outline – inherited age. (c) Concordia U-Pb diagram with all zircon grains. (d) Concordia plot for $^{206}\text{Pb}/^{238}\text{U}$ magmatic, metamorphic and inheritance ages with discordance less than 5%.

Instituto de Geociências
Programa de Pós-Graduação em Geociências

TM 96 A spot	%	ppm	ppm	^{232}Th	\pm	(1) ppm	(1) $^{206}\text{Pb}/$	(1) $^{207}\text{Pb}/$	%	(1) $^{207}\text{Pb}^*$	\pm	(1) $^{207}\text{Pb}^*/$	\pm	$^{206}\text{Pb}^*/$	\pm	err		
	$^{206}\text{Pb}_c$	U	Th	$/^{238}\text{U}$	%	$^{206}\text{Pb}^*$	^{238}U Age	^{206}Pb Age	disc	$/^{206}\text{Pb}^*$	[%]	^{235}U	[%]	^{238}U	[%]	corr		
1,1	0,14	147	46	0,32	0,39	16	755	± 14	752	± 27	-0	0,0643	1,3	1,10	2,3	0,124	1,9	0,82
2,1	--	162	53	0,34	0,65	18	771	± 14	780	± 29	+1	0,0652	1,4	1,14	2,3	0,127	1,9	0,81
3,1	2,02	156	1	0,01	4,29	12	554	± 8	667	± 82	+17	0,0618	3,8	0,77	4,1	0,090	1,5	0,36
3,2	2,08	299	90	0,31	1,22	26	613	± 12	797	± 65	+24	0,0657	3,1	0,91	3,7	0,100	2,1	0,56
4,1	--	168	73	0,45	0,31	18	756	± 15	776	± 20	+3	0,0650	1,0	1,12	2,2	0,125	2,0	0,90
5,1	1,69	152	49	0,33	1,09	30	1297	± 18	1659	± 53	+22	0,1019	2,9	3,20	3,2	0,228	1,5	0,46
6,1	0,36	104	44	0,44	0,75	17	1098	± 16	1646	± 21	+34	0,1012	1,1	2,67	1,9	0,191	1,5	0,80
7,1	0,09	208	127	0,63	1,55	38	1202	± 33	1894	± 11	+37	0,1159	0,6	3,42	2,9	0,214	2,9	0,98
8,1	0,10	218	58	0,27	0,34	23	752	± 15	755	± 21	+0	0,0644	1,0	1,10	2,3	0,124	2,0	0,89
8,2	0,70	1898	11	0,01	0,69	147	554	± 15	646	± 23	+15	0,0612	1,1	0,76	2,9	0,090	2,7	0,93
9,1	--	110	67	0,63	0,34	29	1695	± 25	1814	± 13	+7	0,1109	0,7	4,63	1,7	0,303	1,5	0,91
9,2	0,27	122	6	0,05	1,84	10	571	± 13	655	± 40	+13	0,0614	1,9	0,79	3,0	0,093	2,3	0,78
10,1	0,07	138	40	0,30	0,40	15	788	± 11	824	± 24	+5	0,0666	1,1	1,20	1,9	0,130	1,5	0,80
11,1	0,09	185	63	0,35	0,69	20	769	± 12	760	± 22	-1	0,0646	1,1	1,13	1,9	0,127	1,6	0,84
12,1	0,27	2762	97	0,04	1,57	260	669	± 17	666	± 25	-1	0,0618	1,2	0,93	2,8	0,109	2,6	0,91
13,1	0,15	1837	350	0,20	0,30	122	479	± 11	630	± 12	+25	0,0607	0,6	0,65	2,5	0,077	2,4	0,97
14,1	0,03	384	216	0,58	0,19	38	694	± 12	771	± 17	+10	0,0649	0,8	1,02	2,0	0,114	1,8	0,92
15,1	2,79	110	33	0,31	0,45	9	609	± 15	789	± 121	+23	0,0655	5,7	0,90	6,3	0,100	2,6	0,41
15,2	--	5976	350	0,06	0,13	464	557	± 10	606	± 5	+8	0,0601	0,2	0,75	1,9	0,090	1,9	0,99

Table 8 – Summary of SHRIMP U-Pb zircon data for sample TM 96 A.

Instituto de Geociências

Programa de Pós-Graduação em Geociências

TM 96 A spot	%	ppm	ppm	^{232}Th	\pm	(1) ppm	(1) $^{206}\text{Pb}/^{238}\text{U}$	(1) $^{207}\text{Pb}/^{206}\text{Pb}$ Age	%	(1) $^{207}\text{Pb}^*$	\pm	(1) $^{207}\text{Pb}^*/^{235}\text{U}$	\pm	$^{206}\text{Pb}^*/^{238}\text{U}$	\pm	err		
	$^{206}\text{Pb}_c$	U	Th	/ ^{238}U	%	$^{206}\text{Pb}^*$	Age		disc	/ $^{206}\text{Pb}^*$	[%]	^{235}U	[%]	^{238}U	[%]	corr		
16,1	1,04	1382	120	0,09	2,64	107	555	± 11	665	± 22	+17	0,0617	1,0	0,77	2,2	0,090	2,0	0,88
2,1	--	162	53	0,34	0,65	18	771	± 14	780	± 29	+1	0,0652	1,4	1,14	2,3	0,127	1,9	0,81
3,1	2,02	156	1	0,01	4,29	12	554	± 8	667	± 82	+17	0,0618	3,8	0,77	4,1	0,090	1,5	0,36

Table 8 – Summary of SHRIMP U-Pb zircon data for sample TM 96 A.

5 Discussion and Conclusions

The precise age of the VCC orthogneiss protoliths determined here provides a cryogenian crystallization period of ca. 790-780 Ma for all lithotypes. Most zircon crystals show oscillatory zoning and high Th/U ratios, as well as preserved crystal terminations and prism faces, which is typical of magmatic zircons (Fig. 5, 7a, 8, 10, 12, 14b). The dating of different orthogneiss samples using LA-ICP-MS and SHRIMP has yielded consistent data and indicated Cryogenian ages in the 780-790 Ma range for the VCC magmatism. In addition, the morphological similarity between zircon crystals in these different orthogneisses is consistent with the hypothesis of a common magmatic source for the tectonically interleaved orthogneiss protoliths.

The geochronological data presented in this paper indicate that the VCC magmatism is comparable in time with the DFB arc sequences (Fig. 15), such as the juvenile rocks from western RS (ca. 750-700 Ma) and the ca. 800 Ma orthogneisses from southeastern Uruguay, formed in a continental arc environment (Lenz et al. 2011). Similar age values (ca. 800 Ma – Martil et al. a, submit., Saalmann et al., 2011) are found in acidic metavolcanic rocks of the DFB supracrustal sequences (Fig. 1, 2). Recent provenance studies (Martil et al. a, submit.) pointed out the volcano-sedimentary character of the VCC pelitic gneisses. They also indicate that the original pelites were coeval with the orthogneiss protolith. In association with the present geochronological results, the data point to a genetic link between the VCC gneisses and the supracrustal units of the central part of the DBF. Thus, it is possible that both sequences were formed in the same volcano-sedimentary context and were later interleaved by tectonics.

The presence of Archaean and Paleoproterozoic inheritance indicates the participation of old crustal sources, which is also suggested by geochemical and isotope data and consistent with an active continental margin setting for the generation of the original magmas (Martil et al., 2011 and Martil et al. c, submit.). Furthermore, the predominant Paleoproterozoic inheritance correlate with the age values reported for regional TTG rock associations (Gregory et al., 2015, Saalmann et al., 2011). The same inheritance pattern is played by the VCC orthogneisses – ca. 1.0, 1.1, 1.8 and 2.0 Ga – is found as provenance and inheritance ages in metasedimentary (e.g. Gruber et al., 2011, Hartmann et al., 2004) and metavolcanic (Martil et al. a, submit.) rocks of the supracrustal sequence. This is an additional genetic

Programa de Pós-Graduação em Geociências

similarity between the VCC gneisses and the DFB supracrustal rocks. Xenocryst zircon ages between 1.0 and 2.0 Ga are also described by Lenz et al. (2011) in the arc-related orthogneisses from Uruguay. Inheritance ages (ca. 3.4 Ga) from metatonalites of the Uruguayan Shield (Hartmann et al., 2001).

The age values of 640 - 650 Ma obtained on zircon overgrowths with low Th/U ratios (typically 0.02–0.1) are interpreted as the timing of high-grade metamorphism in the VCC orthogneisses. Such metamorphic overgrowths are virtually restricted to samples where anatexic features are recognized, which is in accordance with the observation of Rubatto et al. (2011) relative to the role played by the presence of melt in promoting zircon growth during metamorphism. These age values agree with those reported by Chemale Jr. et al. (2011) for upper amphibolite facies metamorphism in nearby metagabro-anorthosite association (Fig.2).

The geological and geochronological relations presented here suggest that the time interval between 640-650 Ma represent the timing of the main collisional event. Thus, we interpret younger metamorphic ages (ca. 600 - 620 Ma) reported in previous studies (Gross et al., 2006, Philipp et al., 2016), as related to partial melting during thermal relaxation that commonly follows the main collisional stage in orogens (e.g. Jamieson et al., 2004). Our geochronological data also indicate that both shear regimes (D_1 and D_2) identified in the VCC gneisses are contemporaneous, offering further evidence to the oblique character of the collision.

The ca. 130-140 Ma gap between the magmatic and metamorphic ages found in the VCC orthogneisses is compatible with a prolonged evolutionary history for the Complex, where the generation of a mature arc at ca. 780-790 Ma is followed by continental collision at ca. 640-650 Ma.

Crystallization ages of *ca.* 770 -780 Ma of the granitic vein (sample TM 96 A) suggest that it is coeval with the magmatic event that generated the VCC protoliths. Additionally, the 1.8 Ga inheritance age suggests a common source for the vein and the orthogneiss protoliths. Despite the highly discordant metamorphic age values obtained in this sample, a single spot of 666 ± 25 Ma is, within error, comparable to the ca. 650 Ma rim ages obtained for the orthogneisses. The partial melting event dated at 650 Ma by Lenz et al. (2011) is comparable to the metamorphic ages identified here. However, the authors present metamorphic age values of 670 Ma, indicating a longer time span for the high grade metamorphism of the DFB.

Programa de Pós-Graduação em Geociências

As the granite vein (sample TM 96 A) crosscuts a VCC calc-silicate paragneiss, it is plausible that at least part of the paragneisses are older than this magmatic event. Taken together with the previously discussed data for the VCC pelitic gneisses, and with the structural data from VCC, a geological event capable of thrust-stacking rocks of different ages along the same structure is required, which would be coherent with tectonic interleaving taking place in a continental collision setting.

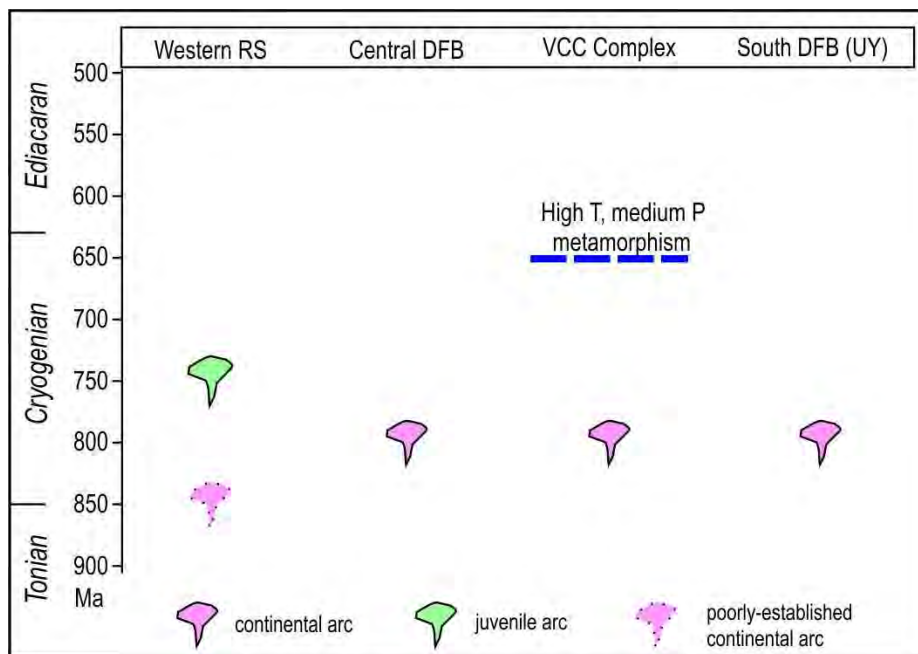


Figure 15 – Schematic time vs. space diagram comparing the VCC magmatism with other arc related units from southern Mantiqueira Province.

Acknowledgements

This work is part of the Ph.D. thesis of Mariana M. D. Martil. We acknowledge financial support provided by CNPq (141209/2010-0 - PhD Grant) and the scholarship from Ciência sem Fronteiras Program of the National Research Council (CSF-CNPq #400252/2012-0). This research was also supported by the State Research Foundation (FAPERGS, 10/0045- 6) and by CNPq Universal Program (471266/2010-8) granted to M.F. Bitencourt.

References

- Albarède, F., Telouk, P., Blichert-Toft, J., Boyet, M., Agranier, A., Nelson, B., 2004. Precise and accurate isotopic measurements using multiple-collector ICPMS. *Geochimica et Cosmochimica Acta* 68 (12): 2725–2744.
- Babinski M., Chemale F. Jr., Hartmann L.A., Van Schmus W.R., Silva L.C. 1996. Juvenile accretion at 750–700 Ma in southern Brazil. *Geology* 24, 439–442
- Babinski M., Chemale F. Jr., Van Schmus W.R., Hartmann L.A., Silva L.C. 1997. U-Pb and Sm-Nd Geochronology of the Neoproterozoic Granitic-Gneissic Dom Feliciano Belt, southern Brazil. *Journal of South American Earth Science* 10 (3-4): 263–274.
- Bom, F.M., Philipp, R.P., Zvirtes, G. 2014. Evolução metamórfica e estrutural do Complexo Várzea do Capivarita, Cinturão Dom Feliciano, Encruzilhada do Sul, RS. *Pesquisas em Geociências* 41 (2): 131-153.
- Bitencourt, M.F., Nardi, L.V.S. 1993. Late to Post-collisional Brasiliano Magmatism in Southernmost Brazil. *Annals of the Brazilian Academy of Science* 65 (1): 3-16.
- Bitencourt, M.F., Nardi, L.V.S. 2000. Tectonic setting and sources of magmatism related to the Southern Brazilian Shear Belt. *Revista Brasileira de Geociências* 30, 184-187.
- Buhn, B., Pimentel, M.M., Matteini, M., Dantas, E., 2009. High spatial resolution analysis of Pb and U isotopes for geochronology by laser ablation multi-collector inductively coupled plasma mass spectrometry (LA-MC-ICP-MS). *Annals of the Brazilian Academy of Sciences* 81, 99–114.
- Chemale Jr., F., Philipp, R.P., Dussin, I.A., Formoso, M.L.L., Kawashita, K., Bertotti, A.L. 2011. Lu-Hf and U-Pb age determinations of Capivarita Anorthosite in the Dom Feliciano Belt, Brazil. *Precambrian Research* 186, 117-126.

Programa de Pós-Graduação em Geociências

Fernandes, L.A.D., Tommasi, A., Porcher, C.C., 1992a. Deformation patterns in the southern Brazilian branch of the Dom Feliciano belt: a reappraisal. *Journal of South America Earth Science* 5, 77-96.

Fernandes, L.A.D., Tommasi, A., Porcher, C.C., Koester, E., Kraemer, G., Scherer, C.M., Menegat, R., 1992b. Granitoides precoces do Cinturão Dom Feliciano: caracterização geoquímica e discussão estratigráfica. *Pesquisas* 19, 197-218.

Garavaglia, L., Koester, E., Bitencourt, M.F., Nardi, L.V.S. 2006. Isotopic Signature of Late magmatic Arc to Post-collisional Magmatism in the Vila Nova Belt, Southern Brazil. In: South-American Symposium on Isotope Geology, 5, 2006, Punta del Este. Short Papers... Punta del Este, Universidad de la Republica. pp. 101-104.

Gollmann, K., Marques, J.C., Frantz, J.C., Chemale, F. Jr. 2008. Geoquímica e Isotópos de Nd de Rochas Metavulcânicas da Antiforme Capané, Complexo Metamórfico Porongos, RS. *Revista Pesquisas em Geociências* 35 (2): 83-95.

Gregory, T.R., Bintencourt, M.F., Nardi, L.V.S. 2011. Caracterização estrutural e petrológica de metatonalitos e metadioritos do Complexo Arroio dos Ratos na sua seção-tipo, região de Quitéria, RS. *Pesquisas em Geociências* 38(1): 85-108.

Gregory, T.R., M.F., Bitencourt, Nardi, L. V., Florisbal, L. M, Chemale, F. Jr. 2015. Geochronological data from TTG-type rock associations of the Arroio dos Ratos Complex and implications for crustal evolution of southernmost Brazil in Paleoproterozoic times. *Journal of South American Earth Science* 57, 49–60.

Gross, A.O.M.S., Porcher, C.C., Fernandes, L.A.D., Koester, E. 2006. Neoproterozoic low-pressure/high-temperature collisional metamorphic evolution in the Varzea do Capivarita metamorphic suite, SE Brazil: thermobarometric and Sm/Nd evidence. *Precambrian Research* 147, 41-64.

Gruber, L., Porcher, C.C., Lenz, C., Fernandes, L.A.D. 2011. Proveniência de metassedimentos das sequências Arroio Areião, Cerro Cambará e Quartz Milonitos no

Programa de Pós-Graduação em Geociências

Complexo Metamórfico Porongos, Santana da Boa Vista, RS. Pesquisa em Geociências 38 (3): 205-223.

Hartmann L.A. 1998. Deepest exposed crust of Brazil—geochemistry of Paleoproterozoic depleted Santa Maria Chico granulites. Gondwana Research 1, 331–341.

Hartmann, L. A., Leite, J.A.D., McNaughton, N.J., Santos, J. O.S. 1999. Deepest exposed crust of Brazil - SHRIMP establishes three events. Geology 27(10): 947-950.

Hartmann LA, Campal J, Santos JOS, McNaughton NJ, Bossi J, Schipilov A & Lafon JM. 2001. Archean crust in the Rio de la Plata Craton, Uruguay – SHRIMP U-Pb zircon reconnaissance geochronology. Journal of South American Earth Sciences 14, 557-570.

Hartmann, L.A., Philipp, R.P., Liu, D., Wan, Y., Wang, Y., Santos, J.O.S., Vasconcellos, M.A.Z. 2004. Paleoproterozoic magmatic provenance of Detrital Zircons, Porongos complex quartzites, southern Brazilian shield. International Geological Review 46, 127–157.

Hartmann, L.A., Dunyi, L., Yenbin, W., Hans, J.M., Santos, J.O.S. 2008. Protolith age of Santa Maria Chico granulites dated on zircons from an associated amphibolite-facies granodiorite in southernmost Brazil. Annals of the Brazilian Academy of Sciences 80(3): 543-551.

Hartmann, L.A., Philipp, R.P., Santos, J.O.S., McNaughton, N.J., 2011. Time frame of the 753–680 Ma juvenile accretion during the São Gabriel orogeny, Southern Brazilian shield. Gondwana Research 19, 84–99.

Heilbron M., Pedrosa-Soares A.C., Campos Neto M., Silva L.C., Trouw R.A.J., Janasi V.C. 2004. A Província Mantiqueira. In: V. Mantesso-Neto, A. Bartorelli, C.D.R. Carneiro, B.B. Brito Neves (Eds.), *O Desvendar de um Continente: A Moderna Geologia da América do Sul e o Legado da Obra de Fernando Flávio Marques de Almeida*. Ed. Beca, São Paulo, cap. XIII, pp. 203-234.

Programa de Pós-Graduação em Geociências

Jackson, S. E., Pearsona, N. J., Griffina, W.L., Belousova, E. A. 2004. The application of laser ablation-inductively coupled plasma-mass spectrometry to in situ U-Pb zircon geochronology. *Chemical Geology* 211, 47-69.

Jost, H., Bitencourt, M.F. 1980. Estratigrafia e tectônica de uma fração da faixa de Dobramentos de Tijucas no Rio Grande do Sul. *Acta Geologica Leopoldensia* 4(7): 27-60.

Jamieson, R. A., Beaumont, C., Medvedev, S., Nguyen, M.H., 2004. Crustal channel flows: 2. Numerical models with implications for metamorphism in the Himalayan –Tibetan orogen. *Journal of Geophysical Research*, 109, B06406.

Koester, E., Porcher, C.C., Fernandes, L.A.D., Lenz, C., Arcelus, H.M., Gross, A.O.M. 2012 Crustal Accretion at 800 Ma In the Eastern Domain of the Dom Feliciano Belt. In: VIII Symposium on Isotope Geology (SSAGI), 2012, Medellin. VIII Symposium on Isotope Geology (SSAGI).Medellin: Corpogemmas, 2012. v. 1., pp. 62.

Košler, J., Fonneland, H., Sylvester, P., Tubrett, M., Pedersen, R.B., 2002. U–Pb dating of detrital zircons for sediment provenance studies—a comparison of laser ablation ICP-MS and SIMS techniques. *Chemical Geology* 182, 605–618.

Leite, J.A.D., Hartmann, L.A., McNaughton, N.J., Chemale Jr., F., 1998. SHRIMP U-Pb zircon geochronology of Neoproterozoic juvenile and crustal-reworked terranes in southernmost Brazil. *International Geological Review* 40, 688–705.

Lenz, C., Fernandes, L.A.D., McNaughton, N.J., Porcher, C.C., Masquelin, H. 2011. U-Pb SHRIMP ages for the Cerro Bori Orthogneisses, Dom Feliciano Belt in Uruguay: Evidences of a 800Ma magmatic and 650 Ma metamorphic event. *Precambrian Research* 185, 149-163.

Lenz, C., Porcher, C.C., Fernandes, L.A.D., Masquelin, H., Koester, E., Conceição, R.V. 2013. Geochemistry of the Neoproterozoic (800 - 767 Ma) Cerro Bori orthogneisses, Dom Feliciano Belt in Uruguay: tectonic evolution of an ancient continental arc. *Mineralogy and Petrology* 107, 785–806.

Programa de Pós-Graduação em Geociências

Ludwig, K.R., 2000. SQUID 1.00. In: A User Manual, vol. 2. Berkeley Geochronology Center Special Publications, Berkeley, CA, 17 pp.

Ludwig, K.R., 2003. Isoplot 3.00: A Geochronological Toolkit for Microsoft Excel_ (revised version). In: Special Publication 4. Berkeley Geochronological Center, Berkeley, CA, 70 pp.

Machado, N., Gauthier, G., 1996. Determination of $^{206}\text{Pb}/^{207}\text{Pb}$ ages on zircon and monazite by laser ablation ICPMS and application to a study of sedimentary provenance and metamorphism in southeastern Brazil. *Geochimica et Cosmochimica Acta* 60, 5063–5073.

Marques, J.C., Jost, H., Roisenberg, A., Frantz, J.C., 1998. Eventos ígneos da Suíte Metamórfica Porongos na área da Antiforme Capané, Cachoeira do Sul. RS. *Revista Brasileira de Geociências* 28, 419-430.

Martil, M.M.D., Bitencourt, M.F., Nardi, L.V.S. 2011. Caracterização Estrutural e Petrológica do Magmatismo Pré-colisional do Escudo Sul-rio-grandense: os ortognaisses do Complexo Metamórfico Várzea do Capivarita. *Pesquisas em Geociências* 38 (2): 181-201.

Martil, M.M.D., Bitencourt, M.F., Schmitt, R., Armstrong, R., Pimentel, M., Nardi, L.V.S. Reconstitution of a volcano-sedimentary environment at 790 Ma obliterated by a collisional thrust tectonics: the Porongos and Várzea do Capivarita Complexes, southern Brazil. *Journal of South American Earth Sciences* (submitted, a).

Martil, M.M.D., Bitencourt, M.F., Weinberg, R., Schmitt, R., Nardi, L.V.S. Structural Evolution of Várzea do Capivarita Complex: a 650 Ma oblique collisional record in southern Brazil. *Journal of Structural Geology* (submitted, b).

Martil, M.M.D., Bitencourt, M.F., Nardi, L.V.S., Koester, E., Pimentel, M.M. Pre-collisional, Neoproterozoic (ca. 790 Ma) arc magmatism in southernmost Brazil: tectono-stratigraphy of the Várzea do Capivarita Complex. *Lithos* (submitted, c).

Programa de Pós-Graduação em Geociências

Nardi, L.V.S. and Bitencourt, M.F. 2007. Magmatismo Granítico e Evolução Crustal no Sul do Brasil. In: J.C. Frantz & R. Ianuzzi (Eds.), 50 Anos de Geologia: Instituto de Geociências. Contribuições. Editora Comunicação e Identidade, Porto Alegre, v.2, pp. 125-141.

Pertille, J.; Hartmann, L.A.; Philipp, R.P., Petry, T.S., Lana, C.C. 2015. Origin of the Ediacaran Porongos Group, Dom Feliciano Belt, southern Brazilian Shield, with emphasis on whole rock and detrital zircon geochemistry and U-Pb, Lu-Hf isotopes. *Journal of South American Earth Sciences* 64, 69-93.

Phillipp, R.P., Lusa, M., Nardi, L.V.S. 2008. Geochemistry and Petrology of dioritic, tonalitic and trondhjemite gneisses from Encantadas Complex, Santana da Boa Vista, southernmost Brazil: a Paleoproterozoic continental arc-magmatism. *Annals of the Brazilian Academy of Sciences* 80(4): 1-14.

Philipp, R.P., Bom, F.M., Pimentel, M.M., Junges, S. L., Zvirtes, G. 2016. SHRIMP U-Pb age and high temperature conditions of the collisional metamorphism in the Várzea do Capivarita Complex: Implications for the origin of Pelotas Batholith, Dom Feliciano Belt, Southern Brazil. *Journal of South American Earth Sciences* 66, 196-207.

Rubatto, D. Williams, I.S., Buick, I.S. 2001. Zircon and Monazite response to prograde metamorphism in the Reynolds Range, central Australia. *Contributions to Mineralogy and Petrology* 140, 458-468.

Saalmann, K., Gerdes, A., Lahaye, Y., Hartmann, L. A., Remus, M.V.D., Läufer, A. 2011. Multiple accretion at the eastern margin of the Rio de la Plata craton: the prolonged Brasiliano orogeny in southernmost Brazil. *International Journal of Earth Sciences* 66, 355-378.

Silva, L. C., McNaughton, N. J., Hartmann, L.A., Fletcher, I. R. 1999. SHRIMP U/Pb zircon dating of Neoproterozoic granitic magmatism and collision in the Pelotas Batholith, Southernmost Brazil. *International Geology Review* 41, 531-551.

Programa de Pós-Graduação em Geociências

Silva, A.O.M.S., Porcher, C.C., Fernandes, L.A.D., Droop, G.T.R. 2002. Termobarometria da Suíte Metamórfica Várzea do Capivarita (RS): Embasamento do Cinturão Dom Feliciano. Revista Brasileira de Geociências 32 (4): 419-432.

Siviero, R. S., Bruguier, O., Koester, E., Fernandes, L.A.D. 2009. Crustal evolution in the Lavras do Sul region, Southern Brazil and the amalgamation of West Gondwana. Goldschmidt Conference Abstracts. A1232.

Soliani Jr., E., Koester, E., Fernandes, L.A.D. 2000. A Geologia Isotópica do Escudo Sul-rio-grandense. Parte II: os dados isotópicos e interpretações petrogenéticas. In: Michael Holz and Luis Fernando De Ros. (Eds.). Geologia do Rio Grande do Sul. Editora da Universidade/UFRGS. Centro de Investigação do Gondwana - Instituto de Geociências, Porto Alegre, v.01, pp. 175-230.

Stacey, J.S., Kramers, J.D., 1975. Approximation of terrestrial lead isotope evolution by a two stage model. Earth and Planetary Science Letters 26, 207-221.

Williams, I.S., 1998. U-Th-Pb geochronology by ion microprobe. In: McKibben, M.A., Shanks, W.C., Ridley, W.I. (Eds.), Applications of Microanalytical Techniques to Understanding Mineralizing Processes. Reviews in Economic Geology, El Paso, 7, pp. 1-35.

Appendix A. Supplementary data

LA-MC-ICPMS and SHRIMP analytical methods from UFRGS, USP, ANU, UnB research laboratories

U-Pb zircon LA-MC-ICP-MS - Laboratório de Geologia Isotópica, Universidade Federal do Rio Grande do Sul (LGI – UFRGS), Brazil

Images of zircons were obtained using the optical microscope (Leica MZ 12₅) and electron microscope (Jeol JSM 5800). Zircon grains were dated using a Neptune ICP-MS multicollector equipment with a UP213 NewWaveTMlaser ablation probe. Conditions of laser at time of measure were: 10 Hz frequency, 30 µm spot size, and energy varied from 0.3 to 1.1

Programa de Pós-Graduação em Geociências

mJ/pulse. Laser-induced elemental fractional and instrumental mass discrimination were corrected by the reference zircon (GJ-1) (Jackson et al., 2004), following the measurement of two GJ-1 analyses to every six sample zircon spots. The external error was calculated after propagation error of the GJ-1 mean and the individual spot. For further detailed analytical methods and data treatment, see Chemale *et al.* (2011).

U-Pb zircon SHRIMP – USP – Centro de Pesquisas Geocronológicas, Universidade de São Paulo (CPGeo-USP), Brazil

The polished zircon mount was examined with a FEI-QUANTA 250 scanning electron microscope equipped with secondary-electron and cathodoluminescence detectors at CPGeo-USP (sample TM 01 E). The same mounts were afterwards analyzed by the U–Pb isotopic technique using a SHRIMP-II also at CPGeo-USP, following the analytical procedures presented in Williams (1998). Correction for common Pb was made based on the ^{204}Pb measured, and the typical error component for the $^{206}\text{Pb}/^{238}\text{U}$ ratio is less than 2%; U abundance and U–Pb ratios were calibrated using the TEMORA standard.

U-Pb zircon SHRIMP – Research School of Earth Sciences at the Australian National University (RSES-ANU), Austrália.

Two samples were analysed using a SHRIMP II instrument. BSE and CL images were acquired on a Hitachi S2250-N scanning electron microscope. The data have been reduced by employing methods similar to those described by Williams (1998), and using the SQUID Excel Macro of Ludwig (2000). For calibration, Pb/U ratios have been normalized relative to a value of 0.1859 for the $^{206}\text{*Pb}/^{238}\text{U}$ ratio of the TEM standard (417 Ma). Common Pb was corrected assuming the model Pb composition from Stacey and Kramers (1975). U and Th concentrations were determined relative to the SL13 standard. Uncertainties given for individual analyses (ratios and ages) are reported at the 1σ level, however uncertainties in the calculated weighted mean ages are reported as 95% confidence limits.

U-Pb zircon LA-MC-ICP-MS - Laboratório de Geocronologia, Universidade de Brasília (UnB), Brazil

In situ U–Pb analyses were performed at the University of Brasília using a Neptune ICP-MS multicollector with a UP213 NewWaveTMlaser ablation probe. Conditions of laser at time of measure were: 9 Hz frequency, 30 μm spot size, and 39–45% energy. The U–Pb

Programa de Pós-Graduação em Geociências

analyses on zircon grains were carried out using the standard-sample bracketing method (Albaréde et al., 2004) using the GJ-1 standard in order to control the ICP-MS fractionation. Two to four samples have been analyzed between GJ-1 standard analyses and $^{206}\text{Pb}/^{207}\text{Pb}$ and $^{206}\text{Pb}/^{238}\text{U}$ ratios have been time corrected. When necessary to correct the laser induced fractionation, the $^{206}\text{Pb}/^{238}\text{U}$ ratio was recalculated using the linear regression method (Kosler et al., 2002). The raw data processed off-line and reduced using an Excel worksheet (Buhn et al., 2009). During analytical session zircon standard UQ-Z1 (Machado & Gautier, 1996) has been analyzed as an unknown sample (1146 ± 47 Ma = $^{207}\text{Pb}/^{206}\text{Pb}$ mean age measured).

3. Artigo 3

Pre-collisional Neoproterozoic (ca.790 Ma) arc magmatism in southernmost Brazil: tectono-stratigraphy of the Várzea do Capivarita Complex

Autores: Mariana Maturano Dias Martil, Maria de Fátima Bitencourt, Lauro Valentim Stoll Nardi, Edinei Koester, Márcio Martins Pimentel.

O objetivo principal deste artigo consistiu em investigar o magmatismo registrado nos ortognaisses do Complexo Várzea do Capivarita. O enfoque petrológico deste trabalho foi dado pelo estudo das fontes e ambientes geotectônicos envolvidos na gênese deste magmatismo. Para tanto, uma abordagem multi-disciplinar foi integrada, incluindo geologia de campo, petrografia, geoquímica de elementos maiores e traços e isótopos de Sr-Nd. Um estudo comparativo com outras associações magmáticas neoproterozóicas existentes no Cinturão Dom Feliciano (CDF) foi também realizado. As associações estudadas foram as seguintes: (i) as rochas de arco do oeste do RS (e.g. Babinski et al. 1996, Saalmann et al., 2005), inclusas no Bloco São Gabriel – BSG (ca. 750-680 Ma – Leite et al., 1998, Hartmann et al., 2011); (ii) os ortognaisses do Cerro Bori (CB – ca. 800 Ma) localizados no sudeste do Uruguai, formados em ambiente de margem continental (Lenz et al., 2011, 2013), (iii) as metavulcânicas ácidas (ca. 800 Ma – Martil et al. a, submit., Saalmann et al., 2011) inclusas nas supracrustais localizadas na porção central do CDF (Complexo Metamórfico Porongos - CMP). A investigação apresentada neste artigo permitiu contribuir para o debate sobre o contexto geotectônico do sul da Província da Mantiqueira, assunto até então controverso na literatura.

Os ortognaisses do Complexo Várzea do Capivarita são rochas cálcio-alcalinas, meta- a peraluminosas, cujo padrão de elementos maiores e traço é compatível com ambiente de arco maduro. Os ortognaisses possuem razões $^{87}\text{Sr}/^{86}\text{Sr}$ (i) variando de 0.71628 a 0.72509 e valores $\epsilon\text{Nd}_{(790)}$ de -7.19 a -10.06. O magmatismo registrado no CVC é compatível com outras sequências de arco Neoproterozóicas, incluindo as metavulcânicas ácidas do CMP e os ortognaisses do CB. Todas essas associações tem assinatura típica de orógenos acrecionários, contendo idade TDM Meso a Paleoproterozóica, além de forte evidência da

Programa de Pós-Graduação em Geociências

participação de processos de assimilação crustal/ contaminação. Desta forma, o conjunto de dados apresentados permite interpretar essas associações como parte do mesmo magmatismo, ou pelo menos como fragmentos de arcos magmáticos similares. Entretanto, o magmatismo registrado no CVC é distinto das sequências de arco continental do BSG, que apresentam assinatura isotópica indicativa de maior contribuição de fontes juvenis neoproterozóicas.

O modelamento binário (*binary mixing models*) realizado neste trabalho indica que o magmatismo estudado teria se originado de fontes mantélicas do tipo EM II. Uma associação de rochas paleoproterozóicas do tipo TTG pertencente ao Complexo Arroio dos Ratos (CAR) é possivelmente o principal contaminante crustal assimilado pelo magmatismo do CVC. Em associação com as idades de herança encontradas no Várzea em ca. 2.0 Ga, é sugerido que a fusão crustal que gerou o magmatismo do CVC em ca. 790-780 Ma foi predominantemente similar ao CAR. O modelamento realizado também indicou que além dos processos de assimilação crustal, a cristalização fracionada também foi importante durante a evolução das fontes magmáticas que geraram os protólitos dos ortognaisses do CVC.

Programa de Pós-Graduação em Geociências

08/08/2016 (20 não lidos) - marianamdmartil - Yahoo Mail

Início Mail Notícias Esportes Finanças Celebridades Vida e Estilo Cinema Respostas Flickr Mais

Todas Buscar Buscar no Mail Buscar na Web Início Mariana

Escrever Resultados da busca Arquivar Mover Apagar Spam Mais

Adicione o Gmail, Outlook, AOL e mais

Caixa de entr... (20) Rascunhos (134) Envíados Arquivo Spam (82) Lixeira (243)

Visualizações inteligentes Importante Não lido FAVORITO Pessoas Social Compras Viagens Finanças

Pastas Recente

LITHOS5644 - Notice of manuscript number

Lithos <ees.lithos.0.387242.52af9b26@eesmail.elsevier.com> Para marianamdmartil@yahoo.com.br Abr 6 em 8:13 AM

Dear Ms. Martil,

Your submission entitled "Pre-collisional, Neoproterozoic (ca. 790 Ma) continental arc magmatism in southernmost Mantiqueira Province, Brazil: tectono-stratigraphy of the Várzea do Capivari Complex" has been assigned the following manuscript number: LITHOS5644.

You will be able to check on the progress of your paper by logging on <http://ees.elsevier.com/lithos/> as Author.

Thank you for submitting your work to this journal.

Kind regards,

Lithos

Responder Responder a todos Encaminhar Mais

Clique para Responder, Responder a todos ou Encaminhar

Enviar

Pre-collisional, Neoproterozoic (ca. 790 Ma) continental arc magmatism in southernmost Mantiqueira Province, Brazil: tectono-stratigraphy of the Várzea do Capivarita Complex

Mariana Maturano Dias Martil^{a1}, Maria de Fátima Bitencourt^b, Lauro Valentim Stoll Nardi^b, Edinei Koester^b, Márcio Martins Pimentel^c.

a - Programa de Pós-Graduação em Geociências, Instituto de Geociências, Universidade Federal do Rio Grande do Sul, Av. Bento Gonçalves, 9500, Porto Alegre 91500-000, RS, Brazil.

b - Centro de Estudos em Petrologia e Geoquímica, Instituto de Geociências, Universidade Federal do Rio Grande do Sul, Av. Bento Gonçalves, 9500, Porto Alegre 91500-000 RS, Brazil.

c- Instituto de Geociências, Universidade de Brasília, Brasília DF 70910-900, Brazil.

¹Corresponding author. Programa de Pós-Graduação em Geociências, Instituto de Geociências, Universidade Federal do Rio Grande do Sul, Av. Bento Gonçalves, 9500, Porto Alegre 91500-000, RS, Brazil. E-mail address: marianamdmartil@yahoo.com.br (M.M.D. Martil).

Abstract

This paper focuses on the pre-collisional mature arc magmatism (ca. 790 Ma) recorded in tonalitic to granitic gneisses from the Várzea do Capivarita Complex (VCC), southern Mantiqueira Province (PM), Brazil. The complex comprises a compositional and age variety of ortho- and paragneisses tectonically interleaved during a transpressive high grade regime (ca. 650 Ma), possibly related to an oblique collision event. In order to investigate the magmatic sources and evolutionary processes of the VCC orthogneisses, a multi-disciplinary approach is taken which includes field geology, petrography, major and trace-element geochemistry and Sr-Nd isotope data. The VCC orthogneisses are metaluminous to peraluminous, calc-alkaline rocks, with high $^{87}\text{Sr}/^{86}\text{Sr}$ (_(i)) ratios from 0.71628 to 0.72509 and

Programa de Pós-Graduação em Geociências

$\varepsilon_{\text{Nd}}^{(790)}$ values from -7.19 to -10.06. VCC magmatism is correlated with other ca. 800 Ma arc sequences from southern PM, including part of the Porongos Metamorphic Complex (PMC) metavolcanic rocks and the orthogneisses from Cerro Bori (CB). All these associations show signatures typical of accretionary orogens, TDM and Meso to Paleoproterozoic inheritance ages, and present strong evidences of crustal assimilation/contamination. The higher contents of K in VCC and PMC rocks, and the tendency to move toward the post-collisional field in the geotectonic diagrams suggest that they were generated in thick-crust, mature arc environments. In contrast, the CB sequence exhibits have a less mature continental-arc character, suggestive of thinner crust or next to the active margin. VCC and CB orthogneisses and part of the PMC metavolcanic rocks may be interpreted as part of the same magmatism, or at least as fragments of similar magmatic arcs. However, VCC magmatism is distinct from continental arc sequences in the São Gabriel Block (ca. 700-750 Ma). Isotope signatures from this younger magmatism indicate major contribution of Neoproterozoic juvenile sources, with only little amounts of reworked old continental crust. In addition to the evidence of similarity between the VCC and the PMC magmatism, geochemical and Sr-Nd signatures presented in this paper suggest that at least part of the PMC metavolcanic rocks may represent the protoliths of the high grade orthogneisses present in Várzea do Capivarita Complex. This, together with the isotope evidence of similarity between VCC and PMC igneous and sedimentary fractions, corroborates the hypothesis that the VCC and PMC are, at least in part, expressions of the same context, wherein the magmatic and sedimentary activity occurred in a single continental arc environment. Binary mixing models indicate that the VCC magmatism originates from evolved EM II mantle sources. A Paleoproterozoic TTG association (ca. 2.0 Ga) from the Arroio dos Ratos Complex (ARC) - seems to be the main crustal contaminant assimilated by the VCC magmatism. Together with the small inheritance contribution at ca. 2.0, this suggests that the melted crust at ca. 790-800 Ma was predominantly like ARC. Our models also indicate that in addition to crustal assimilation processes, fractional crystallization was important during the VCC magmatism evolution.

Key-words: high grade orthogneisses; pre-collisional magmatism; continental arc setting; southern Mantiqueira Province; Neoproterozoic arc magmatism.

1. Introduction

The study area is located in the southern segment of the Mantiqueira Province (MP – Fig. 1), and is largely composed of Neoproterozoic granitic rocks intrusive in a metamorphic basement of predominant Paleoproterozoic age (Hartmann et al., 1999, Soliani Jr. et al., 2000). The MP was constructed during the Brasiliano / Pan-African Orogenic Cycle whose evolution is mainly characterized by diachronic episodes of subduction and arc-continent or continent-continent collision (Heilbron et al., 2004). In the southern segment of MP, this orogenic cycle is characterized by arc magmatism between 900 and 700 Ma (*e.g.* Leite et al., 1998, Lenz et al., 2011, Siviero et al., 2009), and by voluminous post-collisional magmatism active from 650 to 580 Ma (Bitencourt and Nardi, 2000). High grade, collision-related metamorphism is dated at ca. 650-620 Ma (*e.g.* Lenz et al., 2011; Martil et al., submitted a; Philipp et al., 2016). Although the events leading to the formation of the province have been the subject of numerous studies over the past decades, the discrimination of accretionary episodes in the southern Mantiqueira Province is still matter of investigation.

This paper focuses on the pre-collisional magmatism registered in a high grade complex – the Várzea do Capivarita Complex (VCC - Fig. 1, area 1) which represents, according to Martil et al. (submitted a), a Neoproterozoic mature arc association, dated at ca. 790 Ma. In order to investigate the magmatic sources and evolutionary processes of this unit, a multi-disciplinary approach is taken, including field geology, petrography, major and trace-element geochemistry and Sr-Nd isotope data. The correlation with other arc-related terrains in southern Brazil and southeastern Uruguay is established. In order to study the magmatic sources of the orthogneisses from Várzea do Capivarita Complex, binary mixing models were carried out. Determination of the spatio-temporal relations is achieved by integrating these results with other data obtained for the Várzea do Capivarita Complex, including structural (Martil et al., submitted b), U-Pb zircon geochronological data (Martil et al., submitted a) as well as other isotopic and field data (Martil et al., submitted c).

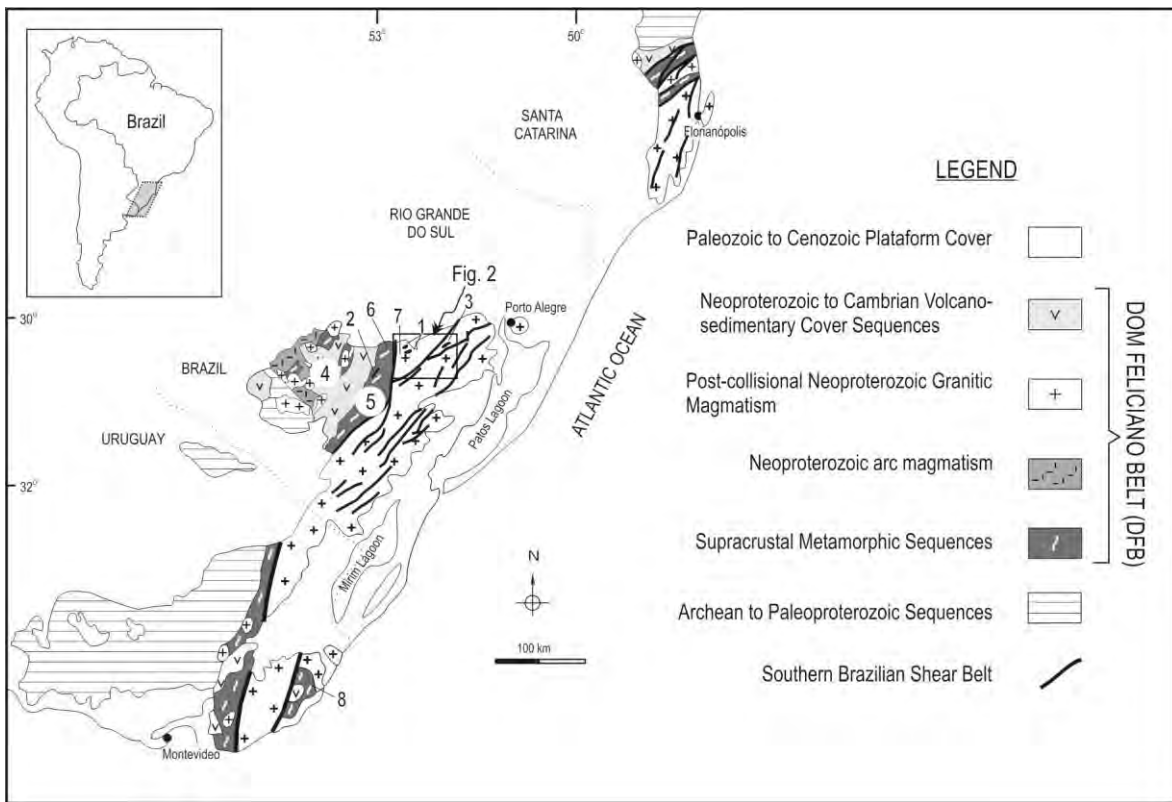


Figure 1 – Main tectonic domains for Southern Mantiqueira Province, with location of figure 2 indicated (modified from Nardi and Bitencourt, 2007). 1 - Várzea do Capivarita Complex, 2 - Encantadas Complex, 3 – Arroio dos Ratos Complex, 4 - São Gabriel Block, 5 – Porongos Metamorphic Complex, 6 – northern Porongos Metamorphic Complex (studied by Goollmann et al., 2008), 7 – Porongos Metamorphic Complex (studied by Martil et al., submitted c); 8 – Cerro Bori orthogneisses.

2. Geological Setting

The distribution of major lithological domains in the southern MP segment indicates the occurrence of Archean to Paleoproterozoic rocks in northeast Santa Catarina (SC), in southwestern Rio Grande do Sul (RS) and in a larger area of the Uruguayan Shield (Fig. 1). In western RS, Neoproterozoic rock sequences are attributed to a juvenile arc (e.g. Babinski et al. 1996, Saalmann et al., 2005a,b), which evolves to post-collisional environment (Garavaglia et al., 2006, Nardi and Bitencourt, 2007). Ages of magmatic-arc activity in this area vary between 750 and 680 Ma (e.g. Hartmann et al., 2011, Leite et al., 1998); however, ages between 900-850 Ma have also been described and interpreted as part of the initial records of the arc magmatism (e.g. Leite et al., 1998; Siviero et al., 2009).

A narrow strip of supracrustal, amphibolite facies metamorphic rocks (Fig. 1) occurs in the central region of the MP southern segment. In RS, this area consists of metapelites, quartzites, metavolcano-sedimentary and metavolcanic rocks. Interpretations of this association tectonic setting to date are controversial, and range from passive margin (Jost and Bitencourt, 1980), passive margin and/or intracontinental setting (Gruber et al., 2011, Hartmann et al., 2004, Saalmann et al., 2006) to back-arc basin (Babinski et al., 1997, Fernandes et al., 1992a,b, Hartmann et al., 1999, Gollmann et al., 2008, Marques et al., 1998,). Provenance studies for metasedimentary rocks in this region indicate a variety of source areas, with significant contribution of Paleo- to Mesoproterozoic ages (Gruber et al., 2011, Hartmann et al., 2004, Pertille et al., 2015, Saalmann et al., 2011). According to Pertille et al. (2015) depositional activity in this area took place in a foreland tectonic setting at 650-570 Ma.

The eastern portion of the MP is represented by a granitic belt that extends from southern Brazil to Uruguay (Fig.1). According to Bitencourt and Nardi (1993, 2000), this granitic belt developed between 650 and 580 Ma in a post-collisional setting. The igneous activity was probably controlled by a set of translithospheric structures known as the Southern Brazilian Shear Belt (SBSB - Fig. 1), being closely associated with transpressive tectonics of the Brasiliano / Pan-African Cycle.

2.1.Paleoproterozoic to Mesoproterozoic magmatism prior to the Várzea do Capivarita Complex

At least two Paleoproterozoic orthogneiss associations of typical continental magmatic-arc signature are recognized (Table 1, Fig.1): the Encantadas Complex (EC, studied by Philipp et al., 2008, among others) and the Arroio dos Ratos Complex (ARC – as defined by Gregory et al., 2011), both compositionally comparable to TTG associations. The EC (Fig. 1, area 2) is exposed as a stratigraphic window in between supracrustal metamorphic rocks, whilst the ARC (Fig. 1, area 3) forms septa and roof pendants on granitoids associated with the Southern Brazilian Shear Belt. SHRIMP U-Pb zircon data from the Encantadas Complex indicate crystallization age of 2234 ± 28 Ma and metamorphism between 2.0 - 2.1 Ga (Saalmann et al., 2011). Petrological and tectonic data for the EC are compatible with parental

Programa de Pós-Graduação em Geociências

magmas derived from the mantle metasomatized by subduction-related fluids in a continental-arc setting (Philipp et al., 2008).

In the ARC three metaigneous associations were described by Gregory et al. (2015) with ages between 2150 ± 28 and 2077 ± 13 Ma (U-Pb LA-MC-ICP-MS data in zircon). The metaigneous associations have $^{87}\text{Sr}/^{86}\text{Sr}_{(i)}$ ratios between 0.701 and 0.715, positive $\Sigma\text{Nd}_{(t)}$ values (+0.47 to +5.19), and T_{DM} ages close to the crystallization ages which indicate the juvenile nature of the parental magma (Gregory et al., submitted). According to these authors, the major and trace element geochemical data, as well as the isotopic data for ARC rocks suggest an origin by melting of a metasomatized mantle (E-MORB type).

The Capivarita Anorthosite (CA) is an extension-related, Mesoproterozoic intraplate association described in the southern MP (Table 1, Fig. 2). For this association, U-Pb zircon data yielded magmatic ages between 1573-1530 and metamorphic ages of 660-601 Ma (Chemale et al., 2011). Babinski et al. (1997) report a T_{DM} age of 2.0 Ga for the anorthosite.

Paleoproterozoic to Mesoproterozoic magmatism prior to the Várzea do Capivarita Complex

Unity	Localization	Rock type	Petrological interpretation	Sr-Nd Isotopic data	Crystallization age	Metamorphic age	Tectonic interpretation
Encantadas Complex (EC) ^a	Fig.1, area 2	Dioritic, tonalitic and trondhjemitic gneisses	TTG – type rock associations	$^{87}\text{Sr}/^{86}\text{Sr}_{(i)} = 0.725262$ to 0.713693 $\Sigma\text{Nd}_{(0)} = -34.2$ to -20.8 and $T_{\text{DM}}=2.4$ to 2.1 Ga	U-Pb LA-MC-ICP-MS zircon 2.2 Ga	U-Pb LA-MC-ICP-MS zircon 2.0-2.1 Ga	Continental arc setting
Arroio dos Ratos Complex (ARC) ^b	Fig.1, area 3	Tonalitic to granodioritic gneisses	TTG – type rock associations	$^{87}\text{Sr}/^{86}\text{Sr}_{(i)} = 0.725262$ to 0.713693 $\Sigma\text{Nd}_{(0)} = -34.2$ to -20.8 and $T_{\text{DM}}=2.3$ to 2.0 Ga	U-Pb LA-MC-ICP-MS zircon 2.1 – 2.0 Ga	-	Continental arc setting
Capivarita Anorthosite (CA) ^c	Fig.2	Anorthosite	Intraplate magmatism	$\Sigma\text{Nd}_{(0)} = -22.6$ and $T_{\text{DM}}=2.0 \text{ Ga}^d$	U-Pb LA-MC-ICP-MS zircon 1573-1530 Ma	U-Pb LA-MC-ICP-MS zircon 660-601 Ma	Extensional setting

a-From Philipp et al. (2008); b- From Gregory et al. (2015, submitted); c-From Chemale et al. (2011); d- From Babinski et al. (1997).

Table 1 – Paleoproterozoic to Mesoproterozoic magmatism prior to the Várzea do Capivarita Complex.

2.2. Neoproterozoic Arc Magmatism

In the southern MP, Neoproterozoic arc magmatism is restricted to southern Brazil and Uruguay (Table 2), as indicated by areas 4 to 8 in Fig. 1.

In southern Brazil (area 4, Fig. 1), it comprises the São Gabriel Block (e.g. Hartmann et al., 2011), where metamorphosed calc-alkaline diorites, tonalites, trondhjemites and granodiorites are intrusive into amphibolite facies metavolcano-sedimentary rocks. Both intrusive and metavolcanic rocks have similar chemical and isotopic composition, and are interpreted as the roots of a magmatic arc (e.g. Babinski et al., 1996). U-Pb zircon dating has yielded values between 680 and 750 Ma for this magmatism (LA-MC-ICP-MS and SHRIMP - Babinski et al., 1996, Hartmann et al., 2011, Leite et al., 1998, Saalmann et al., 2011). Tonalitic calc-alkaline gneisses show $\varepsilon_{\text{Nd}}(t)$ values of +4.34 and +6.3, T_{DM} model ages of 0.89 and 0.72 Ga and $^{87}\text{Sr}/^{86}\text{Sr}_{\text{i}}$ values spread between 0.7000 and 0.70489 (Saalmann et al., 2005a). Major element composition of the ortho-derived rocks indicates a subalkaline character; most orthogneisses have calc-alkaline affinity, and many metavolcanic rocks show signatures of low-K tholeiitic volcanic arc basalts. Relative enrichment in light rare earth elements (LREE), low contents of Nb and other high-field-strength elements, and enrichment in large ion lithophile elements (LILE) are interpreted by Saalman et al. (2005b) as indicative of origin in a subduction zone setting.

Neoproterozoic arc magmatism is also described in the Porongos Metamorphic Complex (Fig. 1, areas 5, 6 and 7). It comprises metapelites, quartzites and acidic to intermediate metavolcanic rocks. The most comprehensive work on the Porongos rocks is that of Saalmann et al. (2006 - Fig. 1, area 5), whilst Gollmann et al. (2008) investigated only the northern part of the Complex (Fig. 1, area 6) and the work of Martil et al. (submitted c) discusses the acidic metavolcanics (Fig. 1, area 7).

The metavolcanic rocks studied by Saalmann et al (2006) are described as subalkaline rhyolites with LREE enrichment and flat HREE patterns similar to those found in rocks of the upper continental crust. Contents of HFS elements, such as Nb and Zr, are slightly lower when compared with those of the average upper continental crust. When normalized to MORB, these rocks exhibit strong enrichment in incompatible and LILE elements. U-Pb zircon data indicate crystallization age of 789 ± 7 Ma (Saalmann et al., 2011 - LA-MC-ICP-MS). Isotope data have lead these authors to recognize two distinct groups: units exposed to

Programa de Pós-Graduação em Geociências

the northwest show $\epsilon_{\text{Nd}}(t=780 \text{ Ma})$ values of -20.6 to -21.7 whereas those in the southeast ones have $\epsilon_{\text{Nd}}(t=780 \text{ Ma}) = -6.9$. Together with trace-element data, the high $^{87}\text{Sr}/^{86}\text{Sr}_{(\text{i})}$ values (0.7064 to 0.7286) support the authors' interpretation of partial melting of, or considerable contamination by, old continental crust during magma generation and evolution.

In the area studied by Gollmann et al. (2008) four groups of felsic to intermediate metavolcanic rocks were identified, here referred as PMC-1, PMC-2, PMC-3, and PMC-4. Rocks of the first three groups are interpreted as formed in an active continental margin magmatic arc due to their LILE- and LREE-enrichment, together with HREE- and HFSE-depletion. $\epsilon_{\text{Nd}}(t = 770)$ values vary from strongly negative (-20) to moderately negative (-6 to -11), with T_{DM} ages ranging from Paleo- to Mesoproterozoic. The fourth group has similar geochemistry features compared with the other groups, but $\epsilon_{\text{Nd}}(t)$ values are slightly negative (-2 to -4) and model ages are restricted to Mesoproterozoic values.

In area 7 (Fig. 1), PMC acidic metavolcanic rocks near the Piquiri Syenite Massif - PSM (Fig.2) are interpreted by Martil et al. (submitted c) to represent the protoliths of the high grade VCC orthogneisses. Provenance studies by the same authors indicate the volcano-sedimentary character of the VCC and that the original pelites are coeval with the orthogneisses. These conclusions are supported by structural, as well as δO^{18} isotope and U-Pb SHRIMP data. Therefore, a genetic link is established between the VCC and the PMC units.

The Cerro Bori high-grade orthogneisses (CB) (Fig. 1, g 8), in Uruguay, which may also be compared with the VCC, comprise tectonically interleaved, arc-related, calc-alkaline, tonalitic and granodioritic gneisses, which are dominant over tholeiitic and ultrapotassic mafic gneisses, as described by Lenz et al. (2013). The calc-alkaline gneisses are enriched in LILE relative to HFS elements, with negative Nb-Ta and Ti anomalies. Negative ϵ_{Nd} values (-2.12 and -6.67), and old T_{DM} model ages (1.29 and 2.09 Ga) are interpreted by these authors as indicative of crustal assimilation/contamination as an important process, together with fractional crystallization. Age data reported by Lenz et al. (2011) comprise U-Pb SHRIMP zircon magmatic ages between ca. 800 and 767 Ma, metamorphic ages of 673 - 666 Ma and partial melting at 654 ± 3 Ma (U-Pb SHRIMP in zircon).

Neoproterozoic Arc Related Associations (ca. 800-700 Ma) in Southern Mantiqueira Province

Unit	Localization	Rock type	Petrological interpretation	Isotopic data	Crystallization age	Metamorphic age	Inheritance ages	Tectonic interpretation
São Gabriel ^a (SG)	Fig.1, area 4	Dioritic, tonalitic, trondhjemitic and granodioritic gneisses and metavolcano -sedimentary sequences	Calc- alkaline or tholeiitic. Ultramafic- relics of OIB	$^{87}\text{Sr}/^{86}\text{Sr}_{\text{J}} =$ 0,7000 to 0,7085 $\epsilon\text{Nd}_{\text{J}} = 4.34$ to 6.3 and TDM=0.89 to 0.72 Ga*	701-750 Ma	-	792-896 Ma	2 suites: Continental Arc and Oceanic Island Arc. Relics of Intraplate magmatism.
Porongos Metamorphic Complex (PMC) ^b	Fig. 1, areas 5 to 7	Metavolcanic rocks from volcano- sedimentary sequence	Calc- alkaline associated tominor OIB- MORB basalts	$^{87}\text{Sr}/^{86}\text{Sr}_{\text{J}} =$ 0.7064 to 0.7286 $\epsilon\text{Nd}_{\text{J}} =$ -20.64 to -21.72 (NW), -6.87 (SE) and -20 to -2 (northern)	780-790 Ma	-	2.0	Controversial: passive margin, continental rift environment, continental arc setting
Cerro Bori (CB) ^c	Fig. 1, area 8	Tonalitic and granodioritic gneisses associated with mafic and ultramafic rocks	Calc- alkaline associated with tholeiitic and ultrapotassic associations	$\epsilon\text{Nd}_{\text{J}} = -2.12$ to -6.67 TDM=1.2 to 2.0 Ga	770-800 Ma	670-650 Ma	1.0 to 2.2 Ga	Continental arc magmatism early phase

Table 2 – Neoproterozoic arc-related associations (ca. 800-700 Ma) in Southern Mantiqueira Province.

3. Geology of the Várzea do Capivarita Complex

The Várzea do Capivarita Complex (Fig. 2) comprises pelitic and calesilicate paragneisses which predominate over the orthogneisses. Subordinate volumes of syntectonic syenites are also part of the complex. The lithological types are tectonically interleaved as tabular or lenticular, decimeter- to meter-thick slices (Martil et al., 2011, Martil et al., submitted b).

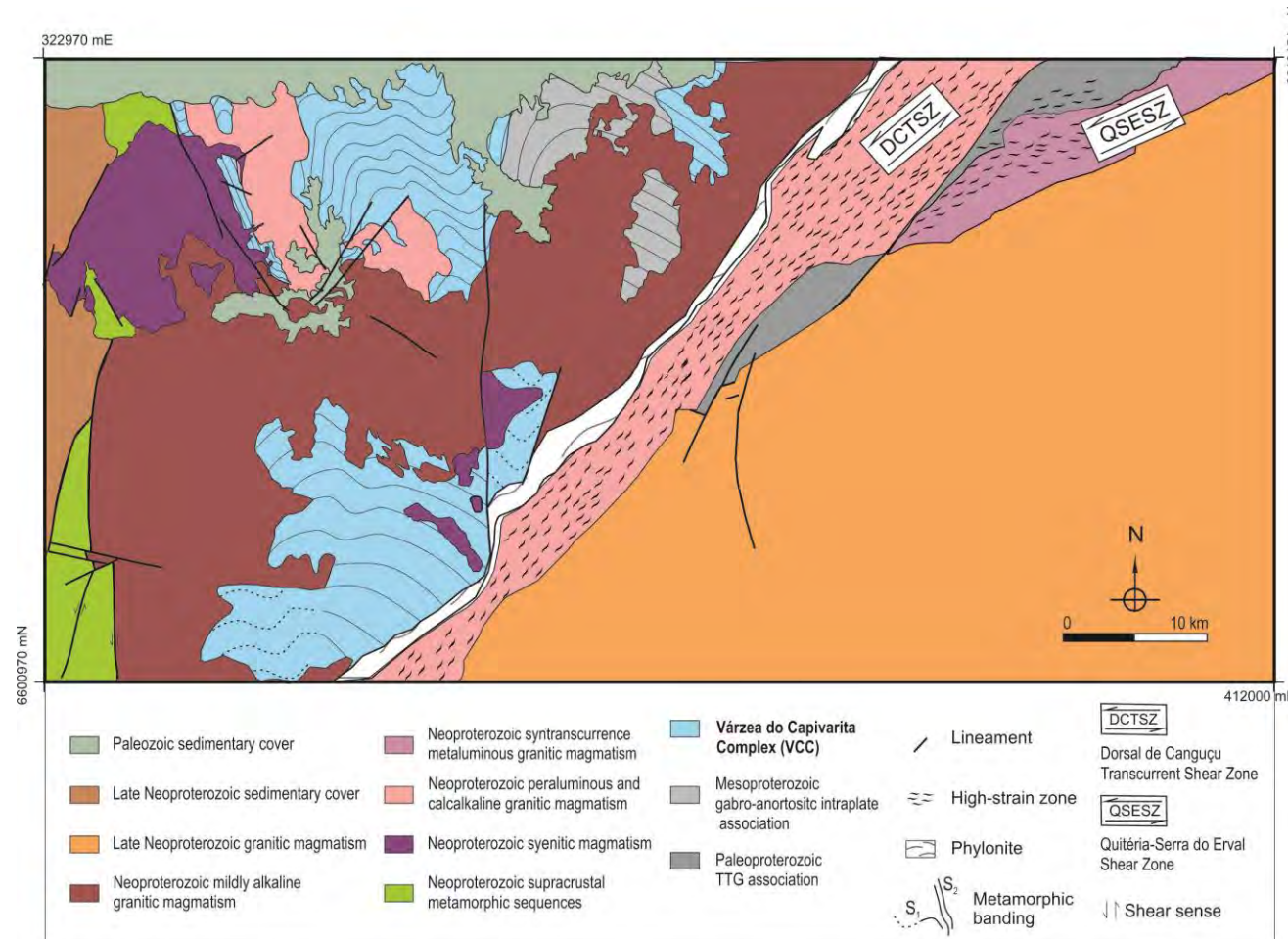


Figure 2 – Regional setting of the Várzea do Capivarita Complex featuring its areal extension and surrounding units. Porongos Metamorphic Complex area 7 indicated.

The VCC metapelites are finely laminated rocks, with mafic and felsic layers. They also contain calcsilicate bands that commonly form disrupted, elongate boudins (Fig. 3a). The metapelitic high grade paragenesis is garnet + cordierite + spinel (Fig. 3b), whilst calcsilicate gneisses have more variable composition, containing sometimes pyroxene-rich bands alternated with fine-grained bands of biotite and Mg-rich amphibole. Although local partial melting evidences are found in all VCC lithological types, as already mentioned by Silva et al. (2002), they are more frequent in the pelitic gneiss, as irregular, garnet-bearing, leucogranitic pockets.

The orthogneisses are fine- to medium-grained rocks (Fig. 3c and Fig. 3d) and comprise tonalitic to granitic compositions. The metamorphic banding is marked by alternating mafic and felsic, mm-thick, regular bands and contains a well-developed stretching lineation (L_X - Fig. 3e) marked by quartz-feldspathic lenticular aggregates. Grain-size banding is also common. Successive generations of granitic veins enhance deformational features.

The dominant texture is polygonal granoblastic (Fig. 3f), with well-developed chessboard pattern quartz subgrains in all compositional types. In the tonalitic gneisses (Fig. 3c) felsic bands contain plagioclase, K-feldspar and quartz, while biotite, hypersthene (Fig. 3g), and diopside are found in the mafic ones. The foliation is sigmoidal and contours plagioclase lenses and quartz large grains. The paragenesis Pl + Bt + Kfs + Qtz + Opx + Cpx indicates metamorphism under granulite facies conditions. In rocks of granitic compositions, biotite is the dominant mafic phase, and garnet occurs as fine-grained crystals. Ribbon-like feldspar and quartz are common (Fig. 3h).

The regional structural framework is marked by two foliations, S_1 and S_2 , formed progressively, under granulite facies conditions. S_1 is an originally sub-horizontal, NNW-trending gneissic banding (Fig. 3c, 4a and 4b) formed during a thrust event – D_1 which resulted in the interleaving of the VCC rocks and development of strong stretching lineations L_{X1} (Fig. 3e and 4a). In areas where the original sub-horizontal position of S_1 is preserved, kinematic indicators, such as feldspar porphyroclasts and intrafolial fold asymmetry indicate top-to-the-W shear sense. The scattering of L_{X1} along a single girdle (Fig. 4a) is due to regional development of F_2 folds. They are nearly upright, asymmetric folds with sub-horizontal, NNW-plunging axis (Fig. 4b) whose axial-planar cleavage grades onto a dextral transposition cleavage (Fig. 4c), and eventually forms a steeply-dipping, S_2 , penetrative

Programa de Pós-Graduação em Geociências

foliation. Progressive dextral shearing along S_2 leads to the formation of regional, strike-slip, NNW-trending shear zones, the most obvious D_2 structural feature (Fig. 4d).

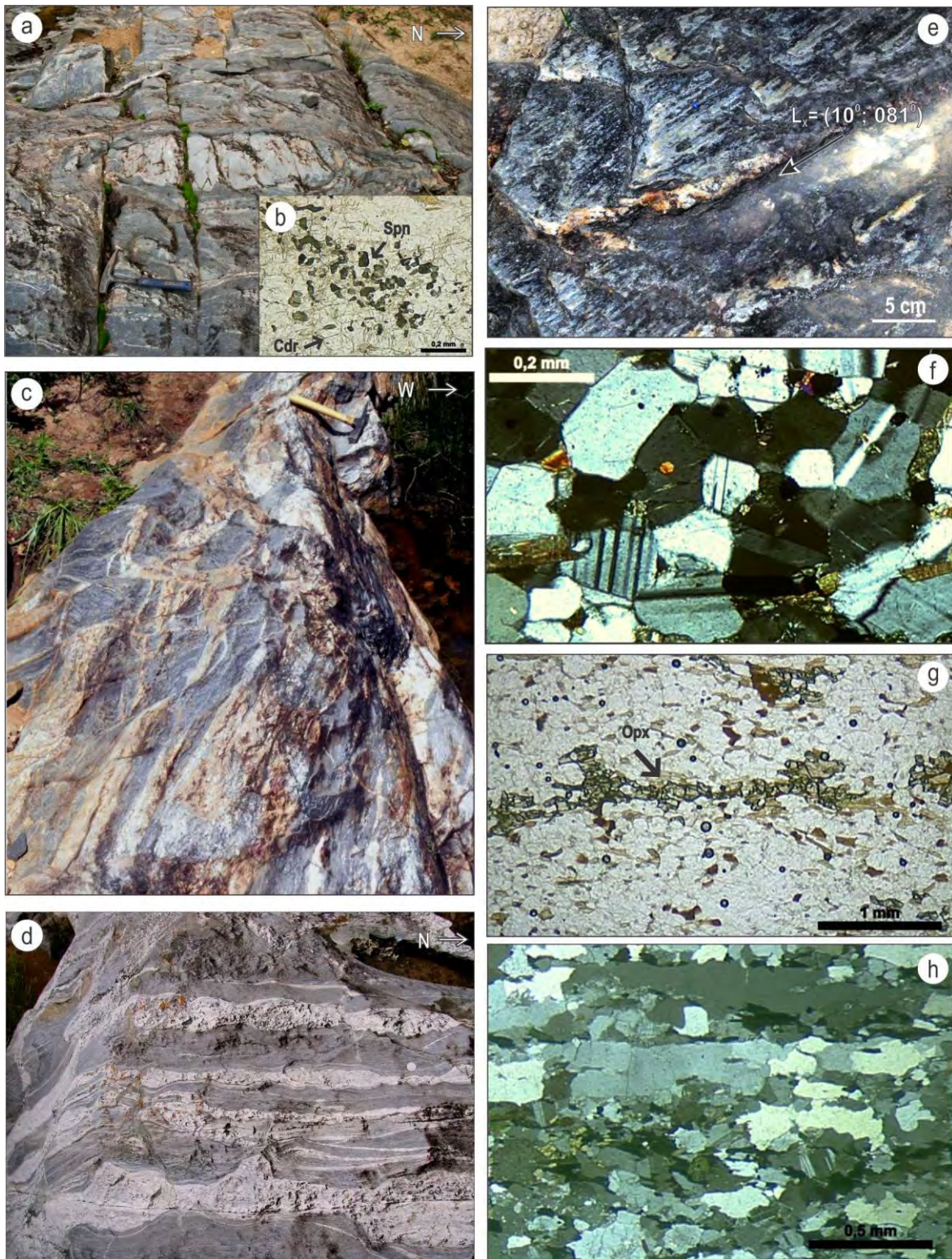


Figure 3 – Main features of the Várzea do Capivari Complex gneisses. (a) Disrupted and partly rotated calc-silicate bands in pelitic gneiss. (b) XZ-plane thin section of metapelite high grade

Programa de Pós-Graduação em Geociências

paragenesis, with cordierite (Cdr) and spinel (Spn) indicated. (c) Tonalitic gneiss with sub-horizontal metamorphic banding. (d) Granitic gneiss with concordant, deformed leucogranitic veins. (e) Pronounced stretching lineation in orthogneiss. (f) Well-developed polygonal texture in orthogneiss. (g) X-Z plane thin section from tonalitic gneiss showing orthopyroxene (Opx) grains aligned parallel to L_x. (h) Granitic gneiss with ribbon-like quartz in elongate grains along the foliation.

Ultrahigh temperature (850-1000 °C) and medium pressure (6 to 11 kbars) conditions are reported for the VCC metapelites by Bom et al. (2014). Philipp et al. (2016) based on the paragenesis garnet-cordierite-sillimanite-biotite, established metamorphic conditions at 720-820° C and of 8 to 9 kbar, characterizing it as of intermediate pressure and high temperature series. Metamorphic age values obtained from Sm-Nd garnet-whole rock data in metapelites are reported by Gross et al. (2006) and range from 604 to 652 Ma, with high associated error, and peak value is interpreted as ca. 604-626 Ma. From the same rock sequence, U-Pb SHRIMP data are reported by Philipp et al. (2016), comprising metamorphic age of 619 ±4.3 Ma. A 620 ±6.3 Ma zircon age from a leucogranite vein is interpreted to indicate partial melting of this sequence. Zircon data reported by Martil et al. (submitted a) for the VCC othogneisses indicate metamorphism at 648 ± 5.4 Ma and magmatic age of *ca.* 790 Ma (U-Pb zircon SHRIMP). T_{DM} model ages (2236 and 1586 Ma – Gross et al., 2006) show predominantly Paleoproterozoic to Mesoproterozoic sources for the VCC metasedimentary rocks.

The VCC orthogneisses and part of the pelitic gneisses were previously interpreted by Martil et al. (2012, submitted a, c) to represent products of pre-collisional, 790 Ma continental arc magmatism. Their modern structural configuration most likely results from a transpressive regime, possibly indicative of an oblique collision event at *ca.* 650 Ma.



Figure 4 – Várzea do Capivarita Complex structural features. (a) Lower hemisphere, equal-area contour plot diagram for the distribution of poles to banding – S_1 indicating preferred orientation along NNW-striking planes of low to moderate dip. The stretching lineation (L_{x1}) is scattered along a single girdle due to regional folding (F_2). (b) Asymmetric folds (F_2) in paragneisses, close to the profile plane,

with poorly-developed axial-planar cleavage. (c) Dextral shearing of orthogneisses along well-developed, axial-planar transposition cleavage (S_2). (d) Lower hemisphere, equal-area contour plot diagram showing distribution of poles to S_2 foliation and L_{x2} lineation which are the main features of D_2 strike-slip deformation.

4. Analytical Procedures

4.1. Major and trace elements

Major and trace element analyses were carried out at AcmeLabs™, Canada, using the techniques of ICP-OES (Inductively Coupled Plasma Optical Emission Spectrometry) for major elements and ICP-MS (Inductively Coupled Plasma Mass Spectrometry) for trace and rare earth elements, after fusion with metaborate/tetraborate. Accuracy better than 2% and 10% was obtained for the major and trace element, respectively. Analytical procedures followed those of Jeffery and Hutchison (1981).

4.2. Sr and Nd isotopes

Rb-Sr and Sm-Nd isotope data for tonalitic/granitic gneisses, and for metavolcanic rocks (Table 3) were obtained at the Laboratório de Geologia Isotópica of the Universidade Federal do Rio Grande do Sul (UFRGS) and the Laboratório de Geocronologia of the Universidade de Brasília (UnB) using thermal ionization mass spectrometry, respectively a VG Sector 54 multicollector and a Finnigan MAT 262 multicollector mass spectrometer. Rb-Sr and Sm-Nd isotope determinations followed the method described by Gioia and Pimentel (2000). Whole rock samples were powdered in agate mortar in order to produce rock powders finer than 200 mesh. Samples were then weighted and spiked with mixed $^{149}\text{Sm}/^{150}\text{Nd}$ and $^{87}\text{Rb}/^{84}\text{Sr}$ tracers and dissolved in concentrate HF-HNO₃ and HCl in 7 mL Teflon vials on a hot plate for seven days. After complete digestion, the samples were dried down and redissolved in 2.5 N HCl. Rb, Sr and REE were separated using standard cation exchange columns with a DOWEX AG 50X8 resin (200-400 mesh). Nd and Sm were separated from the other REE in exchange columns with HDEHP LN resin (50-100 μm) and 0.18 N HCl for Nd and 0.5 N HCl for Sm. Rb, Sr and Sm were run on Re single filaments while Nd isotopes was run on Ta-Re-Ta triple filaments. Rb was deposited with HNO₃, while Sr, Sm and Nd

with H_3PO_4 , and the former also were deposited with silica gel. Sr isotopes were compared to the Sr standard (NBS 987) which yielded values of $^{87}Sr/^{86}Sr$ of 0.71026 ± 0.000011 (1σ ; $n = 100$) and the fractionation was corrected using $^{86}Sr/^{88}Sr = 0.1194$. La Jolla Nd standard measures obtained was 0.511848 ± 0.000021 (1σ ; $n = 100$) and isotopic ratios were normalized to $^{146}Nd/^{144}Nd = 0.7219$. Blanks used for Rb and Sm are < 500 pg, for Sr < 60 pg, for Nd < 150 pg. Typical analytical errors for $^{87}Rb/^{86}Sr$ and $^{147}Sm/^{144}Nd$ ratio are equal or better than 0.1 %. Nd model ages were calculated according to De Paolo (1981). The decay constants used were those recommended by Steiger and Jäger (1977) and Wasserburg et al. (1981). Error for all isotope data presented in Table 3 are better than 0.0010 (SD absolute) for $^{87}Rb/^{86}Sr$, 0.000016 (SD absolute) for $^{87}Sr/^{86}Sr$, 25 ppm for Sm/Nd, 20 ppm for $^{143}Nd/^{144}Nd$ and lower than 0.0020 (SD absolute) and average of analyses was in general 10 blocks of 10 analyses ($n = 100$).

5. Results

5.1. Major and trace element geochemistry

Twenty-six samples were selected to represent the compositional varieties of VCC orthogneisses. Complete major and trace element compositions are presented as supplementary data A. Two metavolcanic samples located southwest of the Piquiri Syenite Massif (area 7, Fig. 1 and Fig. 2) are included for comparison.

The VCC orthogneisses are metaluminous to peraluminous, calc-alkaline rocks. Their composition and trace-element patterns are compatible with a continental-arc magmatism, with crustal contamination pointed by high contents of Rb, Cs and Na₂O (Martil et al., 2011).

The composition of the VCC rocks was compared with that of rocks comprising other Neoproterozoic arcs from the southern Mantiqueira Province, including the São Gabriel Block – SGB, the Porongos Metamorphic Complex – PMC and the Cerro Bori – CB. Most samples from these arcs are peraluminous, with A/CNK values between 1.0 - 1.5. Metavolcanic rocks from the PMC tend to be more peraluminous, with A/CNK values between 1.2 and 1.8.

All samples plot in the subalkaline field of the TAS diagram; PMC is slightly enriched in alkalis (Na₂O + K₂O ca. 6.0 wt %), CB rocks are relatively depleted (Na₂O + K₂O close to 2.5% wt %), and VCC orthogneisses show intermediate values. Metaigneous rocks of the

Programa de Pós-Graduação em Geociências

SGB have variable compositions: there is a group which plots in the andesitic basalt field and others in the dacite-rhyolite field, together with the other associations.

When comparing groups of similar SiO₂ values (61-72 wt %) in a K₂O vs SiO₂ diagram (Fig. 5 - Le Maitre, 2002), the VCC orthogneisses, as well as the PMC metavolcanic rocks, plot in the fields of medium- to high K-series, with the leucocratic samples tending to present lower values of K₂O, which is probably due to the larger fractionation of K-rich mineral assemblages in the late stages of differentiation. CB and SGB rocks plot mostly in the medium-K field. The medium- to high-K character of most rocks in these magmatic arcs suggests that they are predominantly continental arcs, and that VCC and PMC original magmas are the products of melting of more evolved sources. K₂O/Na₂O ratios, as well as Na₂O+K₂O, show the same behavior, which is consistent with this evolution. R1-R2 chemical parameters show that the PMC rocks have compositions which are equivalent to rhyolites, whilst most of VCC, SGB, and CB rocks are dacitic or rhyodacitic. Some basic rocks of the SGB magmatic-arc association show compositions of tholeiites, which suggests an association with oceanic arc magmatism, as proposed by Saalman et al. (2005b). The calc-alkaline affinity of most of the studied associations is indicated in diagrams such as CaO/(Na₂O+K₂O) vs SiO₂, (Fe +Ti - Al - Mg) (Jensen, 1976), AFM plot (Irvine and Baragar, 1971), and SiO₂ vs FeOt/MgO (Myashiro, 1974). In the diagrams of Pearce et al. (1984 – Fig. 6) the VCC, CB, and SGB rocks plot in the field of volcanic arc magmatic rocks, and the PMC samples plot close to the more evolved continental-arc magmatism of New Guinea. The same parameters indicate that according to Peacock's classification, except for PMC, which tend to alkali-calcic, the rocks of VCC, CB and SGB are calc-alkaline.

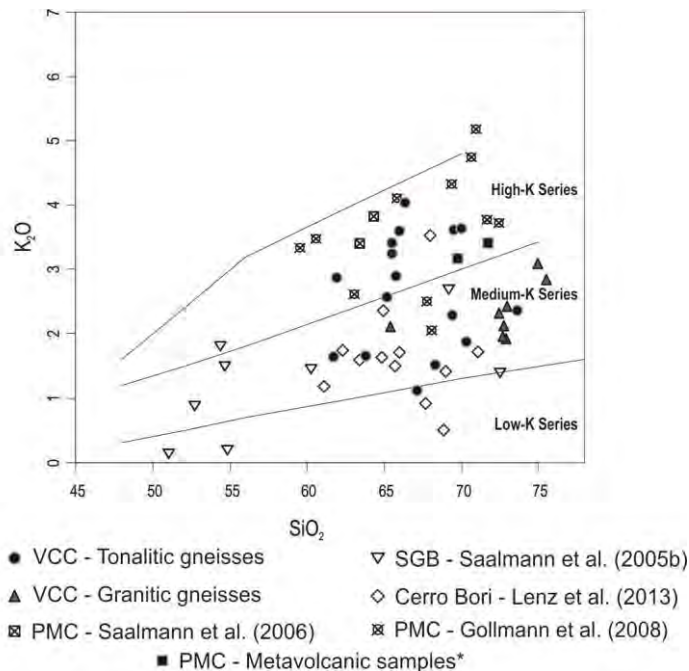


Figure 5 – Studied samples plotted on Le Maitre (2002) K_2O vs SiO_2 diagram. (*) PMC metavolcanic rocks from this study.

Trace element patterns normalized by E-MORB values (Fig. 7a) show strong enrichment of incompatible elements (Cs, Rb, Ba, Th, U) as should be expected, since granitoids are being compared with basaltic compositions. For most elements, however, the values are close to 1 for the E-MORB normalized patterns, except for Nb, Ti, and P, which show prominent negative anomalies. These patterns strongly resemble those of magmas produced from sources previously affected by subduction-related metasomatism of oceanic crust. The PMC rocks are enriched in most trace elements, in relation to other associations, except for Nb, Ti, and P, which is consistent with their production from more evolved arc-related sources.

REE patterns normalized against the chondritic values (Boyton, 1984 - Fig. 7b) for granitoids from all associations are similar, with La_N varying mostly in the 80 to 200 range, Yb_N from 5 to 25, generally with slight negative-Eu anomalies. Basic rocks have less enriched patterns, which lack Eu anomalies, but are parallel to those of granitoids. Values of La_N/Yb_N close to 10, like most rocks from Phanerozoic magmatic arcs, indicate that garnet was not present as a residual phase during melting in the mantle source. The relatively LREE enriched patterns resemble those of mature magmatic continental arcs.

Programa de Pós-Graduação em Geociências

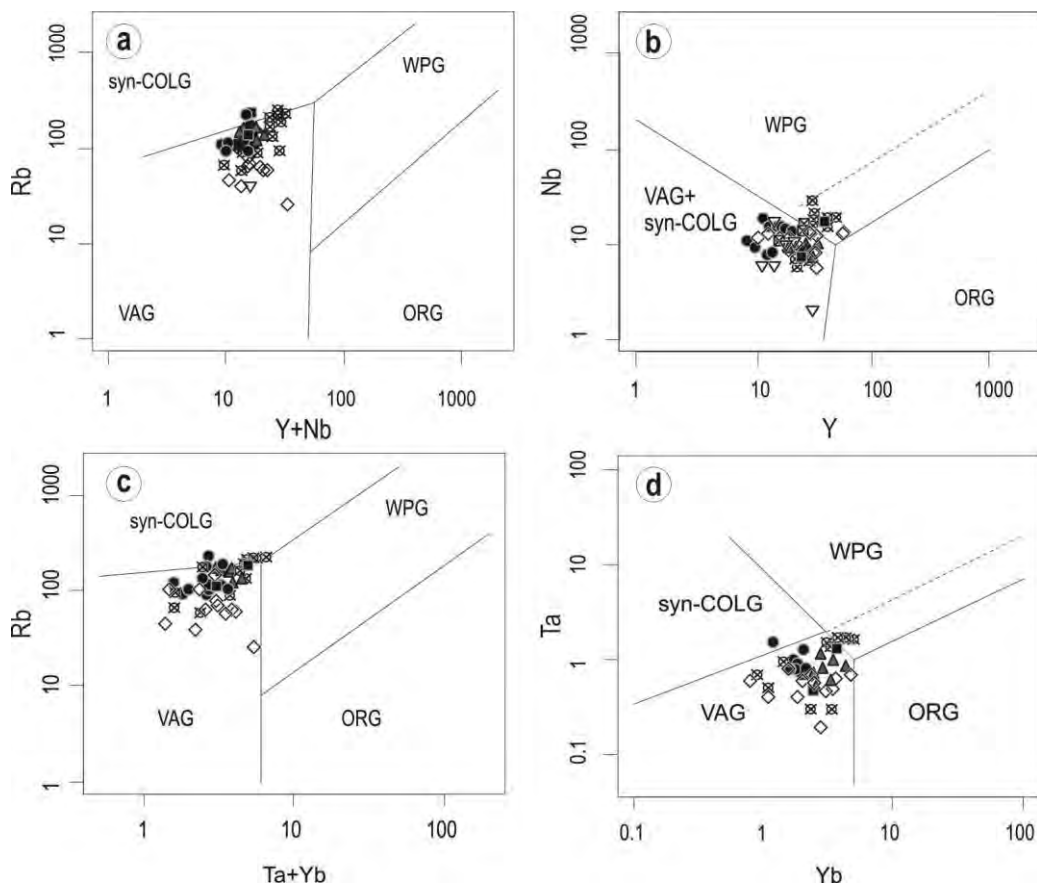


Figure 6 – Tectonic setting discriminant diagrams (Pearce et al., 1984) for the studied samples. Symbols as in figure 5.

In tectonic setting discriminant diagrams (Fig. 8) VCC and SGB rocks plot in the field of volcanic arc granites, whilst the CB and PMC associations are closer to the within plate field. Compared with the Phanerozoic TTG associations of Condie (2005), the rocks discussed here show lower Al_2O_3 contents, and the VCC and PMC rocks have higher K_2O . When the trace elements are taken into account, TTGs show higher amounts of Sr, lower of HFSE (Zr, Nb, Y) and of LREE (La, Ce).

Programa de Pós-Graduação em Geociências

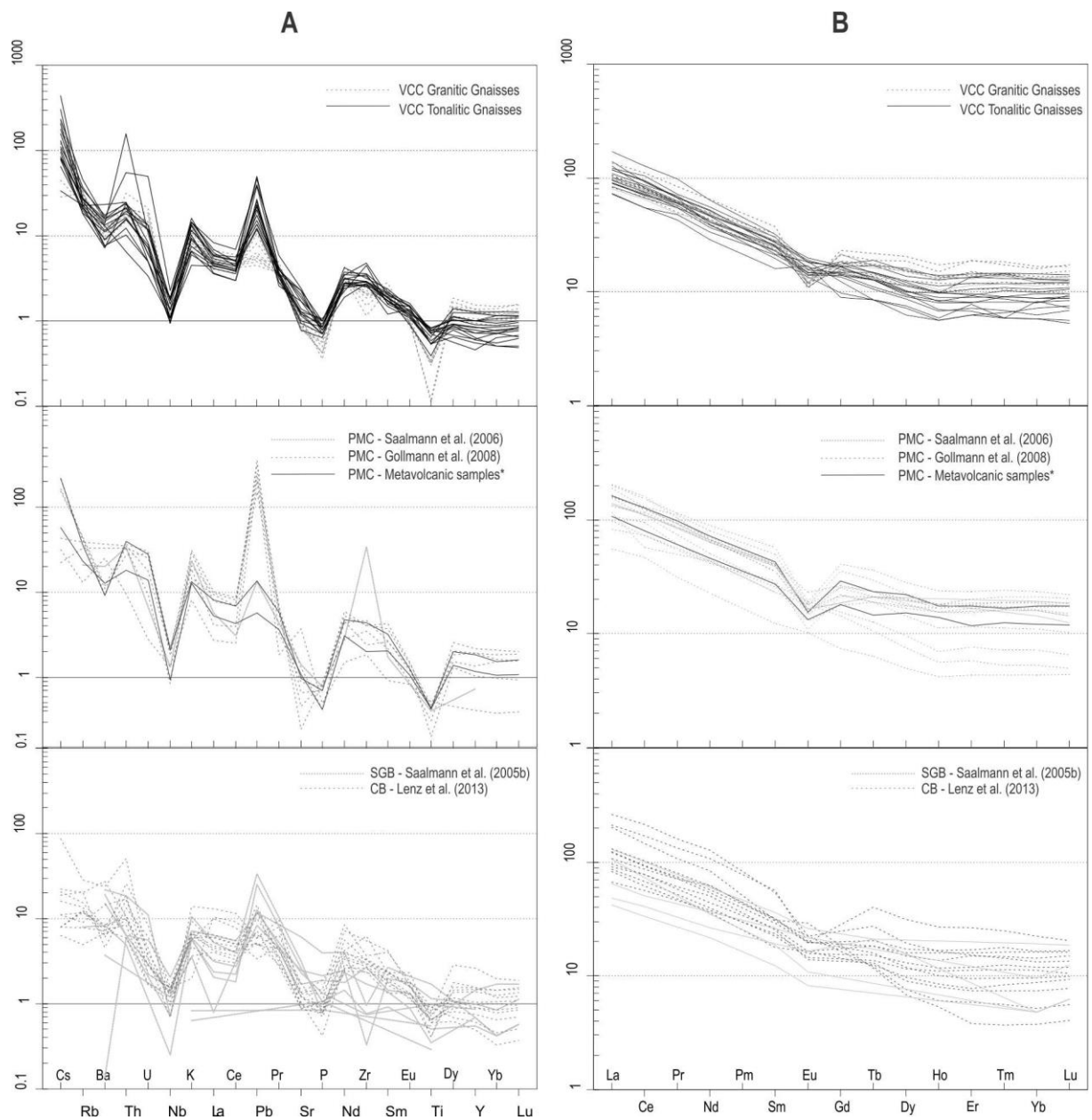


Figure 7 – Spider diagrams for studied associations. (a) Trace-element normalized to E-MORB values of Sun and McDonough (1989). (b) Chondrite normalized REE patterns (values from Boyton, 1984). (*) PMC metavolcanic rocks from this study.

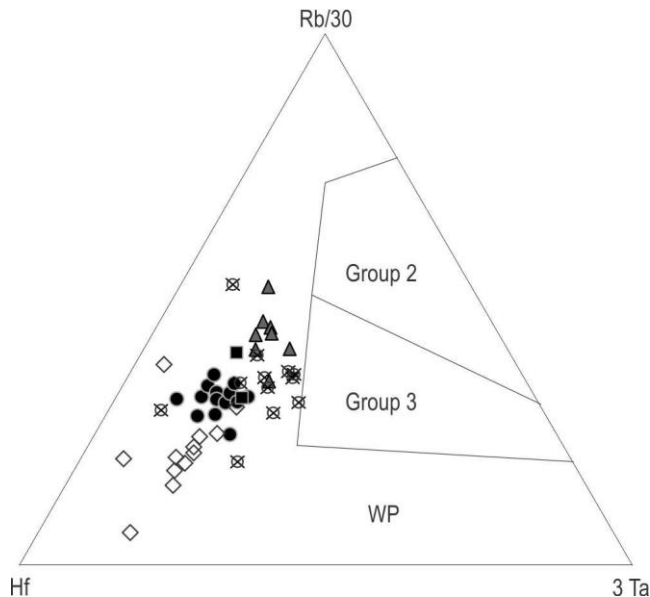


Figure 8 – Rb-Hf-Ta diagram of Harris et al. (1986). Group 2: Syn-collision peraluminous intrusions (leucogranites), Group3: Late or post-collision calc-alkaline intrusions, WP: Whithin Plate Granites. Symbols as in figure 5.

5.2. Isotope Geochemistry: Sm-Nd and Rb-Sr whole-rock results

Whole-rock Sr and Nd isotope data were obtained from 11 samples including tonalitic and granitic gneisses from the Várzea do Capivarita Complex as well as a metavolcanic rock from the Porongos Metamorphic Complex for comparison. The isotopic compositions are shown in Table 3.

The initial Sr and Nd isotopic ratios were calculated for the magmatic crystallization ages of 790 Ma reported by Martil et al. (submitted a). Selected samples have variable $^{87}\text{Rb}/^{86}\text{Sr}$ ratios ranging from 1.538 to 0.247 and $^{87}\text{Sr}/^{86}\text{Sr}$ ratios varying from 0.742873 to 0.758849 with a range of initial $^{87}\text{Sr}/^{86}\text{S}$ ratios from 0.71628 to 0.72509. Sm–Nd isotopic compositions show relatively uniform $^{147}\text{Sm}/^{144}\text{Nd}$ ratios from 0.101 to 0.132, $^{143}\text{Nd}/^{144}\text{Nd}$ ratios from 0.511104 to 0.511251, corresponding to $\epsilon\text{Nd}_{(790)}$ values from -7.2 to -10.1. The metavolcanic sample from the PMC (TM 26 A) has similar Sr-Nd isotopic signatures, similarly to what is observed for the major and trace elements composition.

Instituto de Geociências

Programa de Pós-Graduação em Geociências

sample	group	T (Ma)*	Rb (ppm)	Sr (ppm)	$^{87}\text{Rb}/^{86}\text{Sr}$	$^{87}\text{Sr}/^{86}\text{Sr}$	error (2s)	$^{87}\text{Sr}/^{86}\text{Sr(i)}$	Sm (ppm)	Nd (ppm)	$^{147}\text{Sm}/^{144}\text{Nd}$	$^{143}\text{Nd}/^{144}\text{Nd}$	error (2s)	$\Sigma\text{Nd(0)}$	$\Sigma\text{Nd(t)}$	T_{DM} (Ma)	$^{143}\text{Nd}/^{144}\text{Nd(i)}$
TM 35A	ogT	790	148.26	204.0093	0.283154	0.747762	0.000010	0.72364	5.001	22.90	0.1320	0.511899	0.000006	-14.16	-7.89	2120	0.511215
TM 29B	ogT	790	98.0121	346.1436	0.283154	0.734280	0.000009	0.72501	7.330	43.125	0.1027	0.511697	0.000009	-18.35	-8.88	1834	0.511137
TM 35B	ogT	790	82.4065	333.5077	0.247090	0.731403	0.000013	0.72332	5.278	27.89	0.1144	0.511697	0.000007	-18.35	-10.06	2052	0.511165
TM 01E	ogT	790	110.7028	136.4004	0.811602	0.742873	0.000016	0.71628	4.494	23.46	0.1158	0.511851	0.000007	-15.35	-7.19	1841	0.511104
TM 36G	ogT	790	131.1314	186.5750	0.702835	0.739998	0.000014	0.71698	4.790	22.09	0.1312	0.511799	0.000010	-16.37	-9.77	2287	0.511118
TM 45C	ogG	790	119.8702	116.4998	1.028930	0.758849	0.000016	0.72509	6.510	35.001	0.1124	0.511760	0.000009	-17.13	-8.63	1916	0.511759
TM 45B	ogG	790	133.7828	133.8057	0.999829	0.756701	0.000011	0.72390	4.661	26.92	0.1047	0.511660	0.000013	-19.08	-9.80	1920	0.511251
TM 45H	ogG	790	166.1274	108.0148	1.538007	0.768857	0.000012	0.71834	6.010	32.88	0.1105	0.511709	0.000012	-18.12	-9.84	1956	0.511120
TM 45G	ogG	790	159.1	143.4	1.109483	0.759931	0.000007	0.72352	5.89	29.04	0.1226	0.511787	0.000015	-16.60	-9.13	2087	0.511152
TM 26A	amv	790	116.1	167.8	0.691895	0.745150	0.000010	0.72248	7.023	42.003	0.1011	0.511706	0.000009	-18.18	-8.54	1796	0.511182
PUM ^a	-	recent	0.635	21.1	-	0.7033 ^d	-	0.70232	0.444	1.354	-	0.5130 ^d	-	7.1	6.90	540	0.511973
HIMU ^a	-	recent	16.1	581	-	0.7029	-	0.70200	6.68	32.3	-	0.512857	-	4.27	11.49	351	0.512209
EM1 ^a	-	recent	62.0	792	-	0.7050 ^d	-	0.70244	8.08	40.2	-	0.5112 ^d	-	-28.1	-20.48	3093	0.510570
EM2 ^b	-	recent	73.47	390.83	-	0.7220 ^d	-	0.71585	7.56	42.33	-	0.5121 ^d	-	-10.5	-1.56	1359	0.511541
DMM ^c	-	recent	0.050	7.664	-	0.70263	-	0.70242	0.239	0.589	-	0.51313	-	9.6	4.69	-1318	0.511859

ogT-orthogneiss tonalitic; ogG -orthogneiss granitic; amv- acid metavolcanic rocks. References for mantle reservoirs: a - Sun and McDonough. (1989); b – Workmann et al. (2004); c – Workmann and Hart (2005); d – Rollinson (1993).

Table 3 – Whole rock Sr–Nd isotope data for the Várzea do Capivarita Complex orthogneisses. One sample from Porongos Metamorphic Complex (area 7 in Fig. 1 and 2) is included for comparison.

Sm-Nd model ages (T_{DM}) were calculated using the model of De Paolo (1981). In the ϵNd_0 versus T_{DM} diagram (Fig. 9a) all VCC samples show negative ϵNd_0 (-14.42 to -19.08) values and old depleted-mantle model ages. T_{DM} values between 1.8 and 1.9 Ga are prevalent (Table 2). However, some tonalitic and granitic samples tend to have higher participation of slightly older crustal materials (T_{DM} between 2.3 - 2.0 Ga).

Nd isotope data presented by Lenz et al. (2013), Gollmann et al. (2008) and Saalmann et al. (2005a, 2006) for regional Neoproterozoic arc-related rocks are plotted in figures 09a and 09b for comparison. Metavolcanic acidic to intermediate rocks from group PMC-2, as defined by Gollmann et al. (2008), and the high grade orthogneisses from the Uruguayan shield clearly overlap with the Várzea do Capivarita orthogneisses (Fig 9a). The metavolcanic rocks exposed in the southeastern PMC described by Saalmann et al. (2006) are isotopically similar to the rocks described in the VCC, as well as those from group PMC-2, while metavolcanics in the northwestern part of the Porongos Metamorphic Complex are similar to group PMC-1 (Fig. 9a). VCC orthogneisses exhibit patterns that are distinct from calc-alkaline rocks of group PMC-3 and of the metabasalts in group 4, as well as from the tonalitic gneisses in the SGB (Fig. 9a).

T_{DM} values for metasedimentary rocks shown in figure 9b are comparable to those found in the regional meta-igneous rocks (Fig. 9a). This is also observed when the metapelite data from Gross et al. (2006) are compared with VCC orthogneisses presented in this study. Furthermore, the values reported for the calc-alkaline rocks of the PMC-1 group are correlated with those described by Saalmann et al. (2006) for the metasediments in the northwestern portion of PMC. As observed for the ortho-derived sequences, the isotope composition of the metasedimentary rocks of the southeastern PMC is comparable to the PMC-2 group and to the VCC metapelites.

Basement units, including the Paleoproterozoic continental arc sequences (Arroio dos Ratos and Encantadas complexes) and the Mesoproterozoic (1.5-1.6 Ga) intraplate magmatic rock (Capivarita Anorthosite) were compared to the VCC orthometamorphic association (Fig. 9c). Rocks from the Arroio dos Ratos Complex (ARC) have T_{DM} ages between 1.9 and 2.3 Ga and negative values of $\epsilon Nd_{(790)}$ (-15.0 to -5.8), close to those of the VCC orthgneiss. The Capivarita Anorthosite also shows similar patterns, with $\epsilon Nd_{(790)}$ of -12.0 and a T_{DM} value of 2.0 Ga (Babinski et al., 1997). For the Encantadas Complex (EC), May (1990) reports T_{DM} values of 2.1 to 2.4 Ga and $\epsilon Nd_{(790)}$ between -22.2 and -11.8. Chemale et al. (2000) refer to

Programa de Pós-Graduação em Geociências

ϵNd_0 values between -21.0 and -30.08, and T_{DM} values of approximately 2.8 Ga for the Encantadas Complex orthogneisses. Both sets of data for the EC partially overlap with the VCC isotopic patterns.

In the $\epsilon\text{Nd}_{(790)} \textit{versus} {}^{87}\text{Sr}/{}^{86}\text{Sr}_{(\text{i})}$ diagram (Fig. 10), the VCC orthogneisses exhibit low $\epsilon\text{Nd}_{(790)}$ and high ${}^{87}\text{Sr}/{}^{86}\text{Sr}_{(\text{i})}$ values. ARC lithologies studied by Gregory et al. (2015), and PMC metavolcanic and metasedimentary rocks studied by Saalmann et al. (2006b) show $\epsilon\text{Nd}_{(790)}$ values similar to those of VCC orthogneisses, although the ${}^{87}\text{Sr}/{}^{86}\text{Sr}_{(\text{i})}$ values tend to be slightly lower (0.7109-0.71128). However, one sample representative of a less expressive sequence in the ARC (A3 association), shows atypical, enriched ${}^{87}\text{Sr}/{}^{86}\text{Sr}_{(\text{i})}$ values of 0.75250. Northwestern PMC supracrustal rocks and the Encantadas orthogneisses from Encantadas (May, 1990) tend to have evolved $\epsilon\text{Nd}_{(790)}$ values, ranging from -14.72 to -22.43. VCC orthogneisses were also compared with selected samples of mantle reservoirs, including PUM, HIMU, EMI, EMII and DMM (references in Table 3) and a Garnet Peridotite sample, which represents a xenolith from continental mantle lithosphere (AJE-164 – Hawkesworth et al., 1990). Comparison of VCC orthogneisses with mantle reservoirs and with sample AJE-164 on a $\epsilon\text{Nd}_{(790)} \textit{vs} {}^{87}\text{Sr}/{}^{86}\text{Sr}_{(\text{i})}$ diagram (Fig. 10) indicates that the VCC samples lie close to the EMII reservoir values. All VCC orthogneiss samples plot in the field of crustal component and away from the mantle array field.

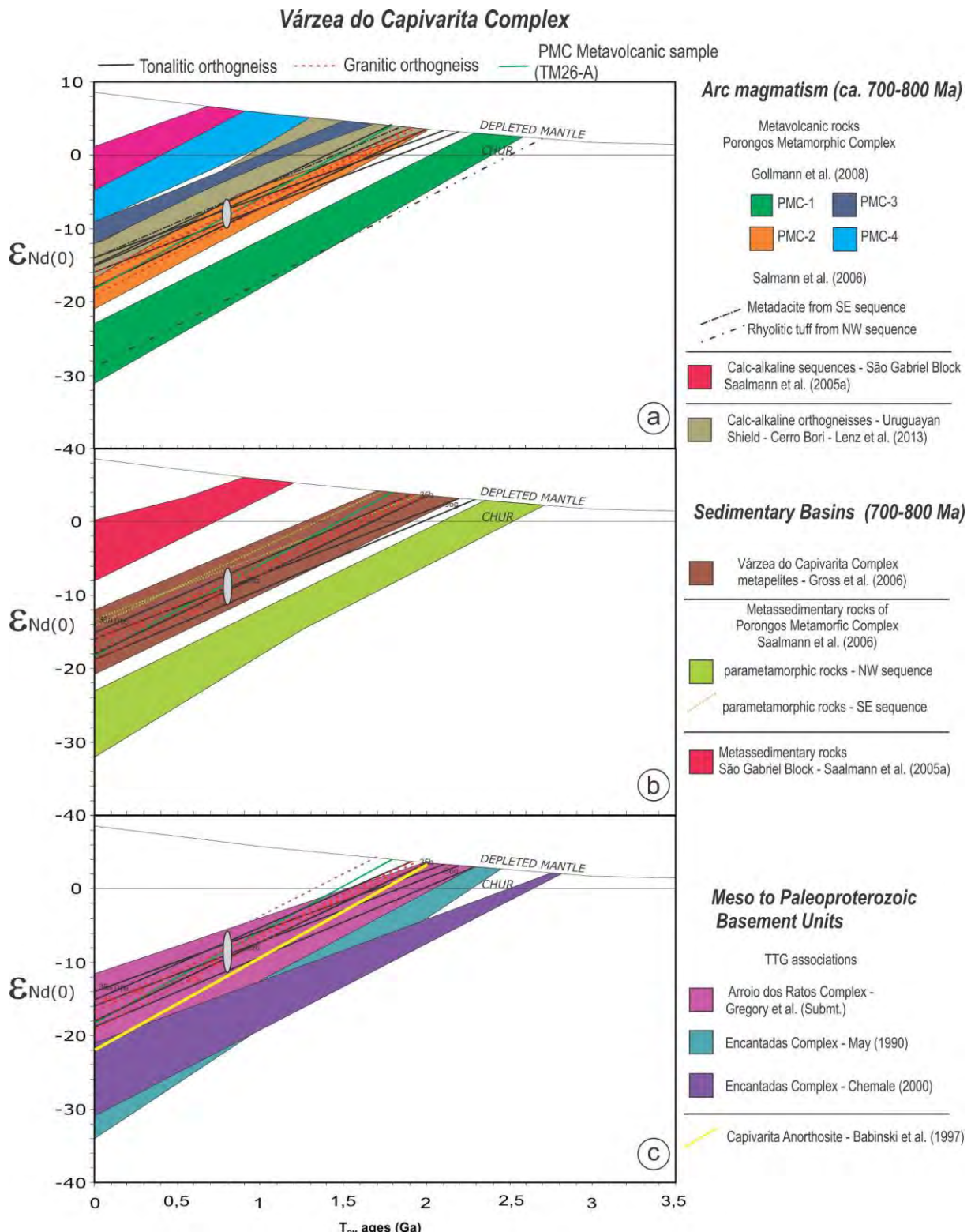


Figure 9 – Isotope correlation diagrams for ϵNd_0 vs T_{DM} ages (Ga) of the Várzea do Capivarita orthogneisses and PMC metavolcanic sample. (a) Arc related magmatism; (b) sedimentary basins; (c) basement units as potential sources. Ellipse indicate $\epsilon\text{Nd}_{(790)}$ values.

Programa de Pós-Graduação em Geociências

Since petrological data of studied orthogneisses suggest crustal participation, mixing models were formulated in order to evaluate the observed Sr-Nd isotope patterns. Figure 11 shows the possible mixing relations. Considering the high $^{87}\text{Sr}/^{86}\text{Sr}_{(i)}$ of the magmatism registered in the VCC orthogneisses, the Paleoproterozoic ARC A3 association was chosen as potential contaminant, since this representative sample has the most radiogenic $^{87}\text{Sr}/^{86}\text{Sr}_{(i)}$ values (Fig. 10). For mantle-derived end-members, the same samples in figure 10 were used. Orthogneisses from the EC were discarded as possible crustal contaminants because they show $^{87}\text{Sr}/^{86}\text{Sr}_{(i)}$ isotope patterns similar to the VCC and therefore, they are not suitable. Despite the former interpretation that volcanism was coeval with sedimentation in the Porongos Metamorphic Complex, one metasedimentary sample from PMC was considered as a potential crustal contaminant due to its high $^{87}\text{Sr}/^{86}\text{Sr}_{(i)}$ value of 0,7286 (Saalmann et al., 2006; Fig. 10). It is assumed that depositional ages could not be well constrained for the entire PMC, and thus some parametamorphic sequences could be older or younger than the 780-790 magmatism. However, all modelling attempts have failed, since all the binary curves show incompatible mixing percentages.

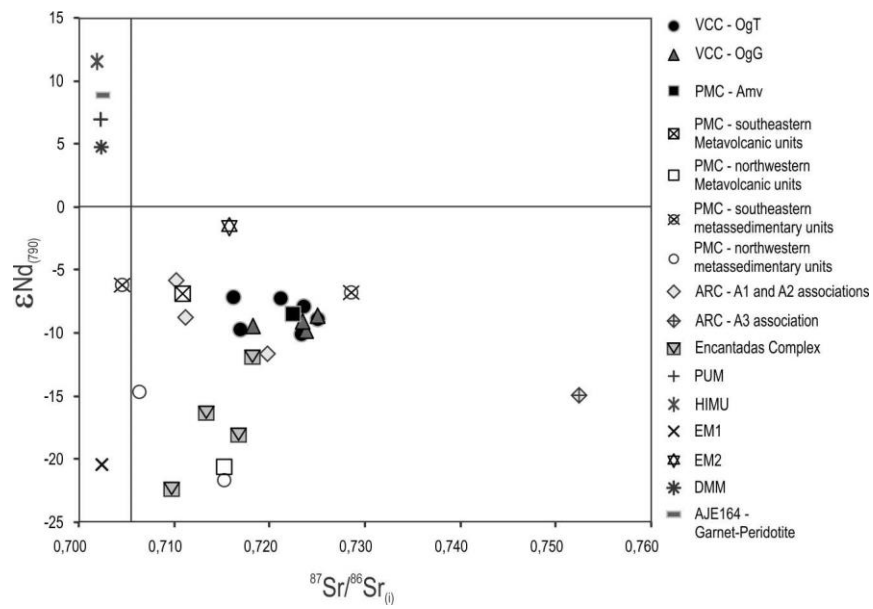


Figure 10 – $^{87}\text{Sr}/^{86}\text{Sr}_{(i)}$ vs $\epsilon\text{Nd}_{(790)}$ for Várzea do Capivarita Complex orthogneisses compared to Neoproterozoic and metasedimentary associations (Saalmann et al. 2006) and to regional basement units Arroio dos Ratos (Gregory et al., submitted) and Encantadas Complex (May, 1990). OgT-orthogneiss tonalitic; OgG -orthogneiss granitic; Amv – acid metavolcanic. Sr-Nd data from mantle reservoirs extracted from Sun and McDonough (1989) – PUM, EM1, HIMU; Workmann et al. (2004) – EM2; Workmann and Hart (2005) – DMM. $^{87}\text{Sr}/^{86}\text{Sr}_{(0)}$ values for PUM, EM1 and EM2 from Rollinson (1993). A garnet peridotite, which represents the continental mantle lithosphere (AJE-164 - Hawkesworth et al., 1990), is included for comparison.

The modelling attempts have failed for most mantle endmembers, including PUM, HIMU, DMM and the peridotite garnet sample (AJE 164), because most of the isotope Sr-Nd ratios of the studied orthogneisses plot away from any possible binary mixing curve. In addition, the binary mixing EMI-A3-ARC was discarded because the trends showed no realistic concentration, as this would require 70-80% mixing.

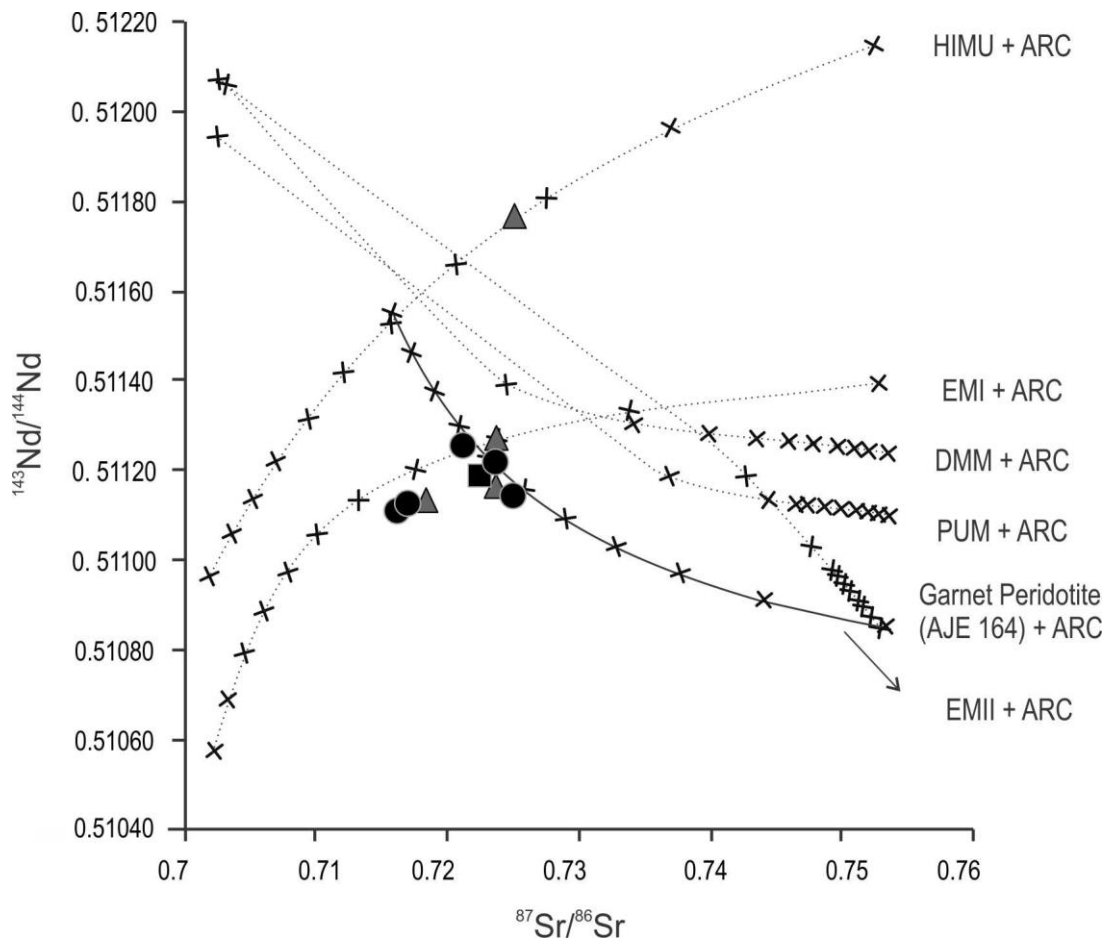


Figure 11 – Mixing model for Várzea do Capivarita Complex orthogneisses and metavolcanic rock sample. Binary mixing curves included a crustal endmember – A3-ARC Association – and selected samples from mantle reservoir, as well as a garnet-peridotite. Symbols as in figure 5.

Our models suggest that the binary mixing (40-60%) of EM II and A3-ARC accounts for the distribution of most of the studied VCC rocks (Fig. 11), and it is the best fit for the studied arc magmatism. Additionally, when the behavior of $^{87}\text{Sr}/^{86}\text{Sr}_{(i)}$ is examined against Sr concentration and $^{144}\text{Nd}/^{143}\text{Nd}_{(i)}$ against Nd concentration, the mixing components yield hyperbolic curves wherein crustal assimilation is followed by mineral fractionation (Fig. 12a

and 12b). From a binary mixture (50-60%) in the $^{87}\text{Sr}/^{86}\text{Sr}_{(i)}$ (i) vs. Sr diagram (Fig. 12a) and in 40-50% $^{143}\text{Nd}/^{144}\text{Nd}_{(i)}$ vs. Nd diagram (Fig. 12b) there is a horizontal displacement also controlled by mineral fractionation. This suggests that from this moment on there has been no further participation of mantle or crustal materials, neither during ascent nor during emplacement.

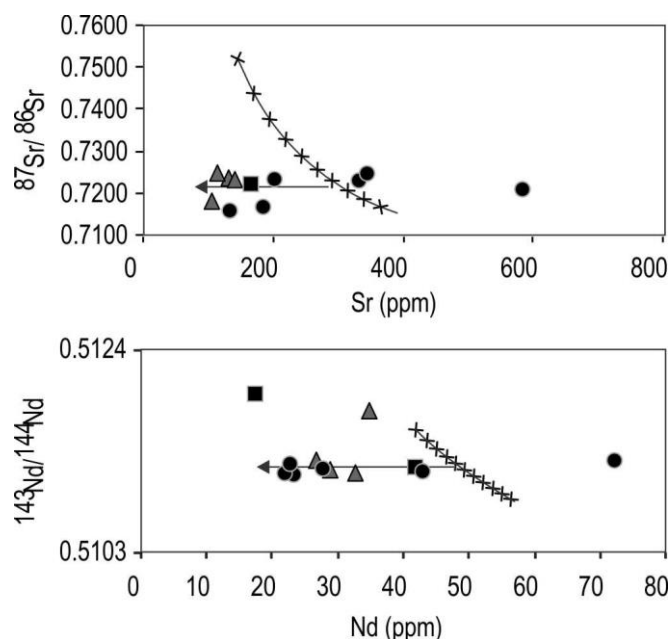


Figure 12 – (a) Plot of Sr isotope ratio against Sr concentration. (b) Plot of Nd isotope ratio against Nd concentration. Symbols as in figure 5.

6. Discussion: magmatic sources, geotectonic settings and correlation with other arc-related magmatism

The major element composition, as well as the calc-alkaline affinity of all studied magmatic associations, is similar to those found in Phanerozoic volcanic arcs described by several authors. Furthermore, Cawood et al. (2013) stated that the magmatic arc activity in accretionary orogens is characteristically calc-alkaline in composition, although it may include tholeiitic, low-K and shoshonitic varieties, depending on the degree and type of interaction with the arc substrate. The PMC rocks described by Gollmann et al. (2008) display a slightly more evolved character, indicated mainly by their higher K contents and lower CaO/(Na₂O+K₂O) values. The trace element patterns are consistent with this interpretation:

Programa de Pós-Graduação em Geociências

the spidergrams normalized to E-MORB show very prominent negative anomalies for Nb, Ti and P, and the studied associations plot in the field of volcanic-arc magmatism in the trace-element diagrams proposed by Pearce et al. (1984 – Fig. 6) and Harris et al. (1986 – Fig. 8). Nb and Ti anomalies found in VCC, PMC and CB arc sequences indicate that these magmas were produced from mantle sources modified by metasomatism caused by previous lithosphere subduction (Thompson et al., 1984). Furthermore, poorly-fractionated REE patterns are similar to those of classical magmatism at island arcs or active continental margins (Wilson, 1989). The LREE-enrichment of granitoids (La_N 80-200) also points to arc-magmatism produced from enriched-mantle sources. PMC rocks (Gollmann et al., 2008) show slight LREE enrichment in relation to other arc associations, and plot closer to the within-plate field in the trace element diagrams for geotectonic discrimination, suggesting a more mature arc setting.

Nd isotope results show similar patterns for CB, PMC and VCC orthogneisses, suggesting similar magma sources (Fig. 9a). In εNd_0 vs T_{DM} diagram, PMC-4 group and samples from the SGB (Saalmann et al., 2005b) exhibit similar values, which are clearly distinct from the VCC orthogneisses. The observed variations, particularly relative to the differences in T_{DM} values (Fig. 9a), in the groups described by Gollmann et al. (2008) may be related to different degrees of mantle-crust interaction, as already mentioned by those authors. However, recent geochronological evidence (zircon U-Pb LA-MC-ICP-MS ages from Kohlrausch, 2013) suggest that at least one of these groups has younger magmatic ages around 618-578 Ma, and thus the εNd_0 vs T_{DM} values observed in figure 9a are probably due to different crystallization ages among the referred groups. Further studies are necessary in order to confirm this hypothesis.

The different signatures observed in figure 9a for the described sequences in northwest and southeast PMC (Saalmann et al., 2006) may be related to distinct magmatic pulses from the same chamber, which have distinct degrees of interaction with crustal magmas. Alternatively, compositionally similar magmatic pulses might have also (i) interacted with different crustal materials, both in terms of composition and age, or even (ii) intermingle with different degrees of crustal contamination due to variable residence times in the crust. These hypotheses can also be applied to the PMC groups discussed by Gollmann et al. (2008), if one considers that the all metaigneous rocks of the PMC are coeval at ca. 800 Ma.

Comparison of VCC orthogneisses and metavolcanic rocks from area 7 (Fig. 1, Fig. 2) with the tonalitic arc sequences from the SGB results in different isotope patterns (Fig. 9a).

Despite their continental arc geochemical patterns, the SGB tonalitic rocks have isotope signatures indicative of Neoproterozoic juvenile sources which contrast with the old and more evolved sources observed in VCC.

The proximal character of sedimentation in the analysed arc environments, as indicated by the T_{DM} and ϵNd_0 values of igneous and sedimentary protoliths, is consistent with the VCC volcano-sedimentary arc-related paleoenvironment, as previously interpreted by Martil et al. (submitted c).

Comparing the composition of the orthogneisses investigated here with the data presented by Saalmann et al. (2006), the VCC rocks are also similar to other volcano-sedimentary sequences from the southeastern PMC. The bimodal pattern of T_{DM} values for sedimentary rocks from southeastern and northwestern PMC may be interpreted as a result of participation of two contrasting sources of the original sediments, as already pointed out by Saalmann et al. (2006). Nevertheless, these distinct isotopic patterns may also be attributed to the erosion of magmatic arc sequences with different degrees of mantle-crust interaction.

The atypical, high $^{87}Sr/^{86}Sr_{(i)}$ values (0.71628-0.72509) found in the VCC arc orthogneisses, together with their variable inheritance zircon ages of 3.1, 2.0, 1.8, 1.6, 1.1 and 1.0 Ga (Martil et al., submitted a), confirm the reworking of older crust and are consistent with the mature-arc signature of these rocks. The predominance of Paleoproterozoic inheritance ages is compatible with the ARC ages reported by Gregory et al. (2015). Younger and older inheritance ages suggest that there are other minor crustal contaminants present during the ascent and emplacement of the magma, even though they do not greatly modify its main composition. Thus, the data indicate that the assimilated crustal material during the 790 Ma arc activity is predominantly similar to A3-ARC association, even though other associations may have also participated.

7. Conclusions

The Várzea do Capivarita Complex orthogneisses are correlated with other associations formed in continental arc environments around 800 Ma, including metavolcanic rocks from southernmost Brazil, and the Cerro Bori orthogneisses, in Uruguay. These sequences show signatures typical of accretionary orogens, have TDM and inheritance ages from Meso to Paleoproterozoic, and present strong evidences of crustal assimilation/contamination. The higher contents of K in VCC and PMC rocks, and the tendency to move toward the post-collisional

Programa de Pós-Graduação em Geociências

field in the geotectonic diagrams suggest that they were generated in a thick-crust, mature arc environment. In contrast, the Cerro Bori sequence exhibits a less mature continental-arc character, positioned in a thinner crust, or closer to the active margin.

The VCC magmatism is clearly distinct from continental, arc-related sequences of ca. 700-750 Ma found in the SGB, as indicated by Sr-Nd isotopes. This younger magmatism shows isotope signatures indicative of major contribution from Neoproterozoic juvenile sources, and with only little amounts of reworked old continental crust.

Binary mixing models suggest that the VCC magmatism originated from evolved EM II mantle sources. A crustal sequence similar to the A3-ARC association described by Gregory et al. (submitted) seems to be the main contaminant assimilated by the VCC magmatism. Together with the small inheritance contribution at ca. 2.0 (Martil et al., submitted a), this suggests that the melted crust at ca. 790-800 Ma was predominantly similar to the Arroio dos Ratos Complex. Our models also indicate that in addition to crustal assimilation processes, fractional crystallization was important during the VCC magmatism evolution.

In addition to the evidence of similarity between the VCC and the PMC magmatism pointed out by the correlation with data in the literature, geochemical and Sr-Nd signatures presented in this paper suggest that at least part of the PMC metavolcanic rocks may represent the protoliths of the high grade orthogneisses present in Várzea do Capivarita Complex, as discussed by Martil et al. (submitted c). This, together with the isotope evidence suggesting similarity between VCC and PMC igneous and sedimentary rocks, corroborates the hypothesis that the VCC and PMC are, at least in part, expressions of the same context, wherein the magmatic and sedimentary activity occurred in a single continental arc environment. VCC and PMC rock types might have been thrust-stacked under granulite facies conditions during the ca. 650 Ma collisional event (Martil et al., submitted c).

The VCC orthogneisses and those described in Uruguay, as well as part of the PMC metavolcanic rocks, may be interpreted as part of the same Neoproterozoic magmatism, or at least as fragments of similar Neoproterozoic magmatic arcs.

Acknowledgements

This work is a part of the Ph.D. thesis of Mariana M. D. Martil. We acknowledge the financial support of the 141209/2010-0 (PhD Grant) as well as the financial support from the State

Programa de Pós-Graduação em Geociências

Research Foundation (FAPERGS, 10/0045- 6) and National Research Council (CNPq, Universal Program 471266/2010-8) granted to M.F. Bitencourt.

References

- Babinski M., Chemale F. Jr., Hartmann L.A., Van Schmus W.R., Silva L.C. 1996. Juvenile accretion at 750–700 Ma in southern Brazil. *Geology* 24:439–442
- Babinski M., Chemale F. Jr., Van Schmus W.R., Hartmann L.A., Silva L.C. 1997. U-Pb and Sm-Nd Geochronology of the Neoproterozoic Granitic-Gneissic Dom Feliciano Belt, southern Brazil. *Journal of South American Earth Science*. 3–4:263–274.
- Bitencourt, M.F. and Nardi, L.V.S. 1993. Late to Post-collisional Brasiliano Magmatism in Southernmost Brazil. *Anais da Academia Brasileira de Ciências*, 65 (1): 3-16.
- Bitencourt, M.F. and Nardi, L.V.S. 2000. Tectonic setting and sources of magmatism related to the Southern Brazilian Shear Belt. *Revista Brasileira de Geociências*, 30: 184-187.
- Bom, F.M., Philipp, R.P., Zvirtes, G. 2014. Evolução metamórfica e estrutural do Complexo Várzea do Capivarita, Cinturão Dom Feliciano, Encruzilhada do Sul, RS. *Pesquisas em Geociências*, 41 (2): 131-153.
- Boynton, W.V., 1984. Geochemistry of the rare earth elements: meteorite studies. In: Henderson, P. (Ed.), *Rare-Earth Element Geochemistry*. Elsevier, pp. 63–114.
- Cawood, P.A., Kröner, A., Collins, W.J., Kusky, T.M., Mooney, W.D., Windley, B.F. 2013. Accretionary orogens through Earth history. *Special Publications, Geological Society of London*, 319:1-36.
- Chemale Jr., F., Philipp, R.P., Dussin, I.A., Formoso, M.L.L., Kawashita, K., Bertotti, A.L. 2011. Lu-Hf and U-Pb age determinations of Capivarita Anorthosite in the Dom Feliciano Belt, Brazil. *Precambrian Research*, 186: 117-126.

Programa de Pós-Graduação em Geociências

Condie, K.C. 2005. TTGs and adakites: are they both slab melts? *Lithos*, 80: 33-44.

DePaolo, D.J. 1981. Neodymium isotopes in the Colorado Front Range and crust–mantle evolution in the Proterozoic. *Nature*, 29(1): 193–196.

Fernandes, L.A.D., Tommasi, A., Porcher, C.C., 1992a. Deformation patterns in the southern Brazilian branch of the Dom Feliciano belt: a reappraisal. *Journal of South America Earth Science*, 5: 77-96.

Fernandes, L.A.D., Tommasi, A., Porcher, C.C., Koester, E., Kraemer, G., Scherer, C.M., Menegat, R., 1992b. Granitóides precoces do Cinturão Dom Feliciano: caracterização geoquímica e discussão estratigráfica. *Pesquisas*, 19: 197-218.

Garavaglia, L., Koester, E., Bitencourt, M.F. and Nardi, L.V.S. 2006. Isotopic Signature of Late magmatic Arc to Post-collisional Magmatism in the Vila Nova Belt, Southern Brazil. In: South-American Symposium on Isotope Geology, 5, 2006, Punta del Este. Short Papers...(p. 101-104). Punta del Este, Universidad de la Republica.

Gioia, S.M.C., Pimentel, M., 2000. The Sm–Nd isotopic method in the Geochronology Laboratory of University of Brasilia. *Anais da Academia Brasileira de Ciências* 72, 219–245.

Gollmann, K., Marques, J.C., Frantz, J.C., Chemale, F. Jr. 2008. Geoquímica e Isotópos de Nd de Rochas Metavulcânicas da Antiforme Capané, Complexo Metamórfico Porongos, RS. *Revista Pesquisas em Geociências*, 35 (2): 83-95.

Gregory, T.R., Bitencourt, M.F. and Nardi, L.V.S. 2011. Caracterização estrutural e petrológica de metatonalitos e metadioritos do Complexo Arroio dos Ratos na sua seção-tipo, região de Quitéria, RS. *Pesquisas em Geociências*, 38(1): 85-108.

Gregory, T.R., M.F., Bitencourt, Nardi, L. V., Florisbal, L. M, Chemale, F. Jr. 2015. Geochronological data from TTG-type rock associations of the Arroio dos Ratos Complex and implications for crustal evolution of southernmost Brazil in Paleoproterozoic times. *Journal of South American Earth Science*. 57: 49–60.

Gregory, T.R., M.F., Bitencourt, Nardi, L. V., Florisbal, L. M, Petrogenesis of Paleoproterozoic TTG-type mafic and felsic rock associations from southernmost Brazil, based on elemental and isotopic geochemistry. (submitted to Lithos).

Gross, A.O.M.S., Porcher, C.C., Fernandes, L.A.D., Koester, E. 2006. Neoproterozoic low-pressure/high-temperature collisional metamorphic evolution in the Varzea do Capivarita metamorphic suite, SE Brazil: thermobarometric and Sm/Nd evidence. Precambrian Research, 147:41-64.

Gruber, L., Porcher, C.C., Lenz, C., Fernandes, L.A.D. 2011. Proveniência de metassedimentos das sequências Arroio Areião, Cerro Cambará e Quartzo Milonitos no Complexo Metamórfico Porongos, Santana da Boa Vista, RS. Pesquisa em Geociências, 38 (3): 205-223.

Harris, N.B.W., Pearce, A.J., Tindle, A.G., 1986. Geochemical characteristics of collision zone magmatism. In: Coward, M.P., Ries, A.C. (Eds.), Collision Tectonics: Geological Society of America Special Papers, 19, pp. 115–158.

Hartmann, L. A., Leite, J.A.D., Mcnaughton, N.J., Santos, J. O.S. 1999. Deepest exposed crust of Brazil - SHRIMP establishes three events. Geology, 27(10):947-950.

Hartmann, L.A., Philipp, R.P., Liu, D., Wan, Y., Wang, Y., Santos, J.O.S., Vasconcellos, M.A.Z. 2004. Paleoproterozoic magmatic provenance of Detrital Zircons, Porongos complex quartzites, southern Brazilian shield. International Geological Review, 46:127–157.

Hartmaan, L.A., Philipp, R.P., Santos, J.O.S., McNaughton, N.J. 2011. Time frame of 753–680 Ma juvenile accretion during the São Gabriel orogeny, southern Brazilian Shield. Gondwana Research. 19: 84–99.

Hawkesworth, C.J., Erlank, A.J., Kempton, P.D., Waters, F.G. 1990. Mantle Metassomatism: Isotope and trace-element trends in xenoliths from Kimberly, South Africa. Chemical Geology. 85: 19-34.

Heilbron, M., Pedrosa-Soares, A.C., Campos Neto, M., Silva, L.C., Trouw, R.A.J., Janasi, V.C. 2004. A Província Mantiqueira. In: Mantesso-Neto, V., Bartorelli, A., Carneiro, C.D.R., Brito Neves, B.B. (Eds.), *O desvendar de um continente: a moderna geologia da América do Sul e o legado da obra de Fernando Flávio Marques de Almeida*, pp. 203-234.

Jost, H., Bitencourt, M.F. 1980. Estratigrafia e tectônica de uma fração da faixa de Dobramentos de Tijucas no Rio Grande do Sul. *Acta Geologica Leopoldensia*, 4(7): 27-60.

Irvine, T.N. and Baragar, W.R.A. 1971. A guide to the chemical classification of the common volcanic rocks. *Canadian Journal of Earth Sciences*, 8: 523-548.

Jeffery, P.G. and Hutchison, D., 1981. *Chemical Methods of Rock Analysis*, 3rd ed. Oxford, Pergamon Press, 379 p.

Jensen, L.S. 1976. A new cation plot for classifying subalkalic volcanic rocks. *Ontario Division of Mines, Miscellaneous Paper*, 6: 1-22.

Kohlrausch, C.B. 2013. Determinação de idades U-Pb em zircão por LA-ICP-MS nas rochas metavulcânicas da Antiforme Capané, Complexo Metamórfico Porongos. Trabalho de Conclusão de Curso. (Graduação em Geologia) - Universidade Federal do Rio Grande do Sul.

Le Maitre, R.W. 2002. Igneous Rocks: A Classification and Glossary of Terms. Recommendations of the International Union of Geological Sciences, Subcommission on the Systematics of Igneous Rocks. Cambridge University Press.

Leite, J.A.D., Hartmann, L.A., McNaughton, N.J., Chemale Jr., F., 1998. SHRIMP U-Pb zircon geochronology of Neoproterozoic juvenile and crustal-reworked terranes in southernmost Brazil. *International Geological Review*. 40, 688–705.

Lenz, C., Fernandes, L.A.D., McNaughton, N.J., Porcher, C.C., Masquelin, H. 2011. U Pb SHRIMP ages for the Cerro Bori Orthogneisses, Dom Feliciano Belt in Uruguay: Evidences of a 800Ma magmatic and 650Ma metamorphic event. *Precambrian Research*, p. 149-163.

Lenz, C., Porcher, C.C., Fernandes, L.A.D., Masquelin, H., Koester, E., Conceição, R.V. 2013. Geochemistry of the Neoproterozoic (800 - 767 Ma) Cerro Bori orthogneisses, Dom Feliciano Belt in Uruguay: tectonic evolution of an ancient continental arc. Mineralogy and Petrology, v. 1, p. 10, 2013.

Marques, J.C., Jost, H., Roisenberg, A., Frantz, J.C., 1998. Eventos ígneos da Suíte Metamórfica Porongos na área da Antiforme Capané, Cachoeira do Sul. RS. Revista Brasileira de Geociências, 28: 419-430.

Martil, M.M.D., Bitencourt, M.F., Armstrong, R., Nardi, L.V.S., Chemale Jr., F. Geochronology of orthogneisses from the Várzea do Capivarita Complex thrust pile and implications for the timing of continental collision in southernmost Brazil. Precambrian Research (submitted a).

Martil, M.M.D., Bitencourt, M.F., Weinberg, R., Schmitt, R., Nardi, L.V.S. Structural Evolution of Várzea do Capivarita Complex: a 650 Ma oblique collisional record in southern Brazil. Journal of Structural Geology (submitted b).

Martil, M.M.D., Bitencourt, M.F., Schmitt, R., Armstrong, R., Pimentel, M., Nardi, L.V.S. Reconstitution of a volcano-sedimentary environment at 790 Ma obliterated by a collisional thrust tectonics: the Porongos and Várzea do Capivarita Complexes, southern Brazil. Journal of South American Earth Science (submitted c).

Martil, M.M.D., Bitencourt, M.F. and Nardi, L.V.S. 2011. Caracterização estrutural e petrológica do magmatismo pré-colisional do Escudo Sul-rio-grandense: os ortognaisse do Complexo Metamórfico Várzea do Capivarita. Pesquisas em Geociências, 38(2): 181-201.

Miyashiro, A. 1974. Volcanic rocks series in island arcs and active continental margins. American Journal of Science, 274: 321-355.

May, E.S.B.A. 1990. Pan-African Magmatism and Regional Tectonics of South Brazil. Ph.D. Thesis, Universidade Federal do Rio Grande do Sul, Porto Alegre, 357 pp.

Nardi, L.V.S. and Bitencourt, M.F. 2007. Magmatismo Granítico e Evolução Crustal no Sul do Brasil. In: J.C. Frantz and R. Ianuzzi (Eds.). Geologia do Rio Grande do Sul - 50 Anos do IG-UFRGS. Porto Alegre, Editora Comunicação e Identidade. CIGO e IG-UFRGS, p. 125-141.

Pearce, J.A. Harris, N.B.W. Tindle, A.J. 1984. Trace Element Discrimination for the tectonics interpretation of granitic rocks. *Journal of Petrology*, 25: 956-983.

Pertille, J.; Hartmann, L.A.; Philipp, R.P., Petry, T.S., Lana, C.C. 2015. Origin of the Ediacaran Porongos Group, Dom Feliciano Belt, southern Brazilian Shield, with emphasis on whole rock and detrital zircon geochemistry and U-Pb, Lu-Hf isotopes. *Journal of South American Earth Sciences*, 64: 69-93

Phillip, R.P., Lusa, M., Nardi, L.V.S. 2008. Geochemistry and Petrology of dioritic, tonalitic and trondhjemite gneisses from Encantadas Complex, Santana da Boa Vista, southernmost Brazil: a Paleoproterozoic continental arc-magmatism. *Anais da Acadêmia Brasileira de Ciências*, 80(4): 1-14.

Philipp, R.P., Bom, F.M., Pimentel, M.M., Junges, S. L., Zvirtes, G. 2016. SHRIMP U-Pb age and high temperature conditions of the collisional metamorphism in the Várzea do Capivarita Complex: Implications for the origin of Pelotas Batholith, Dom Feliciano Belt, Southern Brazil. *Journal of South American Earth Sciences*, 66: 196-207.

Rollinson, H.R. 1993. Using Geochemical Data: Evaluation, Presentation, Interpretation, Longman, UK. 352 pp. Co-published by J. Wiley and Sons. Inc. in the USA.

Saalmann K., Hartmann L.A., Remus M.V.D., Koester E., Conceição R.V. 2005a. Sm-Nd isotope geochemistry of metamorphic volcanosedimentary successions in the São Gabriel Block, southernmost Brazil: evidence for the existence of juvenile Neoproterozoic oceanic crust to the east of the Rio de la Plata craton. *Precambrian Research* 136:159–175.

Programa de Pós-Graduação em Geociências

Saalmann K., Remus M.V.D., Hartmann L.A. 2005b. Geochemistry and crustal evolution of volcano-sedimentary successions and orthogneisses in the São Gabriel Block, southernmost Brazil—relics of Neoproterozoic magmatic arcs. *Gondwana Research* 8: 143–161.

Saalmann K., Remus M.V.D., Hartmann L.A. 2006. Structural evolution and tectonic setting of the Porongos belt, southern Brazil. *Geological Magazine* 143:59–88.

Saalmann, K.; Gerdes, A.; Lahaye, Y.; Hartmann, L. A.; Remus, M.V.D. ; Läufer, A. 2011. Multiple accretion at the eastern margin of the Rio de la Plata craton: the prolonged Brasiliano orogeny in southernmost Brazil. *International Journal of Earth Sciences*, 100: 355-378.

Silva, A.O.M.S., Porcher, C.C., Fernandes, L.A.D., Droop, G.T.R. 2002. Termobarometria da Suíte Metamórfica Várzea do Capivarita (RS): Embasamento do Cinturão Dom Feliciano. *Revista Brasileira de Geociências*, 32(4):419-432.

Siviero, R. S., Bruguier, O., Koester, E., Fernandes, L.A.D. 2009. Crustal evolution in the Lavras do Sul region, Southern Brazil and the amalgamation of West Gondwana. *Goldschmidt Conference Abstracts*. A1232.

Soliani Jr., E., Koester, E., Fernandes, L.A.D. 2000. A Geologia Isotópica do Escudo Sul-riograndense. Parte II: os dados isotópicos e interpretações petrogenéticas. In: Michael Holz and Luis Fernando De Ros. (Eds.). *Geologia do Rio Grande do Sul*. Porto Alegre: Editora da UFRGS/Centro de Investigação do Gondwana - Instituto de Geociências, p. 175-230.

Steiger, R.H. and Jager, E., 1977. Subcommission on geochronology: Convention on the use of decay constants in geo- and cosmochronology. *Earth and Planetary Science Letters* 36(3): 359-362.

Sun, S.S., McDonough, W.F., 1989. Chemical and isotopic systematic of oceanic basalts: implications for mantle compositions and processes. In: Saunders, A.D., Norry, M.J. (Eds.), *Magmatism in the ocean basins: Geological Society of London Special Publication*, 42: 313–345.

Programa de Pós-Graduação em Geociências

Thompson R.N., Morrison M.A., Hendry G.I. And Parry S.J., 1984. An assessment of the relative roles of crust and mantle in magma genesis: an elemental approach. *Philosophical Transactions of the Royal Society of London A*, 310: 549–590.

Wasserburg G.J., Jacobsen S.B., DePaolo D.J., McCulloch M.T., Wen T., 1981. Precise determination of Sm/Nd ratios, Sm and Nd isotopic abundances in standard solutions. *Geochimica et Cosmochimica Acta* 45:2311-2323.

Wilson, M. 1989. Igneous Petrogenesis. Londres, Chapman and Hall, 466p.

Workman, R.K., Hart, S.R. 2005. Major and trace element composition of the depleted MORB mantle (DMM). *Earth and Planetary Science Letters* 231: 53– 72.

Workman, R. K., Hart, S. R., Jackson, M., Regelous, M., Farley, K. A., Blusztajn, J., Kurz, M., Staudigel, H. 2004. Recycled metasomatized lithosphere as the origin of the Enriched Mantle II (EM2) end-member: Evidence from the Samoan Volcanic Chain. *Geochemistry, Geophysics, Geosystems*. 5 (4): 1-44.

Supplementary data A

Major (% wt) and trace (ppm) element data for Várzea do Capivarita Complex orthogneisses. Two metavolcanic samples from Porongos Metamorphic Complex (area 7 in Fig. 1 and 2) are included for comparison.

Programa de Pós-Graduação em Geociências

Tonalitic orthogneisses													TM 60 A
	TM 01 E	TM 12 E	TM-13E	TM 29B	TM 35 A	TM 35 B	TM 36 G	TM 36 J	TM 38 A	TM 39 A	MN 155 G	TM 34 A	65.7
SiO ₂	68.28	69.38	65.93	69.55	65.48	63.8	61.69	67.08	65.16	73.49	69.97	66.27	0
Al ₂ O ₃	14.99	13.43	13.96	13.63	14.51	14.13	16.42	15.62	14.76	12.13	13.35	14.03	14.1
Fe ₂ O ₃ t	5.02	4.75	6.83	3.82	6.01	6.65	7.26	5.24	6.32	3.21	4.02	5.63	5.86
MnO	0.09	0.08	0.1	0.05	0.11	0.12	0.10	0.08	0.11	0.06	0.06	0.09	0.10
MgO	1.67	1.72	2.07	0.97	2.14	2.57	2.07	1.47	2.14	0.95	1.46	2.13	2.29
CaO	4.22	3.78	3.61	2.51	3.23	3.63	5.17	4.67	4.4	2.43	2.67	2.94	3.82
Na ₂ O	3.04	2.32	1.97	2.89	2.56	2.77	2.92	2.9	2.3	2.65	2.67	2.17	2.26
K ₂ O	1.52	2.3	3.63	3.63	3.41	1.66	1.65	1.13	2.59	2.38	3.66	4.07	2.91
TiO ₂	0.535	0.587	0.77	0.53	0.76	0.781	0.816	0.64	0.707	0.388	0.541	0.76	0.73
P ₂ O ₅	0.1	0.1	0.13	0.12	0.14	0.1	0.15	0.12	0.11	0.09	0.11	0.14	0.12
LOI	1.35	1.93	0.8	1.16	0.95	2.5	0.95	1.31	0.98	2.28	1.37	1.5	1.9
Total	100.8	100.4	99.77	98.85	99.31	98.72	99.2	100.3	99.58	100.1	99.87	99.73	9
Sc	16	16	18	12	18	19	24	19	20	9	9	16	17
Be	4	4	3	3	3	5	5	3	3	3	9	4	3
V	78	81	89	61	89	115	105	78	100	32	62	90	96
Ba	427	516	846	1310	796	408	432	508	736	657	937	996	762
Sr	145	177	186.3	372	216	351	199	154	265	121	318	348.4	4
Y	22	18	13.4	14	22	17	22	28	10	27	12	18.4	15.9
Zr	201	211	257.2	229	211	209	329	191	198	206	188	349.9	5
Cr	40	40	< 20	50	90	30	20	40	< 20	30	5	5	5
Co	10	7	13.7	5	12	14	10	7	11	4	6	13.8	14.3
Ni	< 20	< 20	< 20	< 20	< 20	< 20	< 20	< 20	< 20	< 20	< 20	18.1	18.3
Cu	10	10	74.6	30	20	40	40	10	10	< 10	20	24.7	22.1
Zn	90	60	76	60	110	110	120	80	70	70	65	62	62
Ga	17	17	17.1	18	20	21	22	20	18	16	20	16.2	16.0
Rb	114	102	135.2	114	140	92	137	107	106	117	230	178.4	8
Nb	8	9	15.6	8	13	15	11	9	9	8	19	14.4	15.1
Cs	13	4.1	5.1	2.1	9.9	6	27.8	19.2	4.9	6.6	14.6	7.0	8.2
La	26.2	28.3	39.7	52.7	33.9	28.3	22.3	27.7	22.7	29.8	43.4	36.4	36.7
Ce	53.7	56.5	65.3	103	69.9	58.3	44.2	57.5	44.2	60.8	74.9	75.3	77.1
Pr	6.65	6.96	7.44	12	8.5	7.25	5.78	7.27	5.24	7.47	8.13	8.07	8.20
Nd	21.8	23	27.7	38	27.6	24.3	19.9	24.5	17.1	25.1	23.3	30.9	31.2
Sm	4.5	4.4	4.16	6.2	5.5	4.8	4.1	5	3.1	4.9	3.8	5.22	4.84
Eu	1.03	1.02	1.35	1.32	1.45	1.14	1.09	1.07	1.24	0.81	0.99	1.34	1.20
Gd	3.8	3.6	3.17	4.3	4.4	3.8	3.7	4.5	2.3	4.3	2.5	4.25	3.67
Tb	0.7	0.6	0.4	0.6	0.7	0.6	0.6	0.9	0.4	0.8	0.4	0.62	0.52
Dy	3.9	3.2	2.41	3.1	4	3	3.6	4.9	2	4.4	2.3	3.25	2.88
Ho	0.7	0.7	0.42	0.5	0.8	0.6	0.7	1	0.4	0.9	0.4	0.64	0.57
Er	2.8	2	1.63	1.4	2.5	1.7	2.2	3	1.3	2.8	1.3	1.85	1.68
Tm	0.42	0.29	0.19	0.19	0.38	0.26	0.35	0.47	0.21	0.46	0.19	0.29	0.29
Yb	2.7	2	1.71	1.2	2.5	1.7	2.2	3	1.5	2.7	1.2	1.81	1.83
Lu	0.41	0.31	0.23	0.17	0.38	0.27	0.35	0.45	0.24	0.4	0.18	0.28	0.29
Hf	5.8	6.4	6.6	7.1	6.8	6.6	9.2	5.9	6	6.5	5.8	9.2	6.6
Ta	0.7	0.7	1	0.4	0.6	0.9	0.8	0.7	0.5	0.7	1.5	0.8	0.9
Pb	14	13	7.3	24	28	23	12	14	16	15	30	8.2	8.2
Th	7.4	9.3	12.9	14.9	94	14.2	6.1	9.5	3.9	11.6	32.9	14.1	10.8
U	0.9	1.4	1.1	0.9	1.9	1.1	0.9	1.3	0.6	2.4	8.9	2.4	2.1
Tonalitic Orthogneisses				Granitic Orthogneisses							Metavolcanic Rocks		
TM 66 B	TM 38 C	TM 67 A	TM 51 A	TM 45 B	TM 45 C	TM 45 E	TM 45 G	TM 45 H	TM 45 I	TM 69 A	TM-015A	TM-026C	
SiO ₂	61.87	65.49	70.30	65.41	72.75	72.91	75.53	72.95	72.43	72.75	65.95	71.74	70.42
Al ₂ O ₃	16.41	14.31	13.47	14.97	14.02	13.7	13.07	13.88	13.71	14.01	14.43	13.99	13.62
Fe ₂ O ₃ t	6.36	6.23	4.19	6.24	2.68	2.93	1.86	2.68	2.88	2.63	6.2	3.36	4.13
MnO	0.11	0.12	0.05	0.12	0.05	0.06	0.06	0.06	0.06	0.05	0.11	0.07	0.06
MgO	2.18	2.51	1.39	2.65	1.00	1.08	0.27	0.95	1.06	0.93	3.1	0.73	1.25
CaO	3.90	3.53	4.16	4.36	3.24	2.78	1.59	3.09	2.93	2.94	4.41	1.44	2.18
Na ₂ O	3.01	2.33	2.06	1.77	2.99	3.26	3.64	2.67	2.89	3.2	1.31	3.23	2.69
K ₂ O	2.89	3.27	1.88	2.09	1.92	1.9	2.82	2.39	2.3	2.1	2.27	3.4	3.23
TiO ₂	0.82	0.72	0.54	0.62	0.33	0.33	0.12	0.31	0.34	0.3	0.62	0.44	0.43
P ₂ O ₅	0.14	0.12	0.10	0.09	0.07	0.08	0.05	0.06	0.08	0.06	0.09	0.1	0.06
LOI	2.1	1.1	1.6	1.5	0.8	0.8	0.9	0.8	1.2	0.9	1.3	1.3	1.7
Total	99.79	99.77	99.77	99.82	99.85	99.87	99.88	99.86	99.87	99.87	99.83	99.76	99.80
Sc	19	19	14	19	9	10	8	9	9	9	19	7	12
Be	5	3	< 1	2	2	3	4	2	6	2	3	6	3
V	105	102	72	96	35	41	9	36	42	36	101	39	45
Ba	899	889	630	489	709	400	625	610	492	553	457	528	728
Sr	264.0	197.9	190.9	155.0	145.0	135.7	169.1	131.5	117.4	131.2	136.5	150.7	167.8
Y	19.9	15.8	13.0	23.5	20.5	34	29.5	27.4	27.4	26.7	20.5	40.3	26.0
Zr	261.0	208.4	182.2	165.9	151.9	170.8	109.5	135.6	147.2	151.5	164.8	319.2	147.4
Cr	4	62	41	5	3	27	< 13	21	27	21	68	40	50.000
Co	14.8	17.9	12.1	15.8	5.5	6.3	1.5	5.6	6.8	5.5	17	5.8	10.3
Ni	13.5	19.9	11.1	15.9	5.9	8	0.8	6.3	7.5	6.4	18.7	56.2	8.6
Cu	18.0	19.0	67.7	25.8	19.8	2.8	1.6	4.4	8.7	2.4	9.1	10.6	15.7
Zn	84	45	31	64	37	42	37	37	50	40	64	56	47

Programa de Pós-Graduação em Geociências

Cont. suplem. data

Tonalitic Orthogneisses		Granitic Orthogneisses											Metavolcanic Rocks	
	TM	66 B	TM 38 C	TM 67 A	TM 51 A	TM 45 B	TM 45 C	TM 45 E	TM 45 G	TM 45 H	TM 45 I	TM 69 A	TM-015A	TM-026C
Ga	18.1	17.0	15.8	14.7	14.1	17.1	16.6	15.9	16.7	15.5	16.8	18.9	14.4	
Rb	188.1	136.9	94.0	167.7	147.5	129.1	116.5	157.1	166.3	157.6	134.9	179.5	116.1	
Nb	14.3	11.3	7.8	9.0	8.8	9.7	8.2	8.3	9.7	7.7	8.8	17.3	7.7	
Cs	11.3	5.4	5.0	14.3	7.6	7.9	2.8	13.4	9.9	13.2	11.5	13.8	3.6	
Sm	5.82	5.33	4.49	4.41	4.54	7.2	6.26	5.39	5.36	5.42	4.47	8.3	5.29	
Eu	1.15	1.38	1.09	0.96	0.87	0.83	0.87	0.96	0.78	0.86	0.95	1.13	0.97	
Gd	4.71	4.07	3.50	3.99	3.94	5.95	5.42	4.49	4.8	4.7	3.74	7.55	4.64	
Dy	3.71	3.27	2.76	4.01	3.61	6.59	5.95	4.84	5.08	5.08	4.06	7.11	4.88	
Ho	0.71	0.59	0.48	0.85	0.72	1.24	1.07	0.93	0.92	0.98	0.74	1.25	0.99	
Er	1.95	1.92	1.51	2.47	2.19	3.91	3.97	3.08	3.12	2.9	2.38	3.69	2.46	
Tm	0.33	0.28	0.22	0.39	0.34	0.59	0.56	0.46	0.45	0.46	0.38	0.54	0.40	
Yb	2.07	1.67	1.29	2.45	2.08	3.46	3.3	2.84	2.73	2.97	2.35	3.65	2.51	
Lu	0.34	0.30	0.22	0.37	0.31	0.54	0.55	0.43	0.44	0.49	0.4	0.56	0.38	
Hf	7.1	6.3	4.9	4.6	4.1	5.3	4	4.5	4.9	4.9	4.4	9.1	4.30	
Ta	1.3	0.8	0.5	0.7	0.7	1	0.6	0.8	1.1	0.7	0.7	1.3	0.50	
Pb	9.0	10.5	7.1	6.4	3.3	3.1	4.9	3	3.5	3.8	10.2	8.2	3.40	
Th	12.5	14.8	9.8	8.8	11.5	19	11.9	12.7	12.8	12.4	8.7	23.6	10.80	
U	2.1	1.5	1.3	2.1	2.6	3.8	2.2	2.6	3.1	3.3	1.8	5	2.50	

- Capítulo III -

CONSIDERAÇÕES FINAIS

O CVC congrega paragnaisse predominantes de composição pelítica além de rochas calciosilicáticas e ortognaisse tonalíticos a graníticos, tectonicamente intercalados em fatias tabulares ou lenticulares de espessura decimética a métrica. O bandamento principal alinhamento contém minerais de alta temperatura, tais como hiperstênio, cordierita e espinélio, indicando condições de fácie granulito para o metamorfismo que afeta o CVC. O Complexo inclui também granitóides porfiríticos de composição dominante sienítica, que seriam sincrônicos ao evento tectono-metamórfico responsável pelo empilhamento de orto e paragnaisse.

A investigação do arcabouço estrutural que compõe o CVC revela que a deformação principal foi particionada em duas fases dícteis formadas progressivamente - D₁ e D₂. Durante D₁ os gnaisses do CVC foram tectonicamente intercalados ao longo de um bandamento de direção preferencial NNW e atitude original sub-horizontal, contendo lineação de estiramento de alta obliquidade. Essa sucessão teria gerado uma pilha de thrust com sentido de movimento de topo para oeste. A sucessão de rochas de composição contrastante em escala variada é o principal indicativo de embaralhamento tectônico. Entretanto, a hipótese de intercalação tectônica é também amparada pelas evidências geocronológicas e dados de proveniência. Gruber (2016) descreve idades de proveniência paleo- (2.2 – 2.0 Ga), meso- (ca. 1.4 Ga) e neoproterozóicas (ca. 715 Ma) para os metapelitos do CVC. Estes dados são contrastantes com os obtidos por Martil et al. (in prep.) que descreve ortognaisse e gnaisses pelíticos com populações de grãos de zircão com idades bastante similares entre si (ca. 800 Ma), demonstrando que paragnaisse de composição análoga inclusos no CVC podem ser rochas de origem distinta. Além disso, veios graníticos intrusivos em rochas calciosilicáticas e dobrados em D₂ possuem idades de cristalização (ca. 770 Ma) semelhante aos ortognaisse do Complexo (ca. 780 Ma) sugerindo que parte das rochas calciosilicáticas são mais antigas que esse magmatismo.

A deformação D₂ é marcada principalmente pela geração de dobras – F₂ e por uma foliação – S₂ de desenvolvimento heterogêneo. As dobras F₂ são estruturas de

Programa de Pós-Graduação em Geociências

meso e mega escala com plano axial NNW de mergulho alto. A foliação S_2 grada desde uma clivagem plano-axial até uma clivagem de transposição, que eventualmente forma um bandamento penetrativo de direção NNW e mergulho alto. O cisalhamento progressivo ao longo de S_2 leva a geração de uma zona de cisalhamento NNW do tipo *strike-slip* a oblíqua. O sentido de movimento horário é dado pela assimetria de lentes de plagioclásio e quartzo, bem como pelo dragueamento das estruturas relacionadas a D_1 .

A lineação de estiramento transiciona de um padrão *down-dip* (L_{X1}) para um padrão direcional (L_{X2}) o que sugere a conversão de do eixo tectônico de X para Y. Esta transição é comum em áreas transpressivas em que a deformação se particiona em um componente contracional e outro do tipo *strike-slip* (Sanderson and Marchini, 1984, Tikoff and Tessier, 1994).

A relativa coexistência e transição entre a cinemática de empurrão - D_1 e a cisalhamento transcorrente - D_2 , é demonstrada por evidências diversas (i) S_1 e S_2 tem as mesmas assembléias minerais indicativas de fácies granulito, sugerindo que ambas se formaram durante o mesmo evento; (ii) as estruturas S_1 são gradualmente transpostas pelas zonas de alta deformação relacionadas a D_2 ; (iii) o movimento de topo para oeste registrado na D_1 é compatível com o cisalhamento destral encontrado em D_2 ; (iv) Os dados geocronológicos ilustrados nessa tese indicam as mesmas idades para D_1 e D_2 . Adicionalmente, a contemporaneidade entre metamorfismo de alto grau e a tectônica transpressiva registrados no CVC sugere que o Complexo foi originado em um evento colisional oblíquo.

Os dados petrológicos obtidos demonstram que os gnaisses tonalíticos e graníticos do CVC são rochas calcioalcalinas meta- a peraluminosas cuja composição e padrões de elementos traços sugerem que representem um magmatismo de margem continental. Os dados isotópicos Sr-Nd reportados nesta tese sugerem que os protólitos dos ortognaisses foram gerados por assimilação crustal associada a processos de cristalização fracionada. As análises U-Pb em zircão (LA-MC-ICP-MS e SHRIMP) definem idade de cristalização em ca. 790 Ma para os ortognaisses. O magmatismo registrado no Complexo é correlacionável com outras sequências de arco datadas em ca. 800 Ma, incluindo parte das metavulcânicas ácidas inclusas nas supracrustais do sul do Brasil (Complexo

Programa de Pós-Graduação em Geociências

Metamórfico Porongos – CMP), e os ortognaisses de alto grau descritos no escudo uruguai (Cerro Bori – CB). Todas essas associações têm assinatura típica de orógenos acrecionários, contendo idade TDM Meso a Paleoproterozóica, além de forte evidência da participação de processos de assimilação crustal/ contaminação. Os valores elevados de K nas rochas do CVC e CMP, e a tendência dessas unidades de se situarem mais próximas dos campos pós-colisional e intraplaca, nos diagramas descritos por Pearce et al. (1984) sugere sua geração em ambiente de arco mais maduro, com maior espessamento da crosta. Em contraste, os ortognaisses do escudo uruguai exibem um caráter menos maduro de magmatismo, formado em crosta menos espessa.

O conjunto de dados apresentados permite interpretar essas associações como parte do mesmo magmatismo, ou ainda como fragmentos de arcos magmáticos similares.

A caracterização geoquímica e as assinaturas isotópicas Sr-Nd obtidas sugerem que ao menos parte das metavulcânicas do CMP represente os protólitos dos ortognaisses de alto grau inclusos no CVC. Adicionalmente, as evidências isotópicas também apontam similaridade entre as rochas sedimentares de ambas as unidades. Estudos em andamento (Martil et al., in prep.), apontam para o caráter vulcão-sedimentar de uma fração dos metapelitos do CVC e sua relação cogenética com os ortognaisses. Em adição aos dados petrologicos aqui debatidos, é possível que parte das litologias inclusas no CVC e no CMP tenham sido parte de um mesmo ambiente vulcão-sedimentar formado em arco continental. A investigação destas hipóteses é o tema principal de um quarto artigo atualmente em preparação que integrará idades de proveniência (U-Pb – SHRIMP) associadas a determinações de isótopos de oxigênio em zircão (Martil et al., in prep.)

Idades de ca. 640-650 Ma (LA-MC-ICP-MS e SHRIMP) obtidas em sobrecrescimentos de zircão foram interpretadas como representantes do metamorfismo granulítico e do evento colisional que teria gerado o CVC. Estes dados compatíveis com a idade de cristalização em ca. 640 Ma obtida para sienitos sintectónicos inclusos no CVC (U-Pb em zircão obtido por LA-MC-ICP-MS - Bitencourt et al., 2011). Os dados geocronológicos são também consistentes com as idades referidas por Chemale Jr. et al. (2011) para o metamorfismo de fácies

Programa de Pós-Graduação em Geociências

anfibolito superior que afeta a associação metagabro-anortosítica (Anortosito Capivarita) encontrada na região. Idades metamórficas mais jovens em ca. 620 Ma obtidas em metapelitos do VCC e veios leucograníticos e referidas em estudos prévios (U-Pb SHRIMP em zircão - Philipp et al., 2016), são aqui interpretadas como relacionadas a idade fusão parcial comumente associada ao relaxamento termal que sucede o estágio colisional principal (e.g. Jamieson et al., 2004).

O conjunto de dados estruturais, geocronológicos e petrológicos obtidos para o CVC revelam uma história evolutiva prolongada para o Complexo. Os protólitos dos ortognaisses e parte dos paragnaisses estudados teriam se originado em um mesmo ambiente vulcano-sedimentar formado em um arco magmático continental estabelecido em ca. 790 Ma. Posteriormente, essas rochas teriam sido sofrido metamorfismo de alto grau, possivelmente relacionado a um evento de colisão oblíqua em ca. 640 Ma.

Referências

- Bitencourt, M.F., De Toni, G.B., Florisbal, L.M., Martil, M.M.D., Niessing, M., Gregory, T.R., Nardi, L.V.S., Heaman, L.M., Dufrane, S.A., 2011. Structural geology and U-Pb age of unusual Neoproterozoic syn-collisional syenite-tonalite association from southernmost Brazil. In: Seventh Hutton Symposium on Granites and Related Rocks, 2011, Avila. Abstracts Book, p. 21.
- Chemale Jr., F., Philipp, R.P., Dussin, I.A., Formoso, M.L.L., Kawashita, K., Bertotti, A.L., 2011. Lu-Hf and U-Pb age determinations of Capivarita Anorthosite in the Dom Feliciano Belt, Brazil. *Precambrian Research* 186, 117-126.
- Gruber, L., 2016. Geologia isotópica e geocronologia do Complexo Metamórfico Porongos e Suíte Metamórfica Várzea do Capivarita, Cinturão Dom Feliciano, Sul do Brasil: Implicações para a evolução do Gondwana em sua margem ocidental. PhD thesis, Universidade Federal do Rio Grande do Sul, Porto Alegre, p. 117.
- Jamieson, R. A., Beaumont, C., Medvedev, S., Nguyen, M.H., 2004. Crustal channel flows: 2. Numerical models with implications for metamorphism in the Himalayan – Tibetan orogen. *Journal of Geophysical Research*, 109, B06406, doi:10.1029/2003JB002811.
- Martil, M.M.D., Bitencourt, M.F., Schmitt, R., Armstrong, R., Pimentel, M., Nardi, L.V.S. Reconstitution of a volcano-sedimentary environment at 790 Ma obliterated by a collisional thrust tectonics: the Porongos and Várzea do Capivarita Complexes, southern Brazil. (in prep.).
- Pearce, J.A. Harris, N.B.W. Tindle, A.J. 1984. Trace Element Discrimination for the tectonics interpretation of granitic rocks. *Journal of Petrology*, 25: 956-983.
- Philipp, R.P., Bom, F.M., Pimentel, M.M., Junges, S.L., Zvirtes, G., 2016a. SHRIMP U-Pb age and high temperature conditions of the collisional metamorphism in the

Programa de Pós-Graduação em Geociências

Várzea do Capivarita Complex: Implications for the origin of Pelotas Batholith, Dom Feliciano Belt, Southern Brazil. *Journal of South American Earth Sciences* 66, 196-207.

Sanderson, D.J., Marchini, W.R.D., 1984. Transpression. *Journal of Structural Geology* 6, 449–458.

Tikoff, B., Tessier, C., 1994. Strain modeling of displacement field partitioning in transpressional orogens. *Journal of Structural Geology* 11, 1575-1588.